Preface

National Institute of Radiological Sciences (NIRS) has endeavored to promote efficiency, transparency and competitive research atmosphere, which are the essential principle for the Independent Administrative Institution (IAI). Our eventual aim is, needless to say, to achieve outstanding outcomes through research activities.

The fiscal year 2002 (FY2002) was the 2nd year after NIRS was reborn as a IAI in 2001. NIRS has been implementing its activities basically according to mid-term (5 years) plan and annual plan.

We submitted our business report (including the financial report) and the achievement report of FY 2001 to the Ministry of Education, Culture, Sports, Science and Technology (MEXT) in June 2002, which was evaluated by the Evaluation Committee of MEXT. This evaluation process was the first that we have experienced. We need to get accustomed to this annual important event in order not to consume too much energy in this process.

NIRS established a new Research Center for Radiation Emergency Medicine with enforcement of its dose assessment capability for improving the medical preparedness for nuclear emergency and radiation accidents. We also set a program for acquiring external competitive grants and started some leading research with such grants. We also increased the flexibility of research system. Furthermore, NIRS introduced a personnel management system for technologists in order to treat well-trained high grade technologists properly.

NIRS continued research activities according to the mid-term plan, including 5 project researches, I frontier type research, 20 basic researches, and brain function research. Almost all projects progressed as was planned. Additionally, I as president of NIRS took initiative in granting 28 new research proposals after in house competition in order to cultivate research seeds. In FY2002, we produced 244 original papers, which meant 1.4 papers per researcher. Heavy charged particle therapy continued to be successful. Based on the results of clinical trials, we applied to a health system for highly "advanced medical procedures ", which allows us to change patients.

NIRS also increased PR activities such as open lectures for public in Tokyo and Osaka, and two open lectures for researchers, which attracted many participants. NIRS cooperated to the United Nations Scientific Committee on the Effects of Atomic Radiation (UNSCEAR), International Commission on Radiological Protection (ICRP) and the International Atomic Energy Agency (IAEA). We organized several international meetings such as the 3rd Committee for ICRP. NIRS promoted cooperative researches with universities, research institutes and companies, having received many external researchers and students, and organized symposiums. We also set an agreement on cooperation program with Graduate School of Toho University.

It is our great pleasure to publish this annual report for your information and your comments. In the rapidly changing society worldwide, we will continue our efforts as a center of excellence (COE) of radiation medicine applying advantages of IAI. We appreciate your cooperation and would like to ask for your continuous supports.

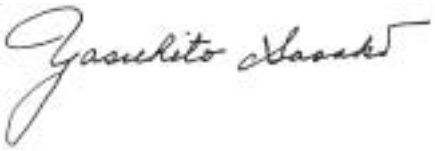

Yasuhito Sasaki, M. D., Ph. D.
President

PHYSICS

1. Basic Study on Pulse Height Distribution of DOI Detectors Constructed of Stacked Crystal Elements

Narimichi Orita, Hideo Murayama, Naoko Inadama, Takaya Umehara, and Takehiro Kasahara

Keywords: *positron emission Tomography(Pet), depth-of-interaction detector, scintillation detector*

As part of the next generation PET development project, performances of one-dimensional GSO crystal arrays were measured and analyzed for the development of the depth-of-interaction (DOI) detector constructed of three-dimensional GSO crystal arrays. We considered two structures of one-dimensional crystal arrays, one is a "straight line type" which has the crystals of the array stacked in series, and the other is a "U shaped type" which is a crystal block of stacked crystals bent at the center. By scanning collimated gamma rays along the crystals, we measured the pulse height distributions from one end or both ends of the crystal array for different conditions of the surface of each crystal (rough or chemical etching) and arrangement of the reflector. On the average, there is almost no position dependence for individual crystals because the gamma ray beam response in each crystal is uniform within 2.0% for chemical etching and 5.6% for rough surface. From this result, we irradiated the gamma ray beam on the center of individual crystals in the following experiments.

The "straight line type" has a better light yield and crystal identification than the "U shaped type". When trying to develop the DOI detector with the "straight line type", DOI information is acquired by arranging a PMT at each end and calculating the ratio from two PMT outputs. However, there are problems on the structure so it is difficult to make a practical application. Then we focused on the "U shaped type". In order to overcome the low light yield of the "U shaped type", we tried to optimize the arrangement of the reflector, and the combination of a crystal surface. In order to examine how the combination of crystal surface and arrangement of the reflector affects the performances, we also measured two-dimensional pulse height distributions for the "U shaped type". The analysis of these data showed how these conditions affected the performances of the DOI detector. Examination results of continuous crystals or discontinuous crystals the "U shaped type" array revealed that using continuous crystals had an advantageous light yield, but crystal identification was not better because there was little position dependence for an individual crystal.

Fig.1 shows a two-dimensional map for the "U shaped type" which allows comparison of the reflector arrangement and conditions of the surface of each crystal. We use "c" to denote the chemical etching surface crystal and "r" to denote the rough surface. The crystal identification by arranging one crystal with the rough surface in the 3rd or 4th stage ("ccrc" or "cccr") was better than the case of "cccc" and as good as the case of "rrrr". By these experiments, we found that various features might be acquired by changing parameters in the discontinuous type detector. And since these results of the "U shaped type" indicated that there was a limitation for this structure, We concluded it was necessary to obtain a larger light yield from the upper stages of the crystal block. One solution would be to make a light path on the upper stages using three-dimensional crystal arrays.

Publication:

Umehara, T. Murayama, H. Omura, T. et al.: *2002 IEEE NSS & MIC Conf. Rec*., M10-29, 2002.

Figure caption:

Fig.1. Two-dimensional map for experimental "U shaped type" array with reflector in 1st and 2nd stages.

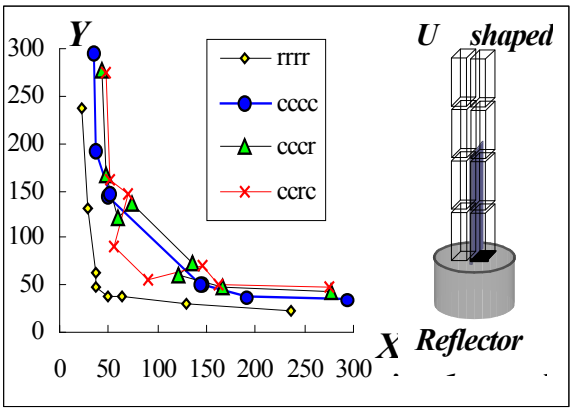

2. DOI-PET Image Reconstruction with Accurate System Modeling that Reduces Redundancy of the Imaging System

Taiga Yamaya and Hideo Murayama

Keywords: *image reconstruction, depth-of-interaction (DOI), positron emission tomography (PET), nuclear medicine*

A high-performance PET scanner, which measures depth-of-interaction (DOI) information, is under development at the National Institute of Radiological Sciences. This scanner is designed to improve spatial resolution and scanner sensitivity simultaneously by the DOI measurement of multi-layered thin crystals. The latest design of the DOI-PET scanner is 5 rings of 24 detector blocks, and each detector block consists of 1,024 GSO crystals of 2.9 mm x 2.9 mm x 7.5mm, which are arranged in 4 layers of 16 x 16 arrays. On the other hand, image reconstruction methods with accurate modeling of the system response functions have been successfully used to improve PET image quality. It is, however, difficult to apply these methods to the DOI-PET scanner because the dimension of DOI-PET data increases in proportion to the square of the number of DOI layers.

In this paper, we propose an image reconstruction approach dedicated for DOI-PET imaging, which reduces computational cost while keeping image quality. The basic idea of the proposed method is that the DOI-PET imaging system is highly redundant because the neighboring spatial response functions of different DOI-layer pairs correlate with each other. First, DOI-PET data are transformed into compact data so that data bins with highly correlating sensitivity functions are combined. Next image reconstruction methods based on accurate system modeling, such as the maximum likelihood expectation maximization (ML-EM), are applied. Four DOI layers result in 16 pairs of DOI layers, and the number of DOI-layer pairs to be preserved, D, works as a tuning parameter that controls the trade-off between computational cost and image quality.

The proposed method followed by ML-EM was applied to Monte Carlo simulated data for the DOI-PET scanner. For comparison, ML-EM with no compression was also applied. The number of DOI-layer pairs to be preserved was chosen as D=1, 2 and 3. We also applied ML-EM to a non-DOI PET scanner to show the effect of DOI information. The non-DOI PET scanner, which had the same geometric size as the DOI-PET scanner, consisted of crystals of 2.9mm x 2.9mm x 30mm arranged in a single layer. The conventional filtered backprojection (FBP) method, which does not deal with the accurate system model, was also applied in order to show the effect of accurate system modeling. At this stage demonstrations have been restricted to 2D implementation, though our final goal is fully 3D image reconstruction. Two figures of merit (FOMs), background noise and spatial resolution, were used to evaluate the image quality. The spatial resolution was measured as the average of radial and tangential full widths at half maximum (FWHM) of three point spread functions. A warm phantom of 100 mm diameter was used to measure the background noise as the normalized standard deviation (NSD). The trade-off between the background noise and the spatial resolution was investigated, using ML-EM with each iteration and FBP with a ramp filter of different cut-off frequencies. Comparison between ML-EM and FBP shows the improvement of image quality by using accurate system modeling. And comparison between DOI-PET and non-DOI PET shows the improvement of image quality by using DOI information. The trade-off results indicate that images reconstructed by the proposed method with D=3 followed by ML-EM have almost the same image quality as ML-EM does although the proposed method with D=1 or 2 shows a slight decline of image quality. The averaged calculation time of the proposed method (D=3) is about 3/16 of the ML-EM with no compression.

In summary, numerical simulation results show that the proposed method followed by ML-EM reduces computational cost effectively while keeping the advantages of the accurate system modeling and DOI information.

Publication:

Yamaya, T., Obi, T., Yamaguchi, M., Kita, K., Ohyama, N., Hasegawa, T., Haneishi, H. and Murayama, H. : *Med. Imag. Tech.*, **21**, 166-169, 2003 (*in Japanese*) .

Figure caption:

Fig. 2. Graph showing the trade-off between background noise (NSD) and spatial resolution. “Proposed method” denotes the proposed method followed by ML-EM, and “ML-EM” denotes ML-EM with no compression. *D* is the number of DOI-layer pairs to be preserved when the DOI-PET data are compressed.

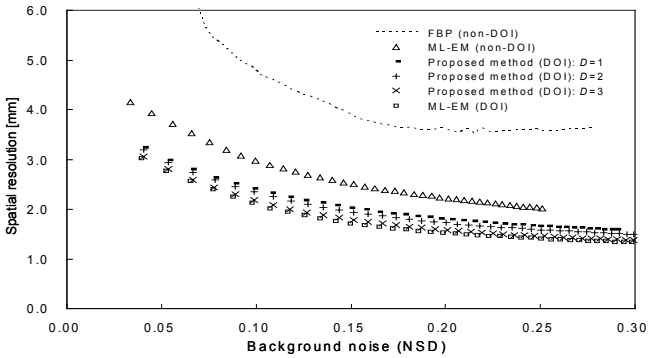

3. Basic Investigation of Data Acquisition System for Next Generation PET Scanner

Eiji Yoshida, Keiji Shimizu, Keishi Kitamura, Hideo Murayama

Keyword: *positron emission tomography (PET), data acquisition, parallel collection, list-mode data*

We are developing a 3D PET scanner with depth-of-interaction (DOI) detector capable of high sensitivity and high resolution. In this work, we estimated the data transfer rate of the data acquisition system of this PET scanner by simulation studies. This PET scanner has a small ring diameter and large axial view. The number of coincidence pairs is 40G for a structure of four stages in the DOI detector. Therefore, measurement data are collected by a list-mode data format (event by event) as opposed to conventional histogram format. The maximum data transfer rate of coincident pair event information is 10 Mcps and one coincidence event has a 64-bit data format. The data acquisition system which fulfills the specifications of this PET scanner is considered for parallel collection with banks including several coincidence units. Fig. 3 shows an example construction of the data acquisition system using several parallel PCs. One node with banks including several coincidence units consists of PCs and has the Small Computer System Interface (SCSI) protocol. Constructions can be applied flexibly; when the composition of a detector system changes, the remaining computer resources can be used for calculation of image reconstruction.

A simulator for the parallel collection system is composed of two stand-alone simulators and the server PC. Each stand-alone simulator is composed of the data generation PC, data processing circuit, SCSI and data acquisition PC. The data generation PC generates list-mode data at imitate counting rate configured in advance. These list-mode data provide for Monte Carlo simulation. Data processing circuits modify the list-mode data format, adjust the timer tag, and so on. The maximum imitate counting rate is 2.5 Mcps per one node, but this value is restricted to the maximum data transfer rate of SCSI (ULTRA SCSI). The data acquisition PC receives modified list-mode data through the SCSI and buffers them for sending to the server PC through Gigabit Ethernet (1000BASE-T). The data acquisition PC has a 32-bit Ethernet board and the server PC has a 64-bit Ethernet board for concentrating the coincidence data.

In simulation studies, the maximum data transfer

rate of the stand-alone simulator was 12.0 MB/s, and the maximum data transfer rates at the server PC with one and two nodes were 11.0 and 21.8 MB/s, respectively. We could expect a good data transfer rate with a full system from these results; 10 Mcps could be achieved for ULTRA-WIDE SCSI which has 2 times the bandwidth of ULTRA-SCSI and a parallel collection of six nodes. Data transfer rate was improved by parameter optimization of message size and multi-processing of data acquisition software using RAM-DISK.

Publication:

Yoshida, E., Shimizu, K., Kitamura K., and Murayama, H.: *Jpn. J. Med. Phys.*, **23**, 65-72, 2003 (*in Japanese*).

Figure Caption:

Fig.3. Example construction of data acquisition system for next generation PET scanner.

Fig.3 Example construction of data acquisition

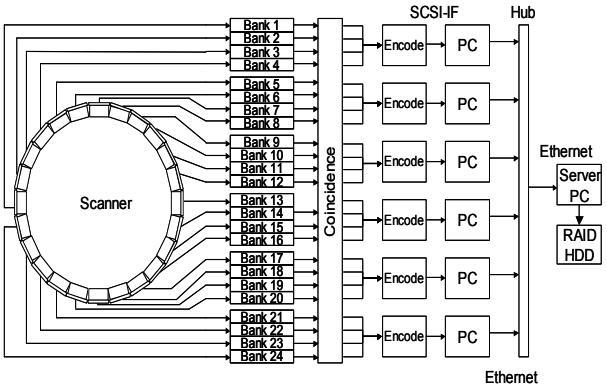

system for next generation PET scanner.

4. Improvement of the Depth-of-Interaction Detector for PET on Full Energy Pulse Height Uniformity

Tomoaki Tsuda, Hideo Murayama, Takaya Umehara,
Takehiro Kasahara, and Naoko Inadama

Keywords: *positron emission tomography, depth-of-interaction detector, GSO scintillation crystal*

For next generation positron emission tomography (PET) that realizes high sensitivity and high resolution, we proposed the design of a depth-of-interaction (DOI) detector. In our previous work, we found the upper stage crystal elements which are further from the photocathode of the PMT have a tendency to show lower energy pulse height and we measured the ratio of the minimum full energy pulse height to the maximum as 0.3. We designed a new DOI detector to overcome this problem by optimizing following the detector parameters; reflector arrangement, condition of crystal surface, and optical coupling between crystal elements.

The DOI detector is constructed of rectangular crystal elements with cross section dimensions of 2.9mm x 2.9mm and 7.5mm depth. They are arranged in 2 by 2 arrays and stacked to four stages. Between stages, silicone oil is inserted. For crystal elements, two kinds of Gd_2SiO_5 (GSO) crystals differing in doped Ce concentration are used; 0.5mol% Ce having a 60 ns scintillation decay time, and 1.5mol% Ce having a 35 ns decay time. The 0.5mol% GSO crystals are used for the 2nd and 4th stages and 1.5mol% GSO crystals are used for the 1st and 3rd stages. The optimized structure was determined through performance tests of DOI detectors in various parameter combinations. Fig.4 illustrates the structure. Crystals in the 1st, 2nd, and 4th stages are replaced by chemically etched ones, while rough surface crystals remain in the 3rd stage. A reflector is inserted between crystals in the 1st and 2nd stages, and there is an air gap in the 3rd and 4th stages. Multilayer polymer mirrors, 65 um thick, is used as the reflector. This optimized DOI detector was optically coupled to a 16ch PS-PMT (H6568MOD Hamamatsu Photonics K.K.) by silicone oil and uniformly irradiated by gamma-rays from a 3.7MBq ^{137}Cs point source placed 10 cm above the top face of the crystal blocks. Pulse height distribution performance, crystal identification performance in 2D

positioning histograms calculated by an Anger-type position calculation, and full energy peak uniformity were assessed.

Fig.5 shows pulse height distributions of all crystal elements in this structure. We got an energy pulse height in the upper stage which was almost the same height as for the bottom stage crystals. The maximum difference in relative full energy peaks of this structure was 0.19. This represented much progress from the previous structure. As a further analysis of this structure, the light yield of individual crystal element was measured to estimate light attenuation by passing through other crystal elements in the same crystal block to reach the PS-PMT photocathode. The results included the interesting fact that the attenuation of light from the 2^{nd} stage crystal was larger than the light from the 3^{rd} stage crystal. This favorable attenuation contributed to achieving full energy pulse height uniformity in this crystal block. Since there was good uniformity of pulse height, photoelectric events could be extracted by applying a threshold at the valley on the pulse height distribution of all events. Misidentification in the pulse shape discrimination process was estimated as less than a few percent after the pulse height discrimination. This good separation and enough distinction in the resultant 2D position histograms indicated the good capability of the optimized DOI detector regarding decay time and light yield fluctuation among so many GSO crystal elements in mass production for a PET system.

Publication:
Kasahara T., Murayama H., Omura T., et al.: *2002 IEEE NSS & MIC Conf. Rec.*, M10-54, 2002.

Figure caption:
Fig.4: Previous structure and optimized structure.
Fig.5: Energy histograms of each crystal element. Vertical axes are normalized by the max value.

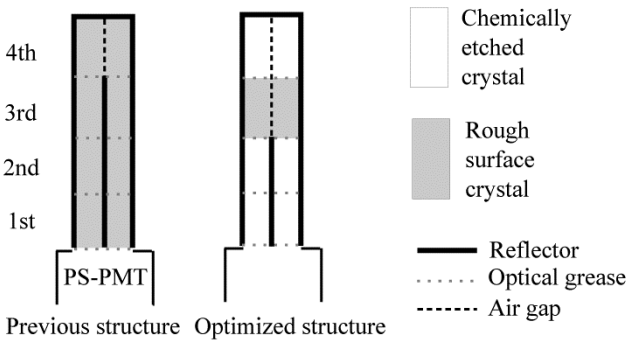

Fig.4

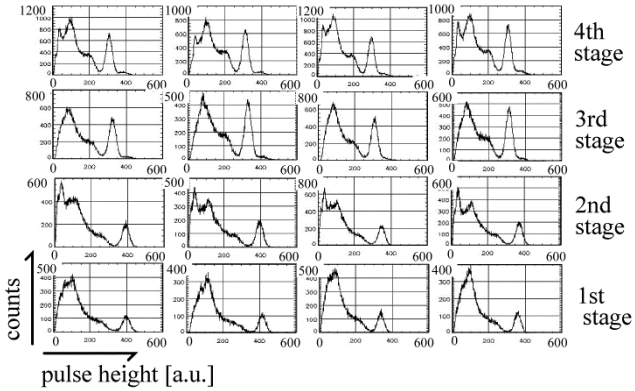

Fig.5

5. Performance of a PET Detector with a 256ch Flat Panel PS-PMT

Naoko Inadama, Hideo Murayama, Takaya Umehara, and Takehiro Kasahara

Keywords: *position sensitive photomultiplier tube, positron emission tomography (PET), scintillation detector*

We plan to utilize a 256ch flat panel position sensitive photomultiplier tube (FP-PMT) for the DOI detector of the next generation PET, jPET-D4, to get high sensitivity while maintaining high spatial resolution. The 256ch FP-PMT having a 52mm x 52mm large opening area and a high 89% effective area ratio was newly designed by Hamamatsu Photonics K.K., Japan (Fig. 6(a)). It contains a 16 x 16 matrix multianode arranged at a 3.04mm interval to each other. The anode configuration contributes to identification of small

crystals even on the peripheral region of its photocathode. Capability of independent processing of all anode outputs will also allow high count rate detection in a PET system. Right now, only a prototype of the 256ch FP-PMT has been produced. To verify the 256ch FP-PMT for application to the jPET-D4 DOI detector, light spread in it and its crystal identification ability were estimated using the prototype and Gd_2SiO_5:Ce (GSO) crystals sized 2.9mm x 2.9mm x 7.5mm which will compose the DOI detector. For latter estimation, GSO crystals assembled in a 16 x 16 array were optically coupled to the 256ch FP-PMT by silicone oil and 511keV gamma-rays from ^{18}F were irradiated onto them uniformly.

Light spread function of the central anode was found to be Gaussian with a 4.9mm full width at half maximum (FWHM). This was comparable with a 16ch position sensitive PMT which is in general use and was obtained despite the rather large difference in thickness of the opening window glass, 2.0mm for the 256ch FP-PMT and 0.8mm for the 16ch PS-PMT. Fig. 6(b) is the resultant 2-dimensional position histogram of the 16 x 16 GSO crystal array. Crystals of interaction could be clearly identified on it. Its profiles and pulse height distributions in some regions of interest (ROIs) indicated lower photoelectron collection at the peripheral region than the central region. However, this can be improved by accurate gain adjustment.

Assuming future applications of the PMT having a large useful area such as the 256ch FP-PMT, we looked at an easier way to construct an array with many crystal elements. The way introduced in Fig. 6(c) using multilayer polymer mirrors as the reflector has possibility of application to detectors containing very small crystals or detectors in complicated structures of crystals and reflector arrangement. It should save much time and labor for quantity detector production for whole PET systems.

Publications:

1) Inadama, N., Murayama, H., Omura, T., *et al.*: *IEEE Trans. Nucl. Sci.*, 49, 629-633, 2002.
2) Inadama, N., Murayama, H., Watanabe, M., *et al.*: *2002 IEEE NSS & MIC Conf. Rec.*, M6-27, 2002.

Figure caption:

Fig. 6. (a) Schematic of a 256ch FP-PMT. (b) Resultant 2-dimensional position histogram of a 16 x 16 GSO crystal array with a 256ch FP-PMT. (c) Proposed way to pack many crystal elements into an array.

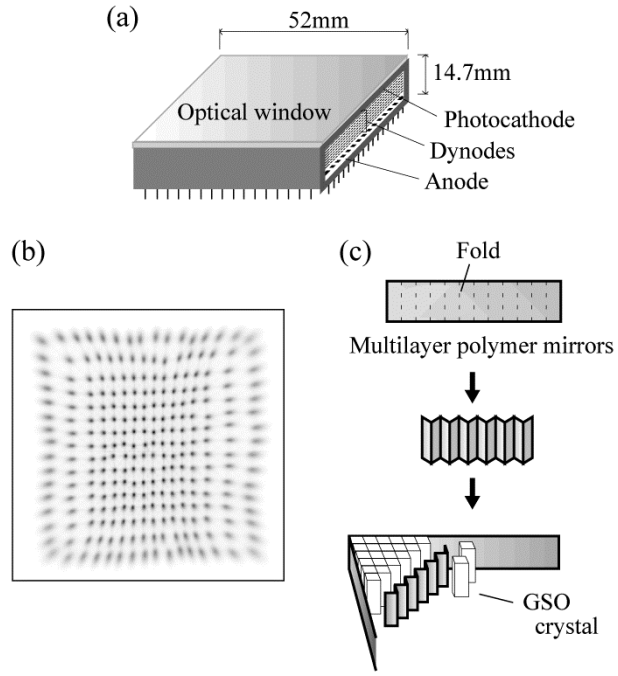

Fig. 6

6. The Polybinary Calibration Method for Radiotherapy Treatment Planning CT Systems

Nobuyuki Kanematsu, Naruhiro Matsufuji, Ryosuke Kohno, Shinichi Minohara and Tatsuaki Kanai

Keywords: *radiotherapy, treatment planning, computed tomography, calibration, quality assurance*

A method to establish the relationship between CT number and effective density for therapeutic radiations is proposed. We approximated body tissues to mixtures of muscle, air, fat, and bone. Consequently, the relationship could be calibrated with just a CT scan of their substitutes, for which we chose water, air, ethanol, and potassium phosphate solution, respectively. With simple and specific corrections for non-equivalencies of the substitutes, the calibration accuracy of 1% was expected to be achieved. We tested the calibration method with some biological materials. Fig. 7 shows an example of the calibration of a CT scanner for the relationship between relative attenuation coefficient (CT number) and stopping power of heavy charged particles (effective density). The calibrated polyline agrees well with the numerically calculated human tissue responses and with the tested biological samples.

The proposed CT calibration method offers accuracy, simplicity, and specificity, which are required for a standard in radiotherapy treatment planning, in particular, with heavy charged particles. Subsequent efforts to establish a standard in quality assurance of CT systems for radiotherapy treatment planning are being made, based on the proposed method.

Publications:

1) Kanematsu, N., Matsufuji, N., Kohno, R., Minohara, S. and Kanai, T.: *Phys. Med. Biol.*, 48, 1053-1064, 2003.

2) Kanematsu, N.: *Jpn. J. Med. Phys.*, 23 (2) (in press), 2003 (in Japanese).

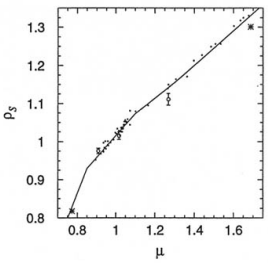

Fig. 7. Test of the polybinary calibration for fine-ground biological materials, where the solid line shows the relationship between relative attenuation coefficient □ and relative stopping power □$_S$ calibrated for body tissues. The circle markers with error bars show the observed responses for fatty meat, lean meat, and hydroxyapatite-added meat, the asterisks show the responses of ethanol and 40% potassium phosphate solution and the dots show the ICRU body tissue responses predicted by the stoichiometric calibration.

7. Electron Density Measurement with Dual-Energy X-ray Computed Tomography

Masami Torikoshi, Takanori Tsunoo, Makoto Sasaki, Masahiro Endo, Yutaka Noda, and Kazuyuki Hyodo[*]([*]High Energy Accelerator Research Organization, Tsukuba-shi, Japan)

Keywords: *CT, electron density, synchrotron radiation, monochromatic x-ray, dual-energy*

Monochromatic x-ray computed tomography (CT) at two different energies provides information about electron density of human tissue without ambiguity due to the beam hardening effect. This information makes the treatment planning for heavy-ion radiotherapy more accurate. We started a feasibility study of the dual energy x-ray CT by using synchrotron radiation. We proved that the electron density was directly measured by dual-energy x-ray CT using monochromatic x-rays with accuracy of 1% or less on average using the one-dimensional scanning system developed in 2001.

When using two monochromatic x-rays individually in the CT scanning, it takes about 15 minutes or even longer to switch the x-ray energy from one to the

other. In the case of clinical practice, this may require an examinee to keep his/her attitude immobile for a while. We have proposed a method to solve this problem that uses two x-rays of different energy simultaneously instead of using monochromatic x-rays individually. Using two mixed x-ray beams with different mixing ratios, transmitted x-rays through an object are described as follows,

$$I_A = I_{1A}\exp\left(-\int \mu(E_1,x)dx\right) + I_{2A}\exp\left(-\int \mu(E_2,x)dx\right)$$
$$I_B = I_{1B}\exp\left(-\int \mu(E_1,x)dx\right) + I_{2B}\exp\left(-\int \mu(E_2,x)dx\right), \quad (1)$$

where indices A and B denote mixing ratios. I_1 and I_2 are incident x-ray intensities of energy E_1 and E_2, respectively. The incident x-ray intensities can be easily measured in a combination of dosimetry and pulse height analysis. Solving the simultaneous equations yields exponential functions of integration of the linear attenuation coefficient. In CT reconstruction algorithms, x-ray attenuation coefficients of $\mu(E_1)$ and $\mu(E_2)$ can be obtained. Then, we obtain the electron density and the effective atomic number employing the algorithm we developed.

We carried out experiments at the beamline of NE5A of the light source facility AR at KEK in Tsukuba. The beamline was equipped with a double crystal monochromator of a silicon crystal with (220) reflection plane. When tuning the angle of the Si(220) crystal plane to the Bragg reflection angle of 40 keV, the 80 keV x-ray beam was reflected simultaneously with the 40keV x-ray beam. A metallic filter could easily change the mixing ratio of the two x-ray beams; that is $I_{1A}/I_{2A} \neq I_{1B}/I_{2B}$ where the indices of A and B denote the different filters. For each projection in CT scanning, two transmission images were taken while alternatively inserting filters one after the other into the beamline. In the experiments, a 1 mm thick copper plate was used as one filter and the other filter was "empty". While the "empty" filter gave the ratio of 40 keV to 80 keV of 1 : 0.04, the copper filter gave a ratio of about 1 : 2.5. The translate-rotate scanning mode CT system (1-D CT system) was used. An ionization chamber was upstream from the rotating table to count the number of incident photons. The rotating table on which a sample was set was moved horizontally in a step of 1 mm. Data were taken every step by being exposed to the x-ray beam for a few hundred ms. At the end of the stroke, the object was rotated by 0.8°. This was repeated until the rotation angle was 180°.

Several samples were used (1) tissue equivalent phantoms: soft tissue, adipose tissue, cartilage bone, compact bone and lung tissue; (2) solutions of K_2HPO_4 in water; (3) sausage; (4) boiled egg; and (5) graphite. In order to verify the electron densities measured with the dual energy x-ray CT, we compared them (i) with the theoretical values for the liquid samples, and (ii) with the reference values which were the electron densities of other samples derived from carbon ranges in water. The electron densities of the liquid samples agree with the theoretical values within about 2 to 3 %. Those of the other samples agree with the reference values within about 1 to 2 %. In the dual-energy x-ray CT using mixed x-rays, the measured electron density is less precise than density measured with the dual-energy x-ray CT individually using monochromatic x-rays. In the 1-D CT system, it took typically about ten hours to scan from 0° to 180°. During the scanning, the mixing ratio of the 40 keV and 80 keV beams varies according to deformation of the crystals of the monochromator due to heat load. The variation in the mixing ratio causes an error in the solution of the simultaneous equations (1). However, this will not be a crucial problem in the case of the 2-D CT system in which CT scanning is carried out in a few minutes.

We conclude that:

(1) The new scenario for dual-energy x-ray CT using two x-ray energies simultaneously is valid to measure the electron density even though the accuracy is less than that by the dual-energy x-ray CT individually using monochromatic x-rays.

(2) The 2-D CT scanning system is likely to improve the accuracy of measurement.

Publications:
1) M. Torikoshi, T. Tsunoo, M. Endo, K. Noda, M. Kumada, S. Yamada, F. Soga and K. Hyodo: *J. Biomed. Opt.* 6, pp.371-377, 2001.
2) M. Torikoshi, T. Tsunoo, M. Sasaki, M. Endo, Y. Noda, Y .Ohno, T. Kohno, K. Hyodo, K. Uesugi and N. Yagi: *Phys. Med. Biol.* 48, pp673-685, 2003.
3) T. Tsunoo, M. Torikoshi, M. Sasaki, N. Yagi, and K. Uesugi: *IEEE Trans. on Nucl. Sci.*, to be published.

8. Design and Performance of a Non-Destructive Beam Profile Monitor Utilizing Charge

Division Method at HIMAC
Toshihiro Honma, Daisuke Ohsawa [1], Koji Noda , Takashi Iwashima [2], Hiroyuki Ogawa [2], Yoshinobu Sano [2], Eiichi Takada and Satoru Yamada

([1]Radioisotope Research Center, Kyoto University; [2]Accelerator Engineering Corporation)

Keywords: *beam profile monitor, non-destructive, residual-gas, ion, MCP, charge-division.*

A non-destructive ionization beam profile monitor has been developed to measure a very narrow beam size, which is expected to be 1 mm (FWHM) or less. The monitor utilizes tandem-type micro-channel plates (MCP) and a resistive anode for the detector, and it is operated by the charge-division method. Two monitor units for measuring the transverse horizontal and vertical density distributions of a circulating beam were installed in the HIMAC synchrotron. The monitor has been used for an electron-cooling experiment with a spatial resolution of less than 0.38 mm, as well as for studies of beam dynamics under routine operation in the synchrotron. Fig. 8 shows a typical example of consecutive variations of the horizontal beam profiles at different times just after injection in an experiment concerned with cooling time measurement. The profiles were measured with an acquisition time of 0.3s during one injection-cycle with an $^{40}Ar^{18+}$ beam of 6 MeV/u. As can be seen from the figure, the measured beam size σ_M (given in r.m.s.) reached an equilibrium size of 0.68 mm at about 3s after injection. The measured beam size, however, included some incidental lateral deviations. Those independent sources are added to the true beam size σ_B as follows:

$$(\sigma_M)2 = (\sigma_B)2 + (\sigma_I)2 + (\sigma_E)2 + (\sigma_N)2 .$$

In this case σ_I is the intrinsic error exists because of an electric field created by the circulating beam itself, the thermal motion of the residual gas molecules, and the resistive noise generated by the detector, itself; σ_E is an external electric field distortion which exists in the work area; and σ_N is the error caused by the noise mixed on the readout circuit.

The error caused by the thermal motion of the residual gas ion was calculated by a simple equation and found to be 0.07 mm with the mean kinetic energy of the residual gas ions being 13 meV for one degree of freedom at room temperature. For the noise mixed in the event signal on the readout circuit, in our case, the noise-to-signal ratio was reduced to less than 0.35 %; the resolution limit of the readout circuit was σ_N = 0.23 mm, where the total noise level was observed to be less than 30 mV_{p-p} with a signal pulse height of around 4 V. The errors caused by the other sources were estimated to be negligibly small. On the whole, the true beam size of σ_B in the measurement was found to be 0.56 mm. The spatial resolution of the monitor was obtained as

less than 0.38 mm for the horizontal direction, represented by as standard deviation of 1σ . Consequently, the emittance-reduction ratio was supposed to be less than $1/270$ compared to that of the injection beam, due to electron cooling.

Publications:

1) Noda, K., Honma, T., Murakami, T., Takada, E., Yamada, S., Fukushima,T., Izumiya, H., Ogawa, H., Sano, Y., Furukawa, T.: *Proc. 7th Epac*, Vienna, June 2000, 1259-1261.

2) Honma, T., Ogawa, H.Y., Sano, Y., Noda, K., Takada, E., Yamada, S.: *Nucl. Instr. and Meth. A* 459, 390-397. 2001.

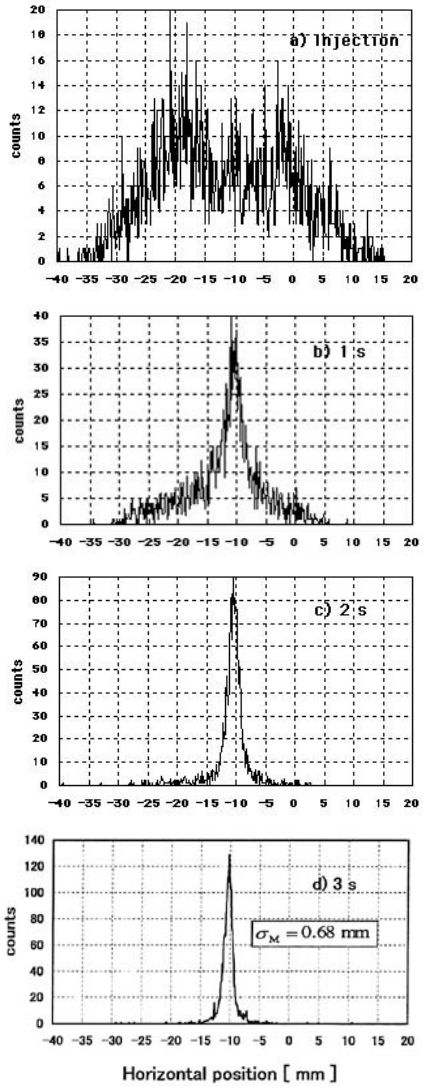

Fig.8. Measured horizontal beam profiles of a cooled $^{40}Ar^{18+}$ beam of 6 MeV/u at different times after injection.

9. Charge Fraction of 6.0 MeV/n Heavy Ions Measured with a Carbon Foil

Yukio Sato, Atsushi Kitagawa, Masayuki Muramatsu, Takeshi Murakami and Satoru Yamada

Keywords: *HIMAC injector linac, carbon foil, heavy ions, charge fraction, equilibrium* condition

We precisely measured the exit charge fraction of 6.0 MeV/n heavy ions (C, Ne, Si, Ar, Fe, and Cu) for carbon foil thicknesses between 10 and 350 μg/cm^2 at the NIRS-HIMAC injector linac facility. In this energy region, few data concerning the charge fraction have been reported yet, particularly for ions heavier than Ne; data are necessary not only to design and operate accelerators, but also to improve model calculations for heavy-ion beam interactions in solids. Accelerators usually require the highest charge states (which occur at the equilibrium charge state distribution) with the thinnest foils, which minimize the energy loss, and multiple scattering and energy straggling. Fig.9 shows the measured charge fractions at the equilibrium charge state distribution. For example for Ar, we found that the fraction of Ar^{18+} ions could be improved to 33% at 320 μg/cm^2 from the previous value of ~15% at 100 μg/cm^2.

An attempt was made to compare our results to the calculations by the computer program ETACHA (Rozet, J.P et al. Nucl. Instrum. and Meth. B107, 67 (2000)). Concerning the fully-stripped fractions, the calculated values were generally larger than our results, except for C; the differences became large as the atomic number (z) of incident ions increased. For C to Ar, the calculations were not very far from our data, and the model calculation seemed basically correct, though the precision in the cross sections used was somewhat unsatisfactory. For Fe and Cu, however, the calculations did not agree with our results. For example, the maximum charge fraction was 47.23% for Fe^{24+} in the calculation, while it was 37.53% for Fe^{23+} in our data; the charge state distribution was considerably shifted to

a higher charge state in the calculation. A similar tendency could also be clearly seen for the case of Cu. The present calculations by ETACHA could not be used for such heavy atoms.

For C to Ar ($6 \leq z \leq 18$), the thickness of the equilibrium charge state increased monotonically from 21.5 μg/cm^2 to 346 μg/cm^2 with increasing atomic number, z, while it rapidly decreased to 121 and 143 μg/cm^2 for Fe and Cu (z=26 and 29). In the latter two cases, the equilibrium condition should be determined primarily by the behavior (loss/capture) of the L- and outer-shell electrons. Since their interaction cross sections are much larger than those of the K-shell electrons in the 6.0 MeV/n region, charge state equilibrium is obtained at a small thickness. In the rest frame of the projectile, the velocity of a 6.0 MeV/n projectile corresponds to an electron energy of 3.26 keV. The binding energies of K-shell electrons are 9.0 keV for Fe and 11.2 keV for Cu, respectively; the energy of 3.26 keV is too small to effectively remove the K-shell electrons.

Publications:

1) Sato, Y., Kitagawa, A., Muramatsu, M., Murakami, T., Yamada, S., Kobayashi, C., Kageyama,
Y., Miyoshi, T., Ogawa, H., Nakabushi, H., Fujimoto, T., Miyata T. and Sano, Y.: *Nucl. Instrum. and Meth*. B201, 571-580, 2003.

2) Miyoshi, T., Kobayashi, C., Ogawa, H., Nakabushi, H., Fujimoto, T., Miyata, T., Kageyama, Y.,
Sano, Y., Kitagawa, A., Muramatsu, M., Murakami, T. and Sato, Y.; *Proc. 21st Int. Conf. on Linac*, Gyeongju in Korea, Aug. in 2002.

Figure caption

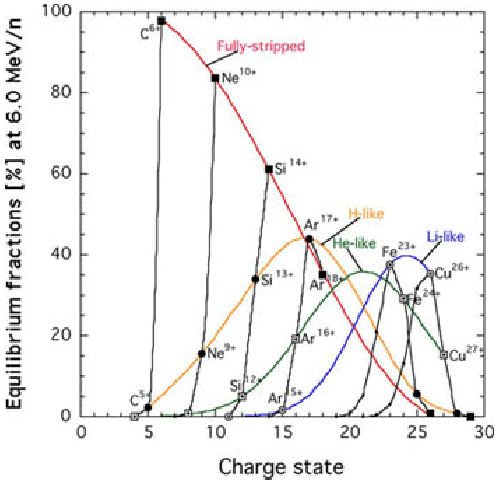

Fig.9. Exit charge fractions at the equilibrium condition.

10. Characteristics of Fast Beam Switching for Spot Scanning

Takuji Furukawa, Koji Noda, Eriko Urakabe, Masayuki Muramatsu, Shinji Shibuya, Mitsutaka Kanazawa, Eiichi Takada and Satoru Yamada

Keywords: *RF-knockout slow extraction, synchrotron, heavy ion therapy, dose management, spot scanning*

An irradiation method for spot scanning has been developed in order to provide accurate irradiation even for an irregular target shape. In spot scanning irradiation, the beam is turned off while the beam position is shifted to the next spot for precise dose management. For this precise dose management in spot scanning, we investigated the characteristics of fast beam switching, which can switch a beam many times during a single flattop by turning on/off both the transverse and longitudinal RF fields. Owing to the fast beam cut-off method, the cut-off time, for each turning off, was kept at around 50 μs. On the other hand, the momentum spread of the extracted beam changes with an increase of the switching number. It was estimated that the momentum spread of the extracted beam changed from 0.02% to 0.1% at σ after switching fifty times.

This change is not very large for practical use, because a ridge filter provides a wider momentum spread of around 0.3-0.5% at σ. In order to maintain the beam size, an achromatic condition was realized. We experimentally verified that the beam size growth rate was suppressed within 10% even after switching a hundred times. The fluctuation of the lateral dose distribution could be suppressed within ±2% in the HIMAC spot scanning system, even under the beam-size fluctuation within 10%. As shown in Fig. 10, in addition, the advanced RF-knockout method makes it possible to supply a smooth spill even under a small chromaticity of –1.

The advanced RF-knockout extraction method and the intensity control method combining with the fast beam switching technique will give a method to play an important role in the precise irradiation with spot scanning.

Publication:
Furukawa T., Noda K., Urakabe E., Muramatsu M., Kanazawa M. and Maeda K.: *Nucl. Instrum. Meth. A* 503 485-495, 2003.

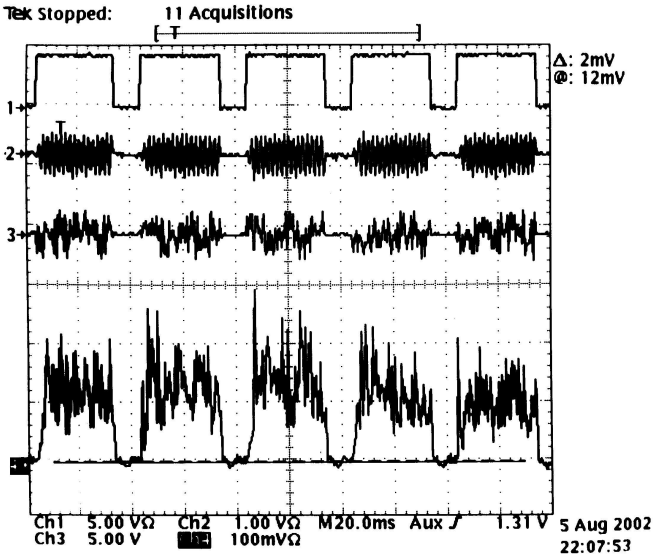

Fig. 10. Spill structure in this switching method with the advanced RF-knockout method. From the bottom, the spill structure, the transverse RF field, the longitudinal RF field and the beam gate signal.

11. Analytical Reconstruction Algorithm for Compton Cameras Applicable to Lower Gamma Energy

Masahiko Hirasawa and Takehiro Tomitani

Keywors: *Compton camera, image reconstruction, angular uncertainty, compensation*

Reconstruction methods of radiation source distribution images from scattering-projection data obtained by Compton cameras can be categorized into two classes: iterative methods and analytical methods. The former were used until analytical solutions appeared. R. Basko *et al.* (1998) presented an analytical algorithm in terms of series expansion with the complex supherical harmonics system. The series expansion gives cone-surface back-projection values: integrated radioactivity on the cone-surface. However, this algorithm requires numerical calculations of complex spherical harmonics, which are associated with computational difficulty at zenith edges of their domain. L.C. Parra (2000) also presented an analytical algorithm based on series expansion with respect to the complex spherical harmonics system. In his algorithm, the series expansion leads to direction-line back-projection values: integrated radioactivity on the direction lines, which contain more infomation than the cone-surface back-projection values. In addition, the complex spherical harmonics are replaced by the singurality-free Legendre functions with the aid of the addition theorem of complex spherical harmonics. However, since these algorithms require scattering-projection data by the Compton scattering in all directions, the rear detector must entirely surround the front detector.

In 2002, we presented an improved algorithm for Parra's algorithm, with which the direction-line back-projection values are derived only from the scattering-projection data with limited Compton scattering angles, ω, of ω_1 to ω_2. This practical

algorithm holds for the ideal scattering-projection data. Real data include scattering angular uncertainties due to the finite energy resolution of the front detector and the Doppler effect from moving electrons. Then in 2003, we have extended the idealized algorithm to compensate for the uncertainties. The compensated algorithm is as follows:

$$\alpha_n(\cos\omega) \equiv \int_{-1}^{1} d\langle \boldsymbol{s},\boldsymbol{t}\rangle \, Br(\boldsymbol{s},\boldsymbol{t};\omega)\, P_n(\langle \boldsymbol{s},\boldsymbol{t}\rangle), \tag{1}$$

$$H_n \equiv \int_{\cos\omega_2}^{\cos\omega_1} d\cos\omega \; h(\cos\omega)\, \alpha_n(\cos\omega)^2 , \tag{2}$$

and

$$f(\boldsymbol{s}) \approx \int_{\cos\omega_2}^{\cos\omega_1} d\cos\omega \int_S d\Omega_t \sum_{n=0}^{n_{max}} \frac{2n+1}{4\pi} \frac{\alpha_n(\cos\omega)}{H_n} P_n(\langle \boldsymbol{t},\boldsymbol{s}\rangle)\, g(\boldsymbol{t};\omega), \tag{3}$$

where P_n and h denote the Legendre function of n-th degree and the normalized Klein-Nishina formula, respectively, $g(\boldsymbol{t};\ \omega)$ represents the scattering-projection datum in a scattered gamma-ray direction vector, $\boldsymbol{t}$, and with a measured scattering angle, ω, and $f(\boldsymbol{s})$ denotes the direction-line back-projection value with the incident gamma-ray direction vector, $\boldsymbol{s}$. $\langle \boldsymbol{s},\boldsymbol{t}\rangle$ is inner product of $\boldsymbol{s}$ and $\boldsymbol{t}$, and Br describes the scattering angle uncertainty defined by

$$Br(\boldsymbol{s},\boldsymbol{t};\omega) \equiv \frac{1}{\sqrt{2\pi}\sigma \sin\omega} \exp\left\{ -\frac{(\langle \boldsymbol{s},\boldsymbol{t}\rangle - \cos\omega)^2}{2(\sigma \sin\omega)^2} \right\}, \tag{4}$$

where σ is the standard deviation of the stochastic distribution on the scattering angle uncertainty.

Fig. 11 shows an example reconstruction simulation with the idealized (pre-compensation) and compensated algorithms. The utilized scattering-projection data include scattering angle uncertainties with σ of 3.8 through 2.0 deg when the Compton scattering angle increases from 10 to 30 deg. These uncertainties degrade spatial resolution of the reconstructed image with the algorithm without compensation (b), but the resolution is recovered with the algorithm with compensation (c). Angular uncertainties are pronounced at low gamma-ray energy. The analytical algorithm with compensation can almost completely recover the spatial resolution even at low energy. Therefore the analytical algorithm with compensation extends the applicability of Compton cameras to lower energy gamma-ray imaging.

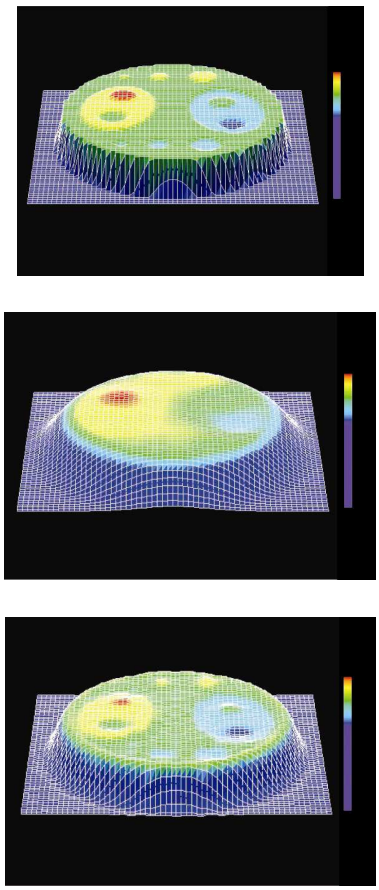

(a) Original phantom (b) Reconstruction without compensation (c) Reconstruction with compensation

Fig. 11 Reconstruction simulation using scattering-projection data with angular uncertainties

Publications:

1) Tomitani, T. and Hirasawa, M.: *Phys. Med. Biol.*, **47**, 2129-2145, 2002.
2) Hirasawa, M. and Tomitani, T.: *Phys. Med. Biol.*, **48**, 1009-1026, 2003.

12. Single Particle Irradiation System to Cell (SPICE) in the ElectrostaticAccelerator Building

Hitoshi Imaseki, Hiroshi Yamaguchi, Yukio Sato, Nakahiro Yasuda, Tsuyoshi Hamano, Yoshiya Furusawa, Masao Suzuki, Takehiro Ishikawa, Teiji Mori, Kenichi Matsumoto, Teruaki Konishi, Masae Yukawa and Fuminori Soga

Keywords*: ionizing, particle, microbeam, radiation biology, radiation protection*

Tandetron (HVEE, High Voltage Engineering Europe Ltd.) was installed for PIXE (Proton Induced X-rays Emission) analysis in 1999 in the NIRS Electrostatic Accelerator Building.

A vertical beam port driven from the horizontal main port by a 90°magnet, as a whole, is installed in a cradle which is hung on a rigid frame structure. In the end of the vertical beam port, a focusing triplet Q-magnet, an automated x-y stage of cell dishes and a video microscope are assembled as a unit solid structure. This special structure of the beam port will ensure the system is relatively insensitive to unavoidable environmental vibrations. At a height of 4.6m from the floor, a platform for a workbench is built on the frame structure with spiral steps to access the platform. This platform is a workspace for the operator when manipulating the modules such as the triplet Q-magnet, beam monitoring, the controller of the cell dish stage, the particle detector, and the PC and electronics, and for users when exchanging sample dishes. The main structure of SPICE is shown in Fig.12(a).

The horizontal beam port is located at a height of 125 cm from the floor. Two frame structures (outer and inner) are built strong enough to support (1) the platform at a height of 460 cm on which the irradiation workroom is built, and (2) the cradle of the vertical beam port for SPICE. The distance between the object slit and focus point is designed as 320 cm to allow focus rate by the triplet Q-magnet from 1/7 to 1/10. Accurate adjustment of width of the object slit in a range of less than 10 μm may achieve a beam spot size as small as 2 μm at the focus point. From the object slit to the upper end, the microscope stage is constructed in a cradle as a solid unit. The irradiation workroom is a working space to which users' access by steps. The electrostatic deflector (not shown in this figure) is located just before or upper stream of the bending magnet.

Effort has been made to reduce irradiation time to as short as possible from data acquisition to repeated irradiations. At present our estimation as best performance is around 2000 cells / h.

Figure caption

Fig. 12. Schematic diagram (a) and a photograph (b) of the SPICE facility

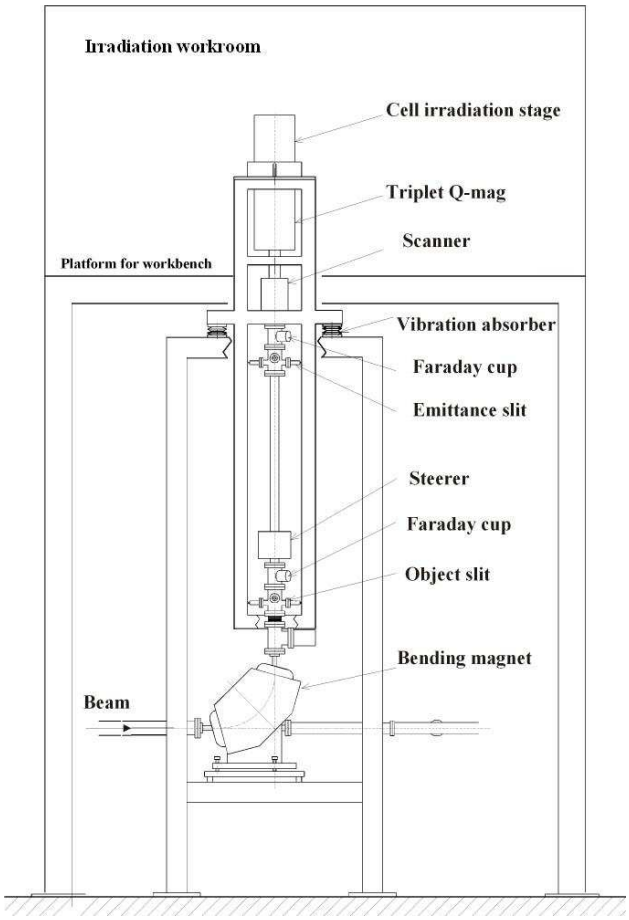

13. Responses of Two Types of Gamma Ray Directional Detectors

oshiyuki Shirakawa

Keywords: *gamma ray, NaI(Tl) scintillator, BGO scintollator, CsI(Tl) scintillator, photomultiplier(PMT), photopeak, direction, energy*

Two types of gamma ray detectors, which positively show directional dependence on incoming gamma rays, have been developed to identify the location of radioactive materials such as lost radiation sources and radioactive contaminations in a field by determining simultaneously directions and energies of incoming gamma rays. In the tandem detector (Fig.13, (a)), a cylindrical NaI(Tl), the same size BGO scintillator and a fitted photomultiplier tube (PMT) are combined optically in this order. In the parallel detector (Fig.13, (b)), a half cylindrical NaI(Tl) is combined, parallel to the same shape CsI(Tl) scintillator. Both scintillators are vertically connected to the PMT. Since the passing lengths of gamma rays in each scintillator will change with directions of incoming gamma rays, the directions can be determined by counting changed photopeak counts in each spectrum obtained from each scintillator and by calculating the ratio of photopeak counts. This procedure for the tandem detector is given by the formula

R = peak counts by BGO / peak counts by NaI(Tl) = f (θ) (1)

where θ is a incoming direction from 0 to 90 deg. The same procedure for the parallel detector is given by a formula of

R = peak counts by CsI(Tl) / peak counts by NaI(Tl) = F(θ) (2)

where θ is a incoming direction from 0 to 180 deg.

Using both detectors, the following experiments were carried out for purposes of 1) confirmation of the measurement principle and 2) verification of the performance. A ^{137}Cs source of 3.7MBq was placed 100cm in front of the detector (θ =0). Incoming gamma rays were counted for 60-300 s and the counting ratio was calculated from the spectrum. The source was moved by 10 deg intervals around the for detector until it reached 90 deg (θ =90) or 180 deg (θ =180) . From the results of the experiments, it was proven that the ratio, f (θ) was changed approximately from 0.5 to 5.0 when the direction θ changed from 0 to 90 deg. The ratio F(θ) was between about 0.5 and 4.0 in the range of 0 and 180 deg. This meant that the incoming direction could be determined when the (photopeak) counting ratio was given. At the same time, it was confirmed that the energy characteristics of both detectors were the same as those of an NaI(Tl), a BGO, and a CsI(Tl) detector.

As a result, it has been shown that both detectors had a possibility of identifying the radioactive materials in a field by determining simultaneously the incoming directions and the energies of gamma rays.

Publications:

1) Shirakawa, Y.: *Radioisotopes*, 52, 111-117, 2003.

2) Shirakawa, Y.: *Radioisotopes*, 50, 117-122, 2001.
3) Shirakawa, Y.: *JASP*, *Radiation Science*, 26, 67-73, 2001.

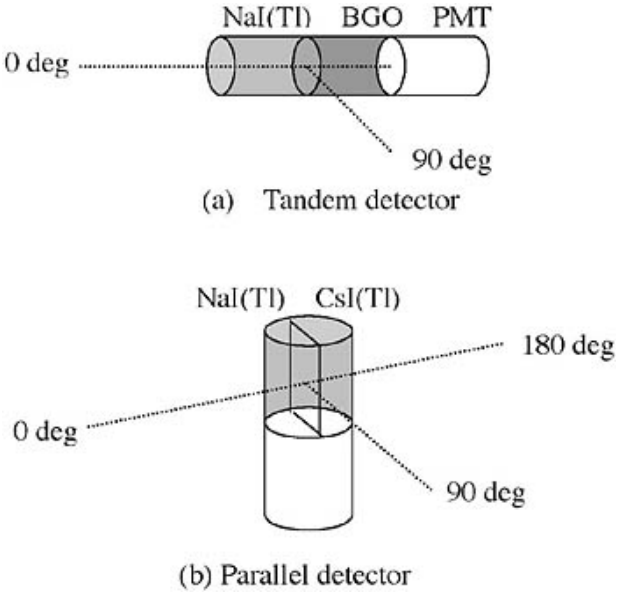

Fig.13. Structures of two types of directional detectors.

CHEMISTRY

14. Production of Semiquinone by Oxidation of *para*Monosubstituted Phenols with Singlet Oxygen

Jun-ichi Ueda, Chiho Nishizawa, Keizo Takeshita and Toshihiko Ozawa

Keywords: *DMPO, singlet oxygen, semiquinone, phenolic compounds, UVA, HPLC*

Reactive oxygen species (ROS) involving singlet oxygen ($^1O_2$) have been implicated both in the aging process and in degenerative disease. $^1O_2$ is produced in biological systems by lipid peroxidation and by enzyme reactions involving lactoperoxidase and chloroperoxidase. $^1O_2$ is also produced through the interaction of the ultraviolet-A component (UVA) and visible light of sunlight with endogenous photosensitizers such as porphyrins and flavins in the skin.

Phenolic compounds are widely used for the production of pharmaceuticals as well as disinfection, cosmetic and food flavoring goods, and the skin is inevitably exposed to these phenolic compounds. Then, an investigation was done by electron spin resonance (ESR) spectroscopy whether phenolic compounds can react with $^1O_2$ to produce the oxidized compounds through the generation of free radical as an intermediate. The phenolic compounds examined were phenol, *o*-methoxyphenol, *p*-cresol, *p*-methoxyphenol, *p*-hydroxyphenylacetic acid, and *p*-hydroxybenzoic acid.

A five-line ESR spectrum was obtained during irradiation with UVA-visible light (> 330 nm) in an air-saturated solution containing 1 mM phenol and 25 M hematoporphyrin (HP) and assigned to semiquinone (SQ). The signal intensity of SQ was diminished by the addition of a singlet oxygen quencher NaN_3, suggesting the participation of $^1O_2$ in the production of SQ. The five-line signal was also observed in other *para*-monosubstitued phenolic compounds such as *p*-methoxyphenol and *p*-hydroxybenzoic acid, but not in *p*-cresol, *p*-hydroxyphenylacetic acid and *o*-methoxyphenol.

The relationship between the signal intensity of SQ and the irradiation time was investigated. In the case of phenol and *p*-hydroxybenzoic acid, the sginal intensity increased gradually with the irradiation time. On the other hand, in *p*-methoxyphenol the signal intensity immediately reached the maximum, although it was the smallest value among the three compounds. These results suggest the formation mechanism of SQ in phenol or *p*-hydroxybenzoic acid differs from that in *p*-methoxyphenol.

The production of hydroquinone (HQ) and benzoquinone (BQ) during the reaction of phenol with $^1O_2$ was confirmed using high performance liquid chromatography (HPLC)-electrochemical detector (ECD). The time course of the yield of BQ and HQ from the reaction of phenol or *p*-hydroxybenzoic acid with $^1O_2$ indicated that BQ is the primary, and HQ the secondary, oxidation product. On the other hand, the increase of equivalent yield of BQ and HQ in *p*-methoxyphenol toward the irradiation time was observed, suggesting that SQ was at first produced, following the production of BQ and HQ by dismutation of SQ. Thus, it is speculated at present that phenol or *p*-hydroxybenzoic acid react with $^1O_2$ to form BQ, and the resulting BQ is reduced with HP anion radical to generate SQ. On the other hand, *p*-methoxyphenol reacts with $^1O_2$ to form the endoperoxide, and the resulting endoperoxide ultimately undergoes a one-electron reduction by *p*-methoxyphenol to generate SQ.

These results indicate that SQ or BQ are conducted by the oxidation of *para*-monosubstituted phenolic compounds and penetrate into skin with $^1O_2$. The resulting SQ may furthermore lead to the formation of O_2^-,

hydrogen peroxide, and ultimately the hydroxyl radical. Production of ROS can cause aging and carcinogenesis through severe oxidative stress within cells. On the other hand, benzoquinone toxicity develops through the depletion of intracellular biological reductant glutathione.

15. DNA Cleavage via Superoxide Anion Formed in Photoinduced Electron Transfer from NADH to -Cyclodextrin-Bicapped C_{60} in an Oxygen-Saturated Aqueous Solution

Ikuo Nakanishi, Toshihiko Ozawa and Nobuo Ikota

Keywords: *fullerene, DNA cleavage, photodynamic therapy, NADH, cyclodextrin, electron transfer, reactive oxygen species*

F ullerenes, such as C_{60} and C_{70}, are sensitive to light at wavelengths longer than 500 nm and thus expected to be an effective photodynamic therapy agent, since bodily tissues are most transparent in this region of wavelengths. Water-soluble -cyclodextrin-bicapped C_{60} (C_{60}/ -CyD) shows an efficient DNA-cleaving activity in the presence of NADH (dihydronicotinamide adenine dinucleotide) in an O_2-saturated aqueous solution under visible light irradiation. No DNA cleavage has been observed without NADH under otherwise the same experimental conditions, although singlet oxygen ($^1O_2$) has been detected by the ESR spin-trapping of the C_{60}/ -CyD-O_2 system. This indicates that neither the triplet excited state of C_{60}/ -CyD ($^3C_{60}$*/ -CyD) nor $^1O_2$ produced via an energy transfer from $^3C_{60}$*/ -CyD to O_2 is an actual reactive species, which is responsible for the DNA damage under the present experimental conditions. In the presence of NADH, photoinduced electron transfer from NADH to $^3C_{60}$*/ -CyD occurs to yield two equivalents of the radical anion ($C_{60}^{\bullet-}$/ -CyD), which exhibits its characteristic NIR band at 1080 nm. The dynamics of the photoinduced electron transfer has been examined by monitoring decay of the triplet–triplet absorption band at 740 nm and concomitant rise of the NIR absorption band at 1080 nm due to $C_{60}^{\bullet-}$/ -CyD with the use of laser flash photolysis for the C_{60}/ -CyD-NADH system. In the presence of O_2, $C_{60}^{\bullet-}$/ -CyD disappears via the electron transfer to O_2 to produce $O_2^{\bullet-}$. An electron transfer from NADH to $^1O_2$ also occurs to produce $O_2^{\bullet-}$. The formation of $O_2^{\bullet-}$ has been confirmed by the spin trapping with DEPMPO (5-diethoxyphosphoryl-5-methyl-1-pyrroline-*N*-oxide), which is an efficient $O_2^{\bullet-}$-trapping agent. The reorganization energy for the reduction of O_2 to $O_2^{\bullet-}$ is evaluated as 43.4 kcal mol^{-1}, which agrees with the literature value determined directly for the self exchange between $^{36}O_2^{\bullet-}$ and $^{32}O_2$. This indicates that the electron transfer from $C_{60}^{\bullet-}$/ -CyD to O_2 proceeds via an outer-sphere pathway. The $O_2^{\bullet-}$ thus produced gives H_2O_2, ultimately yielding hydroxyl radical, which is shown to be the actual DNA-cleaving reagent in this study.

Publications:

1) Nakanishi, I., F ukuzumi, S., Konishi, T., Ohkubo, K., F uj itsuka, M., Ito, O., Miyata, N. *J. Phys. Chem. B* **106**, 2372–2380, 2002.
2) Nakanishi, I., Ohkubo, K., F uj ita, S., F ukuzumi, S., Konishi, T., F uj itsuka, M., Ito, O., Miyata, N. *J. Chem. Soc., Perkin Trans. 2* **2002**, 1829–1833.

16. Effects of Metal Ions Distinguishing between One-Step Hydrogen- and Electron-Transfer Mechanisms for the Radical-Scavenging Reaction of (+)-Catechin and Vitamin E Model

Ikuo Nakanishi, Toshihiko Ozawa and Nobuo Ikota

Keywords: *antioxidant, flavonoid, catechin, vitamin E, hydrogen transfer, electron transfer*

Catechins contained in green tea are a class of bioflavonoids that show a significant antioxidative activity. Vitamin E (-tocopherol, -TOH) is also a very effective biological antioxidant that can scavenge peroxyl radicals in biological membranes, preventing oxidative inj ury by toxic and carcinogenic chemicals. However, little is known about the mechanism of antioxidative radical-scavenging reaction, in which a hydrogen transfer from the phenolic hydroxyl group of catechin or -TOH to radical species occurs to produce the corresponding phenoxyl radical and the hydrogenated radical species. There are two possibilities in the mechanism of hydrogen-transfer reactions from phenolic anitioxidants to radical species, i.e., a one-step hydrogen atom transfer or electron transfer followed by proton transfer. It has previously been demonstrated that the effect of Mg^{2+} on the hydrogen-transfer rates from NADH (dihydronicotinamide adenine dinucleotide) analogues to aminoxyl or nitrogen radicals provides a reliable criterion for distinguishing between the one-step hydrogen atom transfer and the electron-transfer mechanisms.

We report herein the effect of metal ions, such as Mg^{2+} and Sc^{3+}, on the rates of hydrogen transfer from (+)-catechin (**1**) or vitamin E model, 2,2,5,7,8-pentamethyl-6-chromanol (**2**), to radical species, such as 2,2-di(4-*tert*-octylphenyl)-1-picrylhydrazyl ($DPPH^{\bullet}$), galvinoxyl ($G^{\bullet}$), and cumylperoxyl radicals. The detailed kinetic studies provide valuable mechanistic insight into the antioxidative reactions of natural antioxidants: whether the reaction between natural antioxidants and radical species proceeds via one-step hydrogen atom transfer or via electron transfer.

A kinetic study of a hydrogen-transfer reaction from **1** to $G^{\bullet}$ has been performed using UV-vis spectroscopy in the presence of $Mg(ClO_4)_2$ in deaerated acetonitrile at 29 8 K. The rate constants of hydrogen transfer from **1** to $G^{\bullet}$ determined from the decay of the absorbance at 4 28 nm due to $G^{\bullet}$ increase significantly with an increase in the concentration of Mg^{2+}. The kinetics of hydrogen transfer from **1** to cumylperoxyl radical has also been examined in propionitrile at low temperature with use of ESR. The decay rate of cumylperoxyl radical in the presence of **1** was also accelerated by the presence of $Sc(OSO_2CF_3)_3$. These results indicate that the radical-scavenging reaction of (+)-catechin proceeds via electron transfer from **1** to oxyl radicals followed by proton transfer rather than via a one-step hydrogen atom transfer. The coordination of metal ions to the one-electron reduced anions of oxyl radicals may stabilize the product, resulting in the acceleration of electron transfer.

In contrast to the radical-scavenging reactions of **1**, no effect of Mg^{2+} on rates of hydrogen transfer from **2** to $DPPH^{\bullet}$ or $G^{\bullet}$ was observed in deaerated acetonitrile at 29 8 K. Thus, the hydrogen-transfer reaction of **2** proceeds via one-step hydrogen atom transfer rather than via electron transfer followed by proton transfer.

Publications:

1) Nakanishi, I., Miyazaki, K., Shimada, T., Ohkubo, K., Urano, S., Ikota, N., Ozawa, T., F ukuzumi, S., and F ukuhara, K.: *J. Phys. Chem. A* **106**, 11123–11126 , 2002.
2) Nakanishi, I., F ukuhara, K, Shimada, T., Ohkubo, K.,

Iizuka, Y., Inami, K., Mochizuki, M., Urano, S., Itoh, S., Miyata, N., and Fukuzumi, S.: *J. Chem. Soc., Perkin Trans. 2* **2002**, 1520–1524 .

17. Enhanced Radical-Scavenging Activity of a Planar Catechin Analogue

Ikuo Nakanishi, Toshihiko Ozawa and Nobuo Ikota

Keywords: *oxidative stress, antioxidant, flavonoid, catechin, hydroxyl radical*

Oxidative stress is important in the pathogenesis of neuronal cell death in Alzheimer's and Parkinson's disease. The protective role of antioxidants against such pathogens has been widely studied, and this has promoted the development of antioxidants for the treatment of diseases associated with oxidative stress. Flavonoids such as (+)-catechin (**1**) and quercetin (**2**) are plant phenolic pigment products that act as natural antioxidants (Fig. 14). Quercetin, on one hand, has been shown to protect against oxidant injury and cell death by scavenging free radicals, protecting against lipid peroxidation, and thereby terminating the chain-radical reaction. On the other hand, there have been only a few reports on the use of (+)-catechin for the treatment of free radical-associated disease, whereas the mechanism to scavenge oxygen radical has been well-studied. Furthermore, its ability to scavenge free radicals must be improved, and adequate lipophilicity is needed to penetrate the cell membrane before it is suitable for clinical use. We herein describe the first synthesis and characterization of the antioxidative properties of a planar catechin analogue (**3**) (Fig. 14), in which the catechol and chroman structures in **1** are constrained to be planar.

The planar catechin (**3**) was synthesized via an oxa-Pictet–Spengler reaction using catechin and acetone with BF_3•Et_2O as the acid. The structure of **3** was characterized by ^1H and ^{13}C NMR and UV–visible spectroscopy. The planar geometry of **3** was substantiated by single-crystal X-ray crystallography of a tetra-*O*-silylated analogue, in which the four OH groups on the A and B rings are substituted by *t*-Bu$(Me)_2$SiO groups.

The radical-scavenging activities of **1**, **2**, and **3** were compared using galvinoxyl radical as an oxyl radical species in deaerated acetonitrile at 298 K. From the decay of the absorbance at 428 nm due to galvinoxyl radical with respect to the reaction time were determined the rate constants (k) for the radical-scavenging reactions of **1**, **2**, and **3** as 2.34×10^3, 1.08×10^3, and 1.12×10^3 M^{-1} s^{-1}, respectively. Thus, the k value for **3** is about 5-fold larger than that for **1** and approximately the same as that for **2**.

Hydroxyl radical is the most reactive among oxygen-derived free radicals responsible for aging and free radical-mediated injury. Therefore, the effects of **1**, **2**, and **3** on hydroxyl radical-mediated DNA breakage were investigated. DNA-strand scission in supercoiled pBR322DNA was induced by a hydroxyl radical-generating system using hydrogen peroxide in the presence of Fe^{3+} (Fenton reaction). In contrast to the pro-oxidant effects observed for **1** and **2**, the addition of **3** protected DNA from Fenton reaction-mediated damage and **3** exhibited marked hydroxyl radical-scavenging ability. Since **3** is very lipophilic compared to **1**, the high radical-scavenging ability of **3** might be very useful for suppressing free-radical associated events, especially in the cell membrane.

Publication:
Fukuhara, K., Nakanishi, I., Kansui, H., Sugiyama, E., Kimura, M., Shimada, T., Urano, S., Yamaguchi, K., and Miyata, N.: *J. Am. Chem. Soc.* **124**, 5952–5953, 2002.

中西郁夫
レドックス制御研究グループ

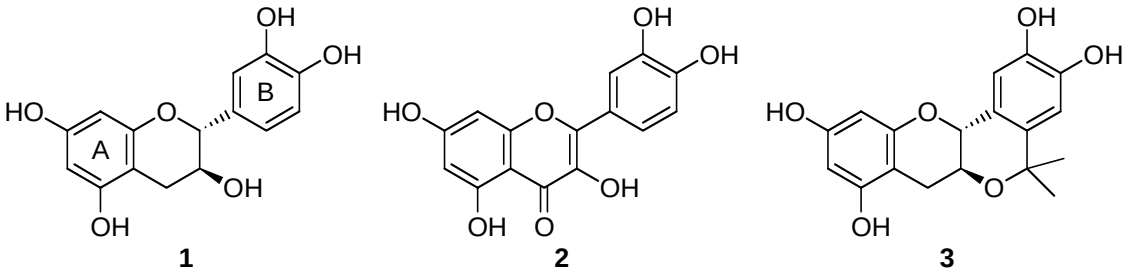

Fig. 14. Chemical structures of (+)-catechin (**1**), quercetin (**2**), and planar catechin (**3**).

18. Scavenging Property of the Indole Derivatives for the Nitrating Intermediate of Peroxynitrite

Hidehiko Nakagawa, Mitsuko Takusagawa, Hiromi Arima, Toshihiko Ozawa, and Nobuo Ikota

Keywords: *peroxynitrite, nitrotyrosine, dityrosine, scavenger, tryptamine derivatives, selenium*

Reactive oxygen species are now well-known and important components of the oxidative stress in several diseases, such as inflammation, Parkinson' s disease, Alzheimer' s disease, etc. It has also been suggested that nitric oxide and its oxidatively activated species, reactive nitrogen species, are involved in the oxidative damage in such diseases. Peroxynitrite (PN) is one reactive nitrogen species, and it has been suggested to be formed from nitric oxide and superoxide *in vivo*. Peroxynitrite is a highly reactive oxidant, and causes nitration on the aromatic ring of free tyrosine and protein tyrosine residues. It was reported that peroxynitrite induced various oxidative damages *in vitro*, for example LDL oxidation, lipid peroxidation, DNA strand breakage and so on. Additionally, tyrosine nitration is assumed to affect the phosphorylation of tyrosine residues in the substrate proteins of tyrosine kinase in the cellular signal transduction. These data imply that the oxidizing and nitrating reactions of peroxynitrite may differently play different pathological roles in the oxidative stress processes. F rom this point of view, it is very useful and important to discriminate the nitrating (nitrative) damage from the oxidative damage reaction in the peroxynitrite-induced damages.

Various antioxidants have been reported to have an inhibitory effect on the nitration of tyrosine, as well as the oxidation reaction by peroxynitrite. However, the relationships between those two types of inhibitory effects of single compound have not been quantitatively discussed. Previously we have briefly reported that 5-methoxytryptamine (5MT) and -lipoic acid (LA) are selective inhibitors for tyrosine nitration by peroxynitrite, but not for oxidative dityrosine formation (NIRS-37 Annual Report). Adding to this result, we report here the evaluation and comparison of the inhibitory activity for the nitration and the oxidation of tyrosine by peroxynitrite for more than 4 0 reagents including natural and synthetic compounds, to elucidate the unique property of tryptamine derivatives and one synthetic compound.

Various compounds including natural and synthetic compounds were subj ected to the assay for the inhibition of tyrosine nitration and oxidation by peroxynitrite. In the presence of the testing compound, 0.2 mM of freshly prepared peroxynitrite solution was mixed with 1 mM of L-tyrosine in sodium phosphate buffer at physiological pH. The products were analyzed by HPLC with a UV and fluorescence detector system. It was confirmed that 3-nitrotyrosine was formed as a maj or product of the reaction. The formation of 3-nitrotyrosine was dependent on the concentration of peroxynitrite and L-tyrosine, as previously reported. The formation of 2,2' -dityrosine was also detected by fluorescence at 4 10 nm (ex. 29 5 nm). The amounts of 3-nitrityrosine and 2,2' -dityrosine were quantified as the nitrated and oxidized products, respectively, and the percent production for the control reaction (containing no testing reagents) was calculated. Among the more than 4 0 compounds showing the inhibitory effect on either nitration or oxidation, the IC50 values were determined for the 28 compounds having sufficient efficacy.

To compare and characterize the inhibitory effect of the 28 effective compounds, the IC50 values for the 3-nitrotyrosine formation and the dityrosine formation were plotted on X- and Y-axes, respectively (F ig. 15). We found

that 22 of 28 compounds had values on the line y = x, meaning that these compounds had the same inhibiting potency for nitration as for oxidation. It was suggested that these compounds scavenged a common intermediate for both nitration and oxidation reactions of peroxynitrite. We also found that the remaining 5 compounds, melatonin, 5-methoxytryptamine, tetrahydro-beta-carboline, tryptophan, lipoic acid and ADCC were off the y = x line. Melatonin, 5-methoxytryptamine, tetrahydro-beta-carboline, and tryptophan, which all have an indole moiety, showed the inhibitory effect only on the nitration of tyrosine, and they were far above the line. This result indicated that these compounds apparently scavenged different intermediate promoting the nitration reaction specifically. However, ADCC, a selenium-containing synthetic compound, was plotted below the line, indicating that it scavenged the intermediate for the oxidation more effectively than that for nitration.

The product of L-tyrosine and peroxynitrite reaction, 3-nitriotyrosine has a characteristic local absorption maximum (lambda max) at 27 4 nm. By monitoring the absorbance change at this wavelength, we measured the production rate of 3-nitrotyrosine. L-Tyrosine solution in 0.1 N HCl and peroxynitrite solution in 0.01 N NaOH were mixed, and the absorbance change at 27 4 nm was recorded with a stopped flow photometer. The reaction rate constant for the tyrosine nitration was found to be 3.6 3-3.8 6 x 10^{2} $M^{-1}s^{-1}$ as the second order rate constant. It is known that the reactivity of peroxynitrite for the oxidation is like that of OH radicals, which can react in a diffusion-rate-limiting manner. However, the rate constant for the nitration calculated in this experiment was much smaller than that for OH radical reaction. This result suggests that the nitrating reaction has different rate limiting reaction step(s). F rom this point of view, the nitrating reaction is not likely to be a direct rebound reaction of caged NO_2 radicals after electron subtraction by caged OH radicals from the aromatic ring of tyrosine. Moreover, the pseudo-first order rates are did not exactly linearly correlated with the concentration of tyrosine, so the nitration by peroxynitrite may be a more complicated reaction.

In conclusion, almost all the compounds tested in this study, including typical antioxidants, showed equal inhibitory activity for both nitration and oxidation, suggesting that these compounds scavenged the common or primary intermediate for nitration and oxidation. However, indole derivatives tested here selectively inhibited the tyrosine nitration, suggesting that they scavenged specific intermediates for nitration, probably in later steps of the reaction mechanism. ADCC, a selenium-containing compound, however, inhibited dityrosine formation preferably. We suggested that there might be specific intermediates for tyrosine nitration by peroxynitrite different from the intermediate for the oxidation reaction. The rate-limiting reaction for the nitration was assumed to be very slow compared with OH radical-like reaction of peroxynitrite. It was also demonstrated that the effects of peroxynitrite due to the nitrating reaction could be distinguished from the oxidizing reaction using these specific inhibiting compounds.

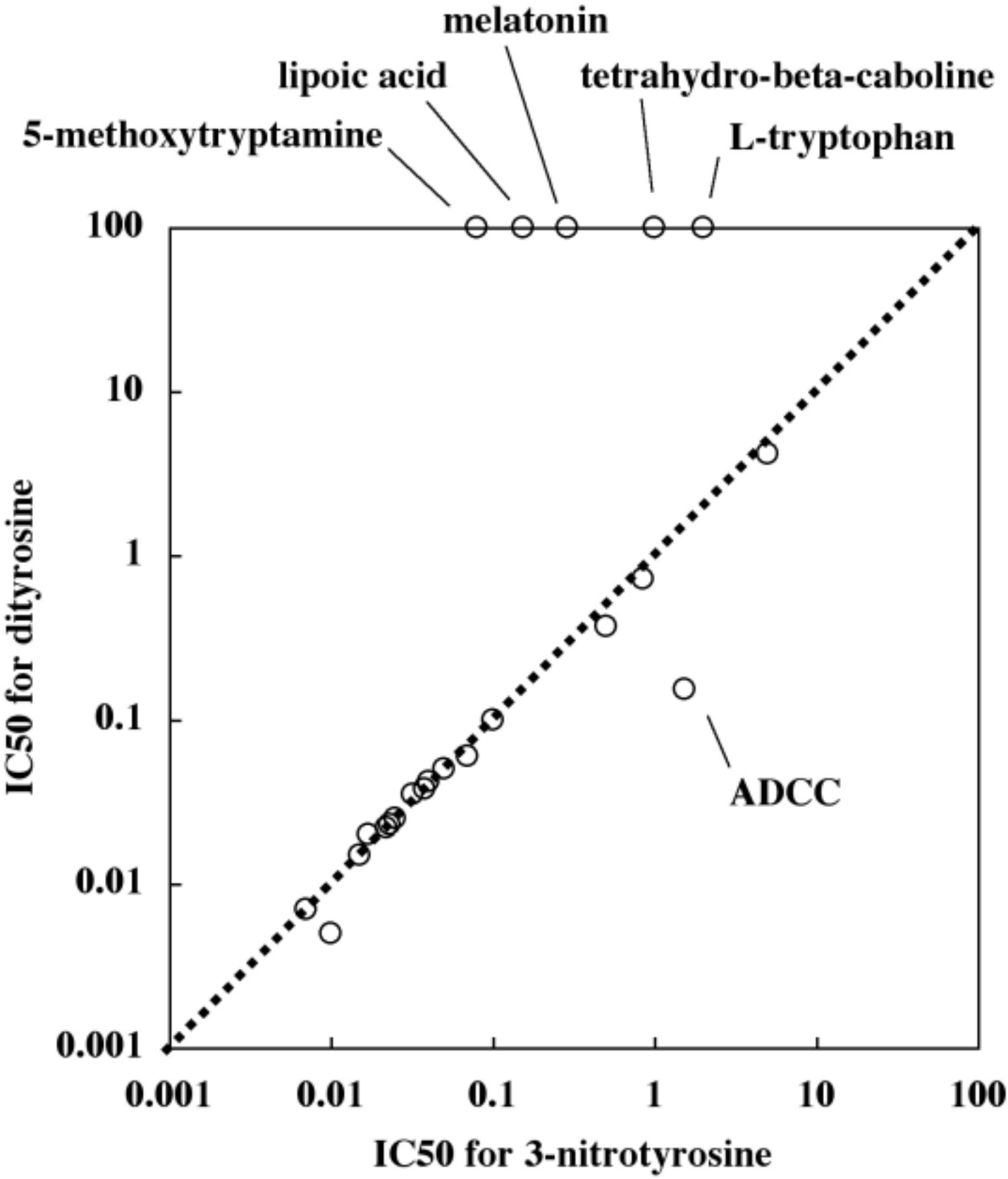
melatonin
lipoic acid
tetrahydro-beta-caboline
5-methoxytryptamine
L-tryptophan
100
10
1
0.1
0.01
0.001
IC50 for dityrosine
ADCC
0.001
0.01
0.1
1
10
100
IC50 for 3-nitrotyrosine

Fig. 15

19. Attenuation of the Ability of Cytochrome c for Caspase Cascade Activation due to Protein Nitration by Peroxynitrite

Hidehiko Nakagawa, Nobuko Komai, Mitsuko Takusagawa, Toshihiko Ozawa, and Nobuo Ikota

Keywords: *peroxynitrite, cytochrome c, apoptosis, caspase, nitration, tyrosine*

Peroxynitrite, or its equivalent species are very strong oxidants, and candidates for in-vitro substances leading to oxidative and " nitrative stress" in various diseases, such as cardiovascular diseases, brain ischemia, Parkinson' s disease, Alzheimer' s disease, sepsis and so on. Nitration of the free and protein tyrosine residues is a unique reaction of peroxynitrite and its equivalents. The protein tyrosine nitration offers clues that reactive nitrogen species (RNS) like peroxynitrite and its equivalents are produced, and that biological systems are damaged with RNS stresses. There are some reports that the nitration of protein tyrosine residues, including cytochrome c, causes some changes in its functions. It was previously reported that the nitration of single tyrosine residue in cytochrome c by a relatively low dose of peroxynitrite results in the upregulation of its peroxidase activity for hydrogen peroxide, and in the actual impairment of the membrane potential formation, which is important for the ATP synthesis, in isolated mitochondrial preparations (NIRS-4 1 Annual Reports).

It is also well known that cytochrome c is an important player in the mitochondria-dependent apoptotic cell death. Regarding the response for apoptotic stimuli, cytochrome c is released from the intermembrane space to the cytosol, and it forms apoptosome complexes with caspase-9 and Apaf-1 to activate caspase-9 and the downstream caspases, resulting in the apoptic death execution. Here, we demonstrate that the nitration of cytochrome c by a prolonged exposure to peroxynitrite attenuated its potency for the mitochondria-dependent caspase activation.

F or the low-dose repetitive treatment of cytochrome c with peroxynitrite, 1 µl of 50 mM peroxynitrite in 0.01 M NaOH was repeatedly added to the solution (1 ml) of 20 µM cytochrome c in PBS 20 times at 5-min intervals while mixing (denoted as PN20X50). Because peroxynitrite is unstable at neutral pH, it is practically fully decomposed 5 min after a treatment in PBS. F or the control treatment, no peroxynitrite was added to the cytochrome c solution containing decomposed peroxynitrite equivalent to the 20 µl of 50 mM peroxynitrite. After the addition of a total of 20 µl of peroxynitrite solution, the resultant solution was confirmed to be neutral (pH 7 to 8). All the peroxynitrite-treated cytochrome c solutions were subj ected to a gel-filtration with Sephadex G 25, and the concentrations were adj usted according to the absorbance at 4 09 nm. With the peroxynitrite treatment at the concentration range in this experiment, the maximum absorbance and wavelength of the Soret-band (4 09 nm) had almost no changes; a blue-shift by only 0.2 nm in wavelength was found. A solution of cytochrome c repetitively treated with low-dose peroxynitrite in the presence of 5-methoxytryptamine (5MT) was also prepared for the experiment on the inhibitory effect of 5MT. Tetranitromethene (TNM)-treated cytochrome c was also prepared. TNM is a well-known protein tyrosine-nitrating reagent. Peroxynitrite-treated cytochrome c was hydrolyzed enzymatically, and analyzed by reversed-phase HPLC, to confirm the nitrotyrosine formation. In the hydrolysate, 3-nitrotyrosine was detected, and it was confirmed that the tyrosine nitration occurred on cytochrome c by a treatment of peroxynitrite.

Caspase activation assay in a cell free system was

carried out using a cytosolic fraction of C6 cells and exogenous peroxynitrite-treated cytochrome c. Peroxynitrite-treated or control cytochrome c was incubated with cytosolic fraction at 30°C for 9 0 min. The samples were subsequently subj ected to SDS-PAGE and immunoblotting with anti-cleaved caspase-3 antibody, and visualized by chemiluminescence with ECL-plus reagents. The cleaved caspase-3 formation indicates the activation of the upstream caspase, caspase-9 , meaning that the cytochrome c holds the ability for the caspase cascade activation.

As shown in F ig. 16 , the peroxynitrite-treated cytochrome c prepared by repetitive low dose treatments showed a very low activity for the induction of the procaspase-3 cleavage in the *in vitro* apoptosis assay. This attenuation of the caspase cascade activation was not observed when the peroxynitrite-treatment was carried out in the presence of 5MT, which is a nitration selective peroxynitrite scavenger. F urthermore, the TNM-treated cytochrome c also lost its ability for the caspase cascade activation. These results suggested that the nitration on cytochrome c proteins resulted in the attenuation of the potency for the caspase cascade activation. They also implied that the nitrating stress by the low dose and repetitive peroxynitrite exposure, which is likely close to the condition *in vivo*, induced cytochrome c nitration and the suppression of the cytochrome c-dependent caspase cascade activation.

Fig. 16

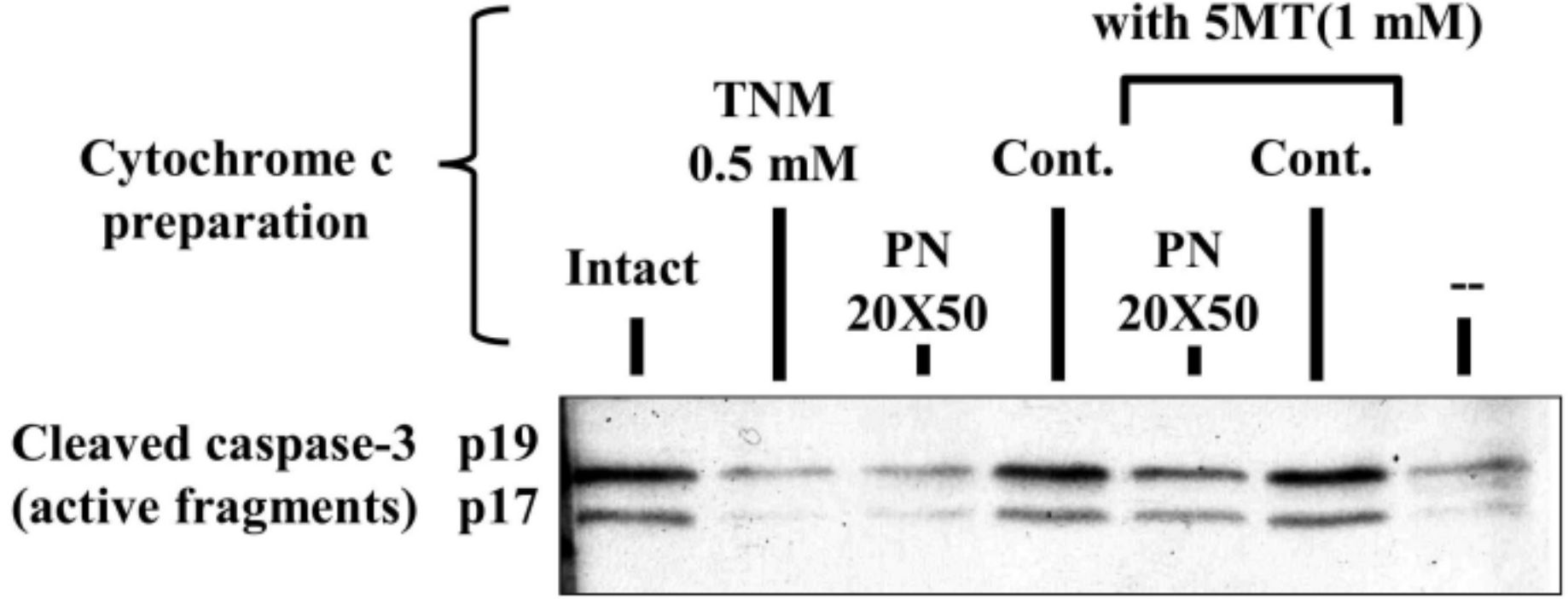
with 5MT(1 mM)
TNM
0.5 mM
Cont.
Cont.
Cytochrome c
preparation
Intact
PN
20X50
PN
20X50
--
Cleaved caspase-3
(active fragments)
p19
p17

BIO-MEDICAL SCIENCES

Biochemistry and Biophysics

20. Disappearance of Nuclear Binding Proteins Bound to the Far-Upstream Region of the Interleukin-1 Gene Immediately after Irradiation of Mouse Macrophages

Hiroshi Ishihara, Izumi Tanaka, Hong Wan and CheerarattanaCheeramakara

Keywords: *interleukin-1 , radiation-inducible, gene expression, nuclear protein, electrophoretic mobility-shift assay*

Interleukin(IL)-1 is a multifunctional cytokine that plays important roles in the immune system and inflammation and is able to survive from death of mice irradiated at lethal doses of X-rays. We previously reported that the induction of the IL-1 gene, not only in the late phase, but also in the immediate-early phase after exposure to ionizing radiation at transcriptional level in primary cultures of mouse spleen cells and macrophage. Since the immediate-early phase of induction probably reflects early responsive mechanisms against radiation in mammalian cells, we explored the molecular events in the macrophage. To demonstrate the immediate-early induction of the IL-1 gene, an electrophoretic mobility-shift assay (EMSA) was used to detect specific binding of nuclear proteins to the upstream region of the gene, since the analysis using conventional reporter assay was intercepted by the late phase induction.

In the consideration of the possibility that the gene is regulated by a far-upstream region from the transcriptional starting site, as in other cytokine genes, we focused on a DNA locus including the IL-1 gene with an upstream region of 9.5 kb that was isolated from the C3H mouse genomic library. Binding activity to the nuclear extract of macrophage-line leukemia cell line L8704 was analyzed using its upstream region that was fragmented by restriction endonuclease. Specific binding activity was detected in three DNA fragments corresponding to the 8500, 8000 and 2500 bases upstream of the gene named B10, B02 and F19, respectively (Fig. 17, lanes 2 and 3). When the nuclear extract from the L8704 cells immediately after irradiation of 20Gy X-rays was used, the binding disappeared (lanes 5 and 6). When non-labeled oligoDNA was added as a competitor or the nuclear extract was replaced by that from non-irradiated cells, the retardation was blocked and the free DNA bands reemerged (lane 4). The retardation effect also vanished upon a pretreatment of the nuclear extract from the irradiated cells with proteinase K (lane 7). These results indicate that the nuclear proteins in the extract contribute to the specific binding to the DNA fragments.

Nucleotide sequences essential for the binding to the nuclear extract in B10, B02 and F19 fragments were shown to be 79, 118 and 137 bases in size, respectively. However, further elimination of the sizes lost the binding activity, unlike target motifs

for transcriptional activators with short-target motifs and giving single retardation bands. It is speculated that the disappearance of binding activity reflects conformational change(s) of DNA-protein complexes besides the IL-1 gene locus during immediate-early induction. The identification of the nuclear components would be important to understand the immediate-early response after exposure to ionizing radiation.

Publication:

Ishihara, H., Tanaka, I. Wan, H. and Cheeramakara, C.: *J. Radiat. Res.*, **44**, 117-123, 2003.

Figure Legend

Fig. 17. Binding of nuclear extract to the upstream region of the IL-1 gene. Short DNA fragments of B10, B02 and F19 correspond to the upstream region of IL-1 gene (upper). The fragments were end-labeled and incubated with stock (c, lanes 2, 4 and 6) and 10-fold-diluted (d, lanes 1, 3 and 5) solutions of the nuclear extract from non-irradiated cells (lanes 2, 3 and 4) or irradiated cells (lanes 5, 6 and 7). During incubation, a 10-fold molar amount of non-labeled DNA was used as a competitor in lane 4. Before incubation, the nuclear extract from irradiated cells was pretreated with proteinase K (final concentration, 100 g/ml) at 37℃, 10 min (lane 7). After the incubation, mixtures were applied onto 6% agarose gel for electrophoresis. The arrows indicate the areas shifted by the retardation of the DNA. Nucleotide sequences showing binding activity on similar analyses (underlined) of these fragments are placed at the bottom.

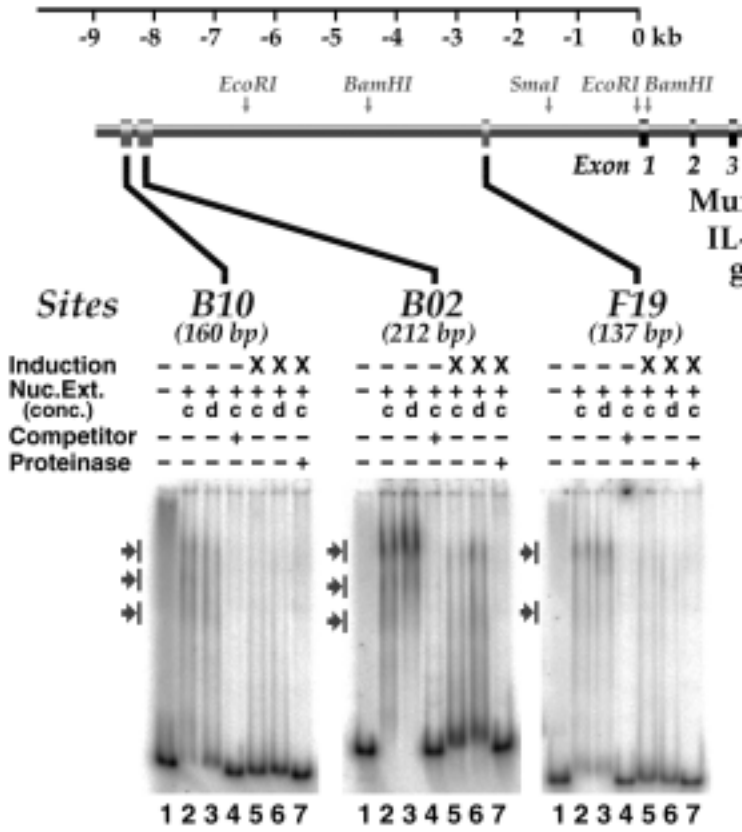

B10 fragment *(160 nt)*

accagccccactactgcctccgccaccaccaacttctccctccttgcgacggcactgccgccatcttgt

ctctttggttgaacaagcagttgtgctacctttggaaggccattgacagcatggcttccctttgcatct

B02 fragment *(212 nt)*

gtcattaaactacctcatgcttttacatcaagatggtcgtctgttcgtgattcttgggtgcacgccgaa

tgggggtttccccactaggttctttcaatggtacagatggtgaggcgaccatcaatgagaccaaagttc

gtacttttccagaagtacctttttggcagagtcatccagagagttcttcaca

F19 fragment *(137 nt)*

ctcgtgcctgtaatctcagtcctttgggagacaaatgcaggagaattgtcatgtacttgaagccagtctg

ggctgcacagtagtcatggttatcacagcaatagaaagtaagtaaaacaggtagcaaggcactttcag

21. Measurement of Hydroxyl Radical Generated in Live Rats during X-Ray Irradiation

Keizo Takeshita, Kaori Fujii, Kazunori Anzai and Toshihiko Ozawa

Keywords: *hydroxyl radical, spin trapping, PBN, dimethyl sulfoxide, rats, X-ray*

The generation of hydroxyl radical believed to be one of the major triggers of radiation injury was monitored in live rats by spin-trapping the secondary radical, methyl radical formed by the reaction of hydroxyl radical with dimethyl sulfoxide (DMSO). The X-ray irradiation of rats administered with a DMSO solution of the spin trap, -phenyl-N-tert-butylnitrone (PBN) resulted in a remarkable increase in the six-line ESR signal in bile. The increase of the signal was dependent on the X-ray irradiation. No increase was observed under sham irradiation. The apparent hyperfine splitting constants for the six-line signal were very close to those reported for PBN/CH_3. Replacement of DMSO with [$^{13}C_2$] DMSO, whose ^{12}C (I= 0) was substituted with a magnetic ^{13}C (I= 1/2), gave the ESR spectrum with another hyperfine structure. Simulation of this spectrum revealed that the observed spectrum was composed of signals for 4 different species: PBN/$^{13}CH_3$; the adduct of the C-centered radical (probably produced by the reaction of intrinsic fatty acid with ˙OH); the unknown radical adduct with broad triplet lines; and ascorbyl radical. The spin ratio calculated from these components strongly indicated that the signal observed in the bile samples collected from rats during X-ray irradiation mainly included the signal of PBN/CH_3. The concentration of the radical adduct in bile was determined by double integration of the doublet line at the lower magnetic field. The strengthened signal was detectable above 20 Gy, and there was a fairly linear relationship between the dose of radiation and the concentration of the radical adducts. Preadministration of cysteamine (4 mmol/kg-b.w.), a radioprotective agent, prevented the signal increase caused by X-ray irradiation at 78 Gy. The effect of cysteamine on the formation of radical adducts was dose-dependent. Cysteamine hardly reduced the signal intensity of the PBN adducts *in vitro*, indicating that the *in vivo* effect of cysteamine resulted from its activity as a radical scavenger. This is the first study of the *in vivo* demonstration of the generation of hydroxyl radical at a radiation dose close to accidental doses and the radical scavenging by a radioprotective agent.

22. Effect of Oxidative Stress on Glutathione Redox Status in Mouse Measured by Simultaneous Determination of GSH and GSSG with HPLC

Kazunori Anzai, Yohei Okuda, Cuiping Chi, Shiro Urano and Toshihiko Ozawa

Keywords: oxidative stress, glutathione, redox state, HPLC, mouse

Glutathione (-Glu-Cys-Gly) is a major antioxidant peptide existing mainly in cytosol at the concentration of 1-11 mM. It occurs as a redox equilibrium between GSH (reduced form) and GSSH (oxidized dimer form) and oxidative stress to living organisms is thought to change the redox balance to a more oxidizing equilibrium (smaller GSH/GSSG ratio). However, experimental evidence proving such an idea is insufficient. In the present study, we tried to establish the method to measure simultaneously the amount of GSH and GSSG in tissue samples with HPLC and to investigate the effect of oxidative stress on the amount of GSH and GSSG in mouse liver and brain.

For the simultaneous detection of both GSH and GSSG, we adopted HPLC using a derivatizing method. Samples were derivatized with 2,4-dinitrofluorobenzene and then applied to HPLC system equipped with an UV/visible detector. Sample pH (authentic GSH and GSSG, mouse liver homogenate, mouse brain homogenate in 6% meta-phosphoric acid and 1 mM bathophenanthroline disulfonic acid) was adjusted to 8.5 with 2.4 M $KHCO_3$ and then the solution was reacted with 2,4-dinitrofluorobenzene for 2 hours at 40°C in the dark. After treatment with 70% perchloric acid, the solution was centrifuged at 5,600 x g for 5 min at 4°C. The resultant supernatant was filtered with a membrane filter (0.22 m) and the filtrate was used as the HPLC sample. The HPLC system (Shiseido Co.) consisted of an auto-sampler (SI-2/3023), two pumps (SI-1/2001 and SI-2/3001), a degasser (SI-2/3009), a column oven (SI-1/2004), an UV/visible detector (SI-1/2002), and a computer-assisted system controller with a data processing software (S-MC). A reverse-phase column (Shiseido Capcel Pak C18 MG120, 2 mm x 250 mm) was used. The mobile phase had a gradient of hydrophobicity by appropriate mixing of two solutions, 0.1% trifluoroacetic acid in acetonitrile and 0.1% trifluoroacetic acid in water.

After establishment of the analytical conditions using HPLC, we measured GSH and GSSG content in liver and brain tissues of normal mice or vitamin E deficient mice to which oxidative stress was applied or not. Two kinds of oxidative stresses, X-ray irradiation (8 Gy) or iron overloading, were applied. Samples were prepared 2 hours post X-ray irradiation and 1 hour post iron injection. Contrary to our initial expectation, neither oxidative stress, X-ray irradiation and iron overloading, changed the GSH/GSSG ratio in the liver and the brain of both normal and vitamin E deficient mice. On the other hand, total glutathione (GSH plus 2GSSG) significantly decreased in the brain of vitamin E deficient mice for both oxidative stresses. Significant change, however, was observed only in this sample.

Since glutathione is in a dynamic equilibrium in living tissues, transient change in the GSH/GSSG ratio might disappear after a certain period of time or the change might be too slow to be detected after a certain period of time. Therefore, it would be better to measure the glutathione content at various timing after applying the oxidative stress.

23. Transient Increase of mRNA of Heme Oxygenase-1 in Rat Liver after a Whole-body X-irradiation

Keiko Suzuki, Masahiko Mori, Fumihiko Kugawa* and Hiroshi Ishihara
(* Nihon Univ.)

Keywords: heme oxygenase, mRNA, X-ray, liver

Heme oxygenase-1 (HO-1) is an enzyme which decomposes heme to biliverdin, Fe^{2+} and carbon monoxide. The transcription of the gene of HO-1 is activated by various stimuli, such as oxidative stress, UVA radiation, heat shock and metal cations.

We had previously reported that the activity of heme oxygenase in the rat liver was stimulated 2.5 times as measured at 7 h after a whole-body irradiation of 17 Gy X-rays, and that the amount of HO-1 protein was also increased after irradiation, reached the maximal level at 4 h and then was decreased slightly until 10 h after irradiation.

In the present study we examined the HO-1 mRNA expression in the livers of irradiated rats by northern blotting to investigate the transcriptional activation of this gene. Male rats were irradiated with X-rays (17 Gy), and the mRNA fraction was prepared from the liver at 2, 4, 7 and 10 h after irradiation. As shown in Fig.18, the mRNA of HO-1 was increased significantly 2 h after irradiation, reached the maximal value at 4 h, and then was declined until 10 h. When the X-ray dose was varied from 4.0 to 21.7 Gy, the transcription of the gene was enhanced with all doses and the level of activation was dependent upon the doses of the X-rays.

Thus in this study, we observed a transient activation of the transcription of HO-1 gene shortly after irradiation, and demonstrated that ionizing radiation is a stressor which induces activation of the HO-1 gene and increases enzyme activity in the liver. It is possible that the products of the heme oxygenase reaction, biliverdin and bilirubin, might scavenge reactive oxygen species produced by radiation to protect tissues from oxidative stress, and might contribute to some extent to attenuate the secondary injuries.

Publication:
Suzuki, K., Mori, M., Kugawa, F. and Ishihara, H.: *J. Radiat. Res.*, **43**, 205-210, 2002.

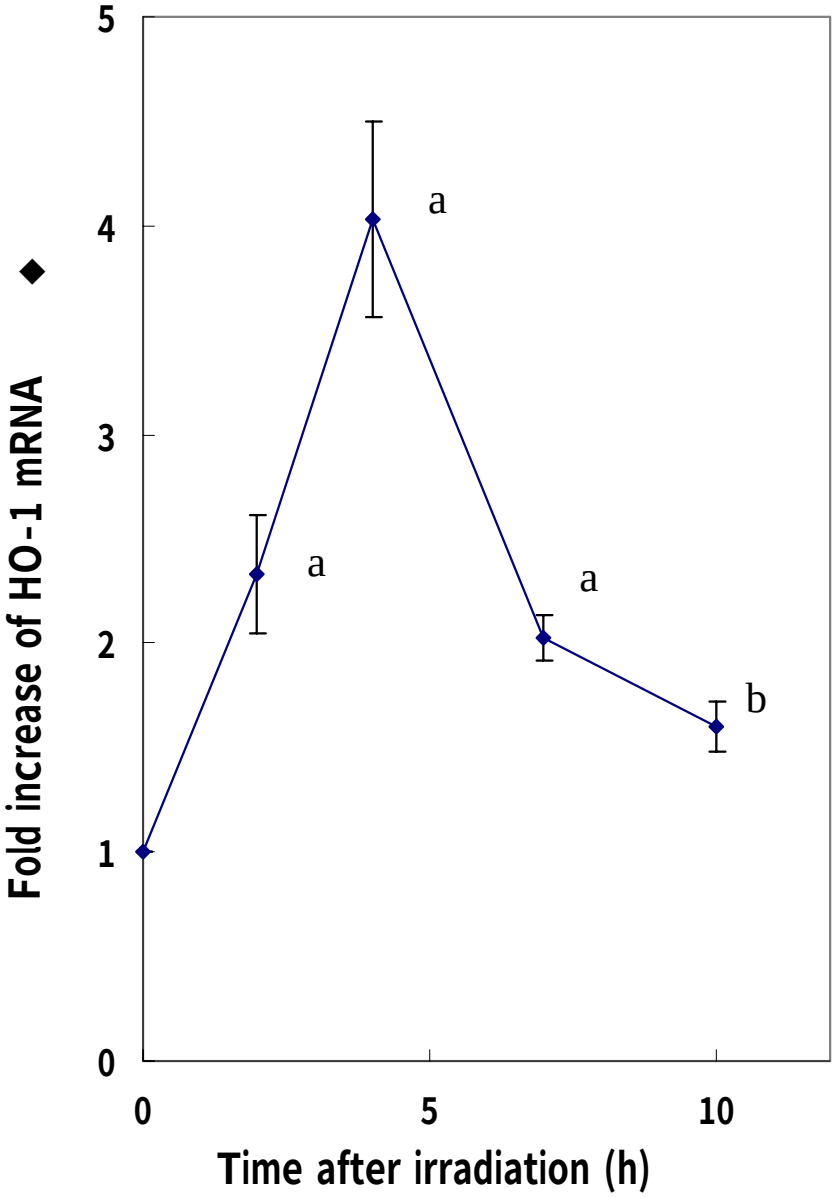

Fig.18. Transient upregulation of rat HO-1 mRNA after 17 Gy X-ray irradiation. a, $P<0.01$; b, $P<0.02$.

24. Analysis of Unrejoined Chromosomal Breakage in Human Fibroblast Cells Exposed to Low- and High-LET Radiation

Honglu Wu[1], Yoshiya Furusawa, Kerry George[1], Tetsuya Kawata[2], and Francis A. Cucinotta[3]

([1]Wyley Lab.; [2]Chiba Univ.; [3]NASA Johnson Space Center)

Keywords: high-LET radiation, chromosome aberration, telomere, unrejoined breaks

Reported studies of DNA breakage induced by radiation of various qualities have generally shown a higher fraction of unrejoined residual breaks after high-LET exposure. This observation is supported by the argument that high-LET radiation induced DNA breaks that are more complex in nature and, thus, less likely to be repaired. In most cases the doses used in these studies were very high. We have studied unrejoined chromosome breaks by analyzing chromosome aberrations using a fluorescence *in situ* hybridization (FISH) technique with a combination of whole chromosome specific probes and probes specific for the telomere region of the chromosomes. Confluent human fibroblast cells (AG1522) were irradiated with -rays, 490 MeV/nucleon Si, or with Fe ions at either 200 and 500 MeV/nucleon, and were allowed to repair at 37°C for 24 hours after exposure. A chemically induced premature chromosome condensation (PCC) technique was used to condense chromosomes in the G2 phase of the cell cycle. Results showed that the frequency of unrejoined chromosome breaks was higher after high-LET radiation, and the ratio of unrejoined to misrejoined chromosome breaks increased steadily with LET up a peak value at 440 keV/μm.

Publication:

Wu, H., Furusawa, Y., George, K., Kawata, T., and Cucinotta, F.A.: *J. Radiat. Res.* **43**, s181-s185, 2002.

25. Models for Mixed Irradiation with a 'Reciprocal-Time' Pattern of the Repair Function

Shozo Suzuki*, Yuri Miura*, Shoichi Mizuno*, and Yoshiya Furusawa.

(* Tokyo Metropolitan Institute of Gerontology)

Keywords: mixed irradiation, theoretical model, LET, reciprocal-time repair, linear-quadratic model

Suzuki presented models for mixed irradiation with two and multiple types of radiation by extending the Zaider and Rossi model, whichis based on the theory of dual radiation action. In these models, the repair function was simply assumed to be semi-logarithmically linear (i.e., monoexponential), or a first-order process, which has been experimentally contradicted. Fowler, however, suggested that the repair of radiation damage might be largely a second-order process rather than a first-order one, and presented data in support of this hypothesis. In addition, a second-order repair function is preferred to an *n*-exponential repair function for the reason that only one parameter is used in the former instead of 2*n*-1 parameters for the latter, although both repair functions show a good fit to the experimental data. However, according to a second-order repair function, the repair rate depends on the dose, which is incompatible with the experimental data. We, therefore, revised the models for mixed irradiation by Zaider and Rossi and by Suzuki, by substituting a `reciprocal-time' pattern of the repair function, which is derived from the assumption that the repair rate is independent of the dose in a second-order repair function, for a first-order one in reduction and interaction factors of the models, although the underlying mechanism for this assumption cannot be well-explained. The reduction factor, which reduces the contribution of the square of a dose to cell killing in the linear-quadratic model and its derivatives, and the interaction factor, which also reduces the contribution of the interaction of two or more doses of different types of radiation, were formulated by using a `reciprocal-time' pattern of the repair function. Cell survivals calculated from the older and the newly modified models were compared in terms of the dose rate by assuming various types of single and mixed irradiation. The result implies that the newly modified models for mixed irradiation can express or predict cell survival more accurately than the older ones, especially when irradiation is prolonged at low dose rates.

Publication: Suzuki, S., Miura, Y., Mizuno, S., and Furusawa, Y.: *J. Radiat. Res.* **43**, 257-267, 2002.

26. Effect of a Hypoxic Cell Sensitizer Dranidazole in Radiation-Induced Apoptosis of Mouse L5178Y Lymphoma Cells

Mizuho Aoki, Yshiya Furusawa, Yuta Shibamoto[1], Ataru Kobayashi[2], and Michihiko Tsujitani[2]
([1]Kyoto Univ.; [2]Pola Chemical Industry Inc.)

Keywords: radiosensitizer, hypoxic cell sensitizer, doranidazole, apoptosis, L5178Y cell

We investigated the sensitizing effect of the 2-nitroimidazole analogue doranidazole, a new hypoxic radiosensitizer, on radiation-induced apoptosis in L5178Y cells. Apoptosis was assessed by checking DNA ladder formation, the presence of sub-G1 peaks in flow cytometry, and chromatin condensation. A radiosensitizing effect of doranidazole was also confirmed by a soft-agar colony assay of surviving cells. In the assay of DNA ladder formation, DNA fragmentation was observed following irradiation under an aerobic or hypoxic condition with or without doranidazole. The proportions of the cells at the sub-G1 peak in a flow cytometric measurement was not very different among the irradiations at 5 Gy under the aerobic condition, 15 Gy under hypoxia, and 10 Gy with 1 mM doranidazole under hypoxia. The fraction of cells with chromatin condensation was found to be significantly increased with doranidazole up to 3 mM when applied under hypoxic irradiation, but did not increase even at 10 mM. The sensitizer enhancement ratio was estimated to be about 1.7 with a concentration of 1 mM. This enhancement ratio was not different from that observed by assaying cell survivals. On the other hand, doranidazole showed no radiosensitizing effect under aerobic conditions with 1 mM. In conclusion, the radiation-induced apoptosis of L5178Y cells was enhanced by doranidazole under hypoxia.

Publication:

Aoki, M., Furusawa, Y., Shibamoto, Y., and Tsujitani, M. *J. Radiat. Res.* **43**, 161-166, 2002.

27. Synthesis and Evaluation of 4-Bromo-1-(3-[^{18}F] fluoropropyl)-2-nitroimidazole with a Low Energy LUMO Orbital Designed as Brain Hypoxia-Targetting Imaging Agent.

Fumihiko Yamamoto*, Mizuho Aoki, Yoshiya Furusawa, Koichi Ando, Yasuo Kuwabara*, Kouji Masuda*, Shigeki Sasaki*, and Minoru Maeda*
(* Kyushu Univ.)

Keywords: nitroimidazole, fluorine-18, brain tissue, biodistribution

In order to develop new imaging markers for brain hypoxia, 4-bromo-1-(3-fluoropropyl)-2-nitroimidazole (4-BrFPN) was designed based on molecular orbital calculations, synthesized and labeled with fluorine-18 as a lipophilic nitroimidazole analog with a lower energy LUMO orbital than those for fluoromisonidazole (FMISO) and 1-(3-fluoropropyl)-2-nitroimidazole (FPN). In an *in vitro* radiosensitization study, the sensitizer enhancement ratio for 4-BrFPN was found to be 1.65 at a 1 mM concentration, in comparison to 1.81 for FMISO. The preparation of ^{18}F-labeled 4-BrFPN (4-Br^{18}FPN) was achieved by [^{18}F] fluoride ion displacement reaction of the tosylate precursor, in a reasonable radiochemical yield (33%, not corrected for decay). Metabolites in tumor and muscle extracts from methylcholanthrene-induced fibrosarcoma mice, as well as the tissue distribution of 4-Br^{18}FPN in normal rats, were studied. The initial uptake into rat brain of 4-Br^{18}FPN was significantly higher relative to ^{18}F-labeled FMISO (^{18}FMISO), followed by a rapid washout from the brain. The tumor uptake of 4-Br^{18}FPN was somewhat enhanced compared to those obtained with ^{18}FMISO and ^{18}F-labeled FPN (^{18}FPN), but with lower tumor localization than ^{18}FMISO. Analyses of tumor and muscle extracts showed metabolites remaining on he base line on the radio-TLC plates, and they were produced to a greater extent in tumor than muscle. The use of two drugs which increase hypoxic cell fraction in tumor, hydralazine or nitro-L-arginine, produced a significant increase in tumor levels of 4-Br^{18}FPN, suggestive of a hypoxic mechanism of accumulation. The results imply that lowering of the LUMO energy of a molecule alone is not sufficient to improve its biodistribution properties for better imaging of regions of hypoxia.

Publication:
Yamamoto, F., Aoki, M., Furusawa, Y., Ando, K., Kuwabara, Y., Masuda, K., Sasaki, S., and Maeda, M.: *Biol. Pharm. Bull.* **25**, 616-621, 2002.

28. Development of a Dielectric Equivalent Gel for Better Impedance Matching for Human Skin

Takahiro Sunaga, Hiroo Ikehira, Shigeo Furukawa, Mitsuru Tamura, Eiji Yoshitome, Takayuki Obata, Hiroshi Shinkai, Shuji Tanada, Hajime Murata and Yasuhito Sasaki

Key words: dielectric constant, bolus gel, dielectric artifact, MRI

It would be useful to develop a tissue equivalent gel, to improve the uniformity of the electromagnetic field in the human body, and for making a tissue equivalent dielectric human phantom.

In this study, solid-type water-based gelatin-honey gels were developed which have the electrical characteristics of skin tissue. It was demonstrated that a stable and homogeneous gel, with a relative dielectric constant (ε') chosen from desired ranges found in skin, can be made.

Above 300 MHz, acquiring MR images of high quality is difficult because of the increase in operating RF (radio frequency). The main factor affecting image quality is a dielectric resonance phenomenon, which can cause distortion. Electromagnetic wave impedance mismatching of the air/tissue interface may also cause dielectric inhomogeneity, especially at the epidermal surface.

We expect that three things will occur when an electromagnetic field propagating in the air encounters human tissue such as the dermis; the RF wave should be reflected, transmitted, and absorbed. All three are related to the dielectric properties of the material. Using suitable impedance-matched materials should reduce the dielectric mismatch between air and the human body.

The simulation and the trial to form phantom for muscle tissue were reported previously. We developed a bolus phantom gel which functions by suppressing the non-uniformity of RF due to impedance mismatching inside the skin at 200MHz up to 400MHz. Data on the dielectric specificity of several human skin conditions were already reported in our previous article.

The basic materials prepared for developing gels are gelatin produced from pigskins, honey syrup, NaCl (100%) and distilled water. Solid-type water-based gelatin-honey gels were developed which have the electrical characteristic of skin tissue. It was demonstrated that stable and homogeneous gels can be made in which values of the relative dielectric constant (ε') can be chosen from desired ranges found in skin. Still, ε' and σ can be varied almost independently, ε' depending on gelatin and honey concentrations, and σ on the salt concentration.

The usage of developed gels would not only improve diagnoses with high Tesla MRI, but also have potential for hyperthermia or the study of the safety of electromagnetic fields.

Publication

Sunaga T, Ikehira H, Furukawa S, Tamura M, et al.: *Bioelectromagnetics* 24, 214-217, 2002.

BIO-MEDICAL SCIENCES

Cell Biology

29. Relationship Between Aberration Yield and Mitotic Delay in Human Lymphocytes Exposed to 200 MeV/u Fe-Ions or X-Rays

Sylvia Ritter[1], Elena Nasonova[2], Yoshiya Furusawa, and Koichi Ando
([1]GSI; [2]JINR)

Keywords: human lymphocytes, heavy ions, time-course of aberrations, calyculin A, apoptosis

The time-course of Fe-ion (200 MeV/u, 440 keV/µm) and X-ray induced chromosomal damage was investigated in human lymphocytes. After cells were exposed in G0 and stimulated to grow, aberrations were measured in first-cycle metaphases harvested 48, 60 and 72h post-irradiation. Additionally, lesions were analysed in G2 and mitotic (M) cells collected at 48h using calyculin A-induced premature chromosome condensation (PCC). Following X-irradiation, similar aberration yields were found in all of the samples scored. In contrast, after Fe-ion exposure a drastic increase in the aberration frequency with sampling time was observed, i.e. cells arriving late at the first mitosis carried more aberrations than those arriving at earlier times. The PCC data indicate that the delayed entry of heavily damaged cells into mitosis observed after Fe-ion irradiation resulted from a prolonged arrest in G2. Altogether these experiments provide further evidence that in the case of high-LET exposure cell-cycle delays of severely damaged cells have to be taken into account for any meaningful quantification of chromosomal damage and, consequently, for an accurate estimate of the RBE.

Publication:

Ritter, S., Nasonova, E., Furusawa, Y., and Ando, K.: *J. Radiat. Res.* **43**, s175-s179, 2002.

30. Induction of Chromatin Damage and Distribution of Isochromatid Breaks in Human Fibroblast Cells Exposed to Heavy Ion

Tetauya Kawata[1], Hisao Ito[1], Ken Motoori[1], Takuya Ueda[1], Naoyuki Shigematsu[2], Yoshiya Furusawa, Marco Durante[3], Kerry George[4], Honglu Wu[4], and Francis A. Cucinotta[4]
([1]Chiba Univ.; [2]Keio Univ.; [3]Univ. Federick II; [4]NASA Johnson Space Center)

Keywords: high-LET radiation, premature chromosome condensation, isochromatid break, calyculin A

The frequency of chromatid breaks and the distribution of isochromatid breaks were measured in G2-phase normal human fibroblasts prematurely condensed a short time after exposure to low- or high-LET radiations. The average number of isochromatid breaks from a single particle traversal increased with increasing LET values, while the average number of chromatid-type breaks appeared to reach a plateau. The distribution of isochromatid breaks after high-LET iron particles exposure was overdispersed compared to -rays, indicating that a single iron particle traversal through a cell nucleus can produce multiple isochromatid breaks.

Publication:

Kawata, T., Ito, H., Motoori, K., Ueda, T., Shigematsu, N., Furusawa, Y., Durante, M., George, K., Wu, H., and Cucinotta, F.A.: *J. Radiat. Res.* **43**, s169-s173, 2002.

31. Nitric Oxide-Mediated Bifunctional Bystander Effect Induced by Heavy-Ion Radiation in Human Salivary Grand Neoplastic Cells

Chunlin Shao, Yoshiya Furusawa, Mizuho Aoki, Hideki Matsumoto* , and Koichi Ando
(* Fukui Medical Univ.)

Keywords: bystander effect, nitric oxide, carbon-ion beam, NO scavenger

Our purpose was to investigate the signal factor and its function in the medium-mediated bystander effect during heavy-ion irradiation of human salivary gland (HSG) neoplastic cells.

Unirradiated recipient HSG cells were co-cultivated with HSG donor cells irradiated with 290 MeV/u carbon beams having different LET values. Cell proliferation and micronucleus (MN) induction in recipient cells with and without treatment of a NO scavenger (PTIO) were measured and the concentration of nitrite in the co-culture medium was detected. As a direct control, the effects of a nitric oxide (NO) generator (sper/NO) on cell proliferation and MN induction were also examined.

Increases in cell proliferation and MN induction were found in the recipient HSG cells as a result of co-culturing and cell proliferation was obviously enhanced during a further subculture. In comparison with 13 keV/μm, 100 keV/μm carbon-ion irradiation was found to be a more efficient inducer of the medium-mediated bystander effect. The treatment of cells by PTIO resulted in elimination of such effects, which supports a role for NO in the medium-mediated bystander effect. As an oxidization product of NO, nitrite was detected in the co-culture medium, and the dose-response for its concentration was similar to that of cell proliferation and MN induction in the recipient cells. When the HSG cells were treated by sper/NO with a concentration of less than 20 μM, cell proliferation was enhanced, whereas MN increased along with sper/NO concentration.

NO participated in the medium-mediated bystander effects on cell proliferation and MN induction, depending on the LET of irradiation.

Publication:

Shao, C., Furusawa, Y., Aoki, M., Matsumoto, H., and Ando, K.: *Int. J. Radiat. Biol.* **78**, 837-844, 2002.

32. Radiation-induced Growth Inhibition in Transplanted Human Tongue Carcinomas with Different p53 Gene Status

Isao Asakawa* , Hitoshi Yoshimura* , Akihisa Takahashi* , Ken Ohnishi* , Hitoshi Nakagawa* , Ichiro Ota* , Yoshiya Furusawa, Tetsuro Tamamoto* , Haj ime Ohishi* , and Takeo Ohnishi*

(* Nara Medical Univ.)

Keywords: X-ray, C-beam, human tongue squamous cell carcinoma. p53, apoptosis

To test p53-dependency in radiation cancer therapy with X-rays (low-linear energy transfer (LET)) or carbon-ion (C-) beams (high-LET heavy ion), we analyzed the radiation-induced growth rate and apoptosis induction in human tongue carcinomas transplanted into nude mice. The SAS cells transfected with mutant p53 gene (SAS/mp53) or a neo control gene (SAS/neo) were transplanted into the thigh of each nude mouse. By measuring the tumor weight (TW), tumor regrowth delay was evaluated when the relative tumor weight (RW) reached 5-fold that of the control group. Apoptosis was analyzed by immunohistochemical and ApopTag stainings.

We found SAS/mp53 tumors were more resistant to X-ray irradiation than SAS/neo tumors, but not to C-beam irradiation. The relative biological effectiveness (RBE) of C-beams compared to X-rays was 2.1 in SAS/neo tumors and 2.6 in SAS/mp53 tumors. Apoptotic cells were more frequently observed in SAS/neo tumors than in SAS/mp53 tumors in X-ray irradiation but not in C-beam irradiation. The radiation-induced growth inhibition of transplanted SAS cells is suggested to be p53-dependent in X-ray irradiation but not in C-beam irradiation. C-beams are proposed as being useful for cancer radiation therapy regardless of p53 gene status.

Publication:

Asakawa I, Yoshimura H, Takahashi A, Ohnishi K, Nakagawa H, Ota I, Furusawa Y, Tamamoto T, Ohishi H, and Ohnishi T.: *Anticancer Res.* **22**, 2037-2043, 2002.

33. Granulocyte-Macrophage Colony-Stimulating Factor Controls the Proliferation and Differentiation of Mouse Epidermal Melanocytes from Pigmented Induced by Ultraviolet Radiation B

Tomohisa Hirobe

Keywords: *melanocyte, keratinocyte, UVB, proliferation, differentiation*

Repeated exposures of ultraviolet radiation B (UVB) on the dorsal skin of hairless mice are known to induce pigmented spots long after the cessation of UVB irradiation. It has been shown that the proliferation and differentiation of epidermal melanocytes from UVB-induced pigmented spots are greatly stimulated, and the stimulations are regulated by keratinocytes rather than melanocytes themselves by using a serum-free culture medium. In this study, to make clear what factors derived from keratinocytes are involved in regulating the proliferation and differentiation of epidermal melanocytes, growth factors were supplemented to the media, and tested for their proliferation- and differentiation-stimulating activities. Of lots of factors tested, granulocyte-macrophage colony-stimulating factor (GMCSF) was effective. Pure cultured primary melanoblasts and melanocytes with a melanoblast-proliferation medium were further cultured with a melanocyte-proliferation media supplemented with GMCSF from 14 days (keratinocyte depletion). GMCSF induced the proliferation and differentiation of melanocytes in keratinocyte-depleted cultures. Anti-GMCSF antibody supplemented to the media inhibited the proliferation of melanoblasts and melanocytes as well as the differentiation of melanocytes from UVB-induced pigmented spots of irradiated mice, but (III-B-5)

not from non-irradiated mice. Enzyme-linked immunosorbent assay of cultured media revealed that GMCSF secreted from irradiated keratinocytes was much greater than that secreted from non-irradiated mice. Moreover, the expression of GMCSF protein was observed in pigmented spots, but not in normal skin areas of irradiated mice. These results suggest that GMCSF is one of the keratinocyte-derived factors involved in regulating the proliferation and differentiation of mouse epidermal melanocytes from UVB-induced pigmented spots.

Publications:

1) Hirobe, T., Kawa, Y., Mizoguchi, M., Ito, S., and Wakamatsu, K.: *J. Exp. Zool.*, **292**, 351-366, 2002.
2) Hirobe, T., Wakamatsu, K., Ito, S., Abe, H., Kawa, Y., and Mizoguchi, M.: *J. Cell. Physiol*., **191**, 162-172, 2002.
3) Hirobe, T.: *J. Cell. Physiol*., **192**, 315-326, 2002.
4) Furuya, R., Akiu, S., Ideta, R., Naganuma, M., Fukuda, M., and Hirobe, T: *Pigment Cell Res*., **15**, 348-356, 2002.
5) Hirobe, T., Furuya, R., Akiu, S., Ifuku, O., and Fukuda, M.: *Pigment Cell Res*., **15**, 391-399, 2002.

34. Effects of Mutations in Ku80 Proteins on Ku-dependent DNA Repair

Koike, M.: J. Radiat. Res. 43, 223-236, 2002.

Manabu Koike and Aki Koike

Keywords: Ku70, Ku80, DNA repair, GFP, localization

The Ku protein is a complex of two subunits, Ku70 and Ku80, and it was originally identified as an autoantigen recognized by the sera of patients with autoimmune diseases. The Ku protein plays a key role in multiple nuclear processes, e.g., DNA repair, chromosome maintenance, replication, transcription regulation, and V(D)J recombination. The mechanism underlying the regulation of all the diverse functions of Ku is still unclear, although it seems that Ku is a multifunctional protein that works in nuclei. On the other hand, several studies have reported cytoplasmic or cell surface localization of Ku in various cell types. To clarify the fundamental characteristics of Ku, we examined the expression, heterodimerization, subcellular localization, chromosome location, and molecular mechanisms of the nuclear transport of Ku70 and Ku80. The mechanism that regulates for nuclear localization of Ku70 and Ku80 appears to play, at least in part, a key role in regulating the physiological function of Ku in vivo. We have generated cell lines expressing the human Ku80 tagged with the green fluorescent protein (GFP) color variants. The tagged Ku80 complements a deficiency in Ku-deficient mammalian cells. Therefore, these cells should prove useful in the analysis of the function of Ku in living cells. We are also investigating the effects of mutations in the Ku80 proteins on Ku-dependent DNA repair.

Publication:

35. Role of Reactive Oxygen Species in Cells Overexpressing Manganese Superoxide Dismutase

Makoto Akashi, Toshiyasu Hiarama, Humiaki Nakayama, Misao Hachiya, Saori Kawamura, Hisayoshi Kondo, Yasunari Takada, Sang-Hee Park and Daisaku Takai

KeyWords: manganese superoxide dismutase (MnSOD), reactive oxygen species (ROS), p38MAPK, radioresistance

Manganese superoxide dismutase (MnSOD) catalyzes the dismutation of superoxide anions (O_2^-) into hydrogen peroxide (H_2O_2). We altered the intracellular status of reactive oxygen species by introducing human MnSOD cDNA into the human ovarian cancer cell line SK-OV-3. The overexpression of MnSOD inhibited cell growth and induced a concomitant increase in the level of H_2O_2 in SK-OV-3 cells. The cells overexpressing MnSOD were more resistant to irradiation than parental cells. MnSOD overexpression shortened the G_2-M duration in irradiated cells. Either inhibition of p38 mitogen-activated protein kinase (p38MAPK) or scavenging free radicals blocked the induction of radioresistance by MnSOD and also abolished the shortening of the G_2-M duration with concomitant inhibition of p38MAPK phosphorylation. Irradiation increased the generation of H_2O_2 even more in these transfectants. These results suggest that the accumulated H_2O_2 potentiated the activation of p38MAPK after irradiation in cells overexpressing MnSOD, which led to the protection of cells from irradiation-mediated cell death through the G_2-M checkpoint. SK-OV-3 cells had no constitutive expression of p53, and the overexpression of MnSOD and/or irradiation did not induce p53 or $p21^{WAF1}$, which causes cell cycle arrest. Thus, our results suggest that MnSOD alters the cell cycle progression of irradiated cells independently of p53 and $p21^{WAF1}$.

Publication:
Takada,Y., Hachiya,M., Park,S.H. and Akashi,M.:*Mol.Cancer Res.*,**1**,137-146,2002..

36. Influence of Nitric Oxide on Cell-Cell Junctions of Mouse Mammary Epithelial Cells

Mami Onoda-Miyoshi, Takanori Katsube and Makoto Onoda

***Keywords*:** nitric oxide, tight junction, occludin, ZO-1, mammary grand, HC11 cell

Nitric oxide (NO) is an important biological molecule that is responsible for cell signaling and physiological action in a number of mammalian tissues. It is now well recognized that mammalian cells produce NO from the amino acid L-arginine with a family of NO synthase (NOS) enzymes. NOS has at least three distinct isoforms, including the neuronal (nNOS), inducible (iNOS), and endothelial (eNOS) types, and the isoforms are now known to distribute across a wide spectrum of cell types and tissues. Recently, we demonstrated that three isoforms of NOS are present not only in the endothelium of blood vessels but also in the parenchymal cells of the rat mammary gland, such as epithelial cells and myoepithelial cells. On the other hand, our previous studies have shown that irradiation of developed mammary glands in rats during pregnancy or lactation induces mammary glands tumors at a higher incidence than in irradiated virgin rats. In addition, a selective inhibitor of iNOS and NO-specific scavenger prevent radiation-induced rat mammary tumors. Therefore, the radiation-induced initiation of mammary tumorigenesis may be partly caused by excessive NO produced by radiation-induced iNOS.

All epithelia serve as selective permeability barriers, separating fluids on either side that have a different chemical composition. This function requires that the adjacent cells be sealed together by occluding junctions. Tight junctions (TJ) comprised of several proteins have this barrier role in vertebrates. This complex includes members of a protein family related to tumor suppression and signal transduction. Therefore, it is plausible that disorder of TJ induced in pathophyiological statuses could be a cause of tumorigenesis. In this context, we undertook an investigation whether nitric oxide (NO) influences tight junctions formed in the mammary epithelium to elucidate the relationship between the retainment of barrier function of mammary epithelium and initiation of mammary tumorigenesis by NO in a culture system of the mouse mammary epithelial cell line (HC11).

Exposure to NO released from a NO donor, NOC18 (400 _ M), caused an acceleration of HC11 cell-detachment from the surface of culture plate in a time-dependent manner (Table 1). However, there was no difference in the proportion of trypan blue-dye exclusion by the detached cells in between non-treated and NOC18-treated HC11 cell cultures (Table 1). Neither leakage of the lactate dehydrogenase nor the chromatin condensation was detected in the cultures treated with NOC18, whereas, exogenous NO inhibited the mitochondrial metabolic activity of HC11 cells. Immunostaining for tight juncion (TJ)-associated proteins, such as occludin and ZO-1 showed honeycomb-like distribution around the cell periphery and colocalized with TJ-associated actin filaments in the region of cell-cell junctional complex on non-treated HC11 cells (Figs. 19A and C). This distribution of occludin and ZO-1 was partially or entirely disrupted by the incubation of the cell monolayer for 48 h with NOC18 (Fig. 19B. and D). Furthermore, expression of both occludin and ZO-1in the cell lysate fraction obtained from NOC18 treated HC11 cells remarkably declined by 56 ± 3 % and 34 ± 8 %, respectively, in comparison with those of control cell extract. These results suggest that excessive NO produced under the successive pathophysiological statuses affects the function of TJ-associated proteins in mammary epithelial cells, and

triggers instability and dysfuction of cell-to-cell adhesion. Hence, in turn such inappropriate circumstances elicited by NO might cause the disorder of development and differentiation of epithelial cells in the mammary glands, which agree with the initiation process of mammary tumorigenesis.

Table 1. Effect of NOC18 on adhesion of HC11 cells monolayer, and viability of detached cells in NOC18-treated cultures.[a)]

	Detached cells number (x 10^6 cells/well)[b)]		Viability of detached cells (%)[b)]	
	24 h	48 h	24 h	48 h
Control	0.099 ± 0.017	0.176 ± 0.017	72 ± 2	65 ± 7
with NOC18 (400 _M)	0.136 ± 0.009[c)]	0.259 ± 0.017[c)]	72 ± 3	63 ± 8

a): Confluent monolayer of HC11 cells was cultured with growth medium containing cytosine arabinoside (1 _ g/ml) for 24 h prior to the treatment with NOC18 (400 _ M). The culture then continued for the indicated periods in growth medium with NOC18 and cytosine arabinoside. The number of cells in each well was (1.82 ± 0.07) x 10^6 cells at the time of NOC18 treatment.

b): Values represent mean ± SE obtained from three independent experiments. Each experiment contained 3-5 cultures per replicate.

c): Significant difference from control, $p < 0.01$.

Figure Legends

Fig. 19. Immunocytochemistry of tight j unction-associated proteins in HC11 cells treated with NOC18. HC11 cells were treated with (B and D) or without (A and C) NOC18 (400 _ M), and then subj ected to immunocytochemistry with specific antibodies against occludin (A, B) and Z O-1 (C, D), respectively. Photomicrographs were taken under either a fluoromicrosope (A - D) or a differential interference microscope (a - d).

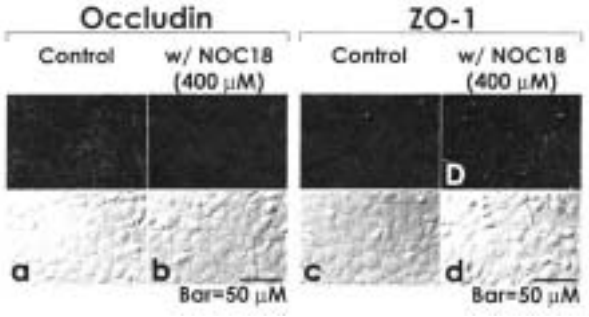

BIO-MEDICAL SCIENCES

Genetics

37. Risk Factors Associated with Adverse Effects of Radiotherapy on Skin among 125 Breast Cancer Patients - Multi-leaf Collimators, Histological Evaluation, Immobilization Devices, or Source Energy of Irradiation -

Mayumi Iwakawa, Shuhei Noda, Shinji Yoshinaga, Akiko Nishitani, Takayuki Nozaki,
Shigeru Yamada, Yoshinobu Harada and Takashi Imai

Keywords: radiotherapy, breast cancer, adverse effects, RadGenomics

Case-control studies are known to possess many advantages when analyzing polymorphisms of genes, including single nucleotide polymorphisms. To apply case-control studies to revealing correlations between genomic variability and sensitivity to radiation, the characteristics and clinical details of 125 breast cancer patients were analyzed, and the associations between these factors and adverse effects on skin during radiotherapy were investigated. Patients were clinically scored by grade defined using RTOG/EORTC (Radiation Therapy Oncology Group and European Organization for Research and Treatment of Cancer) grading system, and classified into two or three groups according to maximum grade within 6 months. Factors were then compared. Use of multi-leaf collimators, immobilization devices and photon-linac 6 were significantly associated ($p=0.008$, 0.008 and 0.020, respectively) with grouping as either radiosensitive or non-radiosensitive patients. Histological evaluation was significantly associated with classification as radioresistant or non-radioresistant ($p=0.021$). Use of multi-leaf collimators, immobilization devices and photon-linac 6 differed significantly between radiosensitive, radioresistant and control groups ($p=0.028$, 0.029 and 0.037, respectively). Other factors, such as total dose, total fraction, total duration, displayed no significant associations. These findings suggest that genetic factors rather than clinical situations are important for regulating radiosensitivity or radioresistance.

38. Chromosomal Instability and the Abrogated G2/M Arrest in X-irradiated MDS Cells

Sadayuki Ban, Hitomi Sudo, Masashi Sagara, Takashi Imai, Kenji Oda, Masaaki Noda, Ken Kuramoto, Hideo Tanaka, Akiro Kimura

Keywords: myelodysplastic syndrome (MDS), chromosome instability, G2/M arrest, radiation

A preliminary epidemiological study demonstrated that MDS has an excess relative risk per sievert of 13 in atomic bomb survivors in Hiroshima. MDS is the only other radiogenic blood disease apart from leukemia. Clinically, MDS involves dysplastic hematopoiesis and an increased risk of leukemic transformation. Because it is uncertain whether MDS pathogenesis affects lymphoid progenitor cells as well as myeloid progenitor cells, we investigated the karyotypes of bone marrow cells and the micronucleus (MN) frequency in peripheral T lymphocytes of atomic bomb survivors with MDS and normal healthy individuals.

Aneuploidy was observed in 10 of 23 patients. Chromosome aberrations were observed in 3 of 12 patients with mild symptoms, and 6 of 11 patients of severe symptoms. The spontaneous- and X-ray-induced-MN frequencies were significantly higher in MDS patients than in normal individuals. Interestingly, radiation sensitivity increased along with the severity of MDS clinical subtypes. Because many of the patients in this study had not been exposed to chemo- or radiation- therapy, their unusual radiosensitivity may be related to their chromosomal or genomic instability. Immortalized lymphoid cell lines were established from B-lymphocytes infected with Epstein-Barr virus *in vitro* and exposed to various doses of X rays. Immediately after EBV infection, EBNA-2 and EBNA-LP proteins are produced in host cells. EBNA-LP protein binds to the p53 and RB proteins and inactivates them. Because the G1 arrest in irradiated cells is controlled by p53, the G1 arrest is not observed in the EBV-infected normal B lymphoid cells. However, since p53 protein is not involved in the G2/M checkpoint, the cells arrested in G2/M phase can be observed in normal B lymphoid cells. The accumulation of cells in G2/M phase was larger in the irradiated normal B lymphoid cells than in the irradiated MDS B lymphoid cells.

Phosphorylation on serine 10 and serine 28 of histone 3 (H3) is an essential step for chromosome condensation at mitosis. Therefore, the cells with the phosphorylated H3 (P-H3) could be recognized as ones that are passed through the G2/M boundary. Cells with P-H3 could be detected with anti P-H3 antibody. Immediately after X-irradiations, decrease of the number of cells with P-H3 was observed in the normal B lymphoid cell population, but not in the MDS B lymphoid cell population. These results meant that the damaged MDS-B cells entered into the mitosis without delay at the G2/M boundary. Condensation of the damaged chromatin may cause various types of chromosome aberrations, such as acentric fragment, reciprocal translocation, dicentric chromosome etc. These chromosomal rearrangements may cause the unbalanced chromosomal segregation, leading to the chromosomal instability. Our data suggested that the control of chromosomal stability was impaired in pluripotent stem cells of MDS patients, and that the abrogated G2/M arrest may be involved in the pathophysiology of disease progression and the unusual radiation sensitivity of patients' blood cells.

39. γH2AX Foci Formation in X-irradiated Human Cells with Varying Radiosensitivity

Masashi Sagara, Sadayuki Ban, Hitomi Sudo, Ryuichi Okayasu, Yoshinobu Harada and Takashi Imai

Keywords: γH2AX, radiosensitivity, DSB

DNA double-strand breaks (DSBs) induced by ionizing radiation represent one of the most serious damages which can occur in living cells. Immediately after the DSB occurs, Ser-139 of histone H2AX in the vicinity of DSB is phosphorylated by the ATM kinase. The phosphorylated H2AX (γH2AX) can be observed as a focus with an immunohistochemical staining using anti-γH2AX antibody. It is also known that each focus corresponds to one DSB and remains until the DSB is rejoined.

Using the immunohistochemical method, we compared the amount of γH2AX at various times after X-irradiation among cell lines with different radiation sensitivities. Foci appeared in less than 3 min after 2Gy-irradiation. The number of foci reached the maximum at 30-60 min after irradiations. However, there was a clear difference in the reduction speed of foci between the radiosensitive cells and the radioresistant cells. Disappearance of foci in the radioresistant cell lines was faster than that in the radiosensitive ones. At 12 h after X-irradiation, few foci were observed in the radioresistant cells, while many foci remained in the radiosensitive cells. HCC1937 cells have mutations in BRCA1, and AT cells, in ATM. Ligase IV is defective in 180BR cells. BRCA1, ATM and ligase IV each play a key role in the repair pathways on DSBs. Therefore, these three cell lines have an unusual radiosensitivity. γH2AX study demonstrated that the DSB rejoining activity in these cell lines was lower than that in the normal human cells. We found that one of 32 esophagus cancer cell lines had an unusual radiosensitivity and reduced rejoining activity. Our preliminary data suggested that DNA-PKcs of this radiosensitive cell line might have genetic or epigenetic alteration. Our data suggested that the rejoining activity on DSBs roughly correlated with the cellular radiosensitivities. To predict the cellular radiosensitivity more precisely, we are trying to establish the method to quantitatively measure the amount of γH2AX.

40. Expression Profiles of Genes Related with Radiosensitivity Indicating Strain Difference in Three Strains of Mice

Shuhei Noda, Mayumi Iwakawa, Chisa Kitazawa, Toshie Ohta, Miyako Goto, Yoshinobu Harada and Takashi Imai

Keywords: *radiosensitivity, mouse, strain difference, microarray, expression profile*

It is well known that there is an interindividual difference in radiosusceptivity caused by genetic factors and side effects of radiotherapy are due to this difference. Analysis of murine strain differences might provide an alternative tool to reveal the mechanism of interindividual radiosensitivity.

Here we analyzed large-scale gene expression profiling of lung to reveal transcriptional regulation following irradiation. Three strains of A/J, C3H/HeMs (C3H) and C57BL/6J (B6) mice were irradiated in their thorax and transcriptome analysis of lung was performed at three time-points by means of cDNA microarray. Ratio of expression level between strains was calculated from the array result. 131 genes for C3H:B6 and 115 for A/J:B6 meet our screening criteria. It is interesting that there are some genes related to immune response or muscle fiber.

41. Gene Expression of Detoxifying Enzymes in AhR and Nrf2 Compound Null Mutant Mouse

Shuhei Noda, Nobuhiko Harada, Azumi Hida, Yoshiaki Fujii-Kuriyama, Hozumi Motohashi and Masayuki Yamamoto

Keywords: *xenobiotics, Phase I enzymes, Phase II enzymes, gene knock-out mouse, 3-methylchoranthrene, butylated hydroxyanisole, phenobarbital*

The arylhydrocarbon receptor (AhR) regulates the expression of cytochrome P450 (CYP)-1 gene family members which catalyse xenobiotic Phase I metabolism, while Nrf2 exerts the concerted regulation of Phase II enzyme genes. We generated AhR and Nrf2 compound null mutant mice to examine the integrated function of AhR- and Nrf2-regulated enzymes in detoxification. Furthermore, we used this mouse model, by administering three different classes of chemical inducers, to examine how xenobiotic metabolism may be influenced in the absence of signals transduced by AhR or Nrf2. The compound mutant mice responded only weakly to AhR ligand or Phase II inducer, while they displayed a clear response to phenobarbital, an inducer of the CYP2B family through another, unrelated transcription factor. Here, we report an initial characterization of the AhR-Nrf2 double mutant mice, which may serve as a simplified bioassay system to evaluate xenobiotic toxicity and metabolic biotransformation of various drugs and environmental chemicals.

42. Radiation-induced chromosomal instability in lymphocytes of cancer patients

Hitomi Sudo, Sadayuki Ban, Masashi Sagara, Chika Knonomi, Shuhei Noda, Yoshifumi Matsui, Mayumi Iwakawa, Yoshinobu Harada, John B. Cologne, and Takashi Imai;

Keywords: chromosomal instability, radiosensitivity, micronucleus assay, lymphocytes, cancer patient

When chromosomes or acentric chromosome fragments fail to be incorporated into the daughter nuclei during mitosis, they form micronuclei in the cytoplasm after one cell division. To discriminate the dividing cells and nondividing cells, the cytokinesis-blocked micronucleus (CBMN) assay was established by Fenech *et al.* The CBMN assay has been extensively used to evaluate the radiation sensitivity of human individuals. Using the CBMN assay, Scott *et al.* demonstrated that the radiation sensitivity of a fraction of breast cancer patients was higher than that of normal individual population. However, Vral *et al.* were very skeptical about the findings of Scott *et al*. The purpose of this work is to test the hypotheses that the chromosomal instability in cancer patients' cells is higher than that in healthy individuals' cells, and that the population of cancer patients may include more radiosensitive individuals than a general population. With the approval from the ethical committee of NIRS, peripheral blood was obtained from 46 normal healthy females (age; 21-58), 131 breast cancer patients (age; 28-74), 32 cervical cancer patients (age; 39-80) and 7 female head & neck cancer patients (age; 51-69). Radiosensitivity of T-lymphocyte was determined with an CBMN assay. Spontaneous MN frequencies in cancer patients were significantly higher than healthy individuals ($p < 0.001$). Radiation-induced MN frequencies of breast- and head & neck-cancer patients were significantly higher than normal individuals ($p < 0.001$). However, the induced MN frequencies of cervical cancer patients were significantly lower than those of healthy individuals ($p < 0.001$), though the statistical power was very weak because of small number of cases. We are considering that the HPV infection lowered the radiation sensitivity of immune-responsible cells, because it is widely believed that one key mechanism which leads to spontaneous micronucleus formation involves an imbalance of chromosomal segregation. Our results suggested the radiation-induced chromosomal instability in cancer patients' lymphocytes was greater than that in normal individuals' lymphocytes. Recently, several reports suggesting that the SNPs on DNA double-strand break repair genes affect the cancer susceptibility or cancer proneness have been published. Kuschel *et al* demonstrated that the ratios in two SNPs on *XRCC3* were significantly different between cancer patients and healthy females. Then, we can suppose that the SNPs variation in radiation-related genes with low penetrance may enhance the risk of mammary- and head & neck-tumorigenesis and the radiation susceptibility of patients' peripheral lymphocyte cells.

43. Developmental Responses of Two Substrains of in Vitro Fertilized C57BL/6J Mouse Embryos to Oxygen and Amino acids

Seiji Kito, Yoshiko Noguchi*, and Yuki Ohta*
(*Science Services)

Key words: *C57BL/6J inbred mice, in vitro development, mouse embryo*

Inbred C57BL/6 strain of mice is the most widely used inbred strain of mice for medical research. Establishment of embryo manipulation of this strain is advantageous for transgenic technology *i.e.* production of gene-modified mice. In this study, developmental response of *in vitro* fertilized embryos to oxygen and amino acids were compared between in-house bred C57BL/6JNrs (Nrs) and commercially available C57BL/6JSlc (Slc) mice. Under 20% oxygen, the percentage of embryos that developed to blastocysts and expanded blastocysts, and nuclear numbers were lower in Slc embryos than in Nrs embryos. Moreover, the nuclear number did not increase in Slc embryos during 72-96 h culture. Effects of amino acids were beneficial on development of Slc embryos under 20% oxygen, but inhibitory on blastocoel formation at 78 h under 5% oxygen. On the other hand, effects of amino acids on Nrs embryos were observed in nuclear number at 72 and 78 h culture under 5% oxygen. Because the present study showed differences in sensitivity to culture conditions between the C57BL/6J substrains, care must be taken in embryo manipulation of this inbred strain in studies of embryo development or other studies.

Publications:

Kito, S., Noguchi, Y., Tateno, S. and Ohta, Y.: *J. Mamm. Ova Res.*, 19, 32-38, 2002.

Kito, S., Noguchi, Y. and Ohta, Y.: *Exp. Ani.*, 52, 63-66, 2003.

44. Analysis of α-and β-tubulin Genes of *Bombyx mori* Using an EST Database

Kimihiko Sugaya, Hideki Kawasaki[1] and Kazuei Mita[2]
([1]Utsunomiya Univ.; [2]Natl. Inst. of Agrobiol. Sci.)

Keywords: *EST, expression, phylogenetic analysis, testis, wing disc*

Tubulin is one of the most widespread classes of multiprotein families and is well known to construct microtubules with two different subunits, α- and β-tubulin. In the course of genome analysis of *Bombyx mori*, we have constructed an EST-database by large-scale sequencing of clones that were randomly selected from cDNA libraries of various tissues and organs belonging to different developmental stages. Using this EST-database, we have identified four types of β-tubulin gene and three types of α-tubulin gene. Based on the analysis of deduced amino acid sequences, we have determined the phylogenetic relationships of tubulins between *Bombyx* and *Drosophila melanogaster* as well as two other moth species, suggesting that each tubulin is classified into at least three distinct subfamilies: a ubiquitously expressed one, a developmentally regulated one and a testis specific one.

45. Diminished Levels of Allelic Losses by Homologous Recombination in Radiation-hypersensitive Cells

Kouichi Tatsumi, Eiko Kubo, Yuko Hoki, Tomoko Ichikawa, Masahiko Mori,
Ryutaro Fukumura, Ryoko Araki, Ikuko Furuno, Akira Fujimori, Masumi Abe, Akira Tachibana[1], Akihiro Kurimasa[2] and Koki Sato[3]
([1]Kyoto Univ., Radiat. Biol. Ctr., [2]Tottori Univ., Fac. Med., [3]Kinki Univ., Fac. Biol. Tech.)

Keywords: APRT, Mitotic, recombination, LOH, XRCC7, 8AA-resistant

Mitotic recombination (MR) due to somatic crossing-over is a predominant mechanism for allelic losses in mammalian cells either spontaneous or radiation-induced. A selectable mutation assay accompanying real-time detection PCR was developed to analyze the second step in loss-of-function mutations, using a human lympho-blastoid cell line derived from an obligate heterozygote of 2,8-dihydroxyadenine urolithiasis, adenine-phospho-ribosyltrans-ferase (APRT) deficiency with a nonsense mutation at exon 3 of the gene. 68 % of spontaneously arising 2,6-diaminopurine resistance (DAP^r) mutant clones were associated with loss of heterozygosity (LOH), while 92 % of 2 Gy gamma-ray induced mutant clones were so associated. Investigation of gene dosage revealed that about one half of the spontaneously arising mutant clones and two-thirds of those induced by gamma-rays showed reduction to homozygosity of the constitutionally inactivated *APRT* allele. In an ataxia telangiectasia (AT) cell subline in which a new inactivation mutation had been introduced into one *APRT* allele by ICR-191, MR rarely occurred and deletion exclusively predominated in both spontaneous and X-ray induced DAP^r with LOH. A similar assay system was also developed with C3H mouse FM3A mammary tumor cells, SR-1, carrying a C->T transition at exon 5 of one *APRT* allele. In an XRCC7 (DNA-PK) deficient subline of SR-1, SX9, spontaneous mutation frequencies for the *Aprt* locus ($8AA^r$) was 10^{-3}, which was about 10 times higher than that in parental SR-1 cells. Mutation frequencies induced by X-rays increased comparably in a dose-dependent manner for the *Aprt* locus in both cell lines. Against our expectation, the lack of an NHEJ pathway for DNA double strand break repair caused a lower proportion (11.1 %) of MR with deletions (77.8 %) as the major molecular cause for $8AA^r$ mutation, while virtually all $8AA^r$ mutant clones were MR in the control SR-1 cells. Factors influencing the mode and the proportion of MR together with their biologically purposeful regulations should be further pursued, since this type of genetic event can well be a rate-limiting step of radiation carcinogenesis.

BIO-MEDICAL SCIENCES

Immunology, Pathology and Physiology

46. Polymerase Chain Reaction with a Primer Pair in the 16S-23S rRNA Spacer Region for Detection of *Mycoplasma pulmonis* in Clinical Isolates

Hiromi Takahashi-Omoe, Katsuhiko Omoe[1], Satoru Matsushita, Hideki Kobayashi[2] and Koshi Yamamoto[2]
([1]Iwate Univ. ; [2]NIAH)

Keywords: *Mycoplasma pulmonis (M. pulmonis), 16S-23S rRNA intergenic spacer region (SR), polymerase chain reaction (PCR)*

To develop a diagnostic tool to identify *Mycoplasma pulmonis* (*M. pulmonis*) in clinical isolates, we developed a polymerase chain reaction (PCR) assay using primers specific for the 16S-23S rRNA intergenic spacer region (SR) of *M. pulmonis.* One pair of PCR primers reacted specifically with two reference strains of *M. pulmonis* tested and seven samples isolated from naturally infected rats. The primer pair did not produce PCR products of the correct size from any other rodent or human mycoplasmas or cellular DNA from rodent lung. Specificity of the PCR assay was confirmed by Southern blotting with probe specific for the SR of *M. pulmonis*. The PCR assay for detection of *M. pulmonis* established in this study is suitable for diagnosis of *M. pulmonis* infection in clinical cases.

Publication:

Takahashi-Omoe, H., Omoe, K., Sakaguchi, M., Kameoka Y., Matsushita, S., Inada, T.: *Comp. Immunol. Microbiol. Infect. Dis.* (in press).

47. Analysis of Protein Expression by Mammalian Cell Lines Stably Expressing Lactate Dehydrogenase-Elevating Virus ORF 5 and ORF 6 Proteins

Hiromi Takahashi-Omoe, Katsuhiko Omoe[1], Masahiro Sakaguchi[2], Yosuke Kameoka[2], Satoru Matsushita and Toshiki Inada[2]
([1]Iwate Univ.; [2]NIID)

Keywords: lactate dehydrogenase-elevating virus (LDV), ORF5, ORF6; VP-3, M/VP-2, stable expression

Lactate dehydrogenase-elevating virus (LDV) has a strict species-specificity. Because only a subset of mouse primary macrophages has been identified that can support LDV replication *in vitro*, the precise molecular mechanism of viral entry and replication remains unclear. To analyze the LDV envelope proteins, which probably mediate viral attachment to the host cell, we developed a mammalian system for stable co-expression of LDV open reading frame (ORF) 5- and ORF 6-encoded proteins (ORF 5 and ORF 6 proteins), which correspond to envelope VP-3 and M/VP-2, respectively, and compared these expressed proteins to the native ones. Western blotting analysis combined with *N*-glycanase digestion revealed that ORF 5 and ORF 6 proteins were similar in size to native VP-3 and M/VP-2, and that ORF 5 protein was *N*-glycosylated, like the native VP-3. Immunofluorescence microscopy revealed that both ORF 5 and ORF 6 proteins were distributed throughout the cytoplasm and were colocalized in most cells. Moreover, ORF 5 protein was localized both in the perinuclear region and the Golgi complex and transported to the cell surface. This mammalian expression system in which the exogenously expressed proteins closely resemble the native proteins will provide the experimental basis for further studies of the interactions between LDV envelope proteins and host cells.

Publications:

1) Takahashi-Omoe, H., Omoe, K., Sakaguchi, M., Kameoka Y., Matsushita, S., Inada, T.: *Comp. Immunol. Microbiol. Infect. Dis.* (in press).
2) Takahashi-Omoe, H., Omoe, K., Sakaguchi, M., Kameoka Y., Matsushita, S., Inada, T.: *Comp. Immunol. Microbiol. Infect. Dis.* (in press).

48. Murine Pre-B-Cell Lymphomas Following Injection of Plutonium Citrate in Comparison to MNU-Induced T-Lymphoblastic Lymphomas

Yoichi Oghiso and Yutaka Yamada

***Keywords**: lymphoma, immunohistochemistry, strain difference, alpha particle, alkylating agent*

Internal radiation exposures by bone-seeking radionuclides occasionally induce malignant and systemic lymphomas in mice other than specific osteosarcomas, although the entity of their pathological features and differences from those by external radiation exposures or chemical carcinogens are not fully elucidated. Lymphoid neoplasms occurring in three different (C3H/He, C57BL/6, and B6C3F1) strains of female mice after injection of the bone-seeking and alpha-emitting radionuclide, ^{239}Pu citrate, were compared by immunohistochemistry with those from the alkylating agent, N-methyl-N-nitrosourea (MNU)-injected mice. There was a variety of phenotypes from either T-cell to B-cell or histiocytic lineages in lymphoid neoplasms of the control, saline-injected mice from three strains. While strain differences were noted in the incidence and proportion, many lymphoid neoplasms occurring early after ^{239}Pu-injection were, however, characterized by B220 $^{+}$ phenotypes but negative for both T-cell-specific markers (Thy 1, CD3) and B-cell markers (CD5, CD19, CD79b) to be classified into pre-B-cell lymphomas derived from progenitor B-cells. In contrast, almost all the MNU-induced lymphomas were shown to be CD3 $^{+}$ or rarely Thy 1 $^{+}$, and B220 $^{-}$ T-lymphoblastic lymphomas. These results indicate differences in immunophenotypic expression but also might reflect different carcinogenic processes between chemical- and radiation-induced murine lymphomas.

Publication:
Oghiso, Y. and Yamada, Y.: J. Toxicol. Pathol., **16**, 93-102, 2003.

49 Life Span and Spontaneous Tumors Incidence of the Wistar Mishima (WM/MsNrs) rat

Satoshi Fukuda and Haruzo Iida

Keywords*: life span, spontaneous tumor, Wistar Mishima (WM/nrs) rat*

The life spans and spontaneous tumors in a total of 1960 Wistar Mishima (WM/Nrs) rats, inbred strain, at 80-130 th generations were examined. The average life span (mean ± SD) was 731 ± 173 days (n = 1053) in the males and 813 ± 214 days (n = 907) in the females ($p<0.0001$). The average life span of the tumors-afflicted females was significantly longer than that in the non-tumor group ($p<0.0001$), while no such difference was observed in males. Tumors were observed in 33 males (3.1%) and 246 females (27.1%). In the males, tumors were often observed under the skin (2.2%). Frequencies of tumors in lung and liver, bones and intestine were less than 0.5 %. In the females, incidence of mammary tumors was 20.1%, and various organs such as ovaries, uterus, bones, lung, and liver had frequencies of less than 3.5 %. It is concluded that WM/Nrs rats might be suitable for life span and age-related studies because of the characteristics of length of longevity and low incidence of spontaneous tumors of both sexes.

Publication:
Fukuda, S. and Iida, H.*: Exp. Anim.* **52**, 173-178, 2003.

BIO-MEDICAL SCIENCES

Radiotoxicology

50. Spin Trapping Reagents as Radioprotectors against Whole Body X-Ray Irradiation of Mice

Kazunori Anzai, Masako Furuse, Azusa Matsuyama and Nobuo Ikota

Keywords: spin trapping, radioprotector, X-ray irradiation, mouse

Spin trapping reagents are used for ESR measurements of short-lived free radicals by extending the lifetime of the radicals via formation of spin adducts. Since the spin trapping reagents react with free radicals, they can be regarded as scavengers of free radicals from another viewpoint. They may function as antioxidants to protect injuries related to reactive oxygen species. In the present study, therefore, we examined *in vivo* radioprotection of spin trapping reagents against whole body X-irradiation of mice. The reagents examined are DMPO (5,5-dimethyl-1-pyrroline-N-oxide), DEPMPO (5-diethoxyphosphoryl-5-methyl-1-pyrroline-N-oxide), PBN (N-*t*-butyl- α -phenylnitrone), and POBN (α -(4-pyridyl-1-oxide)-N-*t*-butylnitrone) as shown in Fig. 19.

The spin trapping reagents were administered intraperitoneally to mice (C3H, male, 10 weeks old) and the mice were irradiated with X-rays at the total radiation dose of 8.0 Gy with the radiation dose rate of 0.6 Gy/min. PBN and POBN showed significant radioprotection, whereas DMPO and DEPMPO showed only slight radioprotection. The radioprotection by POBN was dose-dependent and the dose of 450 mg/kg, which shows no acute toxicity, was chosen as the standard dose for later experiments. POBN injected at 60-120 min before the X-ray irradiation showed the highest radioprotective activity, whereas injection after the X-ray irradiation showed no effect. Dose reduction factor (DRF) of POBN administered at 450 mg/kg was measured as 1.3.

Since the radioprotection is observed only when the reagents were administered before the irradiation, the primary action of the spin trapping reagents may be quenching of the free radicals. However, the effect is different among the reagents examined although the spin trapping activity of them is not very different and relatively long period before the irradiation is required for the protective effect. Therefore, some pharmacological action in addition to the radical quenching might be responsible for the radioprotection.

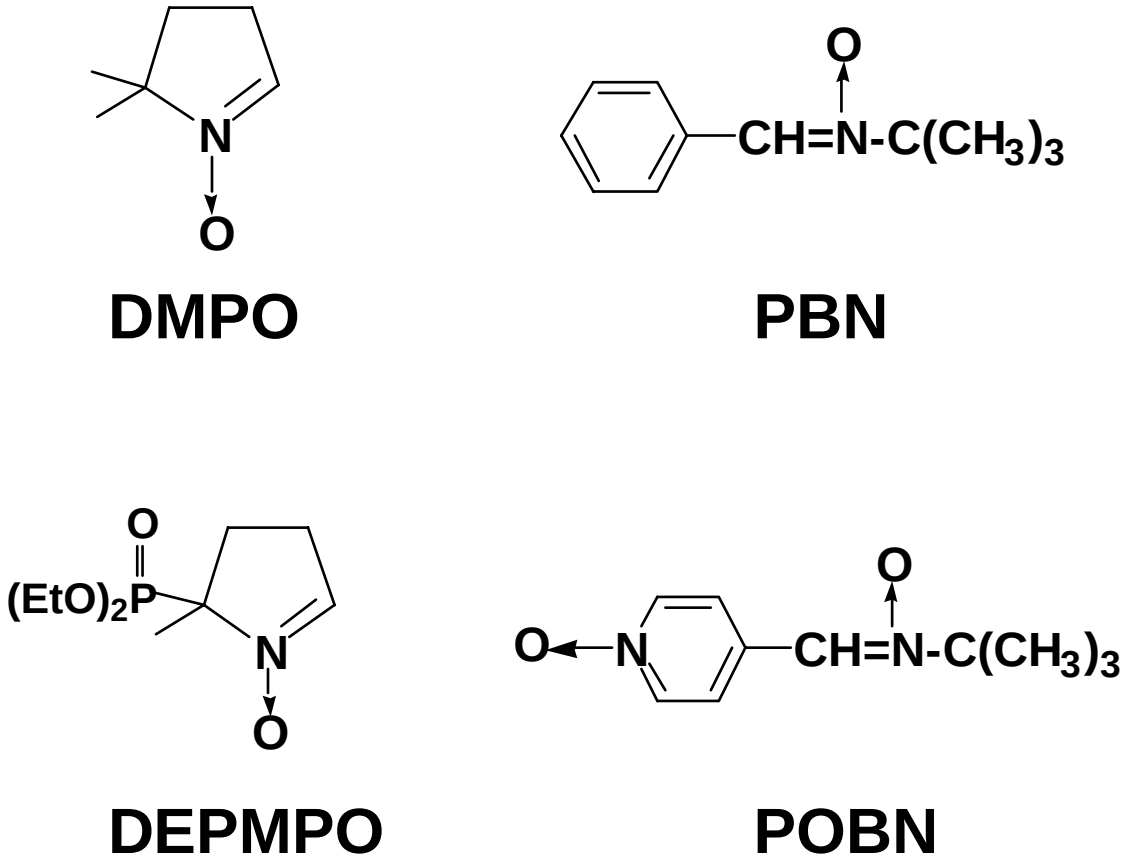

Fig. 19. Structure of spin trapping reagents used in this study.

51. Adaptive Response in Embryogenesis: V. Existence of Two Dose-Rate Ranges for the Same Priming Dose to Adapt Fetal Mice

Bing Wang, Harumi Ohyama, Yi Shang, Masako Nose, Tetsuo Nakajiama, Osami Yukawa and Isamu Hayata

Keywords: embryogenesis, radiation, adaptive response, dose-rate range, mouse

Radioadaptive response (AR) manifests an important phenomenon in radiobiology. Research on the essential conditions for RA induction is of critical significance, and has with an impact on understanding novel biodefense mechanisms against hazardous effects from irradiation. This paper reports the first time evidence on the existence of two dose-rate ranges for the same priming dose of irradiation to successfully induce the AR *in uterus* in fetal mice. A dose of 0.30 Gy given to the fetuses on embryonic day 11 (E11) was adopted as the priming dose according to our previous study. A dose of 3.50 Gy administered to the fetuses on E12, which alone could lead to the death of all neonates within the first postnatal week, was chosen as the challenging dose. Induction of apoptosis in the predigital regions of fetal limb buds, incidences of fetal limb malformations and prenatal fetal death, and postnatal survival of neonates were employed as the biological endpoints. The dose-rate effects in a range from 0.06 Gy/min to 5.00 Gy/min of the priming irradiation on RA induction were investigated. The effectiveness of AR induction was correlated to the dose rate in neither a normal nor a reverse dose-rate effect manner, namely, priming irradiation at a dose-rate range either from 0.18 to 0.98 Gy/min or from 3.50 to 4.20 Gy/min could successfully adapt the fetuses, while giving another dose rate always lead to failed AR induction. Results indicated that dose rate of priming irradiation played a crucial role in AR induction. These findings provided specific information on dose rate to complement the current understanding of AR induction and they suggested that influence of dose rate should be taken into consideration regarding making radiotherapeutic protocols as well as setting standards of radiation protection.

52. Radiation-Induced Teratogenesis in the Late Period of Organogenesis in Mice: Dose Rate Effects

Bing Wang, Harumi Ohyama, Yi Shang, Kaoru Tanaka, Shiro Aizawa and Isamu Hayata

Keywords: *dose-rate effect, apoptosis, teratogenesis, organogenesis, mouse*

The irradiation of fetuses at the late period of organogenesis has been known to induce a dramatic increase in malformations. The mechanisms involved, however, have remained unclear. Using the mouse limb bud system, we first found that radiation-induced apoptosis is involved in the induction of limb malformation, namely, radiation-induced apoptosis in the predigital regions of embryonic limb buds is responsible for digital defects in mice. To investigate the possible dose-rate effects on these radiation-induced phenomena, 3.5 Gy of X-rays at dose rates ranging from 0.06 to 5.00 Gy/min was given to ICR mice on gestation day 12. The dose rate of radiation dramatically affected the consequences of the experiment. Percentages of alive fetuses, malformed fetuses among the alive fetuses, and postnatal survival were significantly higher in the ICR mice irradiated with 3.5 Gy at the dose rates from 2.82 to 3.50 Gy/min when compared to those that received the same dose but at other dose rates. The biological effect as a function of dose rate appeared like a U shape curve. This phenomenon could not be described or evaluated by calculating the dose-rate effectiveness factor. Contrary to both normal and inverse dose-rate effects, which have a regular order of tendency, the dose-rate effects observed in the present study seemed to have an irregular order. As the duration of irradiation at different dose rates in the present study was within 1 h, the results could hardly be simply attributed to the change of cell kinetics. Further studies need to be done on the mechanisms underlying the phenomenon.

53. Comparative Study on *Tp53* Mutations in Rat Lung Tumors Induced by Inhalation Exposure to Alpha Emitters and X-ray Irradiation

Yutaka Yamada, Yoichi Oghiso, Shingo Nakamura[1], Jean-Paul Morlier[2], Kristell Guillet[3], Paul Fritsch[3], Nicolas Dudoignon[4] and Georges Monchaux[4]

([1]IES; [2]LCE/DRR/CEA; [3]LRT/DRR/CEA; [4]IRSN, France)

Keywords: *Tp53, mutation, plutonium, neptunium, radon, X-ray irradiation, rat, lung tumor*

The purpose of this study is to compare the frequency and type of *Tp53* mutations in rat lung tumors after inhalation exposures to three different alpha-emitters, $^{239}PuO_2$ (Pu), $^{237}NpO_2$ (Np) and ^{222}Rn (Rn). In addition, *Tp53* mutations of X-ray-induced lung tumors are also compared with the high LET radiation-induced tumors. Genomic DNA was extracted from tumor sites of paraffin-embedded sections of the tumors. Exon 5 to 8 of *Tp53* were amplified individually from the extracted DNA by PCR method. The exons were amplified in 16 cases of Pu-, 22 cases of Np-, 15 cases of Rn- and 33 cases of X-ray-induced tumors, respectively. PCR products were analyzed for mutations utilizing SSCP and direct sequencing method. Point mutations within exon 6 at codon 219 (G to A transition) and exon 8 at codon 266 (C to T transition) were detected from Pu-induced tumors. Only one point mutation was found in Np-induced tumors within exon 5 at codon 175 (C to T transition) and in X-ray-induced tumors within exon 6 at codon 224 (C to T transition). No mutations, however, were found in Rn-induced tumors (See Table 2). These results indicate that the mutation frequencies of the *Tp53* are inconsistent among the rat lung tumors induced by different irradiation, and G:C to A:T transition is a common mutation in *Tp53* of the tumors. The fact that low frequencies of *Tp53* mutation were observed in the radiation-induced lung tumors indicates that the abnormalities of the *Tp53* might not be so critical for the pulmonary carcinogenesis, although other carcinogenic process for genetic and/or epigenetic changes might also be related to the rat lung tumors induced by alpha-emitters and X-rays.

Yutaka Yamada,
Internal Radiation Effects Research Group

Table 2. *Tp53* mutation in rat lung tumors after inhalation of alpha emitters and X-ray irradiation

Radiation source	No. examined by PCR-SSCP	No. of mutations in direct sequences (%)	Mutation types
$^{239}PuO_2$	**16**	**2 (12.5)**	Exon 6: codon 219, GAG-AAG Exon 8: codon 266, GAC-GAT
$^{237}NpO_2$	**22**	**1 (4.5)**	Exon 5: codon 175, CCC-TCC
^{222}Rn (+BNF)	**15**	**0 (0)**	
X-ray	**33**	**1 (3.0)**	Exon 6: codon 224, GGC-GGT

(BNF: beta-naphthoflavone)

54. Pulmonary Carcinogenesis in the Rat Following Inhalation Exposure to Plutonium Dioxide in Comparison to X-ray Irradiation

Yoichi Oghiso and Yutaka Yamada

***Keywords**: lung tumor, rat, ^{239}Pu, X-ray, relative effectiveness*

Radiation-induced pulmonary carcinogenesis was compared in a total of 1,200 female Wistar rats following either inhalation exposure to alpha-emitting $^{239}PuO2$ aerosols, or whole-body and thoracic X-ray irradiation. No significant differences from the unexposed control rats in survival periods and lung carcinoma induction were observed at the lowest dose of 0.16 Gy in ^{239}Pu-exposed rats, but dose-dependent survival reduction was correlated with increased malignant lung carcinomas at the doses over 0.45 Gy, reaching the maximum incidence of 90 % at 6.6 Gy. While differential dose responses for each histopathological type of tumors were noted, almost 70-80 % were carcinomas among all the primary tumors from ^{239}Pu-exposed rats. As the dose response curves for lung carcinomas were compared, the slope of the fit linear equation and the calculated relative effectiveness for 50 % incidence of lung carcinomas were approximately 11 times as high in ^{239}Pu-exposure as those of thoracic X-irradiation. The numbers of tumor lesions distributed in the lung per tumor-bearing animal were about 2-fold more in ^{239}Pu-exposed rats, while the proportions of their histopathological types were almost similar between ^{239}Pu-exposure and X-irradiation. These results indicate that magnitudes of relative effectiveness or risk for pulmonary carcinogenesis are greater in ^{239}Pu-exposure than X-irradiation, and that radiation-induced lung tumor types appear to originate mostly from the same target epithelial cells.

Publications:

1) Oghiso, Y. and Yamada, Y.: J. Radiat. Res. **43**, 301-311, 2002.

2) Oghiso, Y. and Yamada, Y.: J. Radiat. Res. **44**, 271-280, 2003.

55. Specific Induction of Osteosarcomas in Different Mouse Strains Following Injection of Plutonium Citrate

Yoichi Oghiso and Yutaka Yamada

***Keywords**: bone tumor, soluble ^{239}Pu, strain difference, mouse*

Lifetime bone tumor induction by injection of a bone-seeking alpha-emitter, ^{239}Pu citrate, was compared among a total of 630 female mice from three strains (C3H/He, C57BL/6 and B6C3F1) showing different genetic background for spontaneous and radiation carcinogenesis. Bone tumors, mostly osteosarcomas, appeared relatively early during the periods from 200 to 600 days after the injection of ^{239}Pu, showing an almost similar dose responsiveness with a peak incidence of 50 - 63 % at the skeletal doses of 2-3 Gy, in all the strains of mice. The primary sites of bone tumors from these strains of mice were also predominantly distributed in 80 - 90 % of the skeletal bones including vertebra, femur and tibia which had well-developed trabecular bone surfaces and large vascular sinusoids. Histological appearances of osteosarcomas from three strains of mice were commonly characterized by an irregular growth of osteoblasts along or inside endosteal bone surfaces accompanied by trabecular bone formation. The frequency of lymphoid neoplasms was significantly lower than the control levels, while some appeared earlier at the higher injected doses than those of the controls. Fewer or no myeloid leukemias were found in all the control and ^{239}Pu-injected animals, and the incidences of other solid tumors rather decreased, reaching zero at doses where the maximum incidences of bone tumors were noted. These findings indicate that osteosarcoma is the only specific tumor commonly observed among different mouse strains following the injection of soluble plutonium compounds.

Publication:

Oghiso, Y. and Yamada, Y.: J. Radiat. Res. **44**, 125-132, 2003.

56. Induction of DNA Double Strand Breaks in Scid Cells by Carbon Ions

Tatsuya Shimasaki*, Makoto Ihara*, Yoshiya Furusawa, and Yutaka Okumura*
(*Kumamot Univ.)

Keywords: DNA double strand break, scid cell, DNA-PK, repair, high-LET radiation

The DNA double strand breaks (DSBs) induced by X-ray and carbon ion beam irradiation in scid cells were analysed using pulsed-field gel electrophoresis. Scid cells and hybrid cells were ideal to study the DNA DSB repair mechanisms, because their genetic backgrounds were identical except DNA-PK activity. Induction of DNA DSBs was determined after exposure to X-rays and carbon beams. DNA DSB repair was by biphasic kinetics with a fast and a slow component. For scid cells only a slow component was observed, whereas the kinetics of DSBs repair was biphasic with a fast and a slow component. It was concluded from the experimental data that the induced DSB rejoining in scid cells was due to the lack of DNA-PK activity.

Publication:

Shimasaki, T., Ihara, M., Furusawa, Y., and Okumura, Y.: *Radiat. Protec. Dosim.* **99**, 155-157, 2002.

57. Effects of a Human Dose of Ca-DTPA on Removal of Different Amounts of Plutonium from the Rat

Satoshi Fukuda, Xuemig Yan and Haruzo Iida

Keywords: *daily recommended human dose of Ca-DTPA, plutonium removal, chelation therapy, rat, urinary plutonium excretion*

The effects of the daily recommended human dose (1 g per 70 kg body weight=30 mol/kg) of calcium diethylentriaminepentaacetic acid (Ca-DTPA) on removal of plutonium from rats injected with different amounts of plutonium were examined. Sixty female wistar rats were preinjected with doses of 0.185, 0.37 and 3.7 x10^5 Bq/kg of plutonium as a nitrate, and half of the rats of each dose group were injected with 30 mol/kg of Ca-DTPA for 3 days, beginning 1 h after plutonium injection on the first day. The 24-h urine and feces of rats were collected. The amount of urinary plutonium excretion in the Ca-DTPA groups was found to be significantly greater than that in the respective corresponding control groups on days 1-3. The amount of urinary plutonium excretion in the Ca-DTPA group on the 1st day was increased in response to the plutonium injected dose (correlation coefficient: r=0.628, vs. r=0.573 in the control group, that accumulated in the Ca-DTPA group for 3 days was r=0.800 vs. r=0.669 in the control group), while their rates of plutonium injected dose were decreased. Such findings were not obtained in the feces measurements. In conclusion, the recommended human dose of Ca-DTPA as chelation therapy enhances plutonium excretion for increasing plutonium intake, however the excreted rate of plutonium intake is decreased.

Publication:

Fukuda, S., Yan, X. and Iida, H.: *Jpn. J. Health Phys*., **37**, 158-161, 2002.

CLINICAL RESEARCH

58. Imaging of Each Compartment in PET Dynamic Study with Dual Tracer Injection and 2-Input Compartment Model

Yoko Ikoma*, Hinako Toyama, Akihiko Uchiyama*
(*Waseda Univ.)

Keywords: positron emission tomography (PET), kinetic analysis, 2-input compartment model

Aim: PET kinetic analysis with dual tracer injection is being developed which can assess two different functions, such as cerebral metabolite rate of glucose and distribution volume of benzodiazepine receptor, at the same time, under the same conditions. We investigated the reliability of parameter estimates for various injection protocols, and evaluated the possibility of generating each compartment's kinetic images with a 2-input compartment model by means of a computer simulation.

Methods: The relation between the reliability of parameter estimates and injection interval of two tracers or between the reliability of parameter estimates and administration dose ratio of two tracers was investigated in the computer simulation study, and the injection protocol for reliable estimation was evaluated. Simulated decaying tissue time activity curves were generated with true k-values and input functions by using the 2-input compartment model for various injection intervals and administration dose ratio of two tracers, and the noise which depended on the collected total count was added to each time activity curve. From these activity curves, the rate constants were estimated by nonlinear least square method, and the reliability was evaluated by the mean of absolute differences (MAD) between the true and estimated value for one thousand runs. With the optimal injection protocol determined from the simulation study, dynamic digital phantom was created, parameters were estimated pixel by pixel, and each compartment's activity images of both tracers were created.

Results: The reliability of parameter estimates for various injection protocols were compared, and it was found that parameters could be estimated reliably when the second injection was started 15 minutes later. The reliability did not depend on the administration dose ratio of the two tracers. In the case of [^{18}F]FDG and [^{11}C]flumazenil, the MAD of parameters reflected the cerebral metabolite rate of glucose or the distribution volume of receptor was under 10% at the 5% noise level. The radioactivity image of each compartment represented the accumulation of two tracers.

Conclusion: In the simulation study, the rate constants of two tracers were able to be estimated simultaneously by 2-input compartment model, and the possibility of kinetic analysis for dual tracer injection was shown.

59. Regional Differences of Relationships between Atrophy and Glucose Metabolism of Cerebral Cortex in Patients with Alzheimer's Disease

Hinako Toyama, Shinya Kanekiyo[1], Koji Uemura, Kazunari Ishii[2] and Kenji Ishii[3]

([1]Waseda Univ.; [2]Hyogo Institute for Aging Brain and Cognitive Disorders; [3]Tokyo Metropolitan Institute of Gerontology)

Keywords: *positron emission tomography (PET), magnetic resonance imaging (MRI), Alzheimer's disease, atrophy, cerebral cortical glucose metabolism*

Aim: The purpose of this paper is to estimate a correlation between the extent of atrophy and the decline in the brain function measured with PET study on each brain lobe among patients with Alzheimer's disease.

Materials & Methods: Two groups, the normal controls (male: 8, female: 22 age: 62.4±4.9) and the patients with Alzheimer's disease (male: 6, female: 24, age: 65.9±7.2) participated in this study. The extent of atrophy was evaluated from the extracted gyrus in 2D-projection magnetic resonance imaging (MRI) and the cerebral cortical glucose metabolism was assessed on a 2D-projection positron emission tomography (PET) image. Then a relationship between the cerebral atrophy and the function was evaluated for each brain lobe which was extracted automatically. 2D-projections of PET and MR images were made by the Mollweide method which keeps the area of the brain surface. In order to extract brain lobes from each subject automatically, the bitmap with different value for each brain lobe was made from a standard brain image and was automatically transformed to match each subject's brain image by using SPM99. A correlation image was generated between 2D-projection images of glucose metabolism and the area of the sulcus and the gyrus was extracted from thecorrelation between MR and PET images clustered by the K-means method.

Results: The glucose metabolism of Alzheimer's disease patients was lower than that of normal control subjects at the frontal, parietal, and temporal lobes with the same extent of atrophy as that of the normal. There was a high correlation between the area of gyrus and the glucose metabolism, and the correlation tendency of Alzheimer's disease patients was steeper than that of the normal controls at the parietal lobe.

Conclusions: Combined analysis of regional morphology and function may be useful to distinguish pathological processes, such as the early stage of Alzheimer's disease, from normal physiological aging.

60. Registration of SPECT, PET and/or X-ray CT Images in Patients with Lung Cancer

Koji. Uemura, Hinako Toyama, Tadaaki Miyamoto, Yutaka Mori* and Kyosan Yoshikawa

(*The Jikei University Hospital)

***Keywords**: registration, lung cancer , therapeutic gain of heavy ion therapy*

Aim: We are using the region of interest (ROI) based on anatomical information obtained from X-ray CT to evaluate the therapeutic gain of heavy ion therapy performed on patients with lung cancer, the regional pulmonary functions and the amount of radio tracer accumulation in tumors. There are many registration techniques for brain images, but not so many for other organ images. We have studied registration of chest SPECT, PET and/or X-ray CT images.

Materials and Methods: Perfusion, ventilation and blood pool images with Tc^{99m} labeled radiopharmaceuticals and SPECT, tumor images with ^{11}C-methionine and PET and X-ray CT scans were obtained on several patients with lung cancer before and after heavy ion therapy. The registrations of SPECT-CT, PET-CT and CT-CT were performed by using AMIR (Automatic Multimodality Image Registration), which was developed by Babak et al. for registration of brain images. In the case of SPECT-CT registration, each of the three functional images was registered to the X-ray CT image, and the accuracy of each registration was compared. For PET-CT registration, the transmission images and X-ray CT images were registered at first, because the ^{11}C-methionine PET images bear little resemblance to the underlying anatomical images. Next, the emission images were realigned by using the same registration parameters. The X-ray CT images obtained from a single subject at different times were registered to the first X-ray CT images, respectively.

Results: In the SPECT-CT registration, the blood pool-CT registration is the best among three SPECT images used in visual inspection by radiologists. In the PET-CT registration, the transmission-CT registrations got good results. Therefore, emission-CT registrations also got good results. In the CT-CT registration, the X-ray CT images obtained from a single subject at different times were superimposed well on each other, except for the lower lobe. As a result, it was found to be possible to evaluate the therapeutic gain of heavy particle therapy sequentially by using the same ROI.

Conclusion: This method is useful for evaluating the therapeutic gain of heavy particle therapy performed on patients with lung cancer, quantitatively and sequentially. Registration of chest SPECT, PET and/or X-ray CT images by using the AMIR method gave good results for all of the registrations.

61. Development of a Method of Clustering Multiple Function of the Brain in Hemodynamic Disease with Positron Emission Tomography.

Shinichirou Oohashi[1]、Hinako Toyama、Koji Uemura、Tadashi Nariai[2]、Yoko Ikoma[1]、Kenji Ishii[3]and Akihiko Uchiyama[1]

([1]Waseda Univ.; [2]Tokyo Medical and Dental Univ.; [3]Tokyo Metropolitan Institute of Gerontology)

Keywords: *clustering, positron emission tomography (PET), hemodynamic disease*

Aim: We have investigated post operative changes in CBF and vasodilative and vasoconstrictive reactions for an individual patient with cerebrovascular disease (CVD), by means of segmenting the brain image into some clusters with the varied combination of multiple cerebral functions. In this study, we have developed a new method to classify the combination of the multiple functions by using the common mutual information space generated from the PET images for all subjects.

Materials and Methods: Four patients with CVD (two Moyamoya disease and two ICA occlusion) underwent PET CBF imaging with [^{15}O] labeled water at conditions of rest, hyper ventilation and acetazolamide loading, pre- and post-operation. A mutual information space for all subjects was generated by plotting the values of resting CBF, HV CBF (CBF in hyper ventilation - resting CBF), and AZ CBF (CBF in acetazolamide loading - resting CBF) at the same pixel in the cerebral cortex images for three axes. The space was classified into six segments by hierarchical cluster analysis method. A segmented brain map was created at each study. The characteristic of each segment was described as the mean value of resting CBF, HV and AZ responses as shown on the right side of Fig.20 (#6: normal, #1: decreased CBF and responses).

Results: The segments belonging to the images at pre- and post- operation for each patient are shown on the left of the Fig.20. Black circles show a region including an operated lesion. In case 3 with ICA occlusion, the brain map was classified into three segments, that is #2= ischemic region with decreased resting CBF and poor vaso-reactivity, #6=normal region, #5=decreased resting CBF with high vaso-reactivity before operation. Segments of #2 became #3 and #4 and segment of #5 became normal (#6) 3 months after operation as shown by arrows of the figure. The map 11 months post operation consists of normal function (#6) only.

Conclusion: This method could give some information on correlated cerebral functions and on prognosis after treatment without own-time sequential PET images by using common mutual information data.

62. A Scheduling System for Patient Treatment by Heavy Ion Radiotherapy

Hinako Toyama, Kouichi Shibayama, Syusuke Kanatsu, Toshitaka Kuroiwa, Hideo Watanabe, Mitsuji Wakaisami, Hiroshi Tsuji, Masahiro Endo and Hirohiko Tsujii

Keywords*: heavy ion therapy, treatment scheduler, WEB server, hospital information system, database*

We have developed a scheduling system for heavy ion radiotherapy considering the condition of three treatment rooms and treatment planning for each patient. This system consists of a database (patient information, treatment method and machine schedule), a schedule for radiotherapy and a WEB server. All operation of this system, such as data input, to change and to view the schedule, are performed by using a WEB browser. In order to protect personal information of patients, access privilege to each information entry is limited according to the occupational category. This system is connected with a hospital central information management system (AMIDAS) and an irradiation-managing computer for the heavy ion radiotherapy. Basic information for the patient is got from AMIDAS and the daily schedule is sent to the treatment control computer at each treatment room through the irradiation-managing computer every morning. The daily, weekly and monthly schedules in the treatment room and the treatment condition of each patient are shared on the WEB browser with all participants of the heavy ion therapy. This system could be useful to save time to generate a treatment schedule and to inform staff of the most up-to-date treatment schedule and related information, all at the same time.

1. INTRODUCTION

More than 1000 cancer patients have received carbon-ion therapy as clinical trial since 1994 at the NIRS hospital. Conventionally, a paper schedule of carbon-ion therapy was making manually in each process of machine running time, patient assignment and treatment planning; new copies were distributed to the participants whenever any changes occurred in the schedule. Our purposes of this study were to make a schedule on a computer system which all participants are able to access easily and which gives changes; and to allow sharing of the same information between concerned staff. Cooperation among systems in the hospital has also been tried and the common information is shared between systems and also among doctors, nurses, technologists and paramedical scientists. We also tried to register the record of carbon-ion therapy into the central information management system automatically in order to create an electronic patient record.

2. SYSTEM

The hardware system consists of a unix server with four CPUs, a raid disk for data storage and system backup and a network with gateway for remote access from the maintenance company.

(fig.21). The scheduler consists of the following four processes. 1) To reserve the treatment “frame” on the machine running time table. 2) To assign the patient to the “frame” according to the fraction times (4, 5, 9, 12, 16, 20). 3) To input treatment conditions for each patient. 4) To book the treatment room in the assigned “frame” according to the employing beam energy and direction, treatment position and the other condition such as use of respiratory gate.

In the NIRS hospital, there are four major computer systems (AMIDAS, Order entry system, Radiotherapy planning database and this scheduler). These systems are connected to each other (Fig.22). Basic information on a patient and most entries on of clinical study and clinical

treatment are managed in the order entry system. The results of the study and treatment, patient's clinical record are saved into AMIDAS. In the scheduler, basic information for the patient is got from AMIDAS and the daily schedule is sent to the treatment control computer at each treatment room through the irradiation-managing computer every morning. Carbon-ion therapy is performed by using the data gotten from the scheduler and the radiotherapy planning system. The status of the treatment, such as "under treatment", "completion of treatment" and so on, is received from the irradiation managing computer and transferred to AMIDAS.

3. RESULTS

In order to protect personal information of the patients, access privilege to each information entry is limited according to the occupational category. All participants in radiotherapy are can able to look at all the information, but only certain technologists or medical doctors having privilege can generate and update the schedule.

A schedule to run the accelerator for one year (April to March) is determined every year. We divide a year into two terms. Carbon-ion therapy is planned every term. A technologist reserves a treatment "frame" over the term according to the machine running time (Fig.23). Numbers of patients to be treated per day and No. of fraction are also shown. "S" means start of irradiation, CT means to take CT images for treatment planning. If number of patient a day exceed the arranged number, a warning is given. In the next process, if a doctor assigns a patient to the "frame", the name of the patient is displayed (Pt-1, Pt-2….).

First, the doctor registers the patient ID in this system and the name, gender, etc. appear if the patient is already registered in the hospital. Then the doctor puts in the more information such as the name of the physician in charge, disease name and treatment protocol when the patient is assigned to the "frame".

A technologist for radiotherapy planning input the parameters related to carbon-ion therapy, according to the patient's radiotherapy plan. A treatment room is assigned to the patient depending on the energy and direction of the carbon-ion beam, treatment position (sitting or decubitus) and existence of patch or multi ports irradiation, shrinkage of radiation field and respiratory gating.

After setting the parameters for radiotherapy, a patient is assigned to a treatment room and the order of treatment as shown in Fig. 24. The right side table shows the daily schedule of room A. When the patient ID is clicked on, details of the patient and two types of comments are displayed on the browser as shown on the left side of the figure. A common comment is displayed during irradiation and a daily comment is displayed only on the dedicated day. After irradiation is finished, the color of the patient ID on the display changes to yellow. When irradiation for all reserved patients is finished or a operator pushes the finish button, the status of "completion of treatment" is transferred to AMIDAS automatically.

4. DISCUSSION

We have been using this system for half a year. The daily, weekly and monthly schedules in the treatment rooms and the treatment conditions of each patient are shared on the WEB browser with all participants in the heavy ion therapy. Any schedule change is reflected for all processes immediately. All data on this system are preserved and can be utilized for scheduling in the next term. Most of operations for system maintenance can be done on the WEB browser.

Publication:

Toyama, H., Shibayama, K., Kanatsu, S., Kuroiwa, T., Watanabe, H., Wakaisami, M., Tsuji, H., Endo, M. and Tsujii,H.: J. Jour. *Med. Phys*. **22,** 92-95, 2002.

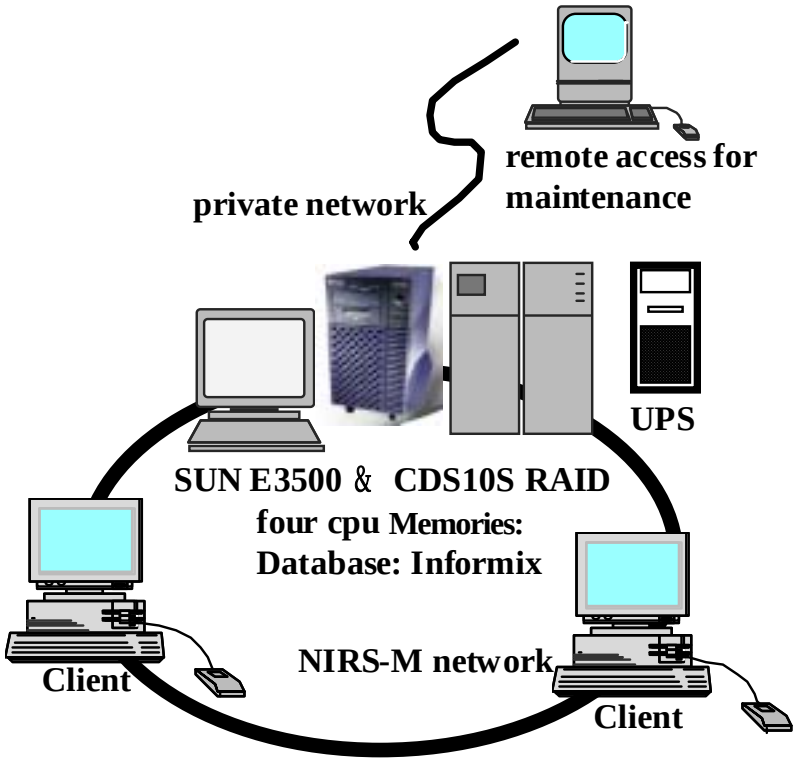

Fig.21 System configuration of the heavy-ion therapy scheduler, consisting of a Unix server with raid and UPS, client PCs and a network with remote access gateway for remote maintenance

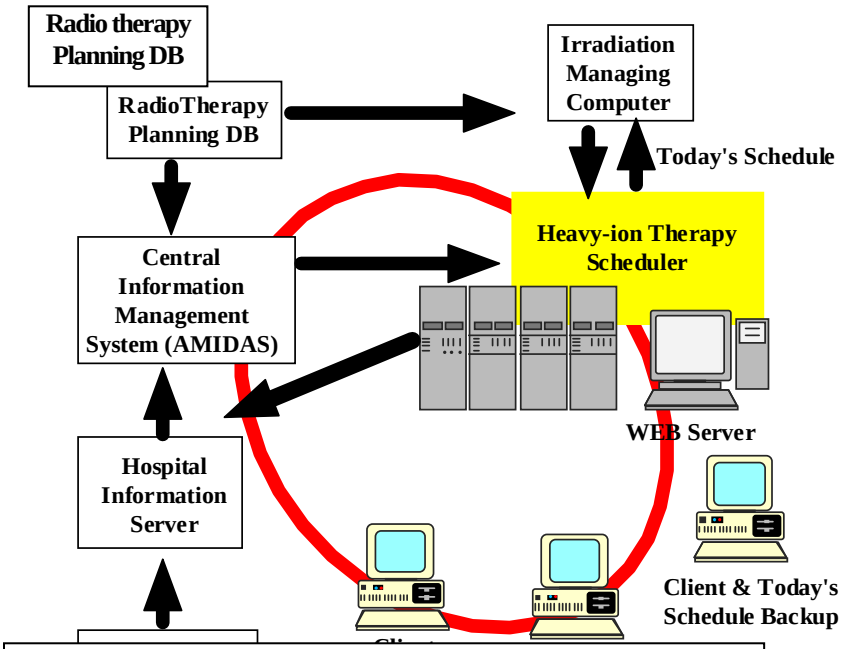

Fig.22 Cooperation with other systems in NIRS hospital. Basic information and clinical record for a patient in the central information management system

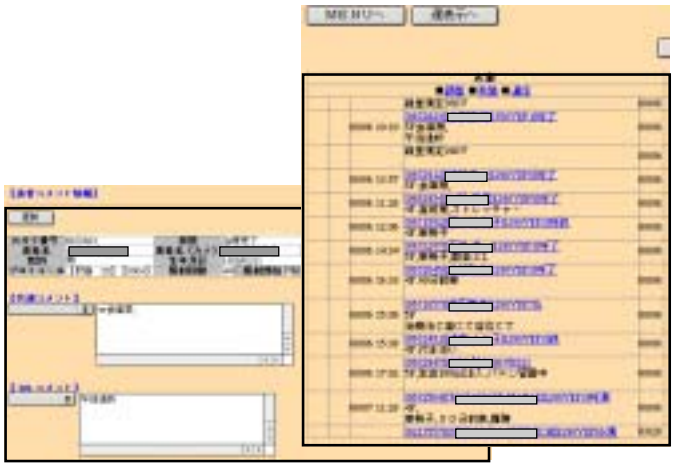

Fig.24 "Today's schedule" of Room A & the information and the comment for a patient, which are displayed when we click the patient ID.

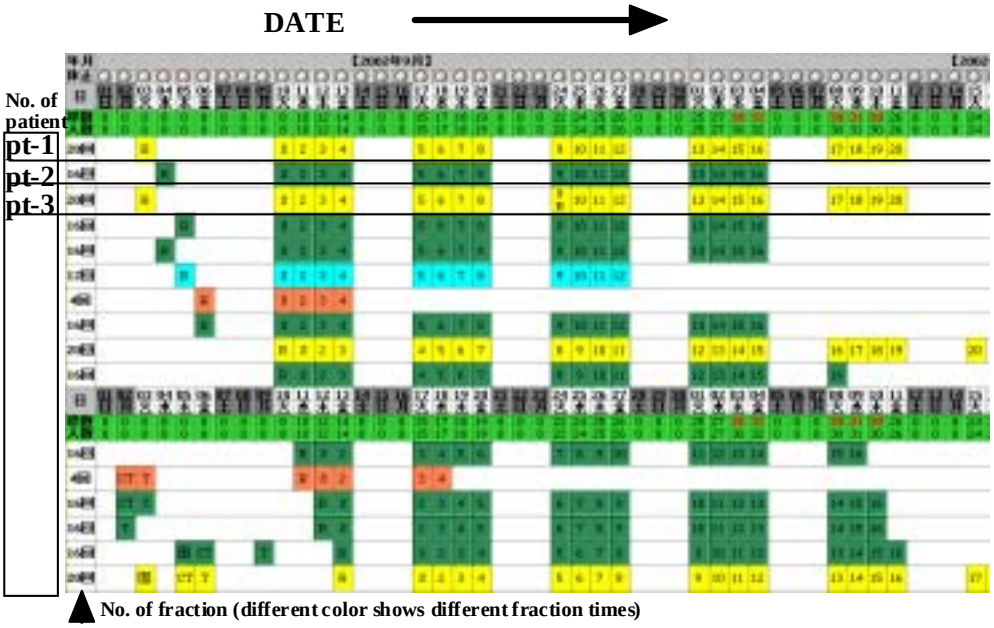

Fig.23 Machine running days & reserved frames for carbon-ion therapy

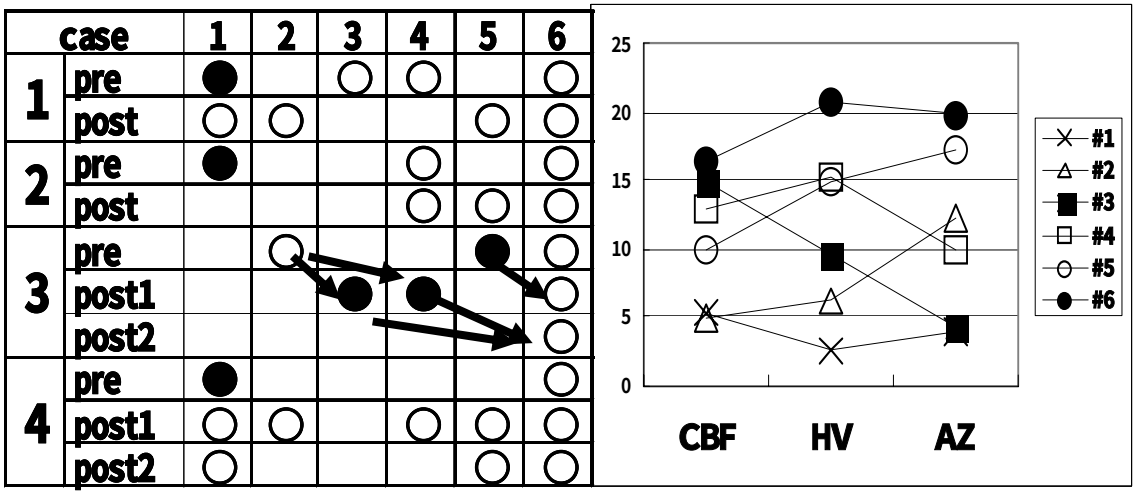
case
1
2
3
4
5
6
1
pre
post
2
pre
post
3
pre
post1
post2
4
pre
post1
post2
25
20
15
10
5
0
CBF
HV
AZ
#1
#2
#3
#4
#5
#6

63. High Levels of Serotonin Transporter Occupancy with Low Dose Clomipramine in Coparative Occupancy Study with Fluvoxamine Using Positron Emission Tomography

Tetsuya Suhara, Akihiro Takano, Yasuhiko Sudo, Tetsuya Ichimiya, Makoto Inoue, Yoshiro Okubo, Fumihiko Yasuno, Yoko Ikoma

Keywords: *serotonin transporter, occupancy, Clomipramine, positron emission tomography*

Context: Serotonin transporters (5-HTT) are regarded as one of the major *therapeutic* target of antidepressants. However, there have only been a few studies about 5-HTT occupancy, and especially data concerning classical antidepressants is still limited.

Objective: The purpose of this study was to investigate the relationship between 5-HTT occupancy and a wide dose-range of antidepressants.

Design, Setting, and Participants: 5-HTT occupancies by antidepressants were measured using positron emission tomography (PET) with [^{11}C](+)McN5652. Twenty-seven normal volunteers were measured with and without pretreatment of single low doses of antidepressants and *chronic doses* were evaluated in *10* patients. Scan data were collected between Dec 12, 1995 and *August 7, 2002*, and data were analyzed in the 2001 – 2002 period at the National Institute of Radiological Sciences, Chiba, Japan.

Intervention: Four different doses of clomipramine (5 - 50 mg) and three different doses of fluvoxamine (12.5 – 50 mg) were used for single administration. Chronic doses were *20* – 250 mg/day for clomipramine and 25 – 200 mg/day for fluvoxamine.

Main Outcome Measure: Occupancies in the thalamus were calculated using the individual *baseline* of [^{11}C](+)McN5652 *for single-dose studies and 2 chronic-dose studies, and the mean value of normal volunteers as the baseline for 8 chronic-dose studies*. The average data of inactive enantiomer [^{11}C](-)McN5652 were used for the estimation of nonspecific binding.

Results: 5-HTT occupancy increased in a curvilinear manner. Even 10 mg of clomipramine showed around 80% occupancy, which was comparable *to* 50 mg of fluvoxamine (Fig. 25). Estimated ED_{50} of clomipramine was 2.67 mg for oral dose and 1.42 ng/ml for plasma concentration; those of fluvoxamine were 18.6 mg and 4.19 ng/ml (Fig. 26).

Conclusions: Clinical doses of clomipramine and fluvoxamine occupied about 80% of 5-HTT, and dose escalation would have minimal effect on 5-HTT blockade. Ten mg of clomipramine was enough to occupy 80% of 5-HTT in vivo.

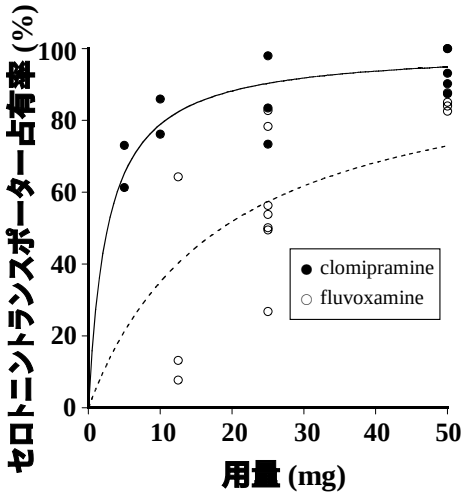

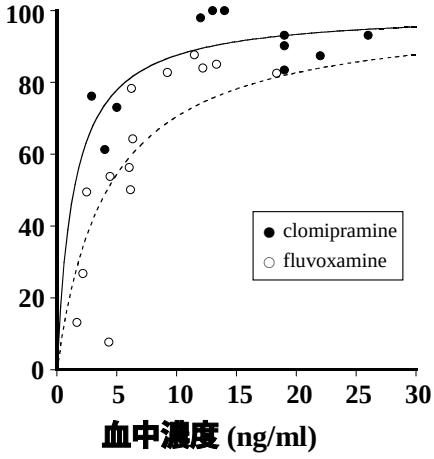

63-Fig. 25 and Fig. 26 (High Levels of Serotonin Transporter Occupancy with Low dose Clomipramine in Coparative Occupancy Study with Fluvoxamine Using Positron Emission Tomography

Tetsuya Suhara, Akihiro Takano, Yasuhiko Sudo, Tetsuya Ichimiya, Makoto Inoue, Yoshiro Okubo, Fumihiko Yasuno, Yoko Ikoma)

Ocuupancy, %

Dose ,mg

Concentration, ng/mL

Fig. 25

Fig. 26

64. No Association Between Genotype of the Promoter Region of Serotonin Transporter Gene and Serotonin Transporter Binding in Human Brain Measured by PET

Kunihiko Shioe, Tetsuya Ichimiya, Tetsuya Suhara, Akihiro Takano, Yasuhiko Sudo, Fumihiko Yasuno, Masami Hirano, Manabu Shinohara, Msato Kagami, Yoshiro Okubo, Masajoro Nankai, Shigenobu Kanba

KEY WORDS: *5-HTTLPR; polymorphism; 5-HTT binding; PET; binding potential*

The human serotonin transporter (5-HTT) gene has a polymorphism in the 5'-flanking promoter region that is called the serotonin transporter gene-linked polymorphic region (5-HTTLPR). In lymphoblast cell lines, the promoter activity of the 5-HTT gene is dependent on 5-HTTLPR allelic variants. The transcriptional activity of the l allele was more than twice as high as that of the s allele. The s allele is considered to be associated with mood disorders and anxiety-related personality traits. To evaluate the functional differences of 5-HTTLPR in the brain in vivo, we examined the allelic variations of 5-HTTLPR and measured 5-HTT binding in the living human brain using positron emission tomography (PET) with C11-labeled trans-1, 2, 4, 5, 6, 10-β-hexahydro-6-[4-(methylthio) phenyl]pyrrolo[2,1-a]isoquinoline (McN5652) as a ligand. Twentyseven healthy male subjects participated in this study. Although the human lymphoblast cells with the l/l genotype was reported to produce higher concentrations of both mRNA and protein of 5-HTT than those with the l/s or s/s genotype in a human lymphoblast in vitro study, 5-HTT binding in vivo was not signi.cantly different among subjects with the three genotypes (l/l: 0.842 ± 0.184, l/s: 0.708 ± 0.118, s/s: 0.825 ± 0.209) as shown in Fig. xx. In conclusion, this study does not support the assumption that the genotypedependent differences of 5-HTTLPR directly contributes to the regulation of the 5-HTT binding site in the living human brain.

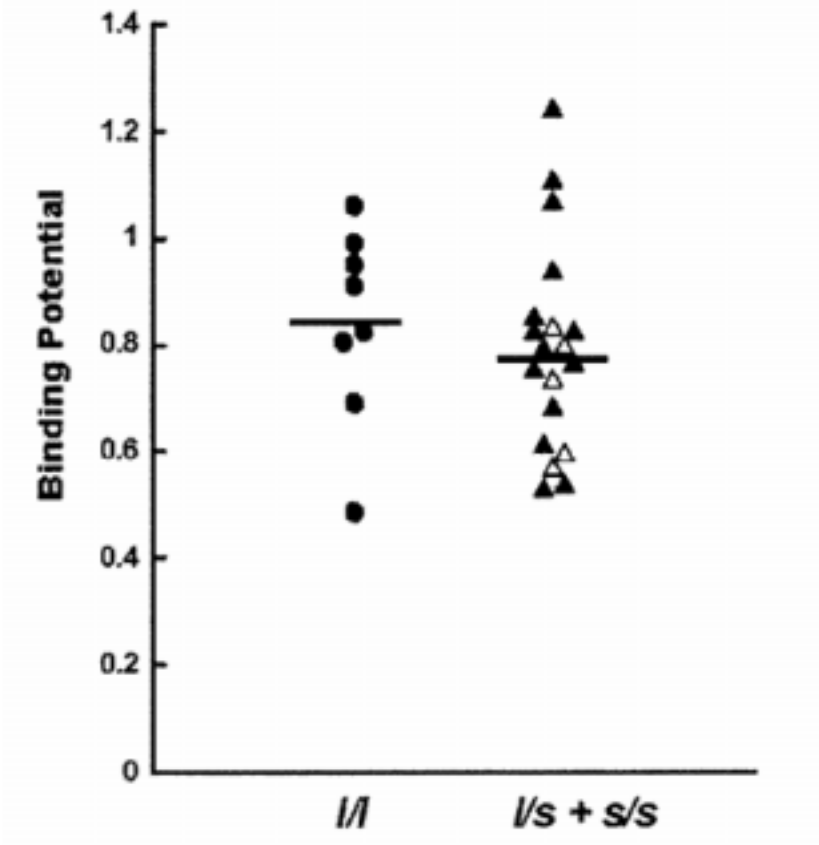

64-Fig. 27 (No Association Between Genotype of the Promoter Region of Serotonin Transporter Gene and Serotonin Transporter Binding in Human Brain Measured by PET

Kunihiko Shioe, Tetsuya Ichimiya, Tetsuya Suhara, Akihiro Takano, Yasuhiko Sudo, Fumihiko Yasuno, Masami Hirano, Manabu Shinohara, Msato Kagami, Yoshiro Okubo, Masajoro Nankai, Shigenobu Kanba)

65. Inhibitory Effect of Hippocampal 5-HT1A Receptorson Human Explicit Memory

Fumihiko Yasuno, Tetsuya Suhara, Takashi Nakayama, Tetsuya Ichimiya,
Yoshiro Okubo, Akihiro Takano, Tomomichi Ando, Makoto Inoue, Jun Maeda, Kazutoshi Suzuki

Keyword: *explicit memory, 5-HT1A, hippocampus, positron emission tomography*

Objective: Recent studies have indicated that the serotonergic system plays important roles in memory functions. However, the specific relationship between 5-HT1A receptors and memory function is not clear in the human brain. To clarify this relationship, we measured the availability of 5-HT1A receptors in the human brain and assessed the relationship between regional receptor binding and memory function.

Method: We examined 5-HT1A receptors using positron emission tomography (PET) with [11C]WAY-100635 and assessed the relationship with memory functions. To interpret the pharmacological implications, we administered the 5-HT1A agonist tandospirone to subjects and investigated the effect of the stimulation of 5-HT1A receptors on cognitive function together with the neuroendocrinological response.

Results: There was a significant negative correlation between explicit memory function and 5-HT1A receptor binding localized in the bilateral hippocampus where the postsynaptic 5-HT1A receptors are enriched (fig.28). Furthermore, we found that the administration of tandospirone dose-dependently impaired explicit verbal memory, while other cognitive functions showed no significant changes. The change in memory function paralleled those of body temperature and secretion of growth hormone, which were reported to be induced by the stimulation of postsynaptic 5-HT1A receptors

Conclusions: The results show that the postsynaptic 5-HT1A receptors localized in the hippocampal formation have a negative influence on explicit memory function. Our findings give rise to the possibility that the antagonistic effect of postsynaptic 5-HT1A receptors in the hippocampus leads to improvement of human memory function. Drugs that work as antagonists on postsynaptic 5-HT1A receptors may be favorable for improved control of memory impairment.

65-Fig. 28. (Inhibitory Effect of Hippocampal 5-HT1A Receptors
on Human Explicit Memory

Fumihiko Yasuno, Tetsuya Suhara, Takashi Nakayama, Tetsuya Ichimiya,
Yoshiro Okubo, Akihiro Takano, Tomomichi Ando, Makoto Inoue, Jun Maeda, Kazutoshi Suzuki)

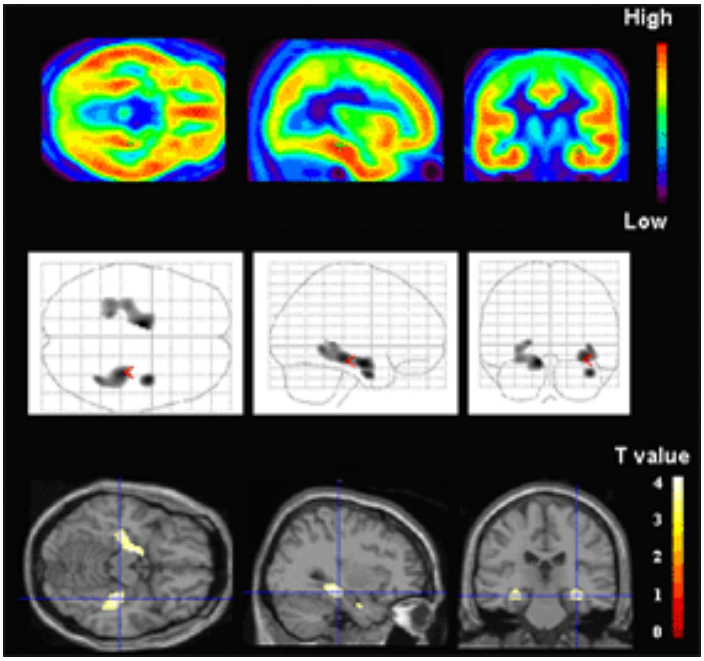

Fig. 28：Averaged BP Images (N=16) of [^{11}C]WAY-100635 (First Row) and Regions with a Significant Inverse Correlation between BP of [^{11}C]WAY-100635 and the General Memory Index on WMS-R(Second and Third Row).

66. The FNCA 2002 Workshop on Radiation Oncology

Hirohiko Tsujii, Shingo Kato, Tatsuya Ohno, Shinichiro Sato, Hideo Tatsuzaki, and Takashi Nakano* (* Gunma Univ. School of Medicine)

Keywords: *radiotherapy, Asian countries, cervix cancer, nasopharyngeal cancer, international clinical trial*

The FNCA (Forum for Nuclear Cooperation in Asia) Application of Radioisotopes and Radiation for Medical Use) 2002 Workshop on Radiation Oncology was held from December 17 to 20, 2002, in Chiba City and Tokyo, Japan. The meeting was jointly organized by the Ministry of Education, Culture, Sports, Science and Technology (MEXT) and the National Institute of Radiological Sciences (NIRS) of Japan, in cooperation with the Japan Atomic Industrial Forum, Inc. (JAIF). Representatives from 8 FNCA countries, China, Indonesia, Japan, Republic of Korea, Malaysia, the Philippines, Thailand and Vietnam, along with a representative from the International Atomic Energy Agency (IAEA) attended the Workshop.

CERVIX-I (standard radiotherapy for uterine cervix cancer): Two hundred and ten patients were registered. The 5-year-local control and survival rates are 81.6% and 52.5%, respectively.

CERVIX-II (accelerated hyperfractionated radiotherapy for uterine cervix cancer): Total number of registered cases was 103. Initial data on the 2-year-local control and survival rates are 94.2 % and 90.4%, respectively.

New protocol (chemoradiotherapy for cervix cancer and nasopharyngeal cancer): The agenda called for reports of experiences of each country and discussions to make a new protocol and to perform multicenter clinical trials. For uterine cervical cancer, treatment protocols for radiotherapy and chemotherapy, tumor response rates and side-effects were discussed. Limitations due to the equipment and economic factors were also discussed as practical aspects for some countries. For nasopharyngeal cancer (NPC), discussions centered on radiotherapy techniques, tumor and critical organ doses and chemotherapy scheduling. It was agreed that pilot studies of weekly chemotherapy at 2 dose levels, 30 and 40 mg/m would be done. Data from these studies will be presented at the next meeting with the view towards an initiation of international randomized clinical trials.

67. Automated Synthesis of the Ultra High Specific Activity of [^{11}C]Ro15-4513 and Its Application in an Extremely Low Concentration Region to an ARG Study

Kazutoshi Suzuki and Junko Noguchi

Key Words: ultra high specific activity, high sensitivity, single pass I_2 method,
in vitro ARG, [^{11}C]Ro15-4513, [^{11}C]CH_3I, automation

In general, it is quite difficult to study *in vivo* behavior of strongly bioactive molecules or toxic molecules and to visualize the distribution of extremely low-density receptors in the brain without somehow affecting the subjects. Radiotracers with a high specific activity would be quite useful in performing these studies since this allows the injection of a sufficiently small amount of tracers into a living subject, but with enough radioactivity. A wide variety of ^{11}C-labeled compounds have been prepared using [^{11}C]CH_3I as a synthetic precursor and used for *in vivo* receptor imaging in the brain by PET. [^{11}C]CH_3I has been prepared mainly by reducing [^{11}C]CO_2 generated directly in a target chamber with $LiAlH_4$ in THF. However, this method has always suffered from contamination by non-radioactive CO_2 from the atmosphere, reagents, etc., which causes a decrease in the specific activity of the product. Alternative methods have been published for the production of [^{11}C]CH_3I, by the reaction of [^{11}C]CH_4 with I_2 vapor at a high temperature. The new method has advantages in simplicity and repeatability of [^{11}C]CH_3I production in a short time interval. In addition, the method has the potential advantage of high specific activity since the $LiAlH_4$/THF solution, the major source of carbon contamination, can be avoided. It might be interesting to produce [^{11}C]CH_4 directly in the target chamber and convert it to [^{11}C]CH_3I by passing through a quartz column with iodine vapor at high temperature since this method might avoid most effectively the possibility to be contaminated by CO_2 and shorten the synthesis time for [^{11}C]CH_3I, i.e., be most suitable for high specific activity and simplicity of the production. It might also be interesting to apply the high specific activity ^{11}C-compounds to *ex vivo* and *in vitro* autoradiography studies in extremely low concentration region.

We have designed and constructed an automated device for the production of ultra-high specific activity ^{11}C-labeled compounds via [^{11}C]CH_3I synthesized by the single pass I_2 method coupled with the *in situ* [^{11}C]CH_4 production method. The optimum conditions for the production of [^{11}C]CH_3I were determined to be 630℃ for the reaction column, 50℃ for the iodine column and 50 ml/min for the He gas flow rate; these gave the maximum conversion ratio of [^{11}C]CH_3I, 44%. [^{11}C]Ro15-4513 was produced by the reaction of the desmethyl compound with the above [^{11}C]CH_3I under the optimized conditions. An i.v. injectable [^{11}C]Ro15-4513 solution of 1500±490MBq (n=6) with specific activity 4700±2500GBq/ mol and a radiochemical purity of 98.2±2% was obtained automatically within 25 minutes (from EOB) by irradiating nitrogen gas containing 5% H_2 with 18 MeV protons (14.2 MeV on target) at 20 A for 20 minutes. The highest specific activity of 9700GBq/ mol (at EOS) could be achieved, although the radiochemical purity was 92.4%. Using the ultra-high specific activity [^{11}C]Ro15-4513, allowed us to clearly visualize the super high affinity binding sites in the rat brain hippocampus even at the extremely low concentration of 0.66 pM Ro15-4513 by *in vitro* autoradiography.

This method could be applied for the syntheses of other ^{11}C-labeled compounds requiring ultra high specific activity which might be quite powerful tool for general studies in an extremely low concentration region.

Publication:

Noguchi, J. and Suzuki, K. : *Nucl. Med. Biol.*, **30, 335 – 343, 2003.**

68. How to Increase the Reactivity of [^{18}F]Fluoroethyl Bromide: [^{18}F]Fluoroethylation of Amine, Phenol and Amide Functional Groups with [^{18}F]FEtBr, [^{18}F]FEtBr/NaI and [^{18}F]FEtOTf

Ming-Rong Zhang and Kazutoshi Suzuki

Keywords: [^{18}F]FEtBr, [^{18}F]FEtBr/NaI, [^{18}F]FEtOTf, [^{18}F]fluoroethylation, PET tracer

[^{18}F]fluoroethyl bromide ([^{18}F]FEtBr) is a useful alkylating reagent for introducing ^{18}F into substrates containing amine, phenol and amide functional groups. However, compared with [^{11}C]methyl iodide ([^{11}C]CH_3I), [^{18}F]FEtBr has been used to a much more limited extent, and for the most part only in research areas. Recently, we developed an automated system for synthesizing ^{18}F-labeled compounds using [^{18}F]FEtBr as a precursor. Using this system, we prepared [^{18}F]FEtBr in a reproducible radiochemical yield of 60 - 75% (corrected for the decay, based on total [^{18}F]F^-) and synthesized several [^{18}F]fluoroethylated ligands. However, in our experiments, we faced a major difficulty, that is, the lower reactivity of [^{18}F]FEtBr with substrates containing amine, phenol and amid functional groups than that of [^{11}C]CH_3I. In this study, the strategies included: 1) adding NaI into the reaction mixture of [^{18}F]FEtBr and nucleophilic substrates, where [^{18}F]fluoroethyl iodide ([^{18}F]FEtI) is reversibly formed and becomes more reactive with the substrates than [^{18}F]FEtBr; 2) converting [^{18}F]FEtBr into [^{18}F]fluoroethyl triflate ([^{18}F]FEtOTf), a highly reactive intermediate by analogy with [^{11}C]methyl triflate ([^{11}C]CH_3OTf). As model substrates, 4-piperidyl acetate (P4A, amine type), *N*-[2-[4-(4-chlorophenyl)piperazin-1-yl]ethyl]-3-hydroxybenzamide (CB, phenol type) and 2a-[4-(4,5,6,7-tetrahydrothieno[3,2-*c*]pyridin-5-yl)butyl]-2*a*,3,4,5-tetrahydro-1H-benz[*cd*]-indole-2-one (DR, amide type) were selected to react with [^{18}F]FEtBr, respectively since the ^{11}C-methyl analogs of these substrates have been developed as putative tracers for brain acetylcholinesterase, dopamine D_4 receptor or 5-HT_7 serotonin receptor . Aqueous [^{18}F]F^- solution was produced according to the same procedure with that of [^{18}F]FDG. The [^{18}F]F^- solution was dried to remove H_2O and CH_3CN, and then 2-trifluoromethanesulfonyloxy ethylbromide in o-DCB was added to form [^{18}F]FEtBr, which was then distilled under a helium flow, passed through a small column filled with Ascarite and phosphorus pentoxide. The [^{18}F]FEtBr was trapped into a solution of anhydrous DMF (300 L) containing substrate (0.8 - 1.1 mg) and base (if required: NaH 1.5 g/20 mL DMF, 10 L or 0.5 N NaOH, 3 L or 10% n-Bu_4NOH/H_2O, 10 L), additionally 1.0 mg of NaI in the case of [^{18}F]FEtI, at -15 - -20 C. [^{18}F]FEtOTf was obtained by passing [^{18}F]FEtBr through a small column containing AgOTf (100 mg) impregnated graphite carbon (300 mg) with a helium gas flow and trapped into the solution described above. The trapped solutions were heated to 25 C, 70 C, 110 C or 130 C and kept for 5 - 30 min. After the reactions were finished, the [^{18}F]fluoroethylation yield for each mixture at 5, 10, 20 or 30 min was determined by the use of radio-HPLC.

As a result, the [^{18}F]fluoroethylation yields for P4A, CB and DR increased significantly by the above improvements, i.e., 74% ([^{18}F]FEtBr/NaI, 130 C, 10 min) and 71% ([^{18}F]FEtOTf, 25 C, 10 min) from 18%([^{18}F]FEtBr, 130 C, 10 min) for [^{18}F]FEtP4A, 68% ([^{18}F]FEtBr/NaI/NaH, 120 C, 10 min) and 68%([^{18}F]FEtOTf/NaH, 25 C, 10min) from 40% ([^{18}F]FEtBr/ NaH, 120 C, 10 min) for [^{18}F]FEtCB, and 26%([^{18}F]FEtBr/ NaI/NaH, 70 C, 10 min) and 82%([^{18}F]FEtOTf/NaH, 25 C, 10min) from 71% ([^{18}F]FEtBr/ NaH, 70 C, 10 min) for [^{18}F]FEtDR, respectively. The lower yield was only observed in the reaction of DR with NaI/NaH, probably due to the instability of DR. In conclusion, the above approaches can be applied in the synthesis of ^{18}F-fluoroethylated compounds starting from [^{18}F]FEtBr as the synthetic precursor.

Publication

Zhang, M-R., Furutsuka, K., Yoshida, Y. and Suzuki, K. : *J. Labelled Cpd. & Radiopharm.*, **46, 587 – 598, 2003.**

69. Preclinical Biological Assessment of Proton and Carbon Ion Beams at Hyogo Ion Beam Medical Center.

Kazufumi Kagawa[1], Masao Murakami[1], Yoshio Hshikawa[1], Mitsuyuki Abe[1], Takashi Akagi[1], Toshihiro Yanou[1], Goh Kagiya[2], Yoshiya Furusawa, Koichi Ando, Kumie Nojima, Mizuho Aoki, and Tatsuaki Kanai ([1]Hyogo Ion Beam Medical Center, [2]Wakasa-wan Energy Research Center)

Keywords: Proton beam, Carbon ion, biological RBE, clinical RBE

The biological effects of proton and carbon ion beams before their clinical use were assassed.

Cultured cells from human salivary gland cancer (HSG cells) were irradiated at 5 points along a 190 MeV per nucleon proton and a 320 MeV per nucleon carbon ion beam, with Bragg peaks modulated to 6 cm widths. A linac 4 MV X-ray besm was used as a reference. Relative biologic effectiveness (RBE) values at each point were calculated from survival curves. Cells were also irradiated in a cell-stack phantom to determine whether localized cell deaths were observed at predefined depths. Total body irradiation of C3H/He mice was performed, and the number of regenerating crypts per jejunal section was compared to calculate intestinal RBE values. For carbon ion and referential 4 MV X-ray beams, mouse right legs were irradiated by four-fractional treatment and followed up for skin reaction scoring.

RBE values calculated from cell survival curves at the dose that would reduce cell survival to 10% (D10) ranged from 1.01 to 1.05 for protons and from 1.23 to 2.56 for carbon ions. The cell-stack phantom irradiation revealed localized cell deaths at predefined depth. The intestinal RBE values ranged from 1.01 to 1.08 for protons and from 1.15 to 1.88 for carbon ions. The skin RBE value was 2.16 at C320/6 cm spread-out Bragg peak (SOBP) center.

The radiobiologic measurements of proton and carbon ion beams at Hyogo Ion Beam Medical Center are consistent with previous reports using proton beams in clinical settings and carbon ion beams with similar linear energy transfer (LET) values.

Publication:

Kagawa, K., Murakami, M., Ishikawa, Y., Abe, M., Akagi, T., Yanou, T., Kagiya, G., Furusawa, Y., Ando, K., Nojima, K., Aoki, M., and Kanai, T.: *Int. J. Radiat. Oncol. Biol. Phys.* **54**, 928-938, 2002.

70. Significance of Fractionated Irradiation for the Biological Therapeutic Gain of Carbon Ions

Sachiko Koike, Koichi Ando, Akiko Uzawa, Nobuhiko Takai, Yoshiya Furusawa, Chisa Oohira, Mizuho Aoki, Manami Monobe, Ryonfa Lee, Masao Suzuki, and Kumie Nojima

Keywords: carbon ion, therapeautic gain, RBE, LET, fractionation,

It is well established that the RBE (relative biological effectiveness) for cell killing depends on LET (linear energy transfer), and that a maximum RBE is observed at ~150 keV• μm^{-1}. However, the therapeutic gain depends on the ratio of the RBEs for the effects on the cancer cell population and the effects on normal tissue. The RBE of a given radiation quality depends not only on LET but also on dose, biological system and effect, and irradiation conditions. There are no data available to answer the question: which LET is suitable to improve the biological therapeutic gain of carbon ions? Here, three different LET values of 290 MeV/u carbon ions were selected, and the relative biological effectiveness was compared between tumor-growth retardation and skin damage using a murine transplantable tumor. Larger RBE values for tumor were obtained when carbon ions were used by intermediate LET delivered daily for 2 to 5 fractions. The biological therapeutic gain would be high for the carbon ion SOBP if the numbers of fractionation were correctly selected in clinical trials.

Publication:

Koike, S., Ando, K., Uzawa, A., Takai, N., Furusawa, Y., Oohira, C., Aoki, M., Monobe, M., Lee, R., Suzuki, M., and Nojima, K.: *Radiat. Protec. Dosim.* **99**, 405-408, 2002.

71. Relative Biological Effectiveness of 290 MeV/u Carbon Ions for the Growth Delay of a Radioresistant Murine Fibrosarcoma

Koike S, Ando K, Oohira C, Fukawa T, Lee R, Takai N, Monobe M, Furusawa Y, Aoki M, Yamada S, Shimizu W, Nojima K, and Majima H

Keywords: RBE, LET, fractionation, Fe-plot, fibrosarcoma

The relative biological effectiveness (RBE) for animal tumors treated with fractionated doses of 290 MeV/u carbon ions was studied. The growth delay of NFSa fibrosarcoma in mice was investigated following various daily doses given with carbon ions or those given with cesium É¡ -rays, and the RBE was determined. Animal tumors were irradiated with carbon ions of various LET (linear energy transfer) in a 6-cm SOBP (spread-out Bragg peak), and the isoeffect doses, i.e. the dose necessary to induce a tumor growth delay of 15 days were studied. The isoeffect dose for carbon ions of 14 and 20 keV/µm increased with an increase in the number of fractions up to 4 fractions. The increase in the isoeffect dose with the fraction number was small for carbon ions of 44 keV/µm, and was not observed for 74 keV/µm. The and values of the linear-quadratic model for the radiation dose-cell survival relationship were calculated by the Fe-plot analysis method. The values increased linearly with an increase in the LET, while the values were independent of the LET. The / ratio was 129 ± 10 Gy for -rays, and increased with an increase in the LET, reaching 475 ± 168 Gy for 74 keV/µm carbon ions. The RBE for carbon ions relative to Cs-137 -rays increased with the LET. The RBE values for 14 and 20 keV/µm carbon ions were 1.4 and independent of the number of fractions, while those for 44 and 74 keV/µm increased from 1.8 to 2.3 and from 2.4 to 3.0, respectively, when the number of fractions increased from 1 to 4. Increasing the number of fractions further from 4 to 6 was not associated with an increase in the RBE. These results together with our earlier study on the skin reaction support the use of an RBE of 3.0 in clinical trials of 80 keV/µm carbon beams. The RBE values for low doses of carbon beams were also considered.

Publication:

Koike, S., Ando, K., Oohira, C., Fukawa, T., Lee, R., Takai, N., Monobe, M., Furusawa, Y., Aoki, M., Yamada, S., Shimizu, W., Nojima, K., and Majima, H.: *J. Radiat Res.*, **43**, 247-255, 2002.

72.Initial Medical Management of Patients Severely Irradiated in the Tokai-mura Criticality Accident

Toshiyasu Hirama, Hisayoshi Kondo, Saori Kawamura, Norikazu Kuroiwa and Makoto Akashi

KeyWords: acute radiation syndrome, criticality accident, haematopoietic stem cell transplantation

A nuclear criticality accident occurred in Japan on September 30, 1999, which resulted in severe exposure of three victims to mixed flux of neutrons and -rays. Estimated average doses for the three victims were 5.4 Gy of neutrons and 8.5 Gy of -rays for Patient A, 2.9 Gy of neutrons and 4.5 Gy of -rays for Patient B, and 0.81 Gy of neutrons and 1.3 Gy of -rays for Patient C. They then suffered the consequences of the effects of ionizing radiation resulting in acute radiation syndrome. In Patients A and B, bone marrow failure was so severe that they received haematopoietic stem cell transplantation. The graft initially took successfully in both patients, although in Patient B it was later taken over by his own haematopoietic cells. They also suffered from severe skin lesions, later exhibited gastrointestinal bleeding and eventually died of multiple organ failure 82 and 210 days after the accident, respectively. The survival of these patients beyond the period of agranulocytosis means that bone marrow failure *per se* caused by exposure to ionizing radiation may now be overcome. Patient C also developed bone marrow failure and was treated with granulocyte colony-stimulating factor as well as supportive care. He recovered without major complications and is now under periodical follow-up. Remarkably, during the prodromal phase, all the patients exhibited hypoxaemia, two of whom also showed interstitial oedema of the lungs. In Patient C these manifestations improved within a week. The circumstances of the accident and the initial medical treatment of the victims are described.

Publication:
Hirama T., Tanosaki S., Kandatsu S., Kuroiwa N., Kamada T., Tsuji H., Ymada S., Katoh H., Yamamoto N., Tsujii H., Suzuki G. and Akashi M.: *Br. J. Radiol.*, **76**, 246-253, 2003.

ENVIRONMENTAL SCIENCE

73. The Involvement of Cell Cycle Checkpoint-mutations in the Mutagenesis Induced in *Drosophila* by a Longer Wavelength Light Band of Solar UV.

Megumi Toyoshima[1], Syogo Takinami[1], Kotaro Hieda[2], Yoshiya Furusawa, and Tomoe Negishi[1]
([1]Okayama Univ.; [2]Rikkyo Univ.)

Keywords: solar UV, mutagenesis, checkpoint, repair, *Drosophila*, mei-9, mei-41

Solar ultraviolet radiation is considered to be injurious rather than necessary for most organisms living on the earth. It is reported that the risk of skin cancer in humans hasincreased by the depletion of the ozone layer. We have examined the genotoxicity of solar ultraviolet light, especially of longer wavelengths, using *Drosophila*. We demonstrated that light of wavelengths up to 340 nm is mutagenic on *Drosophila* larvae. Using an excision repair-deficient *Drosophila* strain (*mus201*), we obtained results suggesting that the lesion caused in larvae by the 320 nm-light irradiation may be similar to the damage induced by irradiation at 310 nm, and that light of 330 and 340 nm may induce damage different from that induced by 310 and 320 nm-light. To examine the difference in DNA damage induced by light of particular wavelength, we performed monochromatic irradiation on larvae of two *Drosophila* strains; one excision repair-deficient (*mei-9*) and another postreplication repair-deficient (*mei-41*). 310 and 320 nm-light were more mutagenic in the *mei-9* strain than *mei-41*, whereas 330 and 340 nm-light were more mutagenic in *mei-41* than in *mei-9*. The *mei-41* gene is a homologue of the human *atm* gene which is responsible for a cell cycle checkpoint. This result suggests that 310-320 nm-light induces DNA damage that is subject to nucleotide excision repair (NER) and that 330-360 nm-light causes damage to be recognized by the cell cycle checkpoint, but it is not repairable by NER.

Publication:

Toyoshima, M., Takinami, S., Hieda, K., Furusawa, Y., and Negishi, T.: *Photochem. Photobiol. Sci.* **1**, 178-183, 2002.

74. Action Spectra of Apoptosis Induction and Reproductive Cell Death in L5178Y Cells in UV-B Region

Mizuho Aoki, Yoshiya Furusawa, Shinnichi Higashi*, and Masakatsu Watanabe*
(*Natl. Inst. Basic Biol.)

Keywords: apoptosis, reproductive cell death, action spectrum, L5178Y cells, monochromatic UV-B light

It is important to determine the action spectrum of UV-B radiation contained in sunlight to estimate the risk of skin cancer. We have investigated action spectra for induction of apoptosis and reproductive cell death in L5178Y cells using the Okazaki Large Spectrograph at NIBB. L5178Y cells were exposed to light at different wavelengths in UV-B or UV-A region. Frequencies of apoptosis induction and reproductive cell death were determined by counting cells with chromatin condensation, and by the colony formation assay, respectively. The measured sensitivity spectra for the two end-points were in very good agreement. Sensitivity decreased steeply with increase of wavelength in UV-B region and remained nearly constant in UV-A region. The action spectra were also slightly steeper than that for the minimum erythematic dose (MED), but very similar to the light absorption spectrum of DNA in UV-B region. On the other hand, the spectra for both endpoints were similar to MED spectrum but not DNA spectrum in the UV-A region. Also different time-course and morphological difference of apoptosis were found between UV-B (long time, fragmentation) and UV-A (short time, shrinkage) regions. These results suggest that DNA damage induced by UV-B light triggers apoptosis and reproductive cell death, but other damaged targets (membrane, protein and so on) trigger these effects in UV-A region.

Publication:

Aoki, M., Furusawa, Y., Higashi, S., and Watanabe, M.: *J. Photosci*. **9**, 454-456, 2002.

75. Database of Calculated Values of Retention and Excretion for Members of the Public Following Acute Intake of Radionuclides

Nobuhito Ishigure, Takashi Nakano, Masaki Matsumoto and Hiroko Enomoto

Key words: *internal dosimetry, public exposure, retention, excretion, database*

The Chernobyl reactor accident has increased concern about the protection of the public in the event of an emergency at a nuclear facility. Since an accident at a nuclear site may result in releases of radioactive material into the environment, provision should be made to assess internal doses to members of the public from possible intakes of radionuclides.

In the case where internal contamination is suspected, measurements of radioactivity in the whole body or in specific organs or in excreta may be made as part of the dose assessment procedure. The magnitude of intakes of radionuclides can then be estimated by comparing the results of these bioassay measurements with predicted retention or excretion data calculated using standard biokinetic models. Monitoring data for occupational exposure are presented by the International Commission on Radiological Protection (ICRP) for 29 radionuclides in Publication 78 (1997) and by the authors for 42 radionuclides in electronic look-up tables on MS Excel® (2001). However, there are no retention or excretion data provided for members of the public in the ICRP publications.

The International Commission on Radiological Protection has developed age-dependent biokinetic models for selected elements and computed age-dependent dose coefficients to meet the necessity for internationally accepted dose coefficients for members of the public.

In the present work, by using such ICRP age-dependent biokinetic models, values of retention and excretion of selected radionuclides inhaled or ingested by members of the public were computed and a graphic database was assembled from the computed results on the web site: http://www.nirs.go.jp/RPD/ to provide a tool for the interpretation of bioassay measurements. Fig. 29 shows an example of graphs called from the database.

Publication:
Ishigure, N., Nakano, T., Matsumoto, M. and Enomoto, H. *Radiat. Prot. Dosimetry*, **105**, 311-316, 2003

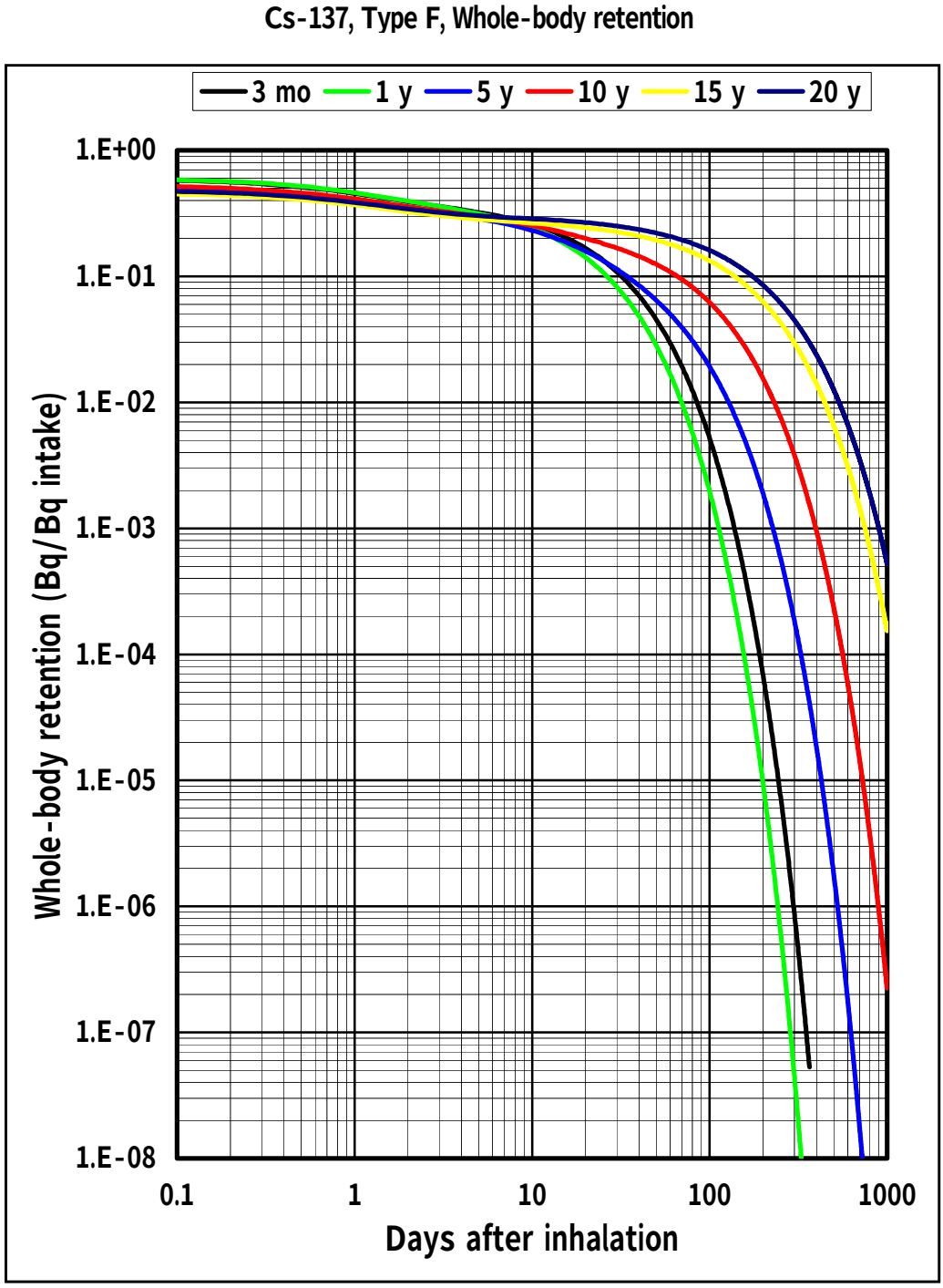

Fig.29 Called graphs for the predicted values of the whole-body retention of ^{137}Cs

76. $^{239+240}$Pu Fluxes on the Continental Margin of the East China Sea

Masatoshi Yamada and Tatsuo Aono

***Keywords**: sediment trap experiment, $^{239+240}$Pu, East China Sea, continental slope, lateral transport*

The plutonium isotopes, ^{239}Pu (half-life=2.44 x 10^4 year) and ^{240}Pu (half-life=6.58 x 10^3 year), have been added to the surface oceans mainly as a consequence of atmospheric nuclear weapons tests. Plutonium has also been deposited in the upper layer of land soil. Large inputs of weathered detrital material in addition to the direct fallout are predicted sources in coastal sea areas. Plutonium is a reactive element, which is adsorbed by particles in seawater and scavenged from the water column. The utility of sediment trap experiments to study the transport process by particles in the ocean is well established. Several studies have been reported on the particle fluxes of plutonium in the open ocean. However, little work has been done on particle fluxes of plutonium in a continental margin such as the East China Sea. The aims of this study were to measure the activities of $^{239+240}$Pu in settling particles collected in the East China Sea continental slope by use of sediment traps, and to discuss the marine processes transporting plutonium on the East China Sea continental margin.

Settling particle samples were collected at three stations. Three moorings of sediment traps were deployed on the continental margin of the East China Sea. Two types of sediment traps were used, cylindrical traps and conical time-series traps. Cylindrical traps consisted of four individual polyvinyl chloride cylinders mounted on a cross frame. Each cylinder was 160 mm in diameter and 480 mm high, yielding an aspect ratio (height/width) of 3. Time-series traps were conical with 0.5 m^2 collecting area and 21 receiving cups; these traps were also covered with polyethylene baffles to decrease the effects of turbulent mixing.

Data from cylindrical traps showed there was a clear tendency for total mass fluxes to increase with depth at all three stations, and there was an especially large increase near-bottom. $^{239+240}$Pu concentrations in settling particles increased with depth from 1.76 mBq/g at 97-m depth to 3.00 mBq/g at 120-m depth and ranged from approximately 3 to 4 mBq/g at depths greater than 120 m. $^{239+240}$Pu concentrations collected in the near-bottom traps were approximately two times higher than those in the underlying surface sediments. Like total mass fluxes there was a clear tendency for $^{239+240}$Pu fluxes to increase with depth at every station, and the highest $^{239+240}$Pu fluxes were observed near-bottom.

$^{239+240}$Pu concentrations in the time-series traps had little variation throughout the sampling period, though the total mass fluxes showed a large variation. A high variability of $^{239+240}$Pu fluxes occurred in very short period of time (1/2 day); such measurements have not been reported previously. From sediment trap experiments on the continental slope in the East China Sea, the following findings were noted: (1) the highest $^{239+240}$Pu fluxes were observed in the near-bottom trap (12 m above the bottom); and (2) there was a large variation of $^{239+240}$Pu fluxes during a short period. The $^{239+240}$Pu concentration in surface sediment was significantly lower than that of the near-bottom trap at every station. The large fluxes of $^{239+240}$Pu in the near-bottom traps could not be explained as coming from resuspension of underlying surface sediments. The large fluxes of $^{239+240}$Pu might be attributed to episodic lateral transport of particles that flow down the continental slope with the nepheloid layer which was considered to be significant for $^{239+240}$Pu transport on the continental slope in the East China Sea.

77. Biokinetics of Radiotellurium in Rats

Yoshikazu Nishimura, Sarat Kumar Sahoo, Hee-Sun Kim*,
Shino Homma-Takeda and Yoshito Watanabe
（*Radiation Health Research Institute, Seoul）

Keywords : radiotellurium, biokinetics, fetal-transfer, milk-transfer

Radiotellurium is present in the environment from nuclear power accidents or as fallout from nuclear weapons tests. However, only a little information on the biokinetics of tellurium in juveniles and fetuses has been reported. The present study was conducted to investigate the whole-body retention of $^{123}Te^{m}$ in juvenile rats after a single oral administration, the fetal uptake of $^{123}Te^{m}$ for different gestational stages, and the transfer of $^{123}Te^{m}$ through milk into pups after a single intravenous administration to pregnant and nursing rats. Wistar strain rats were used to determine the uptake of $H_2{}^{123m}TeO_3$ by the whole-body retention of juvenile rats and the conceptus, corresponding to its gestational stages, by measurements in the placenta, fetal membranes, fetal fluid, and fetuses. For all age groups the retention patterns were similar, but the suckling rats had higher retention values than the weanling and adult rats. From the difference in the whole-body retention curve between oral and intravenous administration, it was estimated that about 10 % of the doses was absorbed from the gastrointestinal tract in adult rats. Whereas the intestinal absorption rate in suckling rat was obviously higher than that of adult rat, the biological half-life was roughly the same (about 10 days) for all age groups in the slowly decreasing phase after oral administration. This seemed to suggest that the whole-body retention of orally dosed radiotellurium in rat of various ages depended mainly on the rate of intestinal absorption rather than that of endogenous excretion. The relative concentrations in the placenta and fetal membranes were higher than in the fetus. No activity was observed in the fetal fluid. These results indicated that the placenta and fetal membranes played significant roles as barriers to the transfer of $^{123}Te^{m}$ into the fetus. The ratio, relative concentration in fetus/relative concentration in mother (C_F/C_M), was calculated. The C_F/C_M ratio was dependent on the stage of gestation and assumed to range from 0.2 to 0.5. The difference with C_F/C_M in the present study may be dependent on the chemical form of tellurium and the difference of tissue to whole-body measurements. The whole-body retention of suckling rats was 2, 3.9 and 5 % of maternal dose, 1 day after administration. The whole-body retention of suckling rats increased slowly during the suckling time and slowly decreased after weaning. However, taking the level of contamination from the mother's urine or feces into consideration, the transfer rate of radiotellurium from the mother to her suckling rats was thought to be relatively low. These results suggested that only a little radiotellurium was transferred to the milk. The present study's findings suggested that 2-5 % of the administered dose were transferred to suckling rats after intravenous administration and the amount of milk in sucklings was dependent on parturition age at the time of dosing.

Publication:

Nishimura, Y., Sahoo, S. K., Kim, H. S., Homma-Takeda, S., Watanabe Y., Inaba, J. , *Workshop on Internal Dosimetry of Radionuclides*, Oxford, Sept. 9-12, 2002

78. Micro-PIXE Application for Analysis of Elemental Distribution in Plant Root

Yoshito Watanabe, Shino Homma-Takeda, Masae Yukawa and Yoshikazu Nishimura

Keywords: *micro-PIXE, ICP-MS, trace element, plant, root*

Elemental mapping by micro-PIXE (Particle Induced X-ray Emission) analysis has a great potential for the examination of elemental behavior in complicated structures of biological tissues. We investigated application of micro-PIXE analysis for plant tissues, in combination with quantitative analysis by inductively coupled plasma mass spectrometer (ICP-MS).

Maize (*Zea mays* L.) seeds were sown on filter papers saturated with distilled water. After being cultured for two days at 24 ℃ in the dark, the seeds germinated and the roots reached about 2 cm in length. The roots were separated into four sections, 0-1 mm, 1-2 mm, 2-3 mm and 3-4 mm from the tip of the roots. The samples from thirty plants were put together, and digested with nitric acid to be introduced into an ICP-MS (HP-4500, Yokogawa Analytical Systems Co., Japan). For the micro-PIXE analysis, root apexes (about 2 mm in length) were sliced thinly (10 μm thick) with a cryo-microtome (CM 1510, Leica Instruments, Germany). The slices were put on a membrane (Pioloform, Agar Scientific Ltd., UK), and set in a micro-PIXE system in the tandem accelerator facility in NIRS.

ICP-MS was so sensitive that a large number of elements including Na, Mg, P, S, K, Ca, Mn, Fe, Cu, Zn, Se, Rb, Sr and Cs could be determined quantitatively. These fourteen elements covered almost all the essential elements for plant growth. The concentrations of the elements varied depending on the sections. The higher concentrations of the elements were observed in the closer section to the root tip, where a meristematic tissue and non-differentiated tissues are distributed. More precise estimation at the tissue level, however, could not be obtained by ICP-MS by analyzing sections from the root tip.

Micro-PIXE was, on the other hand, effective for detailed mappings of elemental distributions. The images of elemental distributions were obtained for Na, Mg, P, S, K, Ca, Mn, Fe and Zn, corresponding to the microscopic images of the root structures. Although Na, Mg, S, Ca, Mn, and Fe distributed uniformly over the root section, K, Zn and P showed localization depending on the tissues. K and P concentrations were higher in the meristematic tissue than differentiated tissues, whereas Zn was excluded from the meristematic tissue.

These results showed that micro-PIXE is of great use for precise estimation of elemental localization at the tissue level. ICP-MS is, on the other hand, a suitable method to detect a large number of elements, and useful for rough estimation of elemental distributions in maize roots. Micro-PIXE and ICP-MS have different, but complementary abilities for the investigation of elemental distributions in root tissues.

Publication:

Watanabe, Y., Takeda, S., Yukawa, M., and Nishimura, Y.: *International Journal of PIXE*, 11,125-131, 2001.

79. Elemental Imaging of Rat Testis by Micro-PIXE Analysis

Shino Homma-Takeda, Yoshikazu Nishimura, Yoshito Watanabe and
Masae Yukawa

Keywords: PIXE, imaging, seminiferous tubules, spermatogonea, spermatocytes, spermatids

Testis is known to be sensitive to radiation. Within the seminiferous tubules of testis, germ cells progress through mitosis, meiosis, and cellular differentiation to become spermatozoa. It has been demonstrated that the germ cells at different stages of the seminiferous tubules respond differently to exogenous stimuti. Elemental dynamics in the process, however, is poorly understood. The micro-PIXE technique was employed with testicular sections to reveal detailed distributions of elements in the testis, which distinguish the cell type-differences corresponding to the germ cell development.

Micro-PIXE measurements were made in the Electrostatic Accelerator Building of NIRS, utilizing a micro-beam scanning PIXE system with Si (Li) X-ray detector. Rat seminiferous tubules are classified into 14 stages and in the seminiferous epithelium, the germ cells are arranged in the following order: spermatogonia, spermatocytes, round spermatids and elongated spermatids. Elongated spermatids are at the innermost area. Corresponding to PIXE imaging with light microscopy, stage- and cell-specific elemental imagings were obtained for P and S. P was higher in the periphery of the seminiferous tubules of stages I, II-III, VII, VIII and XIII, where spermatogonia and spermatocytes were localized, than in the central area, that is, the spermatids. In stages VII and VIII, elongated spermatids, which are the final step in spermatogenesis, contained the lowest level of P among the four types of germ cells. In contrast, elongated spermatids in stages VII and VIII contained a higher level of S than the round spermatids, spermatocytes and spermatogonia in the same seminiferous epithelium as well as other germ cells in Stages I, II-III and XIII. These results suggested that P and S exhibit complementary dynamics in spermatogenesis.

Publications:

1) Homma-Takeda, S., Nishimura, Y., Watanabe, Y., Imaseki, H., and Yukawa, M.: *Int. J. PIXE*, **11**, 103-110, 2001.

2) Homma-Takeda, S., Hiraku, Y., Ohkuma, Y., Oikawa, S., Murata, M., Ogawa, K., Iwamuro, T., Li, S., Sun, G.F., Kumagai, Y., Shimojo, N., and Kawanishi, S.: *Free Radic. Res.*, **36**, 555-566, 2002.

80. Hyperaccumulation of Radioisotopes in Marine Algae

ToshiakiIshii, Shigeki Hirano, Teruhisa Watabe, Motokazu Nakahara and Mitsue Matsuba

***Keywords**: hyperaccumulation, algae, ^{90}Sr, ^{99}Tc, ^{187}Re, ^{226}Ra*

Hyperaccumulator plants are effective for mineral exploration, or biorecovery and detoxification of metal-contaminated soils. We found a new hyperaccumulator useful for estimating marine pollution by radioisotopes and for studying the mechanisms of bioaccumulation of elements by organisms.

Fifty species of marine algae were collected from the coast of Japan in 2001-2003. Ba and Sr were determined by ICP-AES. ^{187}Re ($T_{1/2}$=4.35x10^{10}y, abundance ratio=62.6%) was analyzed by ICP-MS. ^{90}Sr ($T_{1/2}$=28.78y) and ^{99}Tc ($T_{1/2}$=2.111x10^{5}y) were measured by low background β-ray spectroscopy. ^{226}Ra ($T_{1/2}$=1600y) was analyzed by a liquid scintillation counter. Gamma ray spectroscopy was applied to 50 g of ash samples of marine algae.

Table 3 shows concentrations of elements in green algae *Bryopsis maxima* and *Ulva pertusa*. The concentrations of all elements in *B. maxima* were considerably higher than those in *U. pertusa*. In particular, the Re concentration ($^{185+187}$Re=5,490,000 pg/g dry, ^{187}Re=5.6 mBq/g dry) was 22,000 times higher in *B. maxima* than in *U. pertusa*. The Re concentrations in 48 species of algae, excluding the genus *Bryopsis*, ranged from 51 to 29,100 pg/g on a dry weight basis (mean±sd; 5,200±4,800 pg/g). The concentration factor (CF) of *B. maxima* was calculated to be 7.4x10^{5} (7.1x10^{4} on a wet basis) from *ca.*7pg/mL of the Re concentration in Pacific Ocean seawater. *B. maxima* also showed a high concentration (1.03 pg/g dry=660 μBq/g dry) of ^{99}Tc belonging to the same Ⅶ /7 group as Re in the periodic table. Although ^{99}Tc was detected in some species of marine algae, such as *Sargassum thunbergii* (18-270 μBq/g dry), *Sargassum hemiphyllum* (130 μBq/g dry), and *Hizikia fusiformis* (42 μBq/g dry),
the concentration of ^{99}Tc in almost all of Japanese marine algae collected in 2001-2003 was less than the minimum detectable amount (15 μBq/g dry=3 mBq/200g dry).

As shown in Table 3, *B. maxima* had high concentrations of alkali earth elements. For example, the Ba concentrations (4,630 μg/g dry) in *B. maxima* were 2,700 times higher than in *U. pertusa*. *B. maxima* was defined as a Ba hyperaccumulator because the average concentration of Ba in 50 species of marine algae in Japan was 5.19±4.89 μg/g dry wt. The average concentration of ^{226}Ra in 12 species of marine algae was 0.225±0.178 pg/g dry wt. In contrast, *B. maxima* showed a very high concentration of ^{226}Ra (21.4 pg/g dry=780 mBq/g dry). In the case of gamma ray spectroscopy, it was indicated that 185.7155 kev of ^{235}U must be overlapped with 186.1010 kev of ^{226}Ra. We think that no significant amount of ^{235}U was present in *B. maxima*, because 143.762 kev and 163.332 kev of ^{235}U were not observed.
Furthermore, clear peaks of ^{214}Bi ad ^{214}Pb derived from ^{226}Ra were found in the spectrum of *B. maxima*. From the results of radiochemical analyses and gamma ray spectroscopy, *B. maxima* was recognized to be a Ra hyperaccumulator. The Sr in *B. maxima* had the highest value (13,100 μg/g dry) among algae. We think that *B.*

maxima is a Sr hyperaccumulator since the "Hyperaccumulation level of Sr" was 5,000 μg/g dry (hyperaccumulation level -100 times concentration in reference plant). As a result of radiochemical analyses of ^{90}Sr , *B. maxima* showed the highest value (2.8 mBq/g dry= 0.27 mBq/g wet) among algae. Its CF value for wet basis was calculated to be 170, since the radioactivity of ^{90}Sr in the seawater around Japan was approximately 1.6mBq/L.

Table 3. Concentrations (pg/g dry weight) of elements in green algae collected from the same location and at the same month

Element (Isotope)	*Bryopsis maxima* (N=3) (mean±sd)			*Ulva pertusa* (N=3) (mean±sd)		
Ba	4.63×10^{9}	±	1.9×10^{8}	1.72×10^{6}	±	1.1×10^{5}
Ra (as ^{226}Ra)	2.14×10^{1}	±	4.5×10^{0}	1.95×10^{-2}	±	1.6×10^{-3}
Re	5.49×10^{6}	±	3.7×10^{5}	2.51×10^{2}	±	2.3×10^{1}
Sr	1.31×10^{10}	±	1.1×10^{9}	3.21×10^{7}	±	2.7×10^{6}
Tc (as ^{99}Tc)	1.03×10^{0}	±	3.5×10^{-1}	$< 2.36 \times 10^{-2}$	±	

81. Elemental Distribution in Organs of Medaka, *Orysias laptipes*, Burdened with X-ray Irradiation and Salty Water Breeding Determined by PIXE Analysis

Masae Yukawa, Yuji Ishikawa, Hitoshi Imaseki, Kazuko Aoki and Takahiro Okazaki

Keywords: Medaka, elemental distribution, PIXE analysis, X-ray irradiation, salty water breeding

In NIRS, an inbred strain of Medaka, *Oryzias laptipes*, was established and has been maintained for research purposes. Medaka is a small fish like a killifish, 3-4 cm long. We investigated metal balance shift induced in the fish with X-ray irradiation and salty water breeding as environmental stresses. The $LD_{50/30}$ of this fish to X-ray irradiation is 20 Gy, and the survival rate of the fish is about 80% when breed in seawater with 70% NaCl. Fifteen Medaka fish, about 1 year old, were divided into 3 groups and put into 3 separate plastic vessels. The first was for X-ray irradiation, the second was for salty water breeding, and the third was for control. These vessels were kept in a laboratory at room temperature. The fish were used for experiments after become accustomed to the breeding environment. Fish for salty water breeding adapted gradually over 14 days to the 70% NaCl of seawater. On the 16th day after starting to breed Medaka, the first group of five fishes was irradiated with X-rays in a plastic vessel (5mm deep) using PANTAK-320S at 200kV and 20mA. The dose rate was 224R/min and the total dose was 17.00Gy.

On the 18th day, two fish were selected from each group, and were killed and dissected. Ten organs, brain, eye, gill, heart, liver, spleen, intestine, gonad, tail and scale on gill, were sampled from each fish. The weights of the organs ranged from a few mg to about 1g as fresh. After freeze-drying, the organs were analyzed by the Particle Induced X-ray Emission (PIXE) method to determine elemental contents in the organs with 2.6MeV proton beam of 1mm square for 10min at 10nA. In Fig.30, the changes of Fe, Cu, Zn and Mn contents in liver, ovary, spleen, brain, intestine and eye induced by the two types of stresses are shown as the comparison of the stressed fish to the control. In the liver and spleen, both stresses increased the contents of Cu, Zn and Mn. In the case of ovary, the stresses decreased the contents of Fe and Mn. Brain seems to be most stress- resistant organ among these 6 organs. In eye, the content of Fe was most depressed by salty water.

It is well known that radiation like X-rays and γ -rays generate active oxygen species in a living body. Since the active oxygen species is dangerous for organisms due to damages induced in DNA, there are various defensive systems in the animals and plants. Some of them are enzymes for radical scavenging such as super oxide dismutase (SOD), glutathione peroxidase (GPx) and catalase. Cu, Zn and Mn are included in SOD and act as the active center. In the case of GPx, Se is present in this enzyme. Therefore, Cu, Zn, Mn and Se are very important elements in reducing radiation damages. On the other hand, Fe is thought to be one of the factors to make active oxygen. It is necessary to continue the experiments to confirm the results described above. The next step would be an investigation of other environmental stresses such as heavy metals and organic chlorides.

Publications

1) Yukawa, M., Ishikawa, Y., Imaseki, H. and Aoki, K.: *International Journal of PIXE*, **10**, 121-125, 2000.

2) Yukawa, M., Ishikawa, Y., Imaseki, H. and Aoki, K.: *International Journal of PIXE*, **11**, 119-124, 2001.

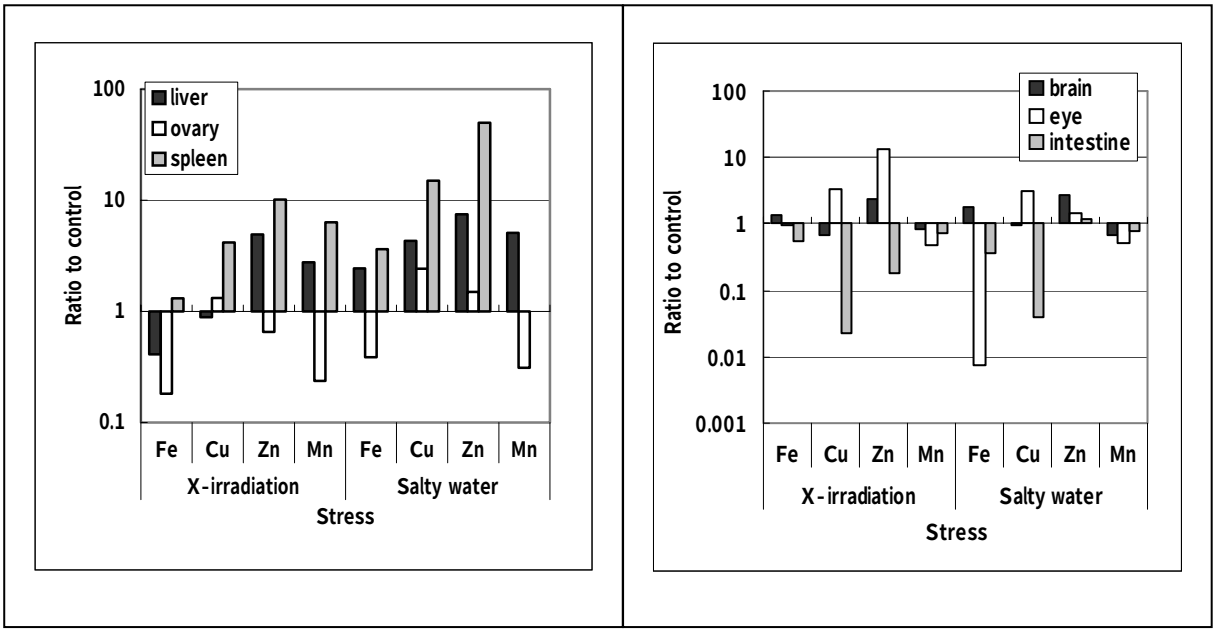
100
10
1
0.1
Ratio to control
liver
ovary
spleen
Fe
Cu
Zn
Mn
Fe
Cu
Zn
Mn
X-irradiation
Salty water
Stress
100
10
1
0.1
0.01
0.001
Ratio to control
brain
eye
intestine
Fe
Cu
Zn
Mn
Fe
Cu
Zn
Mn
X-irradiation
Salty water
Stress

82. Cancer Risks among Radiologists and Radiologic Technologists: A Review of Epidemiological Studies

Shinji Yoshinaga, Kiyohiko Mabuchi*, Alice J. Sig urdson*, Michele M Doody*, and Elaine Ron*

(* Radiation Epidemiology Branch, Division of Cancer Epidemiology and Genetics, National Cancer Institute, NIH)

Keywords: *epidemiology, occupational exposure, cancer, radiologists, radiologic technologists*

Radiologists and radiologic technologists are among the earliest occupational groups exposed to ionizing radiation and represent a large segment of the working population exposed to radiation from man-made sources. We reviewed published and unpublished epidemiological data on cancer risks from eight cohorts of over 270,000 radiologists and technologists in the UK, US, Canada, Denmark, China, and Japan (Table 4). The most consistent finding was increased mortality from leukemia among early workers employed before 1950. This, together with an increasing risk of leukemia with increasing duration of work in the early years, provides evidence of an excess risk of leukemia associated with occupational radiation exposure in that period. While findings on several types of solid cancers were less consistent, there was evidence of a radiation effect for breast cancer mortality, which increased with increasing duration of work in the early years, and skin cancer mortality and incidence, which was increased among the early period workers in several cohorts. Among the most recent workers, there is no clear evidence to date of increased cancer risks associated with occupational

exposures to radiation. However, with the increasing uses of radiation in modern medical practices, the continuing health assessment of medical radiation workers is important. The lack of radiation dose estimates was the major deficiency for these studies and limited the potential usefulness of data. Continued follow-up, with incorporation of dose estimates, would open an opportunity for providing much needed data to advance understanding of the cancer risk from chronic exposure to low to moderate doses of radiation.

83. Relationships between Radiocesium and Stable Cs in Mushrooms and Plants Collected in Forests with Different Contamination Levels

Satoshi Yoshida and Yasuyuki Muramatsu

Keywords: *forest, mushroom, plant, radiocesium, stable Cs*

Forest ecosystems accumulate radiocesium discharged into the atmosphere through nuclear weapons testing and nuclear accidents. Even more than 15 years after the Chernobyl accident, radiocesium contamination of forest products such as mushrooms and berries is high in contrast to agricultural products. Since the removal of radiocesium from a contaminated forest is not feasible on a large scale, studies on the distribution and transfer of radiocesium in forest ecosystems are important from radiation protection viewpoint and geochemical viewpoint. The long-term fate of radiocesium in forest ecosystems is necessary to be predicted for decision-making of the future countermeasures. As the chemical behavior of radiocesium is expected to be almost identical to that of stable Cs, analyses of stable Cs should be useful to understand the long-term behavior of radiocesium and its equilibrium distribution. However, the relationship between radiocesium and stable Cs in forest ecosystems is still unclear because of the lack of analytical data. In this study, we have determined the concentrations of stable Cs in mushrooms and trees collected in forests with different contamination levels in Japan, Germany, Finland, Italy and Ireland. Data of stable Cs were discussed together with those of radiocesium.

Samples were collected from 1989 to 1996. Mushrooms were collected in 5 different forests in Japan, Germany and Finland. For tree samples, one representative Spruce tree was selected for each forest in Italy and Ireland, and different parts of the tree were sampled. Samples were dried, milled and digested with acids. Concentration of stable Cs was determined by inductively coupled plasma-mass spectrometry (ICP-MS). Activity concentration of ^{137}Cs was determined by counting with a Ge-detector.

Relationships between ^{137}Cs and stable Cs for mushrooms collected from 5 different forests were summarized in **Fig. 31**. A good correlation between ^{137}Cs and stable Cs was observed for each site independently, although several different species of mushrooms are included. This finding suggests that mushrooms take up ^{137}Cs together with stable Cs. The ^{137}Cs/stable Cs ratios were fairly constant for samples collected at the same site. The results for different sites, however, showed different degrees of variability. The variability of the ^{137}Cs/stable Cs ratio might be a useful criterion for judging the equilibrium of deposited ^{137}Cs to stable Cs in a forest ecosystem. Standard deviation of the ^{137}Cs/stable Cs ratio for mushrooms was the lowest in Japanese forests (Tokai-mura: 27%), in which most ^{137}Cs originated from the global fallout, and the highest in Hochstadt, Germany (48%). This

finding suggests that ^{137}Cs deposited from the global fallout (mostly in 1960s) has already attained a dynamic equilibrium within the soil-mushroom system.

As shown in the same figure, the good correlation between ^{137}Cs and stable Cs and almost constant ^{137}Cs/stable Cs ratio were also observed in tree samples collected in each site, Italy and Ireland, indicating that ^{137}Cs has well mixed with stable Cs within a tree.

We are currently studying samples, including soils and several different species of plants and mushrooms, collected in 4 different forests with different contamination levels in Belarus. This study is expected to yield comprehensive information of radiocesium and stable Cs and their interrelation in the whole forest ecosystem.

Publication:

Yoshida, S., Muramatsu, Y., Steiner, M., Belli, M., Pasquale, A., Rafferty, B., Rühm, W., Rantavaara, A., Linkov, I., Dvornik, A. and Zhuchenko, T.: *Radioprotection*, **37**, C1-391-396, 2002.

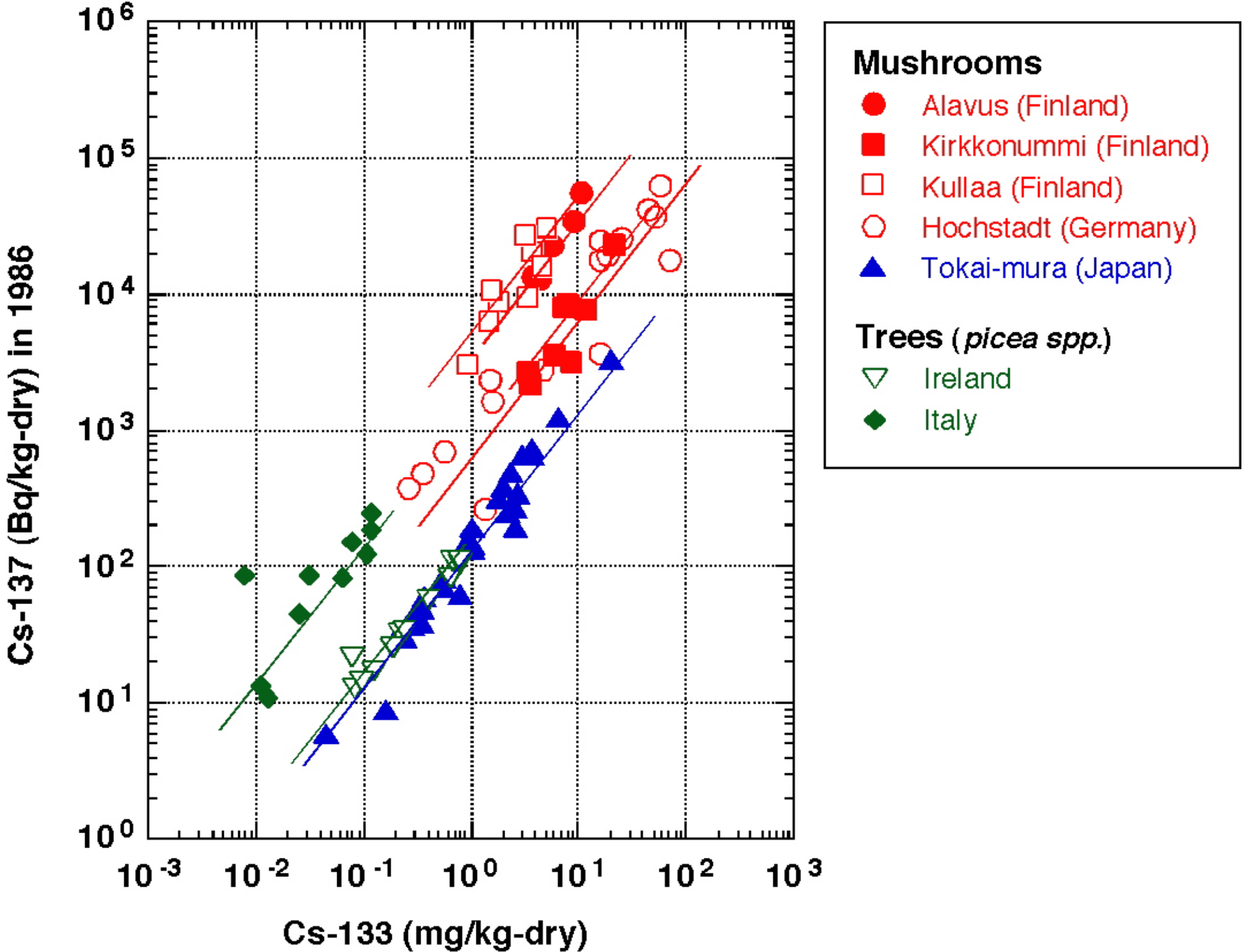
Cs-137 (Bq/kg-dry) in 1986
Cs-133 (mg/kg-dry)
10^6
10^5
10^4
10^3
10^2
10^1
10^0
10^-3
10^-2
10^-1
10^0
10^1
10^2
10^3
Mushrooms
Alavus (Finland)
Kirkkonummi (Finland)
Kullaa (Finland)
Hochstadt (Germany)
Tokai-mura (Japan)
Trees (picea spp.)
Ireland
Italy

図の説明

Yoshida et al.: Relationships between Radiocesium and Stable Cs in *****

Fig. 31. Relationship between stable Cs (Cs-133) and Cs-137 in mushrooms and trees collected from 7 different forests. Straight line corresponds to average Cs-137/Cs-133 ratio in each forest.

84. Determination of Trace Rhenium in River Water Samples by Q-ICP-MS and HR-ICP-MS

Shigeo Uchida and Keiko Tagami

Keywords: rhenium, river water, ICP-MS, chemical separation

In order to understand ^{99}Tc transportation mechanisms in surface water systems, we focused on Re that can be used as a chemical analogue for Tc in the environment, because the two elements are chemically similar. Rhenium is one of the least abundant metals in the earth's surface and its concentration in environmental samples is not well known. The Re concentration in seawater is reported to be between 6-15 pg/mL, but the data in fresh water are quite limited. To measure low-level Re in fresh water samples with inductively coupled plasma mass spectrometry (ICP-MS), we tried two approaches: one was to develop a simple chemical separation before ICP-MS measurement and the other was to make direct measurements with a high sensitivity instrument, such as high resolution ICP-MS (HR-ICP-MS).

River water samples were collected in Osaka and Wakayama Prefectures, Japan, in August 2000. The sample water was pressure filtered through 0.45-μm membrane filters (Millipore Co.). From the filtered sample, ca. 50mL were transferred into an acid-cleaned 50-mL polypropylene bottle. These sub-samples were used for the direct Re determination by a HR-ICP-MS (Finnigan MAT, Element). Chemical separation of Re was performed on 420 – 925 mL of the filtered river water samples using a TEVA resin column. Measurements of Re in the chemically separated samples were carried out with a quadrupole (Q-) ICP-MS (Yokogawa, PMS-2000) and the HR-ICP-MS. To make a standard curve for ICP-MS measurements, multi-element standard solution, XSTC-8 (SPEX Industries Inc.), was used. The instrumental detection limit on the Q-ICP-MS and the HR-ICP-MS was 0.2 and 0.007 pg/mL, respectively.

A simple extraction using the TEVA resin could separate Re from most sample matrices and trace elements. Almost 100% recovery was found throughout the simple separation method as determined with a radioactive tracer. The measured Re contents by Q-ICP-MS and HR-ICP-MS are shown in Fig. 32. The errors (1 sigma) to the individual data by these methods were almost the same: 4.4-6.2% for Q-ICP-MS with the separation method, 4.5-5.3% for HR-ICP-MS with the separation method and 3.9-7.2% for direct HR-ICP-MS. The average value for each sample obtained by these methods had errors of 1-6.6% (1 sigma). The results by these three methods showed good agreement with each other, and no systematical difference was found among them. The Re concentrations in the river water samples ranged from 0.9 to 6.5 pg/mL. Although there was no significant difference between the results of direct HR-ICP-MS and the chemical-separation Q- and HR-ICP-MS, it is better to use the separation method developed in this study to secure a more accurate measurement when a low-level Re content in a sample is expected.

Publication:

Uchida, S. , Tagami, K. and Saito, M. : *J. Radioanal. Nucl. Chem.*, **255**, 329-333, 2003.

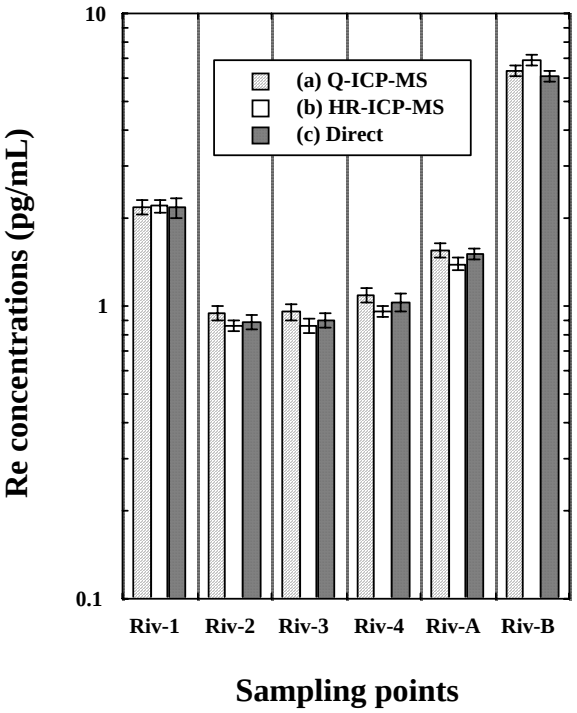

Fig. 32. Concentrations of Re in river water samples determined by (a) chemical separation and Q-ICP-MS, (b) chemical separation and HR-ICP-MS and (c) direct HR-ICP-MS.

85. Global Fallout Technetium-99 Distribution and Behavior in Japanese Soils

Keiko Tagami and Shigeo Uchida

Key words: technetium-99, surface soil, ICP-MS, activity ratio of $^{99}Tc/^{137}Cs$

From a radioecological viewpoint, analysis data on global fallout ^{99}Tc in environmental samples should give useful information for predicting the nuclide behavior. At present, however, due to very low concentration and analytical difficulties for determination of the nuclide in environmental samples, there is a general lack of data on ^{99}Tc levels in the literature. Therefore, the behavior of the nuclide in the terrestrial environment is not well understood.

In this study, we determined concentrations of ^{99}Tc in surface soil samples using inductively coupled plasma mass spectrometry. ^{137}Cs concentration was also measured to use it as a comparative indicator for discussion of the sources of ^{99}Tc, because the fission yields from ^{235}U and ^{239}Pu are about the same (ca. 6%) for the two isotopes, and the behavior and distribution of ^{137}Cs in the environment is reasonably well understood. The activity ratio of ^{99}Tc/^{137}Cs was calculated to understand Tc mobility in the soil environment.

The ranges of ^{99}Tc and ^{137}Cs concentrations in rice paddy fields are 6 – 88 mBq/kg-dry and 1.4 – 14 Bq/kg-dry, respectively. Those in upland field soils are 4.3 – 7.7 mBq/kg-dry and <1.1 – 7.7 Bq/kg-dry, respectively, and those in other soils are 7- 29 mBq/kg-dry and <1.1 – 144 Bq/kg-dry, respectively. Slightly high correlations ($r>0.5$) between ^{99}Tc concentrations and some soil properties, such as CEC, act-Fe, total-C, org-C, and total-N, for upland field soils and other soils are found. No correlation appears for the paddy field soils. The relation has not been explained yet, though there was a possible influence from organic matter and microorganisms in the soils.

The activity ratios of ^{99}Tc to ^{137}Cs for paddy field soils are given in figure 33, and they range from 1.1×10^{-3} to 7.0×10^{-3} with an geometric average of 4.8×10^{-3}. Theoretically, the activity ratio from nuclear fission yield is presently calculated as 3.3×10^{-4} with correction for radioactive decay, because it is assumed that the major source of ^{99}Tc in Japan to now arises from fallout. Compared to the theoretical ratio, the activity ratios in the paddy field soils are one order of magnitude higher. However, the activity ratios in paddy field soils of this study are the same order of magnitude or one order of magnitude less than those in undisturbed soils in Japan reported previously as $(1.2 – 39) \times 10^{-3}$. The average activity ratios found in this study for upland field soils are seven times higher than the theoretical ratio but those for other soils are close to the theoretical one. Among the soils used in this study, the average activity ratio for paddy field soils is the highest. The ratios in paddy field soils are twice as much as those in upland field soils and one order of magnitude higher than those in other soils maybe because of different degrees of the soil reduction. The higher or similar activity ratios found in this study as compared to the theoretical one suggest ^{99}Tc accumulation in the soils, even under aerobic conditions.

Publication:
Tagami, K. and Uchida, S.: *J. Nucl. Radiochim. Sci.* **3**, 1-5, 2002.

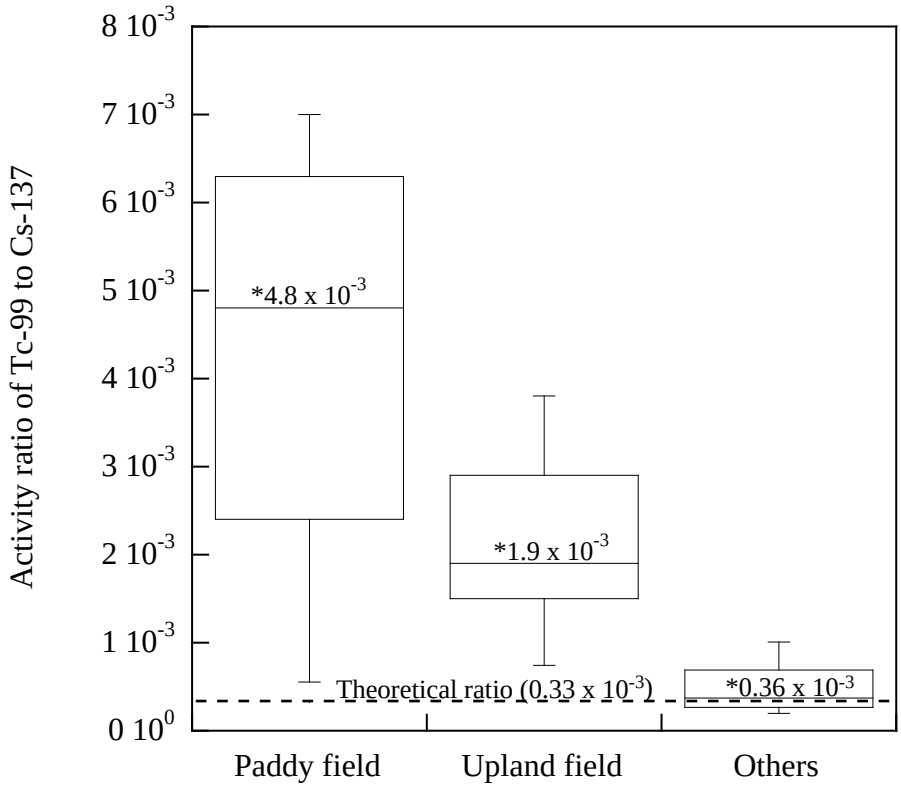

Fig. 33. Activity ratios of ^{99}Tc and ^{137}Cs in soil samples collected in Japan.
(Note) *: geometric average.

86. Changes in Physicochemical Forms of Technetium in the Water Covering Paddy Soils

Nobuyoshi Ishii, Keiko Tagami and Shigeo Uchida

Keywords: technetium, insolubilization, paddy field, bacteria

The radioactive nuclide technetium-99 (^{99}Tc) is a fission product of ^{235}U formed during the reprocessing of nuclear fuel and is a long-lived radionuclide ($T_{1/2}$ = 2.1 10^5 y). This radioactive material has been accumulated and distributed in the environment. The availability of Tc by plants is dependent upon its physicochemical forms. The pertechnetate anion (TcO_4^-), which is most stable form of Tc under aerobic solutions, can be taken up by agricultural crops and vegetables. In extended laboratory and field studies, plant availability of Tc is reduced over time. This phenomenon is considered to be a result of the formation of insoluble Tc by the reduction from Tc (VII) to Tc (IV). We previously suggested that microbial reduction caused the insoluble Tc in waterlogged paddy soils. However, it is not unclear whether the insoluble Tc formed in soils or in water covering paddy soils and whether microorganisms affected physicochemical forms of Tc directly or indirectly. In this paper, we describe the changes of physicochemical forms of Tc in the water covering paddy soils and direct effects of microorganisms on its physicochemical transformation.

Fourteen soils collected from paddy fields (9 samples) and upland (5 samples) were waterlogged and incubated for 7 days at 25˚C. After the incubation, the water covering the soils were collected in newly prepared test tubes. These samples (1.6 – 2.0 ml) were incubated statically with soluble $^{95m}TcO_4^-$ at 25˚C for 4 days again. The cultures were in contact with air. After the incubation with ^{95m}Tc, the samples were sequentially separated into four fractions: one insoluble fraction (> 0.2 μm) and three soluble fractions (TcO_4^-, cationic, and other forms). The radioactivity of ^{95m}Tc in each fraction was measured with a NaI (Tl) scintillation counter.

Dominant species of Tc was pertechnetate anion, but the insoluble Tc was also observed in the samples of the water covering soils (Fig. 34). On an average, 13% of the $^{95m}TcO_4^-$ changed to insoluble forms and the maximum ratio of the insolubilization was 76% of the P38 sample, which was collected from a paddy field (gray lowland soil). No statistically differences in the average amount of insoluble Tc between paddy and upland soils were found. The amount of cationic and the other forms of Tc were less than 1% of total. Although technetium is normally present as the pertechnetate anion in aerobic solutions, our results show that insoluble Tc can occur in the water covering specific soils like P38 even under aerobic conditions.

Pertechnetate could be affected indirectly by physicochemical modifications of the local environment (Eh and pH) leading to reduction of TcO_4^-. Indeed, values of Eh and pH in P38 were low enough to reduce Tc (VII) to Tc (IV). Then, we determined the insolubilization of Tc in a P38 solution passed through a 0.2 μm-pore-size membrane filter. Insoluble Tc was 4.8% of the untreated sample, but when microbial particles, which were killed by autoclaving, were added to the filtrate of P38, insoluble Tc was 2.6% of the untreated sample. These results indicate little indirect insolubilization of Tc in P38.

In order to clarify direct effects of microorganisms on the insolubilization of Tc, organic substrates were added to the P38 sample to promote microbial growth. The addition of substrates resulted in the enhancement of insoluble Tc (115% of untreated sample). The potential direct effects on insolubilization of Tc are biosorption and bioaccumulation. Added pertechnetate

anion added does not sorb on microbial cell surface because the surface generally has a negative charge. From these results, we concluded that insoluble Tc in P38 resulted from bioaccumulation by microorganisms.

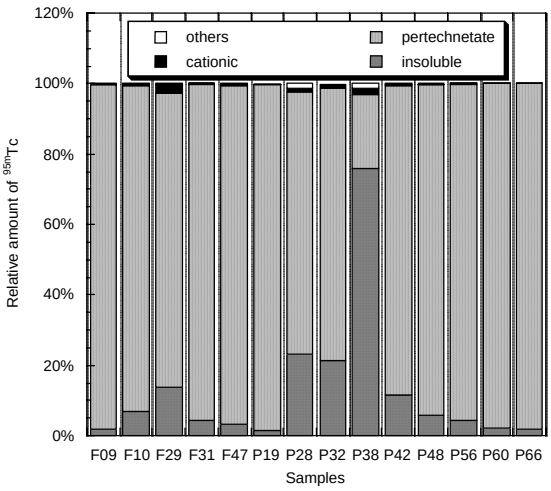

Fig. 34. Relative amount of insoluble, pertechnetate, cationic, and other forms of technetium in the water covering soils. F and P mean upland fields and paddy fields samples, respectively.

87. Bio-kinetics of Radon Ingested from Drinking Water

Tetsuo Ishikawa, Yukinori Narazaki[1], Yasuoka Yasuoka[2], Shinji Tokonami and Yuji Yamada

([1]Fukuoka Institute of Health and Environmental Sciences; [2]Kobe Pharmaceutical University)

Keywords: *ingested radon, drinking water, stomach, dosimetry*

It has been reported that high concentrations of radon can occur in water supplies from groundwater. Since the ingestion of radon-rich water presents a possible risk to human health, several investigators have studied the fate of ingested radon in the body. These studies identified the stomach wall as the most significant organ. An important factor regarding the dosimetry for the stomach is the rate of radon loss from the stomach. The objective of the present study is to estimate the rate of radon loss from the stomach by *in vivo* counting of radon progeny (^{214}Pb and ^{214}Bi).

Two adults served as volunteer subjects for *in vivo* counting. After the ingestion of radon-rich water samples, each subject was measured the stomach. The detector was shielded with lead of 50 mm thickness to minimize effects of gamma rays from other organs than the stomach. *In vivo* counting was started a few minutes after the ingestion. The measurement of each subject lasted more than 100 minutes.

The *in vivo* counting data on ^{214}Pb and ^{214}Bi could give only indirect information on the behavior of radon in the body. This is because (1) the measured gamma rays are the third and fourth emissions in the ^{222}Rn decay chain, and (2) the behavior of radon in the body could be different from that of radon progeny. Thus, a bio-kinetic model was developed to interpret the *in vivo* counting data. The model includes parameters for the behavior of radon as well as its progeny. The retention of radon was estimated by fitting these parameters to the experimental data.

As an example, the fitting process of the ^{214}Bi retention curve for subject A is shown in Fig. 35. Previous models for dosimetric purposes often assumed that radon transfers from the stomach to the small intestine with a half-time of below 20 min. Curve 1 was calculated using a half-time of 20 min for all ingested radon and its progeny. There was a big difference between calculated and experimental data. Thus, the parameters were changed accordingly; first, it was assumed that half the amount of radon progeny stayed as a long-term retention fraction (Curve 2). However, this assumption could not explain the long half-time observed from the experimental data. Even if all of the ingested radon progeny was retained in the stomach (that is, no transfer occurred), the half-time for ^{214}Bi was calculated to be about 40 min. This value was smaller than the half-times observed from the experiments. The long half-time suggested the existence of long-term retention fraction for radon as well as radon progeny. Curve 3 shows a good fitting; this curve was obtained assuming that 60 % of ingested radon decreased with a half-time of 240 min. The value of half-time was much larger than that used in previous dosimetric models (below 20 min). The present research suggested that a part of the radon stayed longer in the stomach than was expected in previous models.

Publication:

Ishikawa, T., Narazaki, Y., Yasuoka, Y., Tokonami, S. and Yamada, Y.: *Radiat. Prot. Dosim.*, **105**, 65-70, 2003.

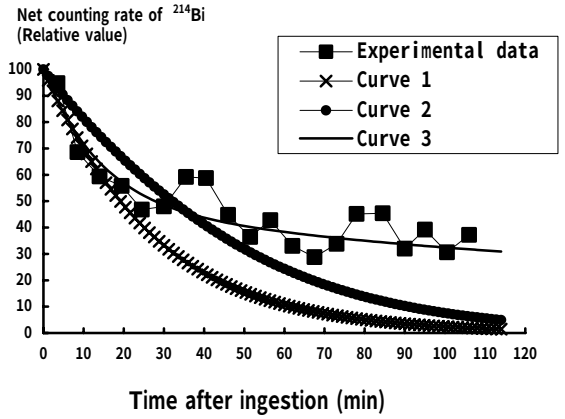

Fig. 35. A model fitting for the ^{214}Bi retention curve

Table 5. Alpha counting efficiencies of the scintillation cell from a Monte Carlo calculation

Cell type	*Radon*	*^{218}Po*	*^{214}Po*	*Thoron*	*^{216}Po*
110A	0.681	0.763	0.884	0.781	0.827
300A	0.637	0.742	0.864	0.736	0.780

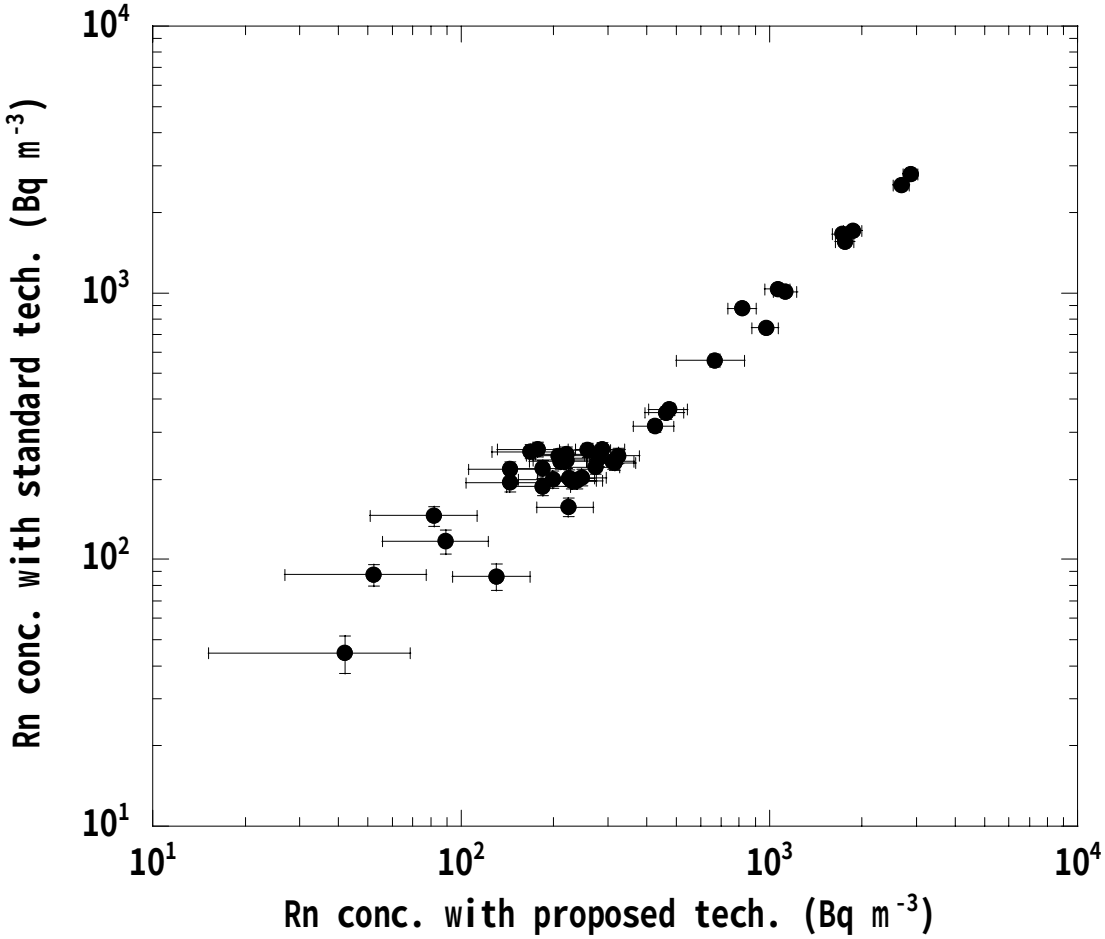

Fig. 36. Comparison of the radon concentration between the standard and proposed techniques.

88. Simple, Discriminative Measurement Technique for Radon and Thoron Concentrations with a Single Scintillation Cell

Shinji Tokonami, Hidenori Yonehara and Yuji Yamada

Keywords: radon, thoron, discriminative measurement

For simplicity and rapidity, a measurement technique was designed so as to measure both radon and thoron concentrations with a single scintillation cell. In principle, it is based on two measurements that use the difference in half life between radon and thoron. (Note that long-lived thoron progeny are not considered in the present study because the measurement terminates within 1 h.)

Alpha counting efficiencies of the scintillation cell were estimated with a Monte Carlo calculation. Both Pylon model 110A and 300A Lucas cells are used in the present study. The 110A cell is a cylindrical vessel, 53 mm in diameter and 70 mm high. Its inner volume and active area are 1.51×10^{-4} m^3 and 1.88×10^{-2} m^2, respectively. On the other hand, the dimensions of the 300A cell are 70 mm diameter and 124 mm height. The inner volume and active area are 2.7×10^{-4} m^3 and 2.77×10^{-2} m^2, respectively. The Pylon model AB-5 scintillation detector is also incorporated into the measuring system. The following conditions are set up in the calculation:

(1) The inner walls are covered with ZnS scintillators except for the transparent plate (glass) at the bottom attached to the detection surface of the photomultiplier.

(2) Radon or thoron gases are uniformly distributed in the cell after injection. ^{216}Po atoms behave like the gases because the half life is very short (0.15 s). The other progeny attach to the inner wall immediately after they are formed in the cell.

(3) If alpha particles reach the wall, the scintillation will definitely occur and can be detected.

Table 5 shows the alpha counting efficiencies for the individual radionuclides of both cells. Using these alpha counting efficiencies, conversion factors for the radon concentration were calculated and compared with experimental values. Since the conversion factor is generally provided at radioactive equilibrium, it can be expressed as the following equation:

$$CF = \frac{1}{\left(\eta_{Rn} + \eta_{RaA} + \eta_{RaC'}\right) \times V_c \times 60} \quad (1)$$

where,

CF: conversion factor of radon concentration (Bq m^{-3} cpm^{-1});

η_{Rn}, η_{RaA}, $\eta_{RaC'}$: alpha counting efficiencies for radon, ^{218}Po and ^{214}Po, respectively;

V_c: inner volume of cell (m^3).

In the case of the 110A cell, a conversion factor of 47.4 was obtained. There is a 3% difference between this and the experimental conversion factor of 48.7. In the case of the 300A cell, this calculation provided 27.9 Bq m^{-3} cpm^{-1}, also within 3% of the experimental value of 27.0. From these two agreements, the counting efficiencies for thoron and ^{216}Po are reasonable in this calculation.

After taking air samples with thoron, the count(C_{Tn}) on the initial phase can be expressed as follows:

$$C_{Tn} = V_c \times \int_{t_0}^{t_0 + t_m} \left(\eta_{Tn} X_{Tn} + \eta_{ThA} X_{ThA}\right) dt \quad (2)$$

where

t_0: beginning of the measurement (s);

t_m: measurement period (s);

η_{Tn}, η_{ThA}: alpha counting efficiencies for thoron and ^{216}Po, respectively;

X_{Tn}, X_{ThA}: activity concentrations for thoron and ^{216}Po, respectively (Bq m^{-3}).

Assuming that $X_{Tn}=X_{ThA}$ because of the radioactive equilibrium between thoron and ^{216}Po, therefore, the initial thoron concentration (X_{Tn0}) can be obtained as follows:

$$X_{Tn0} = \frac{C_{Tn}}{V_c \times (\eta_{Tn} + \eta_{ThA}) \int_{t_0}^{t_0+t_m} e^{-\lambda_{Tn} t} dt} \quad (3)$$

where

λ_{Tn}: decay constant of thoron (s^{-1}).

If radon is present as well as thoron, counts due to radon and its progeny must be subtracted from those in the measurement period. Therefore, another measurement is necessary after the thoron decays. The count comes from radon and its progeny only, so eqn. (3) can be rewritten as follows:

$$X_{Tn0} = \frac{C_1 - kC_2}{V_c \times (\eta_{Tn} + \eta_{ThA}) \int_{t_0}^{t_0+t_m} e^{-\lambda_{Tn} t} dt} \quad (4)$$

where

C_1: counts in the first measurement period;

C_2: counts in the second measurement period.

The constant "*k*" can be determined with the existing ratio of radon and its progeny in the cell and measurement timetable. It can be approximately assigned to be 0.2 with timetables given as below.

For a total measurement period of 15 min, an optimized timetable was determined. Since two measurements have to be made in 15 min, the second measurement period of 5 min was fixed (10-15 min after sampling). The beginning of the first measurement was also fixed to start 20 s after sampling. Relative standard deviations of the thoron concentration were calculated under several different first measurement periods. Thoron and radon concentrations were assumed to be both 100 Bq m^{-3} in the calculation. When the end of the first measurement was set at around 100 to 150 s, the relative standard deviation became the smallest. Thus the first measurement was made between 20 and 120 s. In order to verify the validity of this optimized timetable, the radon concentration was compared between standard and proposed techniques. In the standard technique, the radon concentration was determined after reaching radioactive equilibrium between radon and its progeny. There was a relatively good agreement between the two as shown in **Fig. 36**. It is obvious that an adequate timetable will result in prompt determination of radon and thoron concentrations if alpha counting efficiencies are individually and precisely given.

Publications:

1) Tokonami, S., Yang, M., Yonehara, H. and Yamada, Y.: *Rev. Sci. Instrum*., **73**, 69-72, 2002.

2) Sun, Q., Tokonami, S., Yamada, Y and Akiba, S.: *Radioisotopes*, **51**, 120-126, 2002.

3) Tokonami, S., Sun, Q., Yonehara, H. and Yamada, Y.: *Jpn. Health Phys*., **37**, 59-63, 2002.

4) Tokonami, S., Yonehara, H. Yang, M., Furukawa, M. and Yamada, Y.: *Proc. 5th International Conference on High Levels of Natural Radiation and Radon Areas: Radiation Dose and Health Effects*, 271-273, 2002.

5) Tokonami, S., Yonehara, H. Zhuo, W., Sun, Q. Sanada, T. and Yamada, Y.: *Proc.: Indoor Air 2002*, 665-669, 2002.

89. A New Passive Integrating Radon and Thoron Monitor

Weihai Zhuo, Shinji Tokonami, Hidenori Yonehara and Yuji Yamada

Keywords: *radon, thoron, passive monitor*

Many types of passive integrating ^{222}Rn monitors have been developed for large-scale and long-term measurements. However, most of the monitors are sensitive to not only ^{222}Rn, but also thoron (^{220}Rn) in different extents. To precisely measure ^{222}Rn concentration, it is necessary to evaluate the influence of ^{220}Rn on the ^{222}Rn measurements. On the other hand, recent surveys have revealed that the exposure to ^{220}Rn and its progeny should not be neglected in some areas. Therefore, measurements of ^{220}Rn are indispensable for more precise assessment of public exposure to ^{222}Rn and ^{220}Rn.

Fig. 37 illustrates the construction of the new type of passive integrating ^{222}Rn and ^{220}Rn monitor developed in this study. The ^{222}Rn monitor is commercially available, it is a cylindrical pot made of anti-statically treated plastic. The allyl diglycol carbonate (CR-39) is used as the alpha particle detector. The ^{220}Rn monitor is reformed from the ^{222}Rn monitor by adding 4 holes (□=12 mm) covered with cellulose fiber filter (Whatman® No.41) on the wall of the pot bottom. In order to discriminate ^{222}Rn from ^{220}Rn in the ^{220}Rn monitor, an original ^{222}Rn monitor is attached to the ^{220}Rn monitor using a piece of double-coated tape. The new ^{222}Rn and ^{220}Rn monitor has a total volume of only 110 cm^3 and a weight of as low as 20 g.

The etched-track densities on the CR-39 detectors set in the ^{222}Rn and ^{220}Rn monitors (N_{Rn} and N_{Tn}) can be expressed as the following equations:

$$N_{Rn} = Q_{Rn} CF_{Rn1} T + Q_{Tn} CF_{Tn1} T + B$$
$$N_{Tn} = Q_{Rn} CF_{Rn2} T + Q_{Tn} CF_{Tn2} T + B$$

where Q_{Rn} and Q_{Tn} are the mean concentrations of ^{222}Rn and ^{220}Rn in the exposed period, CF_{Rn1} and CF_{Tn1} are the ^{222}Rn and ^{220}Rn calibration factors for the ^{222}Rn monitor, CF_{Rn2} and CF_{Tn2} are the ^{222}Rn and ^{220}Rn calibration factors for the ^{220}Rn monitor, T is the exposure time, and B is the background track density of the CR-39 detector. Therefore, provided the etched track densities, calibration factors and the exposure time are known, ^{222}Rn and ^{220}Rn concentrations can be derived from the simultaneous equations.

The ^{222}Rn and ^{220}Rn calibration factors for the new monitor were determined through the calibration experiments in a ^{222}Rn/^{220}Rn chamber. The averaged ^{222}Rn calibration factors for 12 sets of ^{222}Rn and ^{220}Rn monitors were estimated to be 2.62 ± 0.20 and 2.64 ± 0.16 tracks cm^{-2} (kBq m^{-3} h^{-1})$^{-1}$, respectively. The mean ^{220}Rn calibration factors were 1.32 ± 0.14 tracks cm^{-2} (kBq m^{-3} h^{-1})$^{-1}$ and 0.10 ± 0.01 tracks cm^{-2} (kBq m^{-3} h^{-1})$^{-1}$ for the ^{220}Rn and ^{222}Rn monitors, respectively. ^{220}Rn calibration factor of the ^{220}Rn monitor was more than 10 times that of the ^{222}Rn monitor. It is expected that ^{220}Rn can be evaluated from the different etched-tracks on the detectors in the ^{222}Rn and ^{220}Rn monitors. Furthermore, ^{220}Rn calibration factor for the ^{222}Rn monitor was also quantified. Therefore, the new monitor is not only useful for ^{220}Rn measurements, but also helpful for more precise measurements of ^{222}Rn. On the other hand, due to its low cost, simple construction and small size, it is considered to be practical for large-scale and long-term field surveys.

Publication:
Zhuo, W., Tokonami, S., Yonehara, H. and Yamada, Y.: *Rev. Sci. Instrum.* **73**, 2877-2881, 2002.

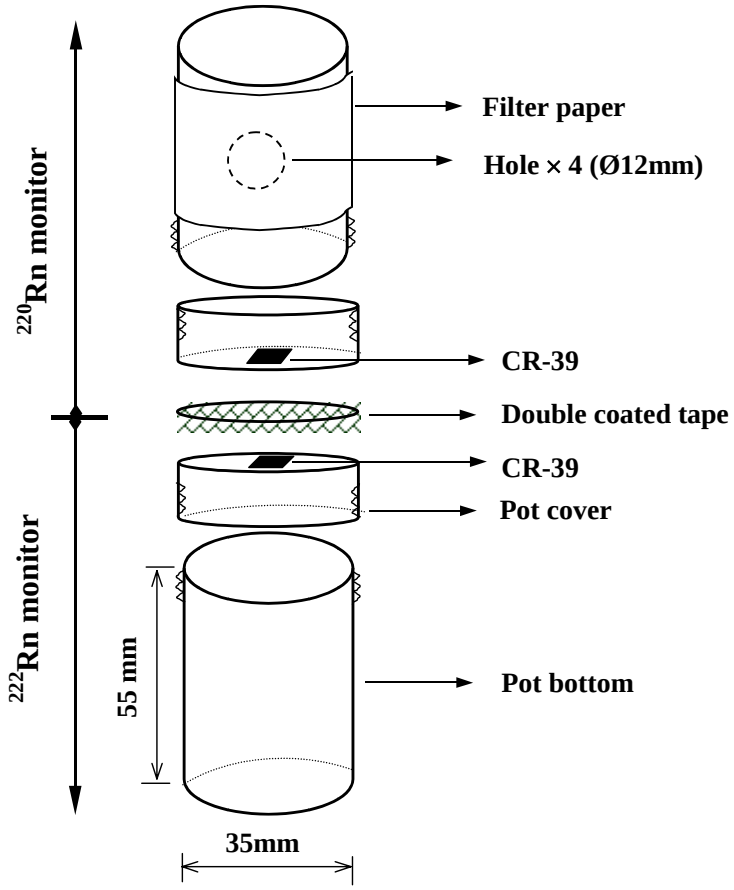

Fig. 37. Schematic construction of the new passive ^{222}Rn and ^{220}Rn monitor.

SPACE SCIENCE

90. Interim Report of Cosmic Ray Doses in Airplanes Measured by a Pocket Dosimeter

Fig.38

Kazunobu Fujitaka

Key words: airplane, dose estimation, solar activity

Neutron doses in airplanes still remain ambiguous. From the viewpoint of health physics, however, it is not bad idea to measure the dose with a small pocket dosimeter (1'' x 1'' silicon ionization chamber: Aloka PDM-101) with a proper conversion factor to the total dose (neutrons involved).

Dose values obtained on board airplanes are summarized in Fig.38. Data include uncertainty which originates from the latitudinal and the flight directional dependences. Solar activity is another source of variation. However, it is most probable that the general public wants to know only how much they receive during an airplane flight to a specific destination. Reasons of variation are not their concern.

Data were collected for 77 flight ranging from domestic flights to long distance flights. About 50 were intercontinental flight. Data collection and analyses were done by the same person. Values were obtained using the same instrument with a few exceptions, so it would be possible to make systematic adjustments for better values later. The total dose shown here was estimated as 2.7 times the indicated value of PDM-101. The measurements were started in 1997, and have been done over 5 years which is almost equal to half the period of solar activity variation. Actually, the dose increases with flight hours wherever the airplane goes, and the maximum dose of a one-way flight would be below 50 Sv. In this figure, the dose is limited to flights only from/to Narita.

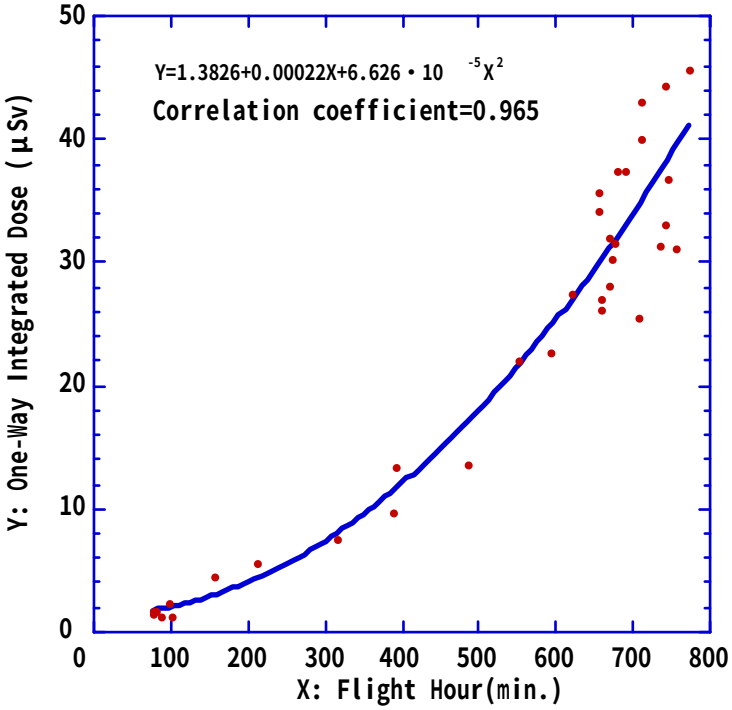

Fig. 38 Estimated dose when an airplane flies from/to Narita. Abscissa represents time length in unit of minute.

91. The Effect of High LET Radiation Is Compromised in NHEJ Deficient Human and Rodent Cells

Shiori Saito and Ryuichi Okayasu

Key words: high LET radiation, non homologous end Joining (NHEJ), cell survival, repair, premature chromosome condensation (PCC)

We have measured radiation cell survival in various human and rodent cell lines exposed to high LET (LET=80keV/ m) carbon ion particles (290MeV/u), and the results were compared with those for cell lines irradiated with X-rays. Non homologous end/joining (NHEJ) deficient human fibroblast (180 BR: Ligase IV mutant) irradiated with carbon ions (LRT=80keV/ m) showed a survival level which was identical to the survival obtained with X-rays. On the other hand, normal human fibroblast showed a significantly higher cell survival when X-rays were used as compared with the survival with high LET carbon ions. Likewise, NHEJ repair deficient hamstar xrs6 cells (Ku80 mutant) showed 180BR-like survival response while wild-type Chinese hamstar ovary (CHO) cells showed a normal human cell-like response. These results may suggest that the initial damage induced by high LET radiation is different from that induced by X-rays, and the regular DSB repair process is not properly functioning in cells irradiated with high LET. Our preliminary results using the premature chromosome condensation (PCC) assay seem to indicate the difficulty in repairing the damage produced by high LET irradiation in normal cells.

No figure

92. Pion-Emission Cross Section in Finite Nuclei at Cosmic Ray Proton Energy

Susumu Kinpara

Key words: pion-emission cross section, effective pion-nucleon coupling model, galactic
cosmic ray proton

Cosmic ray experiments on the earth play a decisive role to determine an abundance of the elementary particles and their energy spectrum. Above all, the pion-emission cross section determines branching ratio that the projectile energy is assigned to the secondary and which dominates the distribution of the radiation field. In the present work we investigate the high energy limiting behavior of the elementary particle reaction for the use of the transport eq uation.

One of the successful treatments on the hadronic phenomena is the meson-nucleon effective field model in the framework of the relativistic nuclear many-body problem. In the effective pion-nucleon coupling model the interaction is represented by either pseudoscalar(PS) or pseudovector(PV) type. In the case of the real pion external line the suppression mechanism is not necessarily applicable so that the PS one is anticipated to make a contribution compared with the PV one exceedingly.

For calculation of the many-body system the Green's function formulation is employed systematically. Incorporating the emitting phenomenon, the external pion is assigned a definite energy and charge in the final state with restriction of their conservation law respectively. It is assumed in this work that the final state momentum distribution of the target nucleus is changed by the uniform displacement in the momentum space. Therefore, the backward scattering of the neutron gets rid of the suppression resulting from the nuclear finite size effect.

It is instructive to derive the high energy limit of the total cross section. Approaching a constant value over TeV region, it gives a remarkable result suitable for the ultra relativistic energy. Because the calculated cross section depends on the range parameter the nuclear density distribution is responsible for the resultant high energy limit to be appropriate definitely. The angular distribution of the neutron spreads with the peak at the backward hemisphere accompanying the oscillatory behavior, in contrary to the pion momentum which is emitted forwards without the modulation by the exclusion effect and serves as the secondary particle.

In summary, we have calculated the pion-emission cross section in the framework of the effective meson-nucleon coupling model. It has been shown that the precise calculation of the pion emitting process is significant for the understanding of the galactic cosmic rays. The high-energy limiting behavior is improved considerably by taking into account the nuclear translational motion. The physical meaning and the role for the cascade process is in current investigation.

93. Resonance Model for Radiation Action

H. Yamaguchi, H. Ohara and A. J. Waker

Key words: biophysical model, radiation action, radiation protection

It is widely recognized that RBE is a multiple-valued function of LET, for both physical reasons (inadeq uateness of LET alone as a microscopic description of radiation q uality) and biological reasons (different biological systems and conditions). Attempts are being made continuously to seek more physically meaningful and practically descriptive radiation q uality in microscopic dimension and also to reassess the numerical values of radiation weighing factors related to the radiation protection.

LET has been used as a q uantitative parameter of radiation q uality in a numberof the attempts to construct a biophysical model of subcellular mechanism of radiation action. No general parameter on radiation q uality, however, has yet been fully identified despite much effort in the field of microdosimetry.

Bearing these facts in mind, we propose a biophysical model in which two processes are assumed for radiation action including damage production and damage repair. The ionization mean free path is proposed as the parameter to describe the damage production process, and LET is ascertained as the parameter of the repair process. Assumptions are as follows: (1) There are two targets in microscopic and macroscopic to explain the radiation action. (2) The entity of initial damage in the microscipic target is DSB (Double Strand Break) of DNA. (3) The microscopic target has structures potentially leading to DSB. (4) As a measure of suchstructures, there are three distributions of distances between atoms, those within DNA, DNA and water, and in pair of water molecules. (5) The yield of initial DSB in the microscopic target can be described by the extent of the ionizing mean free path arising closer to the distance of the target structures leading to DSB (resonance nature). (6) The yield of initial DSB in the macroscopic target is related to biological response observed and the macroscopic target is specified by its mean chord length. (7) The non-repaired or miss-repaired DSB is relevantly expressed to the observable biological endpoint in the cell that has repair ability.

The potential structure leading to DBS was obtained by a model system of B-DNA 5 ' -TCGCGTTGCGCT-3' , 24 Na+ and 7 97 3 water molecules in the box. The first possible distribution of distance(s) is associated with direct radiation action and the other two distributions, with indirect radiation action. Yields of water radicals and their diffusions are involved to estimate occurrences of DSB. Based on the differential cross section of an electron as a function of its kinetic energy, we calculate the integral cross section of the electrons and the total cross section of heavy charged particle of track segment type. The microscopic cross section to produce DSB may associate to form the macroscopic cross sections, suggesting the presence of two sizes of the target. The present model is done with four parameters, i.e. the geometrical cross section of the microscopic target and the mean chord length of the macroscopic target, for each electron and heavy charged particle. Optimization of the initial (DSB production) cross section has been made by fitting the model to the cell killing data with a repair deficient cell line of AT-cells.

The values of the parameter, the geometrical cross section, are σ_0=2.4 3x10^7 μm^2 (r_0=2.8 A) for electrons (X-rays) and heavy charged particles, where r_0 is effective radius of the geometrical cross section, and the mean free paths are 1.31 μm for electrons and 9.4 μm for heavy charged particles. The value r_0 suggests one water molecule as the common microscopic target for electron

and heavy charged particle. The value of the mean chord length suggests different size of the macroscopic target, i.e. the size like chromosome for electron and that like cell nucleus for heavy charged particle.

The probability of repair from the initial cross section may be described with either of three variables, i.e. mean free path, Z^2/β^2 and LET. We found LET as the proper variables to describe the repair probability. Introducing an empirical expression for the repair probability as a function of LET, inactivation cross sections for T1-cell (repair efficient cell line) can be systematically explained and expressed as a function of such measurable variable as the energy of particles (Fig.39). This expression may be important for radiation protection if the scheme of the radiation protection includes that of fluence-based.

Fig. 39. Inactivation cross section (μm^2) for T1 cells as a function of particle energy for fluence-based radiation protection.

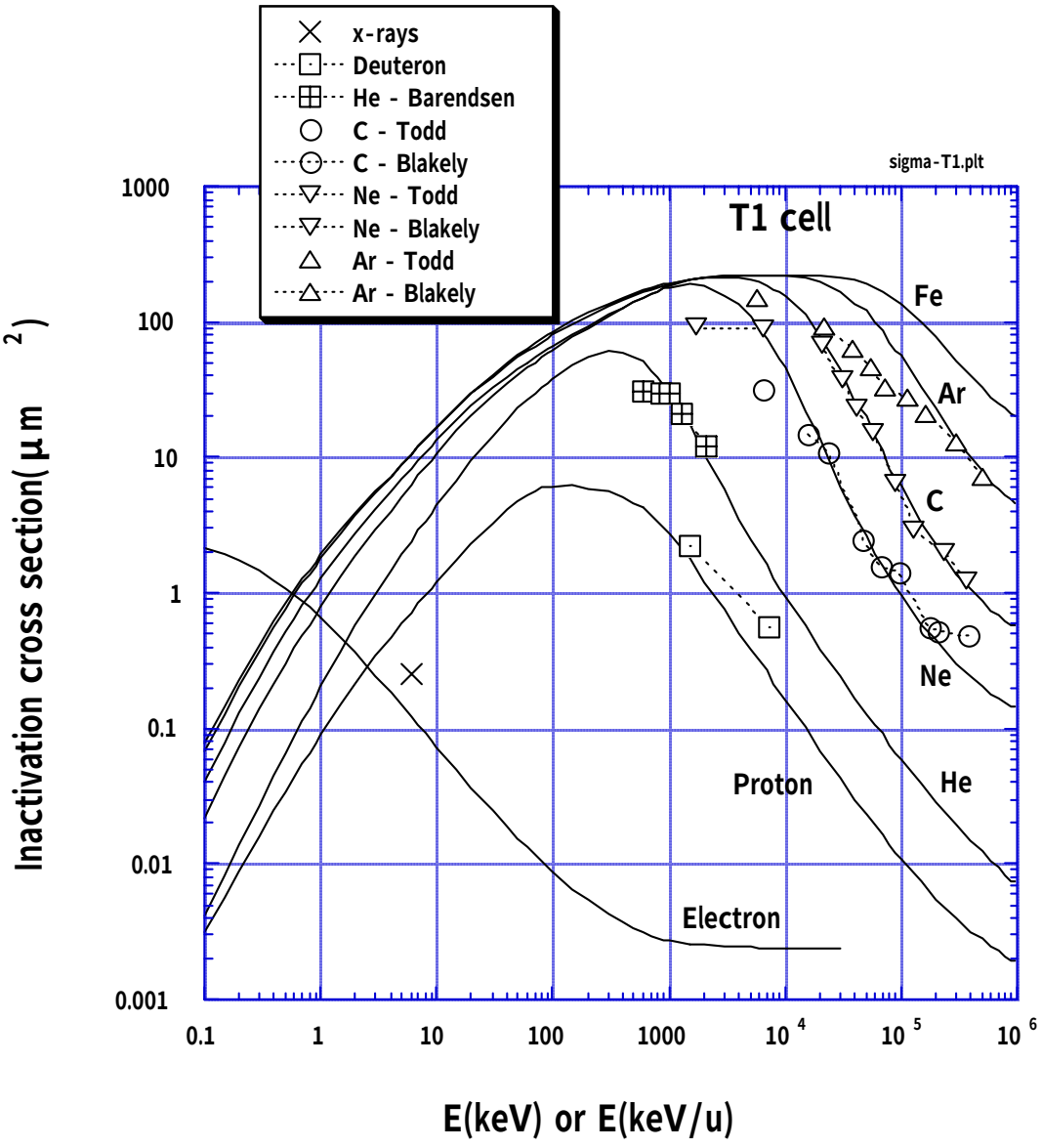

94. ICCHIBAN (InterComparison for Cosmic-rays with Heavy Ion Beams At NIRS) Project

Yukio Uchihori, Nakahiro Yasuda, Kazunobu Fujitaka, Hisashi Kitamura, Kaori Yajima, Masashi Takada and Hiroshi Yamaguchi

Keywords: intercomparison, radiation monitor, space radiation, HIMAC

In order to compare response and sensitivity of various space radiation monitoring instruments for heavy ion and reconcile differences in measurements made during space flights, the intercomparison program, ICCHIBAN (InterComparison for Cosmic-ray with Heavy Ion Beams At NIRS) project, have been carried out in HIMAC. In total 7 0 investigators (including 27 foreign investigators) participated to 4 ICCHIBAN runs during two years. In this fiscal year, 2nd and 3rd ICCHIBAN runs were performed. The former was for passive detectors (TLD, OSL, CR-39 and so on) and the latter was for active detectors (Si Stack detector, Si portable detector and Tissue Eq uivalent Proportional Counter). The results from the detectors have been analyzed by the working group.

Publication:

Uchihori, Y., Fujitaka, K., Yasuda, N. and Benton, E.: *Journal of Radiation Research*, 4 3S, S81-S85 , 2002.

95. Real Time Radiation Measurement by Liulin-4J Spectrometer at High Altitude

Yukio Uchihori

Keywords: high altitude, airplane, space radiation, real time monitor

Radiation environment in an aircraft at high altitudes above 20 km has been measured with Liulin-4 J portable silicon spectrometer. The aircraft (Fig. 4 0) was operated by NASA Dryden Flight Research Center in California, USA for scientific research on high altitude environment. The data from the spectrometer show that the dose rate depends on altitude and geomagnetic latitude. This investigation will help to confirm calculated results by a simulation code for the high altitude environment in which a future supersonic airplane will fly.

Publication List:

Uchihori, Y., Benton, E., Moeller, J. and Bendrick, G.: Advances in Space Research 32(1), 4 1-4 6, 2003.

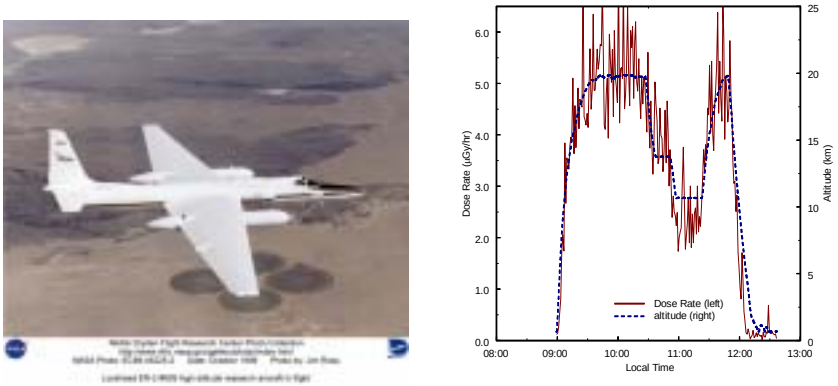

Fig. 40. ER-2 high altitude aircraft and dose rate dependency for altitude. Horizontal axis shows local time and the histogram shows the dose rate. The solid line shows the altitude of the ER-2 at each local time.

96. Preventive Effects of Running Exercise on Bones in Heavy Ion Particle Irradiated Rats

Satoshi Fukuda, Haruzo Iida, and Xueming Yan

Keywords*: heavy ion particle, rat, bone mineral, histomorphometry*

We examined the effects of running exercise on preventing decreases in bone mineral and tissue volume after heavy ion particle irradiation in rats. Male Wistar rats underwent whole-body irradiation by heavy ion particle beam (C-290MeV) at doses of 0.5 , 1.0, and 5 .0 Gy and then were divided into voluntary running groups and control groups. Rats in the running groups ran on the treadmill 15 m/min, 90 min/day for 35 days after exposure. At the end of the experiment, a tibia was obtained from each rat for measurement of bone mineral density (BMD) and cross-sectional area, strength strain index, and bone histomorphometric analysis. The weights of muscles and concentration of serum calcium were measured. Total BMD and trabecular BMD in the metaphysis and cortical BMD of the diaphysis of tibia in the running groups increased. Bone volume and trabecular thickness increased while trabecular separation decreased in the running groups compared to those in the control groups at respective doses. However, the osteoid surface and eroded surface varied in the running groups compared to those of the respective corresponding groups. The dynamic parameters such as mineralizing surface, mineral apposition rate, and bone formation rate in the running groups were varied, probably due to the differences in radiation-induced sensitivities of bones following radiation exposure. The overall results suggest that running exercise might have a beneficial effect on preventing bone mineral loss and changes in bone structure induced by space radiation, but it is necessary to examine the optimal conditions of running exercise response to doses.

Publication:
Fukuda, S., Iida, H. and Yan, X. *JRR*, **43**, Suppl. S233-238, 2002.

97. Genomic Instability in Mutation Induction on Normal Human Cells Exposed to Chronic Low-dose Radiation in Heavy Ion Radiation Field

Masao Suzuki, Chizuru Yamaguchi, Yukio Uchihori, Hiroshi Yasuda and Kazunobu Fujitaka

Keywords: genomic instability, *hprt* locus, scattered low-dose (rate) radiation, heavy ion radiation field

We have been studying cellular responses in normal human fibroblasts exposed to scattered low-dose radiation in a heavy ion radiation field. This year we focused on the induction of genomic instability in mutation induction detected with a 6-thioguanie resistant clone targeted on *hprt* locus. Cells were cultured in a CO_2 incubator, which was placed in the irradiation room for biological study of heavy ions in the HIMAC and exposed to low-dose radiation produced with scattered radiation from heavy-ion beams throughout the life span of the cell population. Genomic instability in cellular response was examined to measure mutation induction in low-dose accumulated cell populations after exposing to X-ray challenging doses as a function of accumulated doses. The mutation freq uency of the low-dose accumulated cell population was 2-5 times higher than that of unaccumulated cell population up to 15 days after being exposed to low-dose radiation (Fig.4 1). The results indicate that very low-dose accumulation of scattered radiation from heavy-ion beams induced genomic instability in mutagenesis.

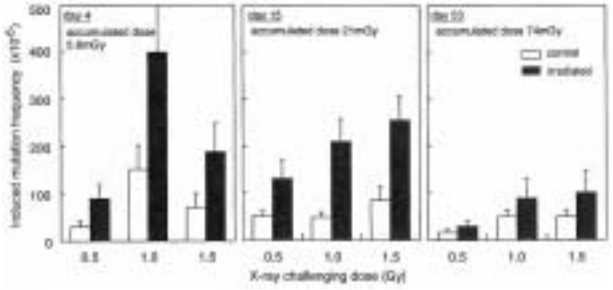

98. LET and Ion Species Dependence of Cell Killing, Mutation Induction and Chromosome Damage on Normal Human Fibroblasts

Chizuru Yamaguchi, Masao Suzuki and Kazunobu Fujitaka

Keywords: LET & ion species dependence, *HZE* particles, *hprt* locus, chromatin breaks, premature chromosome condensation (PCC)

This year, we focused on both cell killing and mutation induction, depending upon both ion species and LETs.

First, we studied both LET and ion species dependence of RBE values for cell killing effect. Normal human fibroblasts were irradiated with heavy ion beams, such as carbon, neon, silicon and iron ions with various LETs ranging from 13 to 400keV/μm. Cell killing effect was detected as a reproductive death using a colony-formation assay. The results clearly indicated that the peak position of RBE at 10% survival level shifted to higher LET region with increasing atomic number of ion sources (Fig.42).

Second, to identify the difference in mutation induction at the cellular level between carbon and neon ions, we examined the induction of 6-thioguanine-resistant clones, concentrated on the *hprt* locus as the target gene of mutation. The cells were irradiated with either carbon or neon ions at various LETs ranging from 13 to 335keV/μm. The dose-response curves for both carbon and neon ions increased steeply up to 0.5Gy and leveled off or decreased above 1Gy, compared to the response to ^{137}Cs γ-rays. However, we observed a large difference in the frequency at the plateau between neon- and carbon-ion-induced mutations. For example, the frequency for carbon-ion-induced mutation at 110keV/μm was around 30 times higher than that for neon-ion-induced mutation at 105keV/μm when compared to a similar LET value. There is circumstantial evidence that the different ion species, such as carbon and neon, led to quantitatively different mutation frequencies even when the LET value was similar.

Publication:
Suzuki, M., Kase, Y., Kanai, T., Kato, T., Yatagai, F. and Watanabe, M.: *Int. J. Radiat. Biol*., 2003. inpress.

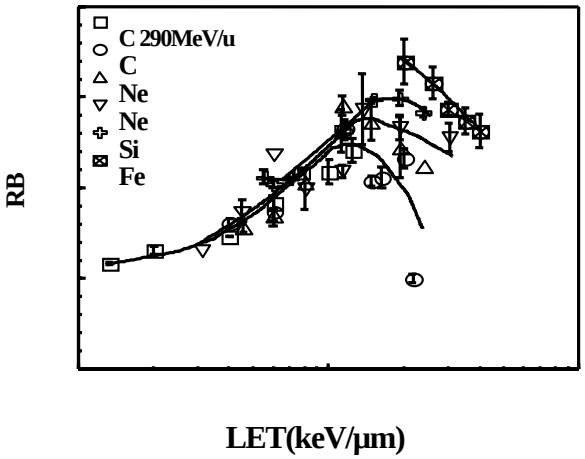

Fig.42. RBE for cell killing as a function of LET

99. Influence of the Shielding on the Space Radiation Radiobiological Effectiveness. II. Chromosomal Aberrations

Marco Durante[1], Giancarlo Gialanella[1], Giafrance Grossi[1], Mariagabriella Pugliese[1], Paola Scampoli[1], Tetsuya Kawata[2], Nakahiro Yasuda, Yoshiya Furusawa
([1]Univ. Federick II; [2]Chiba Univ.)

Keywords: high-LET radiation, chromosome aberration, telomere, unrejoined breaks

Reported studies of DNA breakage induced by radiation of various q ualitis have generally shown a higher fraction of unrejoined residual breaks after high-LET exposure. This observation is supported by the argument that high-LET radiation induced DNA breaks that are more complex in nature and, thus, less likely to be repaired. In most cases the doses used in these studies were very high. We have studied unrejoined chromosome breaks by analyzing chromosome aberrations using a fluorescence *in situ* hybridization (FISH) techniq ue with a combination of whole chromosome specific probes and probes specific for the telomere region of the chromosomes. Confluent human fibroblast cells (AG15 22) were irradiated with rays, 4 90 MeV/nucleon Si, or with Fe ions at either 200 and 5 00 MeV/nucleon, and were allowed to repair at 37 °C for 24 hours after exposure. A chemically induced premature chromosome condensation (PCC) techniq ue was used to condense chromosomes in the G2 phase of the cell cycle. Results showed that the freq uency of unrejoined chromosome breaks was higher after high-LET radiation, and the ratio of unrejoined to misrejoined chromosome breaks increased steadily with LET up a peak value at 4 4 0 keVμm.

Publication:

Durante, M., Gialanella, G., Grossi, G., Pugliese, M., Scampoli, P., Kawata, T., Yasuda, N., and Furusawa, Y.: *J. Radiat. Res.* **43**, s107 -s111, 2002.

100. Simultaneous Exposure of Mammalian Cells to Heavy Ions and X-rays

Yoshiya Furusawa, Mizuho Aoki, and Marco Durante *

(* Univ Napeas Fedelick II)

Keywords: High-LET radiation, synergistic effect, Cell survival, Chromosome aberration

Crews of space missions are exposed to a mixed radiation field, including sparsely and densely ionizing radiation. To determine the biological effectiveness of mixed high-/low-LET radiation fields, mammalian cells were exposed in vitro simultaneously to X-rays and heavy ions, accelerated at the HIMAC accelerator. X-ray doses ranged from 1 to 11 Gy. At the same time, cells were exposed to either ^{40}Ar (5 5 0 MeV/n, 86 keV/µm), ^{28}Si (100 MeV/n, 15 0 keV/µm), or ^{56}Fe (115 MeV/n, 4 4 2 keV/µm) ions. Survival was measured in hamster V7 9 fibroblasts. Structural aberrations in chromosome 2 were measured by chemical-induced premature chromosome condensation combined with fluorescence in situ hybridization in isolated human lymphocytes. For argon and silicon experiments, measured damage in the mixed radiation field was consistent with the value expected using an additive function for low- and high-LET separated data. A small deviation from a simple additive function was observed with very high-LET iron ions combined with X-rays.

Publication:

Furusawa, Y., Aoki, M., and Durante, M.: *Adv. Space Res.* **30**, 87 7 -884 , 2002.

INTERNATIONAL COOPERATION

101. International Activities of NIRS

Hideo Tatsuzaki

Keywords: *ICRP, UNSCEAR, RCA, FNCA*

Exchange of Researchers

In FY 2002, NIRS accepted a total of 77 foreign researchers (for over 7 days) and sent 328 researchers abroad.

NIRS organized seven international meetings as follows:

The 4th Japan-France Workshop on Radiobiology and Isotopic Imaging (June 2002, Paris); A Meeting of ICRP Committee 3 (September 2002, NIRS); International Symposium on Transfer of Radionuclides in Biosphere-Prediction and Assessment- (co-host, December 2002, Mito); Human-Radiation Interface: Application of Radiation in Medical Science-A Course of Nuclear Medicine (October-November 2002, NIRS); FNCA 2002 Workshop on Radiation Oncology (December 2002, Chiba and Tokyo); IAEA/RCA Regional Training Course on "Clinical Aspects of Brachytherpy in Uterine Cervix Cancer"(co-host, July 2002, Maebashi and Chiba); IAEA/ RCA Regional Training Workshop on Myocardial Perfusion Scintigraphy using SPECT for Nuclear Medicine Physicians (February 2003, NIRS).

An open seminar entitled "FNCA Seminar on Radiation Oncology 2002" was held in Toranomon, Tokyo on the final day of the workshop as a part of the FNCA workshop held from 17 to 20 December 2002, drawing about 150 participants both from Japan and abroad.

Cooperation with International Organizations

United Nations Scientific Committee on the Effects of Atomic Radiation (UNSCEAR)

The preparatory committee for Japanese Correspondence for UNSCEAR was newly established at NIRS, including members from outside of NIRS, and 110 corresponding members were appointed in addition to the committee members. Their comments on the UNSCEAR draft were assembled, compiled and passed to the delegation of Japan and also presented to the Nuclear Safety Commission of Japan.

International Commission for Radiological Protection (ICRP)

NIRS sent an expert as a commission member to the meetings of the ICRP Main Commission held in May 2002 in the United Kingdom, in October 2002 in Albuquerque, USA, and in January 2003 in Vienna, Austria.

International Atomic Energy Agency (IAEA)

NIRS hosted two meetings: IAEA/RCA Regional Training Course on "Clinical Aspects of Brachytherpy in Uterine Cervix Cancer"（co-host, July 2002, Maebashi and Chiba） and IAEA/RCA Regional Training Workshop on Myocardial Perfusion Scintigraphy using SPECT for Nuclear Medicine Physicians (February 2003, NIRS). NIRS sent a total of 12 experts to 11 different meetings of IAEA.

APPENDIX

PUBLICATIONS

List of Keywords

Author Index

Organization and Staff

APPENDIX

PUBLICATIONS

This list includes publications by the staff members issued during
the period from April 1, 2002 to March 31, 2003

Low Dose Radiation Effects Project

Masami Yamamoto*,Chie Furihata*,Toshiaki Ogiu,Tetsuya Tsukamoto*,Kenichi Inada*,Kazuyuki Hirano*,Masae Tatematsu*:Independent variation in susceptibilities of six different mouse strains to induction of pepsinogen-altered pyloric glands and gastric tumor intestinalization by N-methyl-N-nitrosourea,Cancer Letters,179,121-132,2002

Kazuei Mita,Mitsuoki Morimyo,Kazuhiro Okano*,Yoshiko Koike*,Junko Nohata*,Masataka Suzuki*,Toru Shimada*:Construction of an EST database for Bombyx mori and its application,Current Science,83,426-431,2002

Yasushi Ohmachi,et.al:Role of endotoxin in 6-Sulfanilamidoindazole(6SAI)-induced arthritis in rats,Experimental and Toxicologic Pathology,53(6),447-452,2002

Masatake Yamauchi,Mayumi Nishimura,Satsuki Tsuji,Minako Terada,Motoe Sasanuma*,Yoshiya Shimada:Effect of SCID mutation on the occurrence of mouse Pc-1 (Ms6-hm) germline mutations.,Fundamental and Molecular Mechanisms of Mutagenesis : A Section of Mutation Research,503,43-49,2002

Yasushi Ohmachi,et.al:Recovery process of arthritis induced by 6-Sulfanilamidoindazole(6SAI) in rats,Histology and Histopathology,17(2),437-444,2002

Yuri Miura*,K Abe*,Shiro Urano*,Takeshi Furuse,Yuko Noda,Kouichi Tatsumi,Shozo Suzuki*:Adaptive response and the influence of ageing: effects of low-dose irradiation on cell growth of cultured glial cells,International Journal of Radiation Biology,78,913-921,2002

Hideki Ukai,Maki Ukai-tadenuma*,Toshiaki Ogiu,Hideo Tsuji:A new technique to prevent self-ligation of DNA.,Journal of Biotechnology,97,233-242,2002

Shizuko Kakinuma,Mayumi Nishimura,Shunichi Sasanuma,Kazuei Mita,Gen Suzuki*,Yoshimoto Katsura*,Toshihiko Sado*,Yoshiya Shimada:Spectrum of Znfn1a1(Ikaros) inactivation and its association with loss of heterozygosity in radiogenic T-cell lymphomas in susceptible B6C3F1 mice,Radiation Research,157,331-340,2002

Tatsuhiko Imaoka,Nelson D. Horseman*,Jason A. Lockefeer*,Takao Mori*,Manabu Matsuda*:Cortactin-Binding Protein 90 (CBP90) Expression in the Mouse Mammary Glands during Prolactin-Induced Lobuloalveolar Development.,Zoological Science,19,443-448,2002

International Space Radiation Laboratory

Jun Sato,Keiji Okada*,Satoshi Fukuda,Reeko Sato*,Jun Yasuda*,Yoshihisa Naito*:Serum activities of tartarate-resistant acid phosphatase and bone specific alkaline phosphatase as indices of bone metabolism in the cow.,64,653-655,2002

Hiroshi Yasuda,Tatsuto Komiyama*,Kazunobu Fujitaka:Probability of cell hits in selected organs and tissues by high-LET particles at the ISS orbit.,Advances in Space Research,30,1011-1015,2002

Hiroshi Yasuda,Kazunobu Fujitaka:Solid-state integrating detectors as an indicator of biological doses from HZE particles.,Advances in Space Research,30,927-932,2002

Yuanlin Peng*,Qinming Zhang*,Hatsumi Nagasawa*,Ryuichi Okayasu,Howard L. Liber*,Joel S. Bedford*:Silencing expression of the catalytic subunit of DNA-dependent protein kinase by small interfering RNA sensitizes human Cells for radiation-induced chromosome damage, cell killing and mutation,Cancer Research,62,6400-6404,2002

Hongning Zhou*,Masao Suzuki,Charles R Geard*,Tom K Hei*:Effects of irradiated medium with or without cells on bystander cell responses.,Fundamental and Molecular Mechanisms of Mutagenesis : A Section of Mutation Research,499,135-141,2002

Hiroshi Yasuda,Ikuo Kobayashi*,Hiroshige Morishima*:Decay patterns of optically stimulated luminescence from Al2O3: C for diffirent quality radiations,Journal of Nuclear Science and Technology,39,211-213,2002

Eiji Kotani*,Toshiharu Furusawa*,Shunji Nagaoka*,Kumie Nojima,Yukio Sugimura*,Aiko Nagamatsu*,Takeshi Todo*,Mituo Ikenaga*:Somatic Mutation in Larvae of the Silkworm, Bombyx mori, induced by Heavy Ion Irradiation to Diapause Eggs,Journal of Radiation Research,43(Suppl.),S193-S198,2002

Satoshi Fukuda,Haruzo Iida,Xueming Yan*:Preventive Effects of Running Exercise on Bones in Heavy Ion Prticle Irradiated Rats,Journal of Radiation Research,43(Suppl.),S233-S238,2002

Hiroshi Yasuda,Tatsuyo Ishidoya*:A Simplified System for Reading Time-resolved Photoluminescence,Journal of Radiation Research,43(Suppl.),S63-S65,2002

Yukio Uchihori,Kazunobu Fujitaka,Nakahiro Yasuda,Eric Benton*:Intercomparison of Radiation Instruments for Cosmic-ray with Heavy Ion Beams at NIRS (ICCHIBAN Project),Journal of Radiation Research,43(Suppl.),S81-S85,2002

Hiroshi Yamaguchi,Yukio Satou,Hitoshi Imaseki,Nakahiro Yasuda,Tsuyoshi Hamano,Masao Suzuki,Takahiro Ishikawa,Teiji Mori,Kenichi Matsumoto,Teruaki Konishi,Masae Yukawa,Fuminori Soga:Single particle irradiation system to cell(SPICE) at NIRS,Nuclear Instruments & Methods in Physics Research Section B,210,292-295,2003

Yukio Uchihori,Hisashi Kitamura,Kazunobu Fujitaka,Tsvetan Dachev*,Borislav Tomov*,Plamen Dimitrov*,Yura Matviichuk*:Analysis of the calibration results obtained with Liulin-4J spectrometer-dosimeter on protons and heavy ions,Radiation Measurements,35,127-134,2002

Hiroshi Yasuda:Application of solid-state integrating dosimeters to biological experiments in space.,Radiation Protection Dosimetry,100,499-502,2002

Hiroshi Yasuda,Kazunobu Fujitaka:Efficiency of a radiophotoluminescence glass dosemeter for low -Earth-orbit space radiation.,Radiation Protection Dosimetry,100,545-548,2002

Hongning Zhou*,Masao Suzuki,Gerhard Randers Pehrson*,Charles Waldren*,Tom K Hei*:Genotoxic damage in non-irradiated cells: Contribution from the bystander effect.,Radiation Protection Dosimetry,99,227-232,2002

Masashi Takada,Hiroshi Yamaguchi,Hisashi Kitamura,Yukio Uchihori,Kazunobu Fujitaka:Microdosimetric Distribution of Protons, Ep=19-65MeV, Measured with a Low-Pressure Proportional Counter.,Radiation Protection Dosimetry,99(1-4),391-392,2002

Kenji Shinozaki*,Michiyuki Chikawa*,Masaki Fukushima*,Naoaki Hayashida*,Naoya Inoue*,Ken Honda*,Kenji Kadota*,Fumio Kakimoto*,Kouichi Kamata*,Setsuo Kawaguchi*,Saburo Kawakami*,Yoshiya Kawasaki*,Norio Kawasumi*,A Mahrous*,Keiichi Mase*,Tomoko Mizobuchi*,Yuichirou Morizane*,Motohiko Nagano*,Hideyuki Ohoka*,Satoko Osone*,Naoto Sakaki*,Nobuyuki Sakurai*,Makoto Sasaki*,Masahiko Sasano*,Masahiro Takeda*,Masahiro Teshima*,Itsurou Tsushima*,Reiko Torii*,Yukio Uchihori,R Vazquez*,Tokonatsu Yamamoto*,Shigeru Yoshida*,Hisashi Yoshii*:UPPER LIMIT ON GAMMA-RAY FLUX

ABOVE 1019 eV ESTIMATED BY THE AKENO GIANT AIR SHOWER ARRAY EXPERIMENT,The Astrophysical Journal,57,L117-L120,2002

Kenichi Kuge*,Nakahiro Yasuda,Hiroshi Kumagai*,Naokazu Aoki*,Akira Hasegawa*:Colored tracks of heavy ion particles using photographic color film,Nuclear Instruments & Methods in Physics Research Section A,482,558-564,2002

Environmental Radiation Protection Research Group

Masatoshi Yamada,Tatsuo Aono:210Pb and 234Th in settling particles collected by time-series sediment traps in the Okinawa Trough,Deep-Sea Research Part II,50(2),487-501,2003

Kazumasa Oguri*,Eiji Matsumoto*,Masatoshi Yamada,Yosiki Saito*,Kazuo Iseki*:Sediment accumulation rates and budgets of depositing particles of the East China Sea,Deep-Sea Research Part II,50(2),513-528,2003

E.T. Natera*,D. Valdez*,Hisao Kawamura*,L. Palad*,Kunio Shiraishi:Estimation of daily micronutirient intake of Filipinos,Food and nutrition bulletin,23,222-226,2002

Shino Takeda,Yusuke Hiraku*,Yasuhiro Ohkuma*,Shinji Oikawa*,Mariko Murata*,Kazuhiko Ogawa*,Taeko Iwamuro*,Song Li*,Gui Fan Sun*,Yoshito Kumagai*,Nobuhiro Shimojo*,Shosuke Kawanishi*:2,4,6-Trinitrotoluene-induced reproductive toxicity via oxdative DNA damage by its metabolite,Free Radical Research,36,555-566,2002

Shino Takeda,Yoshikazu Nishimura,Yoshito Watanabe,Hitoshi Imaseki,Masae Yukawa:Application of microPIXE to elemental imaging of the rat testis,International Journal of PIXE,11,103-110,2001

Masae Yukawa,Yuuji Ishikawa,Hitoshi Imaseki,Kazuko Aoki:Elemental Distribution in organs of Medaka, Oryzias laptipes, burdened with X-ray irradiation and salty water (Part II),International Journal of PIXE,11,119-124,2001

Yoshito Watanabe,Shino Takeda,Masae Yukawa,Yoshikazu Nishimura:Application of micro-PIXE and ICP-MS to analysis of elemental distribution in root apex of plants.,International Journal of PIXE,11,125-131,2001

Motoi Murata*,Toshio Miyake*,Yasushi Inoue*,Sumio Oshima*,Shinichi Kudo*,Takesumi Yoshimura*,Suminori Akiba*,Toshiro Tango*,Yasuhiko Yoshimoto,Yukiko Shimizu*,Tomotaka Sofue*,Shizuyo Kusumi*,Tamiko Iwasaki*,Chikao Yamagishi*,Hiromichi Matudaira*:Life-style and Other Characteristics of Radiation Workers at Nuclear Facilities in Japan:Base-line Data of a Questionnaire Survey ,Journal of Epidemiology,12,310-319,2002

Kunio Shiraishi,Midori Iwasaki*,Chyuzo Miyazawa*,Hidenori Yonehara,Masaki Matsumoto:Dose estimation by ESR on tooth enamel from two workers exposed to radiation due to the JCO accident,Journal of Radiation Research,43,331-335,2002

Sarata Kumar Sahoo,Hidenori Yonehara,Katsumi Kurotaki,Kenzo Fujimoto,Yuuji Nakamura:Precise determination of 235U/238U isotope ratio in soil samples by using thermal ionization mass spectrometry,Journal of Radioanalytical and Nuclear Chemistry,252,241-245,2002

Chushiro Yonezawa*,H Matsue*,Masae Yukawa:Non-destructive determination of trace amounts of iodine in biological samples by epithermal neutron activation and Compton suppression gamma-ray spectrometry,Journal of Radioanalytical and Nuclear Chemistry,255,105-109,2003

Yoshikazu Nishimura,Hiroshi Takeda,Kiriko Miyamoto,Yoshito Watanabe,Fuyuki Kouno,Noriko Kuroda,Hee Sun Kim*,Masae Yukawa:Determination of P-32 in urine for early estimation of the neutron exposure level for three vctims of the JCO criticality accident.,Journal of Radiological Protection,22,25-29,2002

Sarata Kumar Sahoo,Shinzo Kimura,Yoshito Watanabe,Kunio Shiraishi,Akimasa Masuda*:Detection of 236U and variation of uranium isotope composition in the soil samples affected by the JCO criticality accident,Proceedings of the Japan Academy. Ser. B,78,196-200,2002

Kazutoshi Suzuki,Hiroshi Sekimoto*,Nobuhito Ishigure:Effect of Uncertainty in Transfer Rates for the ICRP Publication 67 Bikinetic Model on Dose Estimation for 239Pu From Results of Individual Monitoring.,Radiation Protection Dosimetry,102,333-341,2002

Environmental and Toxicological Sciences Research Group

Tetsuya Sakashita,Masahiro Doi,Hiroshi Yasuda,Shoichi Fuma,Donat P. Haeder*:Effects of gamma-ray and high energy carbon ion irradiation on swimming velocity of Euglena gracilis.,Advances in Space Research,30(4),1023-1030,2002

Tetsuya Sakashita,Masahiro Doi,Hiroshi Yasuda,Hiroshi Takeda,Shoichi Fuma,Yuuji Nakamura,Donat P. Haeder*:Gamma irradiation effect Variation of photosynthetic activity of Euglena.,Biomedical and Environmental Sciences ,15,261-267,2002

Usha Rao*,Udo Fehn*,Yasuyuki Muramatsu,Heather Mcneil*,Pankaj Sharma*,David Elmore*:Tracing the history of nuclear release: Determination of 129I in tree rings,Environmental science & technology,36,1271-1275,2002

Hiroshi Takeda,Shoichi Fuma,Kiriko Miyamoto,Kei Yanagisawa,Nobuyoshi Ishii,Noriko Kuroda:Estimation of internal dose by blood analyses for exposure to tritium in various chemical forms.,Fusion Science and Technology,41,445-449,2002

Tetsuya Sakashita,Masahiro Doi,Hiroshi Yasuda,Hiroshi Takeda,Shoichi Fuma,Yuuji Nakamura,Donat P. Haeder*:High-energy carbon ion irradiation inhibits negative gravitaxis in Euglena gracilis Z.,International Journal of Radiation Biology,78(11),1055-1060,2002

Tadaaki Ban-nai,Yasuyuki Muramatsu:Transfer factors of radioactive Cs, Sr, Mn, Co and Zn from Japanese soils to roots and leaf of radish,Journal of Environmental Radioactivity,63,251-264,2002

Shoichi Fuma,Nobuyoshi Ishii,Hiroshi Takeda,Kiriko Miyamoto,Kei Yanagisawa,Yusuke Ichimasa*,Masahiro Saitou*,Zenichiro Kawabata*,Gennady Polikarpov*:Ecological effects of various toxic agents on the aquatic microcosm in comparison with acute ionizing radiation,Journal of Environmental Radioactivity,67,1-14,2003

Tetsuya Sakashita,Masahiro Doi,Hiroshi Yasuda*,Hiroshi Takeda,Shoichi Fuma,Yuuji Nakamura,Donat P. Haeder*:Comparative study of gamma-ray and high-energy carbon ion irradiation on negative gravitaxis in Euglena gracilis Z.,Journal of Plant Physiology,159(12),1355-1360,2002

Tetsuya Sakashita,Masahiro Doi,Hiroshi Yasuda,Shoichi Fuma,Donat P. Haeder*:Protection of negative gravitaxis in Euglena gracilis Z against gamma-ray irradiation by Trolox C.,Journal of Radiation Research,43(Suppl.),S257-S259,2003

Kei Yanagisawa,Hiroshi Takeda,Kiriko Miyamoto,Shoichi Fuma,Nobuyoshi Ishii:DETERMINATION OF 13C CONCENTRATION IN BIOLOGICAL MATERIALS USING INFRARED ABSORPTION METHOD,Journal of Radioanalytical and Nuclear Chemistry,252,277-280,2002

Tetsuya Sakashita,Takeo Hama*,Shoichi Fuma,Masahiro Doi,Yuuji Nakamura,Nobuyoshi Ishii,Hiroshi Takeda:Effects of gamma irradiation on CO2 fixation and cellular proliferation of Euglena gracilis Z.,Journal of Radioanalytical and Nuclear Chemistry,254(2),401-403,2002

Keiko Tagami,Shigeo Uchida:Pretreatment of Plant Samples for the Determination of Rhenium by ICP-MS.,Journal of Radioanalytical and Nuclear Chemistry,255(3),547-551,2003

Satoshi Yoshida,Yasuyuki Muramatsu,M. Steiner*,M. Belli*,A. Pasquale*,B. Rafferty*,Werner Ruhm*,A. Rantavaara*,I. Linkov*,A. Dvornik*,T. Zhuchenko*:Stable elements - as a key to predict radionuclide transport in forest ecosystems.,Proceedings of the International Congress on the Radioecology-Ecotoxicology of Continental and Estuarine Environments : ECORAD 2001(Radioprotection-colloques ; Vol.37 C1),37(C1),391-396,2002

Yasuyuki Muramatsu,Satoshi Yoshida,Tadaaki Ban-nai,Seigo Amachi:Behavior of iodine in the soil-plant system,Proceedings of the International Congress on the Radioecology-Ecotoxicology of Continental and Estuarine Environments : ECORAD 2001(Radioprotection-colloques ; Vol.37 C1),37(C1),479-484,2002

Kiriko Miyamoto,Hiroshi Takeda,Yoshikazu Nishimura,Masae Yukawa,Yoshito Watanabe,Nobuhito Ishigure,Fuyuki Kouno,Noriko Kuroda,Makoto Akashi:Validation and Verification of the ICRP Biokinetic Model of 32P:The Criticality Accident in Tokai-mura, Japan,Radiation Protection Dosimetry,105,199-208,2003

Tetsuya Sakashita,Donat P. Haeder*:The use of bioassays for studying toxicology in ecosystems. ,Research Trends,2002

Sentaro Takahashi,Hiroshi Sato,Yoshihisa Kubota,Joel S. Bedford*,Ryuichi Okayasu:Inhibition of DNA-double

strand break repair by antimony compounds,Toxicology,180,249-256,2002

Sentaro Takahashi,Yoshihisa Kubota,Kiyo Okinaga*,Keiichi Furuya*:A new method of estimating the cytotoxic effects of suspended particulate matter on cultured alveolar macrophages in vitro,Toxicology Mechanisms and Methods,12,169-180,2002

Radon Research Group

Shinji Tokonami,Hidenori Yonehara,Mingli Yang*,Masahide Furukawa,Yuji Yamada:Thoron and radon exhalation rate measurements performed on building materials using scintillation cells,High Levels of Natural Radiation and Radon Areas : Radiation Dose and Health Effects : Proceedings of the 5th International Conference on High Levels of Natural Radiation and Radon Areas, held in Munich,Germany on September 4 to 7, 2000 vol.II :Poster Presentation(BfS Schriften 24-2002),271-273,2002

Shinji Tokonami,Hidenori Yonehara,Weihai Zhuo,Quanfu Sun,Tetsuya Sanada*,Yuji Yamada:Understanding of high radon concentrations observed in a well-ventilated Japanese wooden house,Indoor Air : International Conference on Indoor Air Quality and Climate,2002(1),665-669,2002

Kumiko Fukutsu,Yuji Yamada,Michikuni Shimo:Refinement of Screen-Type Diffusion Battery for Fast Measurement and Its Validation by Numerical Simulation,Journal of Atmospheric Electricity,22,81-86,2002

Shinji Tokonami,Weihai Zhuo,Hideki Ryuo*,Hidenori Yonehara,Yuji Yamada,Michikuni Shimo:Instrument performance of a radon measuring system with the alpha-track detection technique,Radiation Protection Dosimetry,103,69-72,2003

V Ramzaev*,Tetsuo Ishikawa,P Hill*,T Rahola*,G Kaidanovsky*,Hidenori Yonehara,R Hille*,Masafumi Uchiyama*:Intercomparison of whole-body counters by using a subject who had incorporated Cs-137 into the body,Radiation Protection Dosimetry,98,179-189,2002

Weihai Zhuo,Shinji Tokonami,Hidenori Yonehara,Yuji Yamada:a simple passive monitor for integrating measurements of indoor thoron concentrations,Review of Scientific Instruments,73(8),2877-2881,2002

Hirokazu Ichitsubo,Shinji Tokonami,Katsuhiro Miyamoto,Yuji Yamada:EVALUATION OF THE EFFECTIVE DETECTION AREA OF RADIATION DETECTORS,High Levels of Natural Radiation and Radon Areas : Radiation Dose and Health Effects : Proceedings of the 5th International Conference on High Levels of Natural Radiation and Radon Areas, held in Munich,Germany on September 4 to 7, 2000 vol.II :Poster Presentation(BfS Schriften 24-2002),39-42,2002

Kumiko Fukutsu,Yuji Yamada,Michikuni Shimo:Dose Response of Tracheal Epithelial Cells to Ionizing Radiation in Air-Liquid Interface Cultures,High Levels of Natural Radiation and Radon Areas : Radiation Dose and Health Effects : Proceedings of the 5th International Conference on High Levels of Natural Radiation and Radon Areas, held in Munich,Germany on September 4 to 7, 2000 vol.II :Poster Presentation(BfS Schriften 24-2002),475-477,2002

Redox Regulation Research Group

Keizo Takeshita,Keita Saito,Junichi Ueda,Kazunori Anzai,Toshihiko Ozawa:Kinetic Study on ESR signal decay of nitroxyl radicals, potent redox probes for in vivo ESR spectroscopy, caused by reactive oxygen species,Biochimica et Biophysica Acta General subjects,1573,156-164,2002

Kiyoshi Fukuhara*,Ikuo Nakanishi,Tomokazu Shimada*,Kei Ohkubo*,Kentaro Miyazaki*,Wataru Hakamata*,Shiro Urano*,Nobuo Ikota,Toshihiko Ozawa,Haruhiro Okuda*,Naoki Miyata*,Shunichi Fukuzumi*:A Planar Catechin Analogue as a Promising Antioxidant with Reduced Prooxidant Activity,Chemical Research in Toxicology,16,81-86,2003

Mami Onoda,et.al:Dietary nitrate inhibits stress-induced gastric mucosal injury in the ratstress-induced gastric mucosal injury in the rat,Free Radical Research,37(1),85-90,2003

Hiroshi Inano,Makoto Onoda:Radioprotective action of curcumin extrated from CURCUMA LONGA LINN: Inhibitory effect on formation of urinary 8-hydroxy-2'-deoxyguanosine, tumorigenesis, but not mortality, induced by gamma-ray irradiation.,International Journal of Radiation Oncology Biology Physics,53,735-743,2002

Keita Saito,Keizo Takeshita,Junichi Ueda,Toshihiko Ozawa:Two reaction sites of spin label, TEMPOL (4-hydroxy-2,2,6,6-tetramethylpiperidine-N-oxyl), with hydroxyl radical,Journal of Pharmaceutical Sciences,92,275-280,2003

Keiko Suzuki,Masahiko Mori,Fumihiko Kugawa*,Hiroshi Ishihara:Whole-body X-irradiation induces acute and transient expression of heme oxygenase-1 in rat liver.,Journal of Radiation Research,43,205-210,2002

Kiyoshi Fukuhara*,Ikuo Nakanishi,Hisao Kansui*,Etsuko Sugiyama*,Mitsuhiro Kimura*,Tomokazu Shimada*,Shiro Urano*,Kentaro Yamaguchi*,Naoki Miyata*:Enhanced Radical-Scavenging Activity of a Planar Catechin Analogue,Journal of the American Chemical Society,124,5952-5953,2002

Ikuo Nakanishi,Kiyoshi Fukuhara*,Tomokazu Shimada*,Yuko Iizuka*,Keiko Inami*,Masataka Mochizuki*,Shiro Urano*,Shinobu Itoh*,Naoki Miyata*,Shunichi Fukuzumi*:Effects of Magnesium Ion on Kinetic Stability and Spin Distribution of Phenoxyl Radical Derived from a Vitamin E Analogue: Mechanistic Insight into Antioxidative Hydrogen Transfer Reaction of Vitamin E,Journal of the Chemical Society, Perkin Transactins 2,2002,1520-1524,2002

Ikuo Nakanishi,Kei Ohkubo*,Shunsuke Fujita*,Shunichi Fukuzumi*,Toshifumi Konishi*,Mamoru Fujitsuka*,Osamu Ito*,Naoki Miyata*:Direct Detection of Superoxide Anion Generated in C60-Photosensitized Oxidation of NADH and an Analogue by Molecular Oxygen,Journal of the Chemical Society, Perkin Transactins 2,2002,1829-1833,2002

Ikuo Nakanishi,Kentaro Miyazaki*,Tomokazu Shimada*,Kei Ohkubo*,Shiro Urano*,Nobuo Ikota,Toshihiko Ozawa,Shunichi Fukuzumi*,Kiyoshi Fukuhara*:Effects of Metal Ions Distinguishing between One-Step Hydrogen- and Electron-Transfer Mechanisms for the Radical-Scavenging Reaction of (+)-Catechin,The Journal of Physical Chemistry A,106(46),11123-11126,2002

Ikuo Nakanishi,Shunichi Fukuzumi*,Toshifumi Konishi*,Kei Ohkubo*,Mamoru Fujitsuka*,Osamu Ito*,Naoki Miyata*:DNA Cleavage via Superoxide Anion Formed in Photoinduced Electron Transfer from NADH to g-Cyclodextrin-Bicapped C60 in an Oxygen-Saturated Aqueous Solution,The Journal of Physical Chemistry B,106,2372-2380,2002

Hidekazu Fujimaki*,Keiko Nohara*,Takahihiro Kobayashi*,Keiko Suzuki,Kiyomi Eguchi-Kasai,Shinichi Tsukumo*,Mika Kijima*,Chiharu Tohyama*:Effect of a single oral dose of 2,3,7,8-tetrachlorodibenzo-p-dioxin on immune function in Male NC/Nga mice,Toxicological Sciences,66,117-124,2002

Radiation Hazards Research Group

Kunihiko Fukuchi*,Tamio Hagiwara*,Kenntarou Nakamura*,Sachiko Ichimura,Kouichi Tatsumi,Kunihide Gomi*:Identification of the regulatory region required for ubiquitination of the cyclin kinase inhibitor,p21,Biochemical and Biophysical Research Communications,293,120-125,2002

Hideyuki Tomitori*,Mitsuru Nenoi,Kazuei Mita,Kazuhiro Daino,Kazuei Igarashi*,Sachiko Ichimura:Functional characterization of the human spermidine / spermine N1 - acetyltransferase gene promoter,Biochimica et Biophysica Acta General subjects,1579,180-184,2002

Hisako Sakiyama*,Takashi Nonaka*,Riako Masuda*,Inoue Naokazu*,Yoshinori Kuboki*,Mayumi Iijima*,Yoshio Hirabayashi*,Masahiko Takahagi,Kazuko Yoshida,Kazuko Kuriiwa*,Michiteru Yoshida*,Shinobu Ohmi*:Characterization of mineral deposits formed in cultures of a hamster tartrate-resistant acid phosphatase (TRAP) and alkaline phosphatase (ALP) double-positive cell line (CCP),Cell and Tissue Research,309,269-279,2002

Kimihiko Sugaya:Amino Acid Substitution of the Largest Subunit of Yeast RNA Polymerase II: Effect of a Temperature-sensitive Mutation Related to G1 Cell Cycle Arrest,Current Microbiology,47,159-162,2003

Fumio Yatagai*,Toshihiro Kurobe*,Takehiko Nohmi*,Ken Ichi Masumura*,Teruyo Tsukada*,Hirotake Yamaguchi*,Kiyomi Eguchi-Kasai,Nobuhisa Fukunishi*:Heavy-ion-induced mutations in the gpt delta transgenic mouse: Effect of p53 gene knockout,Environmental and Molecular Mutagensis,40,216-225,2002

Hideki Kawasaki*,Kimihiko Sugaya,Guo Xing Quan*,Junko Nohata*,Kazuei Mita*:Analysis of alfa- and beta-tubulin genes of Bombyx mori using an EST database,Insect biochemistry and molecular biology,33,131-137,2003

Reiko Kanda,Masako Minamihisamatsu,Isamu Hayata:Dynamic analysis of chromosome aberrations in three victims of the Tokai-mura criticality accident. ,International Journal of Radiation Biology,78,857-862,2002

Hiroshi Kimura*,Kimihiko Sugaya,Peter Cook*:The transcription cycle of RNA polymerase II in living cells,Journal of Cell Biology,159,777-782,2002

Tomohisa Hirobe,Kazumasa Wakamatsu*,Shosuke Ito*,Hiroyuki Abe*,Yoko Kawa*,Masako Mizoguchi*:Stimulation of the proliferation and differentiation of mouse pink-eyed dilution epidermal melanocytes by excess tyrosine in serum-free primary culture,Journal of Cellular Physiology,191,162-172,2002

Tomohisa Hirobe:Role of leukemia inhibitory factor in the regulation of the proliferation and differentiation of neonatal mouse epidermal melanocytes in culture,Journal of Cellular Physiology,192,315-326,2002

Tomohisa Hirobe,Yoko Kawa*,Masako Mizoguchi*,Shosuke Ito*,Kazumasa Wakamatsu*:Effects of genic substitution at the pink-eyed dilution locus on the proliferation and differentiation of mouse epidermal melanocytes in vivo and in vitro,Journal of Experimental Zoology,292,351-366,2002

Manabu Koike:Dimerization, translocation and localization of Ku70 and Ku80 Proteins,Journal of Radiation Research,43,223-236,2002

Wang Chun Yan,Zhang Wei,Chen Deqing*,Isamu Hayata,Masako Minamihisamatsu,Hiroshige Morishima*,Yuan Yongling*,Wei Luxin*,Tsutomu Sugahara*:Stable Type Chromosome Aberrations in the Residents of the High Background Radiation Area in China,Journal of Radiation Research and Radiation Processing,20(4),260-264,2002

Masanobu Kitagawa,Shuichi Yamaguchi,Maki Hasegawa,Kaoru Tanaka,Toshihiko Sado,Katsuiku Hirokawa*,Shirou Aizawa:Friend Leukemia Virus Infection Enhances DNA Damage-Induced Apoptosis of Hematopoietic Cells, Causing Lethal Anemia in C3H Hosts,Journal of Virology,76,7790-7798,2002

Kazuko Yoshida,Shirou Aizawa,Keiko Watanabe,Yoko Hirabayashi*,Tohoru Inoue*:Stem-cell leukemia: p53 deficiency mediated suppresion of leukemic differentiation in C3H/He myeloid leukemia,Leukemia Research,26,1085-1092,2002

Marcin Kruszewski*,Hanna Kruszewska*,Masahiko Mori,Kiyomi Eguchi-Kasai,Hiroko Inaba,Iwona Zakierska*,Isamu Hayata:Low frequency of spontaneous rearrangements during plasmid incorporation in CHO-KI mutant cells defective in DNA repair,Nukleonika,47(1),7-11,2002

Rikako Furuya*,Satoru Akiu*,Ritsuro Ideta*,Masako Naganuma*,Minoru Fukuda*,Tomohisa Hirobe:Changes in the proliferative activity of epidermal melanocytes in serum-free primary culture during the development of UVB-induced pigmented spots in hairless mice,Pigment Cell Research,15,348-356,2002

Tomohisa Hirobe,Rikako Furuya*,Satoru Akiu*,Ouji Ifuku*,Minoru Fukuda*:Keratinocytes control the proliferation and differentiation of cultured epidermal melanocytes from ultraviolet radiation B-induced pigmented spots in the dorsal skin of hairless mice,Pigment Cell Research,15,391-399,2002

Kazuhiro Daino,Sachiko Ichimura,Mitsuru Nenoi:Early induction of CDKN1A (p21) and GADD45 mRNA by a low dose of ionizing radiation is due to their dose-dependent post-transcriptional regulation.,Radiation Research,157,478-482,2002

Nobuhiko Ban*,Kazuko Yoshida,Shirou Aizawa,Sachiko Wada*,Michiaki Kai*:Cytogenetic Analysis of Radiation-Induced Leukemia in Trp53-Deficient C3H/He Mice,Radiation Research,158,69-77,2002

Reiko Kanda,Kiyomi Eguchi-Kasai,Hiromi Itsukaichi,Masahiko Mori,Isamu Hayata:Chemically induced premature chromosome condensation in human fibroblast cell lines: Fundamental study for applications to the biodosimetry of local exposure.,Somatic Cell and Molecular Genetics,25,317-325,2002

Kunihiko Fukuchi*,Tamio Hagiwara*,Kenntarou Nakamura*,Sachiko Ichimura,Kouichi Tatsumi,Kunihide Gomi*:Identification of the regulatory region required for ubiquitination of the cyclin kinase inhibitor,p21,Biochemical and Biophysical Research Communications,293,120-125,2002

Hisako Sakiyama*,Takashi Nonaka*,Riako Masuda*,Inoue Naokazu*,Yoshinori Kuboki*,Mayumi Iijima*,Yoshio Hirabayashi*,Masahiko Takahagi,Kazuko Yoshida,Kazuko Kuriiwa*,Michiteru Yoshida*,Shinobu Ohmi*:Characterization of mineral deposits formed in cultures of a hamster tartrate-resistant acid phosphatase (TRAP) and alkaline phosphatase (ALP) double-positive cell line (CCP),Cell and Tissue Research,309,269-279,2002

Yuri Miura*,K Abe*,Shiro Urano*,Takeshi Furuse,Yuko Noda,Kouichi Tatsumi,Shozo Suzuki*:Adaptive response and the influence of ageing: effects of low-dose irradiation on cell growth of cultured glial cells,International Journal of Radiation Biology,78,913-921,2002

Masahiro Muto,Yasuyoshi Kanari*,Eiko Kubo,Takayuki Kurihara*,Akira Fujimori,Kouichi Tatsumi:Targeted disruption of Np95 gene renders murine embryonic stem cells hypersensitive to DNA damaging agents and DNA replication blocks,Journal of Biological Chemistry,277,34549-34555,2002

Akira Fujimori,Hiroshi Hashimoto*,Ryoko Araki,Toshiyuki Saitou,Shinji Sato*,Yasuji Kasama*,Yoko Tsutsumi*,Masahiko Mori,Ryuutarou Fukumura,Tatsuya Ohhata*,Kouichi Tatsumi,Masumi Abe:Sequence analysis of 193.4 and 83.9 kbp of mouse and chicken genomic DNAs containing the entire Prkdc (DNA-PKcs) gene,Radiation Research,157,298-305,2002

Transcriptome Profiling Research Group

Masahiro Muto,Yasuyoshi Kanari*,Eiko Kubo,Takayuki Kurihara*,Akira Fujimori,Kouichi Tatsumi:Targeted disruption of Np95 gene renders murine embryonic stem cells hypersensitive to DNA damaging agents and DNA replication blocks,Journal of Biological Chemistry,277,34549-34555,2002

Akira Fujimori,Hiroshi Hashimoto*,Ryoko Araki,Toshiyuki Saitou,Shinji Sato*,Yasuji Kasama*,Yoko Tsutsumi*,Masahiko Mori,Ryuutarou Fukumura,Tatsuya Ohhata*,Kouichi Tatsumi,Masumi Abe:Sequence analysis of 193.4 and 83.9 kbp of mouse and chicken genomic DNAs containing the entire Prkdc (DNA-PKcs) gene,Radiation Research,157,298-305,2002

Laboratory Animal Development and Research Group

Seiji Kito,Yoshiko Noguchi*,Yuki Oota:Different developmental responses against oxygen and amino acids of in vitro fertilized embryos between two substrains of C57BL/6J inbred mice.,Experimental Animals,52,63-66,2003

Akihiko Koga*,Hiroshi Hori*,Yuuji Ishikawa:Gamera, a family of LINE-like repetitive sequences widely distributed in medaka and related fishes,Heredity,89,446-452,2002

Seiji Kito,Shintarou Tateno*,Yuki Oota,Yoshiko Noguchi*:Kinetics of in vitro fertilization and development of an inbred mouse strain: study using RFM/Ms compared with C57BL/6J.,Journal of Mammalian Ova Research,19,32-38,2002

Hiromi Omoe,Katsuhiko Omoe,Masahiro Sakaguchi,Yousuke Kameoka,Satoru Matsushita,Toshiki Inada: production of virus-specific antiserum corresponding to sequences in the lactate dehydrogenase-elevating virus (LDV) ORF6 protein. Comparative Immunology, Microbiology & Infectious Diseases

Internal Radiation Effects Research Group

Yoichi Oghiso,Yutaka Yamada:Immunohistochemical study on cellular origins of rat lung tumors induced by inhalatiion exposures to pultonium dioxide aerosols as compared to those by X-ray irradiation.,Journal of Radiation Research,43,301-311,2002

Head of Special Research (on Hereditary Effects)

Keiko Tagami,Shigeo Uchida:Global Fallout Technetium-99 Distribution and Behavior in Japanese Soils,Journal of Nuclear and Radiochemical Sciences,3,1-5,2002

Shigeo Uchida,Keiko Tagami,Masahiro Saitou*:Determination of trace rhenium in river water samples by Q-ICP-MS and HR-ICP-MS.,Journal of Radioanalytical and Nuclear Chemistry,255(2),329-333,2003

Research Center for Radiation Emergency Medicine

Naoyuki Anzai,Yonghee Lee*,Byung Youn*,Seiji Fukuda*,Young Kim*,Charlie Mantel*,Makoto Akashi,H. E. Broxmeyer*:c-kit associated with the transmembrane 4 superfamily proteins constitutes a functionally distinct subunit in human hematopoietic progenitors,Blood,99,4413-4421,2002

Sang-hee Park,Yun Sil Lee*,Yoshiaki Osawa*,Misao Hachiya,Makoto Akashi:Hsp25 Regulates the Expression of p21(Waf1/Cip1/Sdi1) through Multiple Mechanisms.,Journal of Biochemistry,131,869-875,2002

Kazuko Yoshida,Shirou Aizawa,Keiko Watanabe,Yoko Hirabayashi*,Tohoru Inoue*:Stem-cell leukemia: p53 deficiency mediated suppresion of leukemic differentiation in C3H/He myeloid leukemia,Leukemia Research,26,1085-1092,2002

Yasunari Takada,Misao Hachiya,Sang-hee Park,Yoshiaki Osawa*,Toshihiko Ozawa,Makoto Akashi:Role of reactive oxygen species in cells overexpressing manganase superoxide dismutase: Mechanism for induction of radioresistance.,Molecular Cancer Research,1,137-146,2002

Nobuhiko Ban*,Kazuko Yoshida,Shirou Aizawa,Sachiko Wada*,Michiaki Kai*:Cytogenetic Analysis of Radiation-Induced Leukemia in Trp53-Deficient C3H/He Mice,Radiation Research,158,69-77,2002

Hospital

Akira Iyoda*,Kennzou Hiroshima*,Masayuki Baba,Yukio Saitoh*,Hidemi Owada*,Takehiko Fujisawa*:Pulmonary large cell carcinomas with neuroendocrine features are high grade neuroendocrine tumors.,Annals of Thoracic Surgery,73,1049-1054,2002

Kennzou Hiroshima*,Akira Iyoda*,Kiyosi Shibuya*,Hidehisa Hoshino*,Yukiko Haga*,Tetsuya Toyozaki*,Mitsutosi Shiba*,Masayuki Baba,Takehiko Fujisawa*,Hidemi Owada*:Evidence of neoangiogenesis and an increase in the number of proliferating cells within the epithelium of smokers.,Cancer,95,1539-1549,2002

Akira Iyoda*,Masayuki Baba,Yukio Saitoh*,Hidehisa Hoshino*,Kiyosi Shibuya*,Yasushi Nomoto*,Fumio Horiuchi*,Kennzou Hiroshima*,Hidemi Owada*,Takehiko Fujisawa*:Imprint cytologic features of pulmonary sclerosing hemangioma-comparison with well differentiated papillary adenocarcinoma.,Cancer,96,146-149,2002

Kennosuke Kadono*,Toshiaki Honnma*,Kazuyuki Kamahara*,Mika Nakayama*,Hiroaki Satoh*,Kiyohisa Sekizawa*,Tadaaki Miyamoto:Effect of heavy-ion radiotherapy on pulmonary function in stage I non-small cell lung cancer patients,Chest,122,1925-1932,2002

Katsuhiro Uzawa*,Kanae Ono*,Chihaya Tanaka*,Takashi Yakushiji*,Nobuharu Yamamoto,Hidetaka Yokoe*,Hideki Tanzawa*:High prevalence of decreased expression of KAI1 metastasis suppressor in human oral carcinogenesis.,Clinical Cancer Research,8,828-835,2002

Minoru Suzuki*,Mizuto Otsuji*,Masayuki Baba,Yukio Saitoh*,Toshihiko Iizasa*,Kiyosi Shibuya*,Yasuo Sekine*,Seiri Yoshida*,Takehiko Fujisawa*:Bronchopleural fistula after lung cancer surgery.,Journal of Cardiovascular Surgery,43,263-267,2002

Masayuki Baba,Akira Iyoda*,Kazuhiro Yasafuku*,Yukiko Haga*,Hidehisa Hoshino*,Yasuo Sekine*,Kiyosi Shibuya*,Toshihiko Iizasa*,Yukio Saitoh*,Kennzou Hiroshima*,Takehiko Fujisawa*:Preoperative cytodiagnosis of very small-sized peripheral-type primary lung cancer.,Lung Cancer,37,277-280,2002

Kiyosi Shibuya*,Hidehisa Hoshino*,Masako Chiyo*,Kazuhiro Yasafuku*,Toshihiko Iizasa*,Yukio Saitoh*,Masayuki Baba,Kennzou Hiroshima*,Hidemi Owada*,Takehiko Fujisawa*:Subepithelial vascular

patterns in bronchial dysplasias using higt-magnification bronchoscope.,Thorax,57,902-907,2002

Riwa Kishimoto,Yoshiaki Watanabe*,Michio Shimizu*:Best cases from the AFIP : invasive ductal carcinoma with osteoclast-like giant cells.,Radiographics,22,691-695,2002

Yasutaka Itani*, Shigeru Watanabe*, Yoshiaki Masuda*, Kazuhisa Hanamura*, Kazuhiro Asakura*,Shusuke Sone*, Yuko Sunami*, Tadaaki Miyamoto: Measurement of aortic diameters and detection of asymptomatic aortic aneurysms is a mass screening program using a mobile helical computed tomography

Yojiro Hashiguchi*,Takeshi Sekine*,Shingo Katou,Hirohiko Sakamoto*,Yoji Nishimura*,Tomoko Kazumoto*,Mizuyoshi Sakura*,Yoichi Tanaka*:Indicators for Surgical Resection and Intraoperative Radiation Therapy for Pelvic Recurrence of Colorectal Cancer,Diseases of the Colon and Rectum,46,31-39,2003

Department of Accelerator Physics and Engineering

Tetsumi Tanabe*,Katsuhisa Chida*,Kouji Noda,Ikuo Watanabe*:An electrostatic storage ring for atomic and molecular science,Nuclear Instruments & Methods in Physics Research Section A,482,595-605,2002

Masayuki Muramatsu,Atsushi Kitagawa,Yukio Satou,Satoru Yamada,Toshiyuki Hattori*,Mitsuru Hanagasaki*,Toshitaka Fukushima*,Hirotsugu Ogawa*:Development of an ECR ion source for carbon therapy,Review of Scientific Instruments,2001

Atsushi Kitagawa:Study of the extracted beam and the radial magnetic field of ECR ion source,Review of Scientific Instruments,73,604-606,2002

Yukio Satou:Effects of Ion-Pumping in a Pulsed Penning Source,Review of Scientific Instruments,73,720-722,2002

T. Furukawa and K. Noda : Fast beam cut-off method in RF-knockout extraction for spot scanning ; Nucl. Instr. Meth. Res. A489 (2002) 59-67.

T. Honma, D. Ohsawa, K. Noda, T. Iwashima, H. Y. Ogawa, Y. Sano, E. Takada, S. Yamada : Design and performance of a non-destructive beam-profile monitor utilizing charge-division method at HIMAC ; Nucl. Instr. Meths. Res. A490 (2002) 435-443.

K. Noda, T. Furukawa, S. Shibuya, M. Muramatsu, T. Uesugi, M. Kanazawa, M. Torikoshi, E. Takada and S. Yamada : Source of spill ripple in the RF-KO slow-extraction method with FM and AM;Nucl. Instr. Meth. Res. A492 (2002) 241-252.

K. Noda, T. Furukawa, S. Shibuya, T. Uesugi, M. Muramatsu, M. Kanazawa, E. Takada and S. Yamada : Advanced RF-KO slow-extraction method for the reduction of spill ripple;Nucl. Instr. Meth. Res. A492 (2002) 253-263.

T. Tanabe and K. Noda: Storage of Bio-molecular Ions in Electrostatic Storage Ring;Nucl. Instr. Meth. Res. A496 (2003) 233-237.

T.Katsuno, S.Nitta, D.Ohsawa and Y.Sato, Detection of heavy ions for cancer therapy using amorphous carbon nitride a-CN_X films produced by a nitrogen radical sputter method, Diamond and Related Materials 12 (2003) 672-676.

Y.Sato, A.Kitagawa, M.Muramatsu, T.Murakami, S.Yamada, C.Kobayashi, Y.Kageyama, T.Miyoshi, H.Ogawa, H.Nakabushi, T.Fujimoto, T.Miyata and Y.Sano, Charge fraction of 6.0 MeV/n heavy ions with a carbon foil: dependence on the foil thickness and projectile atomic number, Nucl. Instrum. and Meth. B201 (2003) 571-580.

Department of Medical Physics

Masahiro Endo,Takanori Tsunoo,Susumu Kandatsu,Shuji Tanada,Hiroshi Aradate*,Yasuo Saito*:Four-dimensional computed tomography (4D CT) - Concepts and preliminary development,Radiation Medicine,21,17-22,2003

Naoko Inadama,Hideo Murayama,Tomohide Omura,Takaji Yamashita*,Seiichi Yamamoto*,Hiroyuki Ishibashi*,Hideyuki Kawai,Kenji Omi*,Takaya Umehara,Takehiro Kasahara:A depth of interaction detector for PET with DSO crystals doped with different amount of Ce.,IEEE Transactions on Nuclear Science,49(3),629-633,2002

Tomoyuki Hasegawa,Eiichi Tanaka,Mitsuo Watanabe*,Takaji Yamashita*,Taiga Yamaya,Hideo Murayama:A Monte-Carlo simulation study on coarse septa for scatter correction in 3D PET.,IEEE Transactions on Nuclear Science,49(5),2133-2138,2002

Keishi Kitamura,Masaharu Amano*,Hideo Murayama:Count rate analysis of PET scanner designs based on a GSO depth of interaction detector

with a large area PS-PMT.,IEEE Transactions on Nuclear Science,49(5),2218-2222,2002

Ayuchi Nakamura,Hiroyuki Takahashi,L Zhang*,Daichi Fukuda*,Takaaki Ishizu*,Masaharu Nakazawa*,Masaki Misawa*,Hideo Murayama:Clustering algorithm with adaptive shaping method for CdZnTe detectors.,IEEE Transactions on Nuclear Science,49(6),3295-3299,2002

Nobuyuki Kanematsu, Masahiro Endo, Yasuyuki Futami, Tatsuaki Kanai, Hiroshi Asaskura*, Hiroyoshi Oka*, Ken Yusa*: Treatment planning for the layer-stacking irradiation system for three-dimensional conformal heavy-ion radiotherapy,Medical Physics, 29(12), 2823-2829, 2002

Manabu Mizota, Tatsuaki Kanai, Munefumi Shinbo, Yasuyuki Futami, Masahiro Endo: Reconstrubtion of Biologically Equivalent Dose Distribution on CT-image from Measured Physical Dose Distribution of Therapeutic Beam in Water Phantom,Physics in Medicine and Biology, 47, 923-945, 2002

Akifumi Fukumura,Tatsuaki Kanai,Nobuyuki Kanematsu,Ken Yusa,Akira Maruhashi*,Akihiro Nohtomi*,Teiji Nishio,Munefumi Shinbo,Takashi Akagi,Toshihiro Yanou*,Shigekazu Fukuda*:Proton beam dosimetry/Protocol and intercomparison in Japan,International Symposium on Standards and codes of Practice in Medical Radiation Dosimetry,in press,2003

Satoru Endo*,Masashi Takada,Masayori Ishikawa*,Masaharu Hoshi*,Shuzou Uehara*,Hiroshi Yamaguchi,Tatsuaki Kanai,Naruhiro Matsufuji,Kiyoshi Shizuma*,Yoshihiko Onizuka*:Microdosimetric study for 400 MeV/A Carbon-beam.,Radiation Protection Dosimetry,99,421-424,2002

Hiroshi Yashima*,Yoshitomo Uwamino*,Hiroshi Sugita*,Takashi Nakamura,Sachiko Ito*,Akifumi Fukumura:Projectile dependence of radioactive spallation products induced in copper by high-energy heavy ions,Physical Review C,66,044607-1-044607-11,2002

Michiya Sasaki*,Noriaki Nakao*,Takashi Nakamura,Tokushi Shibata*,Akifumi Fukumura:Measurements of the response functions of an NE213 organic liquid scintillator to neutrons up to 800 MeV.,Nuclear Instruments & Methods in Physics Research Section A,480,440-447,2002

Michiya Sasaki*,Noriaki Nakao*,Tomoya Nunomiya*,Takashi Nakamura,Akifumi Fukumura,Masashi Takada:Measurements of high energy neutrons penetrated through iron shields using the Self-TOF detector and an NE213 organic liquid scintillator,Nuclear Instruments & Methods in Physics Research Section B,196,113-124,2002

Michiya Sasaki*,Eunju Kim*,Tomoya Nunomiya*,Takashi Nakamura,Noriaki Nakao*,Tokushi Shibata*,Yoshitomo Uwamino*,Sachiko Ito*,Akifumi Fukumura:Measurements of High-Energy Neutrons Penetrated Through Concrete Shields Using Self-TOF, NE213 and Activation Detectors,Nuclear Science and Engineering,141,140-153,2002

Narufumi Suganuma*, Yukinori Kusaka*,Yomei Hiraga*, Yutaka Hosoda*, Hisao Shida*, Hiroshi Morikubo*, Toru Matsumoto.: Asbests-related pleural abnormalityes detected by chest X-ray: Fair agreement with detection by computed tomography, J Occup Health 43:365-370, 2001

Norinari Honda*, Kikuo Machida*, Makoto Hosono*, Tohru Matsumoto ,Hiroshi Matsuda*, Motoo Oshima*, Kiyoshi Koizumi*, Shigeru Kosuda*, oshimitsu Momos*, Yutaka Mori*, Jun Hashimoto*, Yuji Shimizu*: Interobserver variation in diagnosis of dementia by brain perfusion SPECT, Radiation Medicine 20(6):281-289,2002

K Nishizawa, M Matsumoto, K Iwai, A Tonari, T Yoshida, M Takayama: Dose evaluation and effective dose estimation from multi detector CT Jap. J. Med. Phys: 22, 155-158, 2002

Takehiro Tomitani,Masahiko Hirasawa:Analytical image reconstruction of cone-beam projections from limited angle Compton camera data,IEEE Transactions on Nuclear Science,50,1602-1608,2003

Masahiko Hirasawa,Takehiro Tomitani:An analytical image reconstruction algorithm to compensate for scattering angle broadening in Compton cameras,Physics in Medicine and Biology,48,1009-1026,2003

Masahiko Hirasawa,Takehiro Tomitani:Tracer imaging with a Compton camera,Proceedings of International Symposium on Bio-Trace Elements,2002,40-42,2003

Department of Medical Imaging

Yoshinori Ishiguro*,Tatsuya Kikuchi,Hiromi Etsuki,Toshiaki Irie:Does Xenon Anesthesia Inhibit Cholinesterases?,Anesthesiology,98(3),791-792,2003

Zhang Ming-rong*,Akio Tsuchiyama*,Terushi Haradahira,Yuichirou Yoshida*,Kenji Furutsuka*,Kazutoshi Suzuki:Development of an automated system for synthesizing 18F-labeled compounds using [18F]fluoroethyl bromide as a synthetic precursor,Applied Radiation and Isotopes,57,335-342,2002

Zhang Ming-rong,Tatsuya Kikuchi,Yuichirou Yoshida*,Jun Maeda,Takayo Kida*,Takashi Okauchi,Toshiaki Irie,Kazutoshi Suzuki:N-[18F]Fluoroethyl-4-piperidyl acetate ([18F]FEtP4A): A PET Tracer for Imaging Brain acetylcholinesterase in vivo. ,Bioorganic & Medicinal Chemistry,11,2519-2527,2003

Mikio Sato,Tetsuya Toyozaki*,Kenichi Odaka,Tomoya Uehara*,Yasushi Arano*,Hiroshi Hasegawa,Katsuya Yoshida,Kyoko Yoshida*,Toshimichi Yoshida*,Michiaki Hiroe*,Hiroyuki Tadokoro,Toshiaki Irie,Shuji Tanada,Issei Komuro*:Detection of experimental autoimmune myocarditis in rats by 111In monoclonal antibody specific for Tenascin-C.,Circulation,106,1397-1402,2002

Naoyuki Watanabe*,Shuji Tanada,Hajime Murata,Yasuhito Sasaki:I-123 IMP Pulmonary SPECT in a Patient with Acute Pulmonary Thromboembolism,Clinical Nuclear Medicine,27,460-461,2002

Zhang Ming-rong*,Terushi Haradahira,Jun Maeda*,Takashi Okauchi*,Takayo Kida*,Shigeru Obayashi,Kazutoshi Suzuki,Tetsuya Suhara:Synthesisi and preliminary PET study of the 5-HT7 receptor antagonist [11C]DR4446,Journal of Labelled Compounds & Radiopharmaceuticals,45,857-866,2002

Zhang Ming-rong,Kenji Furutsuka,Yuichirou Yoshida*,Kazutoshi Suzuki:How to increase the reactivity of [18F]fluoroethyl bromide: [18F]fluoroethylation of amine, phenol and amide functional groups with [18F]FEtBr, [18F]FEtBr/NaI and [18F]FEtOTf,Journal of Labelled Compounds & Radiopharmaceuticals,46,587-598,2003

Hiroki Namba,Kiyoshi Fukushi,Shin-ichiro Nagatsuka,Masaomi Iyo*,Hitoshi Shinotoh,Shuji Tanada,Toshiaki Irie:Positron emission tomography: quantitative measurement of brain acetylcholinesterase activity using radiolabeled substrates,Methods,27,242-250,2002

Zhang Ming-rong*,Terushi Haradahira,Jun Maeda*,Takashi Okauchi*,Koichi Kawabe*,Takayo Kida*,Junko Hojo*,Kazutoshi Suzuki,Tetsuya Suhara:Synthesis and Pharmacological Evalution of Two Potent Antagonists for Dopamine D4 Receptors:[11C]YM-50001 and N-[2-[4-(4-Chlorophenyl)-piperizin-l-yl]ethyl]-3-[11 C]methoxybenzamide. ,Nuclear Medicine and Biology,29,233-241,2002

Zhang Ming-rong*,Terushi Haradahira,Jun Maeda*,Takashi Okauchi*,Koichi Kawabe*,Takayo Kida*,Shigeru Obayashi,Kazutoshi Suzuki,Tetsuya Suhara:Synthesis and evaluation of 3-(4-chlorobenzyl)-8-[11C]methoxy-1,2,3,4-tetrahydr omeno[3,4-c]pyridin-5-one:a PET tracer for imaging sigma1 receptors,Nuclear Medicine and Biology,29,469-476,2002

Terushi Haradahira,Jun Maeda*,Takashi Okauchi*,Zhang Ming-rong*,Junko Hojo*,Takayo Kida*,Takuya Arai,Fumihiko Yamamoto*,Shigeki Sasaki,Minoru Maeda*,Kazutoshi Suzuki,Tetsuya Suhara:Synthesis,in vitro and in vivo pharmacology of a C-11 labeled analog of CP-101,606,(+-)threo-1-(4-hydoxyphenyl)-2-[4-hydr oxy-4-(p-[11C]methoxyphenyl)piperidino]-1-propan ol,as a PET tracer for NR2B subunit-containing NMDA receptors,Nuclear Medicine and Biology,29,517-525,2002

Junko Hojo*,Kazutoshi Suzuki:Automated synthesis of the ultra high specific activity of [11C]Ro15-4513 and its application in an extremely low concentration region to an ARG study,Nuclear Medicine and Biology,30,335-343,2003

Toshimitsu Fukumura,Shihoko Akaike*,Yuichirou Yoshida*,Kazutoshi Suzuki:Decomposition of an aqueous solution of [11C]Ro 15-4513: implication of hydrated in the radiolyisis of[11C]Ro 15-4513Abbreviated Title: Radiolysis of[11C]Ro 15-4513,Nuclear Medicine and Biology,30,389-395,2003

Zhang Ming-rong,Takayo Kida*,Junko Noguchi*,Kenji Furutsuka,Jun Maeda,Tetsuya Suhara,Kazutoshi Suzuki:[11C]DAA1106: Radiosynthesis and In Vivo Binding to Peripheral Benzodiazepine Receptors in Mouse Brain,Nuclear Medicine and Biology,30,513-519,2003

Takahiro Sunaga*,Hiroo Ikehira,Shigeo Furukawa,Mitsuru Tamura,Eiji Yoshitome,Takayuki Obata,Hiroshi Shinkai,Shuji Tanada,Hajime Murata,Yasuhito Sasaki:Development of a Dielectric Equivalent Gel for Better Impedance Matching for Human Skin.,Bioelectromagnetics,24,214-217,2003

Junichi Takanashi*,Hiroo Ikehira,Shuji Tanada:Distinctly abnormal brain metabolism in late-onset ornithine transcarbamylase deficiency,Neurology,59,210-214,2002

Hong Zhang,Tian Mei*,Noboru Oriuchi*,Tetsuya Higuchi*,Shuji Tanada,Keigo Endou*:Oncological diagnosis using postiron coincidence gamma camera with fluorodeoxyglucose in comparison with dedicated PET,British Journal of Radiology,75,409-416,2002

Heavy-Ion Radiobiology Research Group

Yoshiya Furusawa,Mizuho Aoki,Marco Durante*:Simultaneous exposure of mammalian cells to heavy ions and X-rays,Advances in Space Research,30,877-884,2002

Kaoru Kobayashi*,Rie Hosoi*,Sotaro Momosaki*,Sachiko Koike,Koichi Ando,Tsunehiko Nishimura*,Osamu Inoue*:Enhancement of the relative uptake of 18F-FDG in mouse fibrosarcoma by rolipram,Annals of Nuclear Medicine,16,507-510,2002

Isao Asakawa*,H Yoshimura*,Akihisa Takahashi*,Ken Ohnishi*,H Nakagawa*,I Ota*,Yoshiya Furusawa,Tetsurou Tamamoto*,H Ohishi*,Takeo Oonishi*:Radiation-induced growth inhibition in transplanted human tongue carcinomas with different p53 gene status,Anticancer Research,24,2037-2043,2002

Fumihiko Yamamoto*,Mizuho Aoki,Yoshiya Furusawa,Koichi Ando,Yasuo Kuwabara*,Kouji Masuda*,Shigeki Sasaki*,Minoru Maeda*:Synthesis and evaluation of 4-Bromo-1-(3-[18F]fluoropropyl)-2-nitroimidazole with a low energy LUMO orbital designed as brain hypoxia-targetting imaging agent,Biological and Pharmaceutical Bulletin ,25,616-621,2002

Kazufumi Kagawa*,Masao Murakami*,Yoshio Hishikawa*,Mitsuyuki Abe*,Takashi Akagi*,Toshihiro Yanou*,Gou Kagiya*,Yoshiya Furusawa,Koichi Ando,Kumie Nojima,Mizuho Aoki,Tatsuaki Kanai:Preclinical biological assessment of proton and carbon ion beams at Hyogo Ion Beam Medical Center,International Journal of Radiation Oncology Biology Physics,54,928-938,2002

Mizuho Aoki,Yoshiya Furusawa,Yuta Shibamoto*,Ataru Kobayashi*,Michihiko Tsujitani*:Effect of a hypoxic cell sensitizer Dranidazole in radiation-induced apoptosis of mouse L5178Y lymphoma cells,Journal of Radiation Research,43,161-166,2002

Manami Monobe,Manami Monobe*,Koichi Ando:Drinking Beer Reduces Radiation-induced Chromosome Aberrations in Human Lymphocytes,Journal of Radiation Research,43,237-245,2002

Sachiko Koike,Koichi Ando,Chisa Oohira*,Takeshi Fukawa,Ryonfa Lee,Nobuhiko Takai,Akiko Uzawa,Manami Monobe,Yoshiya Furusawa,Mizuho Aoki,Shigeru Yamada,Wakako Shimizu*,Kumie Nojima,Hideyuki Majima*:Relative biological effectiveness of 290 MeV/u carbon ions for the growth delay of a radioresistant murine fibrosarcoma,Journal of Radiation Research,43,247-255,2002

Shozo Suzuki*,Yuri Miura*,Shoichi Mizuno*,Yoshiya Furusawa:Models for mixed irradiation with a 'Reciprocal-Time' pattern of the repair function,Journal of Radiation Research,43,257-267,2002

Marco Durante*,G Gialanella*,Malia Antonella Pugliese*,Tetsuya Kawata*,Nakahiro Yasuda,Yoshiya Furusawa:Influence of the shielding on the space radiation radiobiological effectiveness. II. Chromosomal aberrations,Journal of Radiation Research,43(Suppl.),s107-s111,2002

Tetsuya Kawata*,Hisao Ito*,Ken Motoori*,Takuya Ueda*,Naoyuki Shigematsu*,Yoshiya Furusawa,Marco Durante*,Kerry George*,Honglu Wu*,Francesca A Cucinotta*:Induction of chromatin damage and distribution of isochromatid breaks in human fibroblast cells exposed to heavy ion,Journal of Radiation Research,43(Suppl.),s169-s173,2002

Sylvia Ritter*,E Nasonova*,Yoshiya Furusawa,Koichi Ando:Relationship between aberration yield and mitotic delay in human lymphocytes exposed to 200 MeV/u Fe-ions or X-rays,Journal of Radiation Research,43(Suppl.),s175-s179,2002

Honglu Wu*,Yoshiya Furusawa,Kerry George*,Tetsuya Kawata*,Francesca A Cucinotta*:Analisis of unrejoined chromosomal breakage in human fibroblast cells exposed to low- and high-LET radiation,Journal of Radiation Research,43(Suppl.),s181-s185,2002

Sachiko Koike,Koichi Ando,Akiko Uzawa,Nobuhiko Takai,Takeshi Fukawa,Yoshiya Furusawa,Chisa Oohira*,Mizuho Aoki,Manami Monobe,Ryonfa Lee*,Masao Suzuki,Kumie Nojima:Significance of fractionated irradiation for the biological therapeutic

gain of carbon ions,Radiation Protection Dosimetry,99,405-408,2002

Chunlin Shao,Yoshiya Furusawa,Mizuho Aoki,Hideki Matsumoto*,Koichi Ando:Nitric oxide-mediated bifunctional bystander effect induced by heavy-Ion Radiation in human salivary grand neoplastic cells,International Journal of Radiation Biology,78,837-844,2002

Megumi Toyoshima*,Shogo Takinami*,Kotaro Hieda*,Yoshiya Furusawa,Tomoe Negishi*:The involvement of cell cycle checkpoint-mutations in the mutagenesis induced in Drosophila by a longer wavelength light band of solar UV,Photochemical and Photobiological Sciences,1,178-183,2002

Director of Special Research (on Information Management)

Kiichi Ishiwata*,Nobuo Ogi*,Nobutaka Hayakawa*,Keiichi Oda*,Tsukasa Nagaoka*,Hinako Toyama,Fumio Suzuki*,Kazutoyo Endo*,Akira Tanaka*,Michio Senda*:Adenosine A2A receptor imaging with [11C]KF18446 PET in the rat brain after quinolinic acid lesion:Comparison with the dopamine receptor imaging,Annals of Nuclear Medicine,16(7),467-475,2002

Yuhei Shimada*,Motohiro Kiyosawa*,Keiichi Oda*,Fumio Suzuki*,Kiichi Ishiwata*,Nobuo Ogi*,Nobutaka Hayakawa*,Hiroyuki Umegaki*,Tsukasa Nagaoka*,Kazutoyo Endo*,Akira Tanaka*,Michio Senda*,Tadashi Nariai*,Hinako Toyama,Kenichirou Ono*:Mapping adenosine A1 receptors in the cat brain by positron emission tomography with [11C] MPDX.,Nuclear Medicine and Biology,29,29-37,2002

Kiichi Ishiwata*,Nobuo Ogi*,Nobutaka Hayakawa*,Hiroyuki Umegaki*,Tsukasa Nagaoka*,Keiichi Oda*,Hinako Toyama,Kazutoyo Endo*,Akira Tanaka*,Michio Senda*:Positron emission tomography and ex vivo and in vitro autoradiography studies on dopamine D2-like receptor degeneration in the quinolinic acid-lesioned rat striatum:comparison of [11C] raclopride, [11C] nemonapride and [11C] N-methylspiperone,Nuclear Medicine and Biology,29,307-316,2002

Director of Special Research (on Brain Imaging)

Tetsuya Suhara,Yoshiro Okubo*,Fumihiko Yasuno*,Yasuhiko Sudo*,Makoto Inoue*,Tetsuya Ichimiya*,Yoshifumi Nakashima*,Kazuhiko Nakayama*,Shuji Tanada,Kazutoshi Suzuki,Christer Halldin*,Lars Farde*:Decreased dopamine D2 receptor binding in the anterior cingulate cortex in schizophrenia.,Archives of general psychiatry,59,25-30,2002

Tetsuya Ichimiya*,Tetsuya Suhara,Yasuhiko Sudo*,Yoshiro Okubo*,Kazuhiko Nakayama*,Masahiro Nankai*,Makoto Inoue*,Fumihiko Yasuno*,Akihiro Takano*,Jun Maeda*,Haruo Shibuya*:Serotonin Transporter Binding in Patients with Mood Disorders: A PET Study with [11C](+)McN5652,Biological Psychiatry,51(9),715-722,2002

Akihiro Takano,Tetsuya Suhara,Yasuhiko Sudo*,Makoto Inoue,Kenji Hashimoto*,Zhang Ming-rong*,Tetsuya Ichimiya*,Fumihiko Yasuno*,Kazutoshi Suzuki:Comparative evaluation of two serotonin transporter ligands in the human brain: [11C](+)McN5652 and [11C]cyanoimipramine,European Journal of Nuclear Medicine,29,1289-1297,2002

Youko Ikoma*,Tetsuya Suhara,Hinako Toyama,Tetsuya Ichimiya*,Akihiro Takano*,Yasuhiko Sudo*,Makoto Inoue*,Fumihiko Yasuno*,Kazutoshi Suzuki:Quantitative analysis for estimating binding potential of brain serotonintrasporters with [11C]McN5652.,Journal of Cerebral Blood Flow and Metabolism,22,490-501,2002

Soutarou Momosaki*,Sun Xue Zhi,Nobuhiko Takai,Rie Hosoi*,Osamu Inoue*,Sentaro Takahashi:Changes in histological construction and decrease in 3H-QNB binding in the rat brain after prenatal X-irradiation,Journal of Radiation Research,43,277-282,2002

Masahiro Yamamoto*,Tetsuya Suhara,Yoshiro Okubo*,Tetsuya Ichimiya,Yasuhiko Sudo*,Makoto Inoue,Akihiro Takano,Fumihiko Yasuno,Kyosan Yoshikawa,Shuji Tanada:Age-related decline of serotonin transporters in living human brain of healthy males,Life Sciences,71,751-757,2002

Fumihiko Yasuno*,Akterh Hasnine*,Tetsuya Suhara,Tetsuya Ichimiya*,Yasuhiko Sudo*,Makoto Inoue*,Akihiro Takano*,Ou Tan*,Tomomichi Ando*,Hinako Toyama:Template-Based Method for MultipleVolumes of Interest of Human Brain PET Images,NeuroImage,16,577-586,2002

Jun Maeda,Tetsuya Suhara,Takashi Okauchi,Junichi Senba:Different roles of group I and group II metabotropic glutamate receptors on phencyclinine-induced dopamine release in the rat prefrontal cortex,Neuroscience Letters,336(3),171-174,2003

Shigeru Obayashi,Tetsuya Suhara,Koichi Kawabe*,Takashi Okauchi,Jun Maeda,Yuji

Nagai,Atsushi Iriki*:Fronto-parieto-cerebellar interaction associated with intermanual transfer of monkey tool-use learning,Neuroscience Letters,339,123-126,2003

Takeshi Sassa,Tetsuya Suhara,Hiroo Ikehira,Takayuki Obata,F Girard*,Shuji Tanada,Yoshiro Okubo:19F-magnetic resonance spectroscopy and chemical shift imaging for schizophrenic patients using haloperidol decanoate,Psychiatry and Clinical Neurosciencis,56,637-642,2002

Tetsuya Suhara,Takashi Okauchi*,Yasuhiko Sudo*,Akihiro Takano*,Koichi Kawabe*,Jun Maeda*,S Kapur*:Clozapine can induce high dopamine D2 receptor occupancy in vivo.,Psychopharmacology,160,107-112,2002

Takashi Nakayama,Tetsuya Suhara,Yoshiro Okubo,Tetsuya Ichimiya,Fumihiko Yasuno,Jun Maeda,Akihiro Takano,Tomoyuki Saijo,Kazutoshi Suzuki:In vivo drug action of tandospirone at 5-HT1A receptor examined using positron emission tomography and neuroendocrine response,Psychopharmacology,165,37-42,2002

Taeko Miyazaki,Tetsuo Iwami*,Hiroaki Somiya*,Benno Meyerrochow*:Retinal Topography of Ganglion Cells and Putative UV-Sensitive Cones in Two Antarctic Fishes: Pagothenia borchgrevinki and Trematomus bernacchii (Nototheniidae),Zoological Science,19,1223-1229,2002

Frontier Research Center

Masashi Sagara,Eri Takeda*,Akiyo Nishiyama*,Shunsaku Utsumi*,Yoshirou Toyama*,Shigeki Yuasa*,Yasuharu Ninomiya,Takashi Imai:Characterization of functional regions for nuclear localization of NPAT,Journal of Biochemistry,132,875-879,2002

Toshiji Sitara, Yoshiaki Tsuchida, Akira Shimada, Hideaki Mura, Minoru Kuroiwa , Mayumi Iwakawa:PLUMONARY METASTASES AFTER NEPHRECTOMY ONLY FOR SMALL, STAGE I /FAVORABLE HISTOLOGY WILMS'TUMOR,Journal of Pediatrics,in press,2003

Mayumi Iwakawa,Syuuhei Noda,Toshie Oota,Chisa Kitazawa,Ryonfa Lee,Miyako Gotou,Miyuki Wakabayashi,Yoshifumi Matsui,Yoshinobu Harada,Takashi Imai:Different radiation susceptibility among five strains of mouse detected by skin reaction. ,Journal of Radiation Research,44,7-13,2003

Ken Kuramoto*,Sadayuki Ban,Kenji Oda*,Hideo Tanaka*,Akiro Kimura*,Gen Suzuki*:Chromosomal Instability and Radiosensitivity in Myelodysplastic Syndrome Cells.,Leukemia,16,2253-2258,2002

Yuichi Michikawa,Giuseppe Attardi*:Screening for aging-dependent point mutations in mtDNA.,Mitochondrial DNA : methods and protocols(Methods in molecular biology ; 197),197,75-92,2002

Guang Gao*,Adrian Bracken*,Karina Burkard*,Dieo Pasini*,Marie Classon*,Masashi Sagara,Takashi Imai,Kristian Helin*,Jiyong Zhao*:NPAT expression is regulated by E2F and is essential for cell cycle progression,Molecular and Cellular Biology,23,2821-2833,2003

Kurisaki Tomohiro*,Aki Masuda*,Katsuko Sudo*,Junko Sakagami*,Shigeki Higashiyama*,Yoichi Matsuda*,Akira Nagabukuro*,Atsushi Tsuji,Youichi Nabeshima*,Masahide Asano*,Youichirou Iwakura*,Atsuko Sehara*:Phenotypic analysis of Meltrin alpha (ADAM12)-deficientmice: involvement of Meltrin alpha in adipogenesis and myogenesis.,Molecular and Cellular Biology,23,55-61,2003

Zhang Jin*,Asin-cayuela Jordi*,Jennifer Fish*,Yuichi Michikawa,Bonafe Massimiliano*,Olivieri Fabiola*,Passarino Giuseppe*,Giovanna De.benedictis*,Franceschi Claudio*,Giuseppe Attardi*:Strikingly higher frequency in centenarians and twins of mtDNA mutation causing remodeling of replication origin in leukocytes.,Proceedings of the National Academy of Sciences of the United States of America,100(3),1116-1121,2003

Yuichi Michikawa,Kenneth Laderman*,Richter Katherine*,Giuseppe Attardi*:Role of nuclear background and in vivo environment in variable segregation behaviorof the aging-dependent T414G mutation at critical control site for humanfibroblast mtDNA replication.,Somatic Cell and Molecular Genetics,25,333-342,2002

List of Keywords

Author Index

Organization and Staff

Status of March 31, 2003

Yasuhito Sasaki, M.D., PhD., President

Keiko Yumino, Secretary

Toshihiko Ozawa, PhD., Executive Director

Haruo Suzuki, Executive Director

Masaoki Terashima, Auditor

Takashi Murai, Advisory Auditor

Low Dose Radiation Effects Research Project

Toshiaki Ogiu, M.D., Ph.D., Director

Mitsuoki Morimyo, Ph.D., Vice-Director*

Yoshiya Shimada, Ph.D., Vice-Director

Biological Effects of Neutrons

Toshiaki Ogiu, M.D., Ph.D., Team Leader*

Yasushi Ohmachi, D.V.M., Ph.D.

Shin Saigusa, Ph.D.****

Tsuyoshi Hamano, Ph.D. ††

Yuka Ishida, M.S.†

Takeshi Hiraoka, Ph.D.****

Shinji Fushiki, M.D., Ph.D.****

Radiation and Environmental Carcinogenesis

Yoshiya Shimada, Ph.D., Team Leader*

Mayumi Nishimura

Tatsuhiko Imaoka, Ph.D.

Shizuko Kakinuma, Ph.D.****

Mie Murata, D.V.M., Ph.D.+++++

Toshihiko Sado, Ph.D.***

Masahiko Hatano, M.D., Ph.D.***

Kyoko Yasumura, M.S.†††

Atsushi Inoue, M.D.†††

Genetic Effects on Radiation Carcinogenesis

Hideo Tsuji, Ph.D., Team Leader

Hiroko Ishii, Ph.D.

Takanori Katsube, Ph.D.

Hideki Ukai, Ph.D. ††

Hereditary Effects of Radiation

Masatake Yamauchi, Ph.D., Team Leader*

Tomoyasu Higashi, M.S.

Etsuko Hongo

Satsuki Tsuji

Mitsuoko Morimyo, Ph.D.*

Katsuyoshi Fujikawa, Ph.D. (May 2002～Oct. 2002)††

Wu Jian Yu, M.S.+++++

Radiation Effects on Germ Cells

Tadahiro Shiomi, Ph.D., Team Leader

Masahiko Takahagi, Ph.D.

Naoko Shiomi†

Takeshi Yasuda, Ph.D. (Jan.2003～) ††

Nakaminoto Laboratory for Marine Radioecology

Masashi Kusakabe, PhD.,Director

Management Section

Naokata Suzuki,Head and 7staffs

International Space Radiation Laboratory

Kazunobu Fujitaka, Ph.D., Director

Masahide Furukawa, Ph.D.*

Masahiro Doi, Ph.D.*

Etsuko Ito+++

Satomi Onuma

Radiation measurements in space

Hiroshi Yamaguchi, Ph.D., Team leader

Masashi Takada, Ph.D.

Yukio Uchihori, Ph.D.

Tatsumi Koi, Ph.D.+++

Nakahiro Yasuda, Ph.D.+++

Hisashi Kitamura, M.S.+++

Takashi Nakamura, Ph.D.+

Toshisuke Kashiwagi, Ph.D.+

Mieko Kurano

Dairo So

Kazuko Kaiho

Radiation protection in space.

Kazunobu Fujitaka, Ph.D., Team leader*

Hiroshi Yasuda, Ph.D.

Susumu Kinpara, Ph.D.

Cellular and molecular effects in Space

(Kazunobu Fujitaka, Ph.D., Team leader*)

Ryuichi Okayasu, Ph.D., Team leader

Kumie Nojima, B.S.

Masao Suzuki, Ph.D.

Sizuo Tomita***, &

Chizuru Tsuruoka***

Rekiko Bando

Chikako Kizu

Keiko Sekita

Liu Chihua

Setsuko Kawai

Shiori Saito
Preventive medicine in space
Satoshi Fukuda, D.V.M., Ph.D.,Team leader
Haruo Iida
Naoko Yayoshi, D.V.M.
Kuniyo Tarumi

Environmental Radiation Protection Research Group
Kenzo Fujimoto, Ph. D., Director*
Masashi Kusakabe, Ph. D., Vice-Director
Radionuclide Behavior around the Living Environment
Kunio Shiraishi, Ph. D., Team Leader*
Sarata Kumar Sahoo, Ph. D.*
Shinzo Kimura, Ph. D.
Toshiyuki Nakajima, Ph. D.***
Yoshiko Kawabata, Ph. D.***
Hitoshi Iwahashi, Ph. D.***
Emi Ishido†††
Internal Exposure
Yoshikazu Nishimura, D. V. M., Ph. D., Team Leader*
Yoshito Watanabe, Ph. D.*
Shino Homma-Takeda, Ph. D.
Masae Yukawa, Ph. D.*
Shiro Sakurai, Ph. D.***
Masahito Wada, Ph. D.***
Izuru Kakuta, Ph. D.***
Atsuko Shinohara, Ph. D.***
Hiroyuki Fukuda, M. D.†††
Hiromichi Oobu, M. D.†††
Radiation Protection Dosimetry
Nobuhito Ishigure, Ph. D., Team Leader*
Takashi Nakano, Ph. D.*
Masaki Matsumoto, M. S.*
Hiroko Enomoto*
Masaharu Okano, Ph. D.***
Radiation Epidemiology and Risk Assessment
Yasuhiko Yoshimoto, Ph. D., Team Leader
Shinji Yoshinaga, Ph. D.
Radiation Exposure Mitigation
Katsumi Kurotaki, Ph. D., Team Leader
Masafumi Uchiyama, Ph. D.***
Distribution of Radionuclides in the Ocean
Teruhisa Watabe, M. S., Team Leader
Masatoshi Yamada, Ph. D.
Tatsuo Aono, Ph. D.
Zhong-Liang Wang, Ph. D.***
Miki Amou†††
Mechanism of Accumulation of Radionuclides and Stable Isotopes by Marine Organisms
Toshiaki Ishii, Ph. D., Team Leader
Motokazu Nakahara, B. S.
Ryoichi Nakamura, B. S.
Mitsue Matsuba
Assessments of Radiological Impacts of Releases of Radioactive Substances into the Marine Environment
Shigeki Hirano, Ph. D., Team Leader
Setsuko Yokosuka

Environmental and Toxicological Science Research Group
Ysuyuki Muramastu, Ph.D., Director
Environmental Toxicology
Yasuyuki Muramatsu, Ph.D., Head
Hiroshi Sato, Ph.D.
Yoshihisa Kubota, D.V.M.
X.Z.Sun,Ph.D.††
Model Ecosystem Studies
Hiroshi Takeda, Ph.D., Head
Kiriko Miymoto, Ph.D.
Kei Yanagisawa, Ph.D.
Shoichi Fuma, M.S.
Nobuyoshi Ishii, Ph.D††
Methodology Development
Masahiro Doi, Ph.D., Head
Tetsuya Sakashita, Ph.D.
Biogeochemical Research
Yasuyuki Muramatsu * ,Ph.D., Head
Shigeo Uchida, Ph.D.
Satoshi Yoshida, Ph.D.
Keiko Tagami, Ph,D.
Tadaaki Ban-nai,M.S.

Radon Research Group
Yuji Yamada, Ph.D. Director
1st Team
Masahide Furukawa, Ph.D Team Reader.
Shinji Tokonami, Ph.D.
Hirokazu Ichitsubo, Ph.D.
2nd Team
Yuji Yamada, Ph.D. Team Reader.
Takeko Odaka
Kumiko Fukutsu, B.S.
Tetsuo Ishikawa, Ph.D.
Weihai Zhuo, Ph.D.
Akira Koizumi,* B.S.
Hidenori Yonehara*, Ph.D.

Redox Regulation Research Group
Nobuo Ikota, Ph.D. Director
1st Team
Jun-ichi Ueda, Ph.D. Team Leader

Hidehiko Nakagawa, Ph.D.,
Ikuo Nakanishi, Ph.D.
Akira Hanaki, Ph.D.***
Megumi Ueno, M.S.+++++

2nd Team
Kazunori Anzai, Ph.D. Team Leader
Masako Furuse,
Keizo Takeshita, Ph.D.
U. Winn Aung, Ph.D. ††
Takashi Moritake, M.D.***
Ragchaa Khoroljav, Ph.D.***
Badal Mandal, Ph.D. ††
Kaori Fujii,†††††
Keita Saito,+
Chiho Nishizawa,††††
Yo-hei Okuda,††††

3rd Team
Nobuo Ikota, Ph.D.* Team leader
Makoto Onoda, Ph.D.
Hiroshi Inano, Ph.D.***
Mami Miyoshi, Ph.D. †

4th Team
Nobuo Ikota, Ph.D.* Team leader
Keiko Suzuki, Ph.D.
Hiroshi Ishihara, Ph.D.
Izumi Tanaka,
Haruko Yakumaru, M.S. †

Radiation Hazards Research Group
Isamu Hayata, Ph.D.,Director

1st Team
Isamu Hayata, Ph.D.Team leader
Masako Minamihisamatsu, B.S.
Reiko Kanda, Ph.D.
Akira Furukawa, Ph.D.
Wang Chunyan***
Zhang Wei, B.M.***

2ndTeam
Shiro Aizawa, Ph.D.Team Leader
Kazuko Yoshida, Ph.D.
Kaoru Tanaka, B.S.
Yoko Hirabayashi, M.D.,Ph.D.***
Tohru Inoue,M.D.,Ph.D.***
Keiko Watanabe, B.S. ††
Masanobu Kitagawa, M.D.,Ph.D††

3rdTeam
Osami Yukawa, Ph.D.,Team Leader
Masako Nose,B.S.
Mitsuru Nenoi, Ph.D.
Wang Bing, Ph.D.
Tetsuo Nakajima,Ph.D.
Kazuhiro Daino,M.S. ††
Takeshi Yamada, Ph.D***
Harumi Ohyama, Ph,D***
Sachiko Ichimura,Ph.D***
Hiroko Hama-Inaba, Ph.D***
Chihiro Azuma,B.S. ††††

4thTeam
Tomohisa Hirobe, Ph.D,Team Leader
Hiromi Itsukaichi
Kiyomi Eguchi-Kasai, Ph.D
Masahiko Mori, Ph.D.
Masahiro Murakami, Ph.D.
Manabu Koike, Ph.D.
Kimihiko Sugaya, Ph.D.
Yasuharu Ninomiya, Ph.D.
Motoi Ohba, Ph.D.***
Haruki Ootaka, B.S. ††
Kori Ohno, M.S.

Transcriptome Profiling Research Group
Kouichi Tatsumi, M.D., Ph.D., Director
Masumi Abe, Ph.D., Team leader
Toshiyuki Saito, Ph.D., Team leader
Ikuko Furuno-Fukushi, Ph.D., Senior Researcher
Yuko Noda, Senior Researcher
Eiko Kubo, Senior Researcher
Ryoko Araki, M.D., Ph.D., Postdoctoral Fellow
Ryutaro Fukumura, Ph.D., National Institute Post Doctoral Fellow
Hirakazu Takahashi, Ph.D., Visiting Researcher
Akira Fujimori, M.D., Ph.D., Visiting Researcher
Masahiro Muto, Ph.D., Visiting Researcher
Yoshihiko Chiba, Ph.D., Visiting Researcher
Yuko Houki-Fujimori, B.Ph., Visiting Technical Staff
Akiko Hayashi, B.S., Visiting Technical Staff
Tatsuya Asano, B.S., Visiting Technical Staff
Tsuyoshi Kuroda, B.S., Visiting Technical Staff
Yoshinori Takano, B.S., Visiting Technical Staff
Tatsuya Ohhata, Graduate Student of Cooperation Program
Yoko Tsutsumi, Ph.D., Visiting Scientist
Syunsuke Ando, B.S., Visiting Scientist
Yoshimichi Tabata, Postgraduate Fellow
Eiko Sameshima, Postgraduate Fellow
Takeshi Furuse, Ph.D., Visiting Cooperative Researcher
Hiroshi Tanooka, Ph.D., Visiting Cooperative Researcher
Takayuki Kurihara, Ph.D., Visiting Cooperative Researcher
Akiko Ueno, Ph.D., Visiting Cooperative Researcher
Naokazu Sasaki, B.S., Visiting Cooperative Researcher
Maki Nakahara, M.S., Visiting Cooperative Researcher

Etsuko Mitsui, B.S., Visiting Cooperative Researcher
Joseph John Rodrigue, Ph.D., Visiting Cooperative Researcher
Takayuki Akimoto, Ph.D., Visiting Cooperative Researcher
Ichiro Kouno, Ph.D., Visiting Cooperative Researcher
Charles A.Waldren, Ph.D., Cooperating Researcher
Akiko Ueno, Ph.D., Cooperating Researcher
Diane B. Vannais, B.S., Cooperating Researcher

Laboratory Animal Development and Research Group
Satoru Matsushita, D.V.M.,Ph.D., Director
Yuji Ishikawa, Ph.D., Team Leader
Seiji Kito, Ph.D.
Masanori Okamoto, Ph.D.*
Akihiro Kawano, D.V.M., M.S.*
Hiromi Omoe, D.V.M., Ph.D.*
Atsuko Matsumoto, M.S.+
Kouichi Maruyama, M.S.++
Kazuko Aoki, Ph.D.,***

Internal Radiation Effects Research Group
Yoichi Oghiso, D.V.M., Ph.D., Director
Yutaka Yamada, D.V.M., Ph.D., Team Leader

The Research center for Radiation Emergency Medicine
Yasuhiro Takeuchi, M.D., Ph.D,Director
Makoto Aakshi, M.D.,Ph.D.,Project Leader
Pathophysiological Study on Tissue Injury due to Acute High dose Irradiation Toshiyasu Hirama, M.D., Ph.D.,Head
Naoyuki Anzai, M.D., Ph.D.
Misao Hachiya, Ph.D.
Hisayoshi Kondo,M.D.
Saori Kawamura,M.D.
Daisaku Takai,Ph.D.***
Sang-Hee Park,Ph.D.***
Rika Kawaguchi,M.S.***
Yasunari Takada††
Kazumi Harada†††
Manabu Koike, Ph.D.
Yasuharu Ninomiya, Ph.D.
Kaori Ohno, M.S.
Tomoe Yamauchi
Aki Koike
Motoi Ohba, Ph.D.***
Development of Chelating Agents for Internal Contaminations
Satoshi Fukuda,D.V.M.,Ph.D.,Head.
Haruzo Iida
Yan Yueming****
Makoto Akashi,M.D.,Ph.D.
Development Program of a System for dose Assessment and Evaluation in Radiation Emergency
Yutaka Noda,B.S.,Head
Makoto Akashi*,M.D.,Ph.D.
Shinji Sato
Yoshikazu Kumamoto,Ph.D.
Isamu Hayata*,Ph.D.
Masako Minamihisamatsu,B.S.
Reiko Kanda*,Ph.D.
Akira Furukawa*,M.S.
Study for Reduction of Detriment Induced by Ionizing Irradiation
Makoto Akashi*,M.D.,Ph.D.,Head
Yoshiko Kawase,B.S.
Reina Kondo††††
Nobuo Ikota*,Ph.D.
Kazuki Anzai*,Ph.D.
Hiroshi Ishihara*,Ph.D.
Masako Furuse*
Hiroshi Inano* ,Ph.D.
Shiro Aizawa*,Ph.D.
Kazuko Yoshida*,Ph.D.
Kaoru Tanaka*,B.S.
Emergency Response on Accidental Environmental Contamination
Kenzo Fujimoto*,Ph.D.,Head
Hiroshi Takeda*,Ph.D.
Shinzo Kimura*,Ph.D.
Katsumi Kurotaki*,Ph.D.
Masae Yukawa*,Ph.D.
Yoshikazu Nishimura*,D.V.M.,Ph.D.
Nobuhito Ishigure*,Ph.D.
Kiriko Miyamoto*,Ph.D.
Yasuyuki Muramatsu*,Ph.D.
Takashi Nakano*,Ph.D.
Reiko Kanda*,Ph.D.
Sarata Kumar Sahoo*,Ph.D.
Yoshito Watanabe*,Ph.D.
Masaki Matsumoto*,B.S.
Kunio Shiraishi*,Ph.D.

Hospital
Hirohiko Tsujii, M.D.,Director
Section of Clinical Oncology
Shinroku Morita, M.D.,Section Head
1st Room
Tadaaki Miyamoto, M.D.
Hiroshi Kato, M.D.
Shigeru Yamada,M.D.
Naoyoshi Yamamoto, M.D.
3Resident Doctors
2nd Room

Junetsu Mizoe, M.D.
Takeshi Yanagi,M.D.
Hiroshi Tsuji, M.D.
Tatsuya Ohno , M.D.
3Resident Doctors
Clinical Radio-Technology
Kunio Sakashita and 10 Staff Members
Section of Clinical Diagnosis
Susumi Kandatsu, M.D., Section Head
Laboratory Examinations
Hidehumi Ezawa, M.D.
Hiroko Moriya and 3 Staff Members
Imaging Diagnosis
Tadashi Kamada, M.D.
Tkayuki Obata, M.D.
Kyosan Yoshikawa, M.D.
Ryuuichi Yoneyama, M.D.
And 2 Resident Doctors
Section of Nursing
Mitsuko Matsuda, Section Head
Tamiko Satoh
Fusako Kitane
Chiemi Murakami, Noriko Tokuyama
30 Staff Members and 4 Assistants
Pharmacy
Shin Watanabe, Kazuo Seki and Takashi Nakano

Department of Accelerator Physics and Engineering
Satoru Yamada, Ph. D., Director
Cyclotron Operation Section
Toshihiro Honma, Ph. D., Section Head
Koji Kono*
Satoru Hojo
Yukio Sakamoto
HIMAC Operation Section
Eiichi Takada, Ph. D., Section Head
Koji Kono
Mitsuru Suda
Masayuki Muramatsu
Mitsuo Yoshimoto
Technical Management Section
Takeshi Murakami, Ph. D., Section Head
Akinori Sugiura
Low Energy Beam Research Section
Yukio Sato, Ph. D., Section Head
Atsushi Kitagawa, Ph. D.
Valeri Kapin, Ph. D.(JSPS Fellow)
Takashi Fujisawa, Ph. D.#####
High Energy Beam Research Section
Satoru Yamada, Ph. D., Section Head*
Masayuki Kumada, Ph. D.
Mitsutaka Kanazawa, Ph. D.
Koji Noda, Ph. D.
Yoshiyuki Iwata, Ph. D.(JISTEC Fellow)
Makoto Sasaki, Ph. D.††
Toshiyuki Misu, Ph. D. ††
Takuji Furukawa, M. S. †
Tetsumi Tanabe, Ph. D.****
Fuminori Soga, Ph. D.
Takehiro Tomitani, Ph. D.
Masami Torikoshi, Ph. D, Section Head
Shinji Shibuya, Ph. D. †††
Medical Physics Research Section
Shinichi Minohara, Ph. D.
Naruhiro Matsufuji, Ph. D.

Department of Medical Physics
Masahiro Endo, Ph.D., Director
Mitsue Takeshita, Secretary
Therapy Biophysics Section
Tatsuaki Kanai, Ph.D., Section Head
Akifumi Fukumura, Ph.D.
Nobuyuki Kanematsu, Ph.D.
Masaaki Hirai, Ph.D.††
Masataka Komori, Ph.D.††
Eriko Urakabe, Ph.D.††
Ryosuke Kohno, Ph. D.††
Manabu Mizota, Ph. D.****
Ken Yusa, Ph.D.***
Haruo Yamashita, Ph.D.***
Yasuyuki Futami, Ph.D.***
Teiji Nishio, Ph.D.***
Takashi Akagi, Ph.D.***
Munefumi Shinbo, Ph.D.***
Akio Higashi, Ph.D.***
Takeshi Hirooka, Ph. D.***
Li Qiang, Ph. D.***
Yasushi Iseki, M.S.†
Yuki Kose, M.S. †
Hiroki Otani, Ph.D.†††
Therapy System Section
Masahiro Endo, Ph.D., Section Head*
Hiroko Koyama-Ito, Ph.D.
Nobuyuki Miyahara, Ph.D.
Takanori Tsnoo, Ph.D. ††
Masao Matsumoto, Ph. D.****
Shigeo Furukawa***
Yuzuru Nakamura, Ph.D.***
Naoki Suzuki, Ph. D.***
Yukio Nakatsuch, M.D.***

Masahiro Husakabe, Ph. D.***
Kazumasa Satoh, B.S.†††
Satoshi Matsusita, M.S.†††
Satoshi Umeda, M.D.†††

Imaging Physics Section
Hideo Murayama, Ph.D., Section Head
Toru Matsumoto, Ph.D.
Taiga Yamaya, Ph.D.****
Tomoyuki Hasegawa, Ph.D.****
Keishi Kitamura, Ph.D.****
Takeshi Iinuma, Ph.D.****
Norimasa Nohara, Ph.D.****
Eiichi Tanaka, Ph.D.***
Hideharu Yoshida, M.S.††
Sigenori Shimizu, M.S. †
Naoko Inadama, M.S. †
Hiroyuki Takahashi, Ph.D.***
Hideaki Haneishi, Ph.D.***
Hideyuki Kawai, Ph.D.***
Yoshihisa Akiyama, Ph.D.***
Takeshi Obi, Ph, D.***
Yuichi Kimura, Ph. D.***
Seiichi Yamamoto, Ph. D.***

Medical Exposure Assessment Section
Kanae Nishizawa, Ph.D.
Yutaka Ito, Ph.D.****
Takashi Maruyama, Ph.D.****
Kazuo Iwai, Ph.D., D.D.S†††

Department of Medical Imaging
Shuji Tanada, M.D., Director
Taiko Joshima, Secretary

Radiopharmaceutical Chemistry Section
Kazutoshi Suzuki, Ph.D.,Head
Terushi Haradahira, Ph.D.
Kazuyosyi Nemoto
Masayuki Suzuki
Ryuji Nakao
Osamu Inoue, Ph.D.++++
Ren Iwata, Ph.D.***
Tomoko Nakanishi, Ph.D.***
Kiyoshi Matsumura, Ph,D.***
Toshimitu Fukumura, M.S. †††
Keitarou Tanoi, M.S. †††
Keiko Kawahara, Secretary

Radiotracer and Radiopharmacology Section
Toshiaki Irie, Ph.D., Head
Sadao Shibata, B.S.
Kiyoshi Fukushi, M.S.
Hitoshi Shinotoh, M.D.****
Masahiko Hirasawa, M.S.****
Hiroki Namba, M.D.****
Noriko Tanaka,M.D. †††
Tsuneyoshi Oota, M.D. †††
Shinichiro Nagatsuka, M.S.***

Clinical Imaging Section
Shuji Tanada, M.D., Head*
Tetsuya Suhara, M.D.*
Yukio Tateno, M.D.***
Hiroshi Fykuda, M.D.****
Katsuya Yoshida, M.D.***
Hiroyuki Tadokoro, M.D.***

Informative Molecular Research Section
Hiroo Ikehira, M.D.,Head
Tsutomu Nakada, M.D.****
Hiroshi Shinkai, M.D.***
Takayuki Aoki, Ph.D.***

Medical Information Processing Office
Hinako Toyama, Ph.D.,Head*
Shinichiro Sato, M.D.,Ph.D.
Eiko Takeda
Koji Uemura, Ph. D.
Yoko Ikoma†††
Shinichiro Ohashi†††
Ikuma Takahashi††††
Keisuke Yamakawa††††

Heavy-Ion Radiobiology Research Group
Koichi Ando, D.D.S., Ph.D., D.M.Sc., Group Leader
Yoshiya Furusawa, Ph.D.
Akiko Uzawa, B.Sc.
Sachiko Koike B.Sc.
Nobuhiko Takai, Ph.D.
Mizuho Aoki, Ph.D.††
Hiroshi Ohara, Ph.D.****
Chunlin Shao, Ph.D.***
Guangming Zhou, Ph.D.***
Manami Monobe, M.Sc.+
Yasuyuki Miyato, M.Sc.+
Takeshi Fukawa, M.Sc.+
Yayoi Shino, M.Sc.†††
Kazumi Nakata,
Michiko Takakura,
Eriko Satoh,
Noriko Kameyama,
Tetsuya Kawata, Ph.D., MD.†††
Francis A. Cucinotta, Ph.D.†††
Honglu Wu, Ph.D.†††
Hideki Matsumoto, Ph.D.†††

Akihisa Takahashi, Ph.D.†††
Ken Ohnishi, Ph.D.†††
Kerry George M. Sc.†††
Teruaki Konishi, M.Sc.†††
Kyoko Takahashi,+++
Chisa Ishizawa,+++
Shin Yamaura,+++
Yuichi Kanasugi,+++
Daichi Yoshihara,+++
Takahiko Ishida,+++
Yosuke Izawa,+++
Tadahiro Shiraishi,+++
Kyoko Nohara,+++

Bio-Emission Laboratory
Mikio Yamamoto,Ph.D., Head^t
Nobuo Fukuda,Ph.D., M.D.**
Hideyuki Kokubo,B.S.***
Yoshio Machi,Ph.D.***
Kimiko Kawano,Ph.D.***
Junichirou Kotake,Ph.D.***
Hideo Yoichi,M.E.***
Tomoko Kokado,B.S.***
Tong Zhang,M.D.***
Weizhong Chen,M.E.***
Fengtong Wang, M.D.***
Masataka Tanaka,B.S.***
Suzue Haraguchi,B.S.***
Dmitri V. Parkhomtchouk,Ph.D.***
Takao Soma,Ph.D.***
Mitsumori Tsuchida, M.E.†††
Yuka FukushimaA.A.***
Masako Baba, M.Ph.***
Yuko Furuya, B.A.***
Mamiko Kotake, B.A.***
Mayumi Shibuya, B.A.***
Yasushi Saito, B.A.***
Kazue Hashimoto, A.A.***
Mariko Fujita, M.Sc***
Namiko Tsunoda.††††
Kensaku Fujimura.††††
Takashi Marui.††††

Frontier Research Center
Hajime Murata, M.D., Ph. D. Supervisory Director RedGenomics
Takashi Imai, Ph.D., Director
Yoshi-nobu Harada, Ph.D., Vice-Director
Mayumi Iwakawa, M.D.,Ph.D., Vice-Director
Sadayuki Ban, D.M.Sc.,Ph.D
Yuichi Michikawa, Ph.D.
Kumiko Saegusa, Ph.D.
Masashi Sagara, Ph.D
Atsushi Tsuji, Ph.D
Syuhei Noda, M.D.,Ph.D.
Ken-ichi Ishikawa, M.S.
Atsuko Ishikawa, B.S.
Yoshimi Ohtsuka.
Tomo Kimura, M.S.
Aya Sugyo, M.S.
Hitomi Sudo, M.S.
Miyuki Ohta.
Chisa Oohira, M.S.
Miyako Goto, B.S.
Toshie Ohta, M.S.
Masakazu Kouda, M.S.
Seiko Kawai.
Aki Furuno, M.S.
Hiroko Tanaka, M.S.

Division of Technical Support and Development
Masae Yukawa, Ph.D., Director
Technical Service and Development Section
Hitoshi Imaseki, B.E., Head
and 6 Staff
Information Network System Development Section
Shozo Hongo, B.S., Head
Hiroshi Takeshita, B.S. and 1 Staff
Shinichiro Sato*

Laboratory Animal Development and Management Section
Satoru Matsushita, D.V.M., Ph.D., Head*
Masanori Okamoto, Ph.D.
Akihiro Kawano, D.V.M., M.S.
Hiromi Omoe, D.V.M., Ph.D. and 6 Staff
Seiji Kito, Ph.D.*
Kazuaki Ichinohe, B.S.††
Mikio Saito, Ph.D.††
Fumiaki Sato, Ph.D. ***
Tsuneya Matsumoto, Ph. D.***

Office of Planning and Coordination
Yuji Nakamura, PhD., Director
Yasuhiro Yukimatsu, Head
Masahiro Yamauchi, PhD., Planning Manager
Kazunori Anzai, PhD., Evaluation Manager and 5 staff.

Office of Public Relation
Osamu Hongo, PhD,. Director and 2 staff.

Department of Management
Masakazu Murakami, Director
Personnel and General Affairs Section
Yukio Sakurai, Head and 12 staff
Budget and Accounting Section
Syoichi Sasaki, Head and 8 staff
Contract and Property Management Section
Masanori Hirokami, Head and 9 staff
Facility Management S4ecytion
Masakichi Sakai, Head and 8 staff

Department of International Co-operation, Research Exchange and Training
Yoshiklazu Inoue, Director
International Co-operation Section
Hideo Tatsuzaki, head and 1 staff
Research and Scientific Information Exchange Section
Yukio Kamakura, Head and 2 staff
Training School
Hsamasa Joshima, PhD, Head
Yoshiyuki Shirakawa, PhD.
Itsuro Tamanoi, PhD.**
Kazuo Watari, PhD.** and 2 staff

Audit Office
Tsukasa Sato, Head

Department of Radiation Protection and Safety
Terumi Aoki, Director
Radiation Safety Section
Koji Suzuki, Head and 8 staff
Emergency Preparedness and Monotoring Office
Mitsuhiro Kuchigi, Head and 4 staff

Safety Control Section
Tsuneo Komaya, Head and 2 staff
Radiotoxicology Building Operation Office
Akira Koizumi, Head and 4 staff
Radiation Safety Technology Developement Section
Noriyoshi Yoshida*, Head

* Dual Capacity
** Honorary Scientist
*** Visiting Cooperative Researcher
**** Visiting Researcher
† Visiting Technical Staff
†† Post Doctorial Fellow
††† Post Graduate Fellow
†††† Trainee
+ Graduate Student of Cooperation Program
++ Senior Consultant
+++ Cooperative Researcher
++++ HIMAC Machine Time Coordinator
+++++ Staff Technologist of Priority

NATIONAL INSTITUTE OF RADIOLOGICAL SCIENCES
4-9-1, Anagawa,Inage-ku,Chiba-shi 263-8555 JAPAN
TEL:043-251-2111　FAX:043-256-9616
Email:kouryu@nirs.go.jp　http://www.nirs.go.jp

NAKAMINATO LABORATORY FOR MARINE RADIOECOLOGY
NATIONAL INSTITUTE OF RADIOLOGICAL SCIENCES
Isozaki 3609, Hitachinaka-shi, Ibaraki, 311-1202 JAPAN
TEL:0292-65-7141　FAX:029-265-9214